[redacted]

CENTRAL RESEARCH LIBRARY
DOCUMENT COLLECTION

MARTIN MARIETTA ENERGY SYSTEMS LIBRARIES
3 4456 0349821 2

ORNL-1853
Progress
Cy. 7A

HOMOGENEOUS REACTOR PROJECT

QUARTERLY PROGRESS REPORT

FOR PERIOD ENDING JANUARY 31, 1955

OAK RIDGE NATIONAL LABORATORY
CENTRAL RESEARCH LIBRARY
CIRCULATION SECTION
4500N ROOM 175
LIBRARY LOAN COPY
DO NOT TRANSFER TO ANOTHER PERSON
If you wish someone else to see this report, send in name with report and the library will arrange a loan.
UCN 7969 (3 9-77)

OAK RIDGE NATIONAL LABORATORY
OPERATED BY
CARBIDE AND CARBON CHEMICALS COMPANY
A DIVISION OF UNION CARBIDE AND CARBON CORPORATION
UCC
POST OFFICE BOX P
OAK RIDGE, TENNESSEE

[redacted]

[redacted]

[redacted]

[redacted]

CLASSIFICATION CHANGED TO: DECLASSIFIED

BY AUTHORITY OF: TID-1148

BY: B. Mannon 7/26/57

ORNL-1853

This document consists of 229 pages.

Copy 7 of 257 copies. Series A.

Contract No. W-7405-eng-26

HOMOGENEOUS REACTOR PROJECT

QUARTERLY PROGRESS REPORT

For Period Ending January 31, 1955

Project Director – J. A. Swartout
Associate Director – C. E. Winters

Experimental Reactors – S. E. Beall
Thorium Breeder Reactor – J. A. Lane and R. B. Briggs
Corrosion – E. G. Bohlmann
Engineering Development – J. A. Lane
Chemical Engineering Development – F. R. Bruce
Supporting Chemical Research – E. H. Taylor

Compiled by

H. F. McDuffie
D. C. Kelly

DATE RECEIVED BY INFORMATION AND REPORTS DIVISION

(FEBRUARY 16, 1955)

DATE ISSUED

MAR 21 1955

OAK RIDGE NATIONAL LABORATORY
Operated by
CARBIDE AND CARBON CHEMICALS COMPANY
A Division of Union Carbide and Carbon Corporation
Post Office Box P
Oak Ridge, Tennessee

[redacted]

MARTIN MARIETTA ENERGY SYSTEMS LIBRARIES

3 4456 0349821 2

[redacted]

[redacted]

[redacted]

[redacted]

INTERNAL DISTRIBUTION

1. C. E. Center
2. Biology Library
3. Health Physics Library
4. Metallurgy Library
5-6. Reactor Experimental Engineering Library
7-9. Central Research Library
10-16. Laboratory Records Dept.
17. Laboratory Records, ORNL R.C.
18-19. ANP Reports Office
20. R. E. Avery
21. S. E. Beall
22. D. S. Billington
23. E. P. Blizard
24. E. G. Bohlman
25. C. J. Borkowski
26. G. E. Boyd
27. R. B. Briggs
28. F. R. Bruce
29. A. D. Callihan
30. D. W. Cardwell
31. W. L. Carter
32. G. H. Cartledge
33. R. A. Charpie
34. W. E. Clark
35. G. H. Clewett
36. T. E. Cole
37. E. L. Compere
38. D. D. Cowen
39. S. Cromer
40. F. L. Culler
41. J. S. Culver
42. J. S. Drury
43. M. C. Edlund
44. W. K. Eister
45. L. B. Emlet (K-25)
46. D. E. Ferguson
47. W. J. Fretague
48. J. L. Gabbard
49. W. R. Gall
50. H. E. Goeller
51. C. B. Graham
52. J. C. Griess
53. W. O. Harms
54. P. N. Haubenreich
55. C. J. Hochanadel
56. A. Hollaender
57. A. S. Householder
58. H. K. Jackson
59. G. R. Jenkins (C&CCC, South Charleston)
60. G. H. Jenks
61. W. H. Jordan
62. C. P. Keim
63. M. T. Kelley
64. R. B. Korsmeyer
65. A. S. Kitzes
66. J. A. Lane
67. C. E. Larson
68. R. E. Leuze
69. S. C. Lind
70. R. B. Lindauer
71. R. S. Livingston
72. M. I. Lundin
73. R. N. Lyon
74. W. L. Marshall
75. H. F. McDuffie
76. J. P. McBride
77. R. A. McNees
78. J. R. McWherter
79. O. Menis
80. E. C. Miller
81. K. Z. Morgan
82. E. J. Murphy
83. E. O. Nurmi
84. J. P. Murray (Y-12)
85. L. F. Parsly
86. H. F. Poppendiek
87. L. R. Quarles
88. P. M. Reyling
89. A. M. Rom
90. W. L. Ross
91. H. C. Savage
92. C. H. Secoy
93. C. L. Segaser
94. E. D. Shipley
95. M. J. Skinner
96. W. Stoughton
97. H. Snell
98. I. Lewak
99. C. Musano
100. J. A. Martout
101. E. H. Taylor
102. D. G. Thomas
103. P. F. Thomas

[redacted]

[redacted]

[redacted]4. M. Tobias
[redacted]. W. E. Unger
1[redacted] W. P. Walker
10[redacted]B. Weaver
108[redacted]. M. Weinberg
109. [redacted] A. Welton
110. [redacted]P. Wigner (consultant)
111. G[redacted] Williams
112. J. C. Wilson
113. C. E. Winters
114. F. C. VonderLage
115. F. C. Zapp
116. P. C. Zmola
117. ORNL Document Reference Library, Y-12 Branch

EXTERNAL DISTRIBUTION

118. AF Plant Representative, Burbank
119. AF Plant Representative, Seattle
[redacted]120. AF Plant Representative, Wood-Ridge
[redacted]21. American Machine and Foundry Company
[redacted]2. ANP Project Office, Fort Worth
123-[redacted]. Argonne National Laboratory
1[redacted] Armed Forces Special Weapons Project (Sandia)
13[redacted] Armed Forces Special Weapons Project, Washington
136-140[redacted]tomic Energy Commission, Washington
141. [redacted]bcock and Wilcox
142. [redacted]telle Memorial Institute
143. B[redacted]ix Aviation Corporation
144-149. Be[redacted] Laboratories (WAPD)
150-152. Brod[redacted]ven National Laboratory
153. Bured[redacted]f Ships
154. Bureau [redacted] Yards and Docks
155. Chicago [redacted]erations Office
156. Chicago [redacted]nt Group
157. Chief of N[redacted] Research
158-159. Commonwea[redacted] Edison Company
160. Department o[redacted] Navy – Op-362
161. Detroit Edison [redacted]mpany
162. Division of Rese[redacted]h and Medicine, AEC, ORO
163-166. duPont Company, [redacted]usta
167. duPont Company, [redacted]ington
168. Duquesne Light Co[redacted]y
169. Engineer Research a[redacted]evelopment Laboratories
170. Foster Wheeler Corpor[redacted]
171-174. General Electric Compa[redacted]ANPD)
175. General Electric Company [redacted]PS)
176-183. General Electric Company, [redacted]hland
184. Hanford Operations Office
185. Iowa State College
186. Kaiser Engineers
187-190. Knolls Atomic Power Laboratory
191-192. Los Alamos Scientific Laboratory
193. Massachusetts Institute of Technology [redacted]enedict)
194. Materials Laboratory (WADC)
195. Monsanto Chemical Company
196. Mound Laboratory

[redacted]

[redacted]

197. National Advisory Committee for Aeronautics, Cleveland
198. National Advisory Committee for Aeronautics, Washington
199-200. Naval Research Laboratory
201. Newport News Shipbuilding and Dry Dock Company
202. New York Operations Office
203-204. North American Aviation, Inc.
205. Nuclear Development Associates, Inc.
206. Nuclear Metals, Inc.
207. Pacific Northwest Power Group
208. Patent Branch, Washington
209. Pennsylvania Power and Light Company
210-215. Phillips Petroleum Company (NRTS)
216. Powerplant Laboratory (WADC)
217. Pratt and Whitney Aircraft Division (Fox Project)
218. San Francisco Operations Office
219. Sylvania Electric Products, Inc.
220. Tennessee Valley Authority (Dean)
221. USAF Headquarters
222. USAF Project Rand
223. U.S. Naval Postgraduate School
224. U.S. Naval Radiological Defense Laboratory
225-226. University of California Radiation Laboratory, Berkeley
227-228. University of California Radiation Laboratory, Livermore
229. Vitro Engineering Division
230. Vitro Laboratories
231. Walter Kidde Nuclear Laboratories, Inc.
232. Westinghouse Electric Corporation (IAPG)
233-257. Technical Information Service, Oak Ridge

[redacted]

[redacted]

Reports previously issued in this series are as follows:

ORNL-527	Date issued, December 28, 1949
ORNL-630	Period Ending February 28, 1950
ORNL-730	Feasibility Report – Date Issued, July 6, 1950
ORNL-826	Period Ending August 31, 1950
ORNL-925	Period Ending November 30, 1950
ORNL-990	Period Ending February 28, 1951
ORNL-1057	Period Ending May 15, 1951
ORNL-1121	Period Ending August 15, 1951
ORNL-1221	Period Ending November 15, 1951
ORNL-1280	Period Ending March 15, 1952
ORNL-1318	Period Ending July 1, 1952
ORNL-1424	Period Ending October 1, 1952
ORNL-1478	Period Ending January 1, 1953
ORNL-1554	Period Ending March 31, 1953
ORNL-1605	Period Ending July 31, 1953
ORNL-1658	Period Ending October 31, 1953
ORNL-1678	Period Ending January 31, 1954
ORNL-1753	Period Ending April 30, 1954
ORNL-1772	Period Ending July 31, 1954
ORNL-1813	Period Ending October 31, 1954

[redacted]

[redacted]

HRP QUARTERLY PROGRESS REPORT

SUMMARY

PART I. EXPERIMENTAL REACTORS

1. Homogeneous Reactor Test

1.1 Project Status. A hazards report was issued for the Advisory Committee on Reactor Safeguards; a summary is presented.

The reactor equipment cell is expected to be completed by February 15. While filled with water, the tank was inspected for leaks, and the few leaks found will have been repaired by February 15.

All orders for construction materials placed prior to this quarter have been received. New requisitions issued during the quarter total $16,600. Work orders were issued, and fabrication of all low-pressure-system components was begun in the ORNL shops.

The thermal shield around the reactor vessel was specified as a 2-ft-thick cylindrical concrete wall. With this shield, the fast-neutron flux in the equipment area will be reduced to 7×10^9 neutrons/cm^2/sec, the slow flux to 4×10^7 neutrons/cm^2/sec, and the gamma intensity to less than 10^5 r/hr.

The possible blast effects from a rupture of the pressure vessel were studied and are judged to be sufficient to justify the inclusion of a 1.5- to 2-in.-thick blast shield around the pressure vessel. The blast shield eliminates the danger of damaging the leaktight equipment-cell liner.

Pressures in the reactor equipment cell, as a result of vessel failure, were calculated in order to arrive at a safe design pressure for the reactor equipment cell. For the case of instantaneous release of the core and pressure-vessel liquids and release of the heat-exchanger liquids through 6-in. steam lines, a maximum cell pressure of 29 psig is expected.

A study was made of the problem of uranium peroxide precipitation at places where the reactor solution is cooled soon after leaving the reactor core. A curve is presented to show the temperatures, for various decay times, at which the peroxide might form.

1.2 Design. Approximately 80% of the effort required for design of the HRT has been expended. Drawings for the reactor and auxiliary facilities are 50% complete. The design of the reactor core and pressure vessels has been approved for construction.

1.3 Nuclear Calculations. *1.3.1 Safety Considerations.* A parameter study was conducted with the use of the Oracle to find the influence of particular parameters upon the maximum core-pressure rise, and the results were analyzed. Relations, good for parameter deviations about HRT values, were obtained which show the maximum core-pressure rise for a given reactivity addition. The parameters varied were the temperature coefficient of reactivity, length of piping between core and pressurizer, friction coefficient, fluid compressibility, volume of pressurizing fluid, and lifetime of prompt neutrons. For a given reactor system, various rates of reactivity addition and initial reactor powers could be expressed in terms of an equivalent instantaneous reactivity addition.

1.3.2 The HRT and the "Walk-Away" Phenomenon. The findings of ORNL CF-54-12-206, *The HRT and the "Walk-Away" Phenomenon,* are reported and supplemented by additional results. The HRT should be stable against "walk-away" without the use of automatically controlled steam reducing valves and at average core temperatures below 293 and 273°C at 5 and 10 Mw, respectively, if enough copper is used to recombine all the gas produced in excess of that corresponding to operation at 1 Mw. While "walk-away" may be prevented by employing automatic controls (such as are presently provided in the HRT) in the heat-removal system, inherent reactor properties such as fuel feed pump rate, overpressure, etc., can also make homogeneous reactors stable against "walk-away."

1.4 Component Development. Four of the five HRT-size pumps ordered for development have been received. The 200A and 230A models are being installed for testing. One 400A pump had a defective casing, which was returned to Westinghouse for repair or replacement. The other 400A pump had operated on water for 80 hr and on UO_2SO_4 (10 g of uranium per kilogram of solution) for 70 hr when the thrust bearing failed from unknown cause. The bearing was replaced and the test on the UO_2SO_4 solution continued for an additional 522 hr.

[redacted]

Fabrication of stainless steel fuel and blanket circulating pumps for the HRT is approximately 60% complete. Fabrication of two titanium-reinforced spares will be started soon.

The HRT feed and purge pumps will combine diaphragm pumping heads, being made at ORNL, with Scott & Williams hydraulic drive units. The operating characteristics of the feed pumps are being determined in a system simulating reactor geometry and conditions.

Fabrication of the HRT fuel and blanket heat exchangers at the Foster Wheeler plant in Carteret, N. J., is proceeding on schedule. All tubing which is scheduled for installation in the two units was accepted by ultrasonic and magnetic eddy-current inspection methods, as well as more conventional tests.

A titanium sleeve resembling that of the HRT gas separator was fabricated and then thermal cycled inside a stainless steel pipe. There was no tendency to vibrate after 21 thermal cycles between room temperature and 280°C.

Some experiments on the fluid flow in a model of the HRT pressurizer were reported earlier. Due to a change in reactor layout, the former arrangement of the pressurizer inlet was modified so that it branched directly from a tee above the reactor core. This new arrangement was tested and shown to work satisfactorily.

Construction of the first phase of the HRT dump test, which involves the study of dumping from a single vessel, was completed, and trial dumps were carried out successfully.

The construction of the HRT mockup is near completion. The 3000-psi air compressor which provides gas to the loop for letdown was operated satisfactorily. Final testing of other components is proceeding.

1.5 Controls and Instruments. Design of the nuclear instrument thimble, through which the chambers for measuring reactor power will be inserted in the shield, was completed. Component testing of pressure seals for wires resulted in the selection of Stupakoff seals for electrical wires and crushed lava for thermocouple wires. Evaluation tests on the Jordan radiation monitoring system suggested that the system will be satisfactory for the HRT process monitoring applications.

Conduit layouts for electrical distribution in the control area were completed. Re-evaluation of the procurement status showed an estimate of $20,000 for equipment to be specified. The revised total estimate for procurement is $146,000.

PART II. THORIUM BREEDER REACTOR

2. Conceptual Design

2.1 Reactor Analysis. Investigation of the relative effects of major design variables and changes in nuclear constants on the cost of electrical power and on the characteristics of two-region thorium breeder reactors has been essentially completed. The cost of power is fairly insensitive to changes in the process variables and to rather large variations in the nuclear constants.

2.2 Engineering Studies. The immediate design program was expanded to include consideration of four basic schemes: (a) low-pressure recombination of radiolytic gases, (b) high-pressure recombination, (c) recombination *in situ*, and (d) a boiling-blanket reactor.

The cost influence of the larger turbine-plant components and of operating conditions for the first optimization of the TBR has been determined. With the temperature span of the core solution confined to 250 to 300°C because of corrosion limitations, the optimum saturated steam temperature is about 436°F for a blanket span of 473 to 599°F. For this steam condition at the throttle, the turbine cycle will comprise one stage of moisture separation and three stages of regenerative feed-water heating, exhausting to a pressure of 1.5 in. Hg absolute. Since the net station efficiency will be only about 23%, as compared with the previously assumed value of 26%, the heat generation in the reactor (and hence power density) was raised to maintain 100 Mw net electrical output per reactor. Consequently, the reactor characteristics were re-evaluated.

An investigation of the influence of changes in fixed charges on the design steam temperature showed that quite large changes in such items as inventory charges and depreciation of reactor equipment altered the optimum steam temperature only a few degrees.

Preliminary consideration of equipment design has shown that:

(a) The core-system gas separator will be equivalent to a 2-ft-dia pipe of sufficient length to accommodate an 11-ft void length.

(b) The core and blanket pressurizers will require a gas volume of not less than about 1000

[redacted]

liters, or at least half the core volume, and must be located within about 10 ft of the reactor.

(c) Criticality calculations of U^{233} uranyl sulfate solutions of interest in horizontal cylindrical tanks indicate that dump tanks for the TBR may be limited to lower linear uranium concentrations than the 0.5 kg of uranium per foot considered permissible for the HRT. (The preliminary design will be limited to about 0.4 kg of uranium per foot.)

(d) The core shell, assumed to be ½-in.-thick Zircaloy-2, will be subject to heat generation from radiation absorption of about 21 w/cm^3. Removal of the heat at such a high rate indicates the probability of boiling next to the core vessel wall in spite of the overpressure relative to the fluid bulk temperature.

PART III. CORROSION

3. Pump-Loop Corrosion Tests

3.1 Pump-Loop Operation and Maintenance. One type 347 stainless steel loop has accumulated more than 6700 hr of operating time with various concentrations of uranyl sulfate solutions at 320 °C. Visual inspection of the loop revealed no serious corrosion of parts exposed to the circulating solution. Total weight loss of the type 347 stainless steel impeller used during this period was negligible.

Preliminary testing of a plastic model of the sample unit designed for corrosion studies in a thorium oxide slurry circulating loop indicated satisfactory flow characteristics. One of the new 100A pump loops designed for corrosion studies of thorium oxide slurries is virtually completed and will be put in operation during the next quarter.

3.2 Results of Loop Tests. A series of tests was completed in the 100A loops in which 0.06 *m* uranyl sulfate containing 0.006 *m* sulfuric acid was circulated at 320°C. The results indicated that the critical velocity of the system was greater than 100 fps, and, generally, all the austenitic stainless steels showed corrosion rates of less than 1 mpy.

Loop runs were made in an effort to determine the relevance of cavitation to the phenomenon of critical velocity. The results gave indications that cavitation may have a slight effect on the critical velocity. Other variables are at least as important and perhaps more important than cavitation. For example, the presence of only small amounts of hexavalent chromium in the corrodent has a very pronounced effect in increasing the critical velocity in a given system.

A variety of different alloys was tested in dilute uranyl sulfate solutions. Relatively few of the alloys other than the austenitic stainless steels showed a high degree of corrosion resistance. Notable among those which suffered little attack were types 322W, 17-4 PH, 17-7 PH, 443, and 446 stainless steels and Incoloy. Other tests indicated that uranyl sulfate solutions containing oxygen and either iodide or chloride ions were capable of dissolving both gold and platinum at a measurable rate.

3.3 Sedimentation Rates of Thorium Oxide Slurries at Elevated Temperatures. The sedimentation rates of thorium oxide slurries ranging in concentration from 250 to 1000 g of thorium oxide per kilogram of water were determined at 250 and 300°C. The sedimentation rate of a slurry containing 500 g of thorium oxide per kilogram of water was 0.14 cm/sec at 250°C and 0.18 cm/sec at 300°C. At the 1000-g/kg level no free settling was apparent; settling appeared to be in the compaction zone at all times. Generally, the data indicated a strong correlation between the viscosity of water and the settling rate.

4. Radiation Corrosion

4.1 In-Pile Loop. *4.1.1 In-Pile Loop Development and Construction.* Out-of-pile testing of loop FF, containing Zircaloy-2 corrosion specimens, was completed, and the loop was installed in beam hole HB-4 of the LITR for the second radiation-corrosion test. In-pile loop GG, also containing Zircaloy-2 corrosion specimens, has been completed and is now under test in the mock-up. Loop GG will replace loop FF in hole HB-4 at the LITR for the third in-pile test.

The ORNL 5-gpm in-pile circulating pump was modified by incorporating "outboard" bearings for improved operation. It is hoped that this design will allow the use of sintered aluminum oxide bearings and journals for increased corrosion resistance and longer bearing life. A modified pump is now being equipped with sintered aluminum oxide for operational testing.

4.1.2 In-Pile-Loop Corrosion Test DD. The first in-pile-loop radiation-corrosion experiment is now essentially complete. The loop package was dismantled. The type 347 stainless steel specimens and representative portions of the loop were examined for corrosion. Metallographic examination

[redacted]

of portions of the loop has not been completed. A major portion of the data obtained during operation and from the examination of the loop has been analyzed and correlated.

A second in-pile-loop radiation-corrosion experiment is under way with loop FF. This loop contains Zircaloy-2 corrosion specimens; type 347 stainless steel coupons were used in loop DD.

4.2 Bomb Tests. The addition of 0.04 *m* sulfuric acid to a solution 0.15 *m* in UO_2SO_4 and 0.01 to 0.02 *m* in $CuSO_4$ was found to decrease the in-pile corrosion rate of Zircaloy-2 from 9.6 mpy to 6.4 mpy at 250°C. Experiments with this same solution at 275 and 280°C indicated a positive temperature coefficient of corrosion of approximately 0.2 mpy/°C. Fission power density in these experiments was between 5.4 and 5.9 w/ml. Measurement of the steady-state pressure of the radiolytic gases and analysis of solution before and after pile exposures indicate losses of copper varying from 21 to about 60% of the original amounts in various experiments.

It was found that irradiated Zircaloy-2 pins can be stripped cathodically in 5% sulfuric acid after pretreatment with acetone and air-drying.

An in-pile experiment at 250°C employing a titanium bomb and the same solution as that tested on Zircaloy-2 has been in progress for four weeks. Results thus far indicate a rate under irradiation of 2 mpy or less.

5. Laboratory Corrosion Studies

Although both hardened and annealed pin-type specimens showed good corrosion resistance in dynamic loop tests, fully hardened types 17-4 PH and 17-7 PH stainless steels did not give satisfactory performance when exposed to various simulated reactor environments in static tests. Cracks and blisters were observed after the specimens were boiled in 0.02 *m* UO_2SO_4 + 0.005 *m* H_2SO_4 and in 1.3 *m* UO_2SO_4. At higher temperatures, unduly high corrosion rates were observed. Fully annealed material showed better characteristics.

HRT pool water conditions appeared somewhat corrosive to many materials, particularly carbon steel. The resultant voluminous rust would be expected to diminish visibility in the pool to a considerable degree. Sodium metasilicate as a corrosion inhibitor was only indifferently satisfactory, but sodium chromate appeared to give quite satisfactory corrosion inhibition. Tap-water corrosion of chromium-molybdenum alloy-steel flange bolts for the HRT did not cause nuts to freeze on the bolts, although voluminous rusting resulted in the absence of inhibitors.

A satisfactory, simple twin-strip stress-corrosion specimen was developed for use in the stress-corrosion cracking program.

Thorium slurries containing from 100 to 2275 g of thorium per kilogram of water, produced from Ames, Lindsay batches Nos. 7 and 8, and a pyrohydrolyzed, 900°C fired thorium oxide, were circulated in stainless steel toroids at 26 fps relative velocity and temperatures from 200 to 300°C with oxygen or inert-gas atmospheres. The corrosion rates of pin specimens of type 347 stainless steel, titanium (75A), and Zircaloy-2 were generally less than 4 mpy. The corrosion rates of these slurries on type 347 stainless steel under selected experimental conditions were, statistically, sufficiently different in some cases as to distinguish the slurries.

PART IV. ENGINEERING DEVELOPMENT

6. Development of Fuel-System Components

The high-pressure H_2-O_2 recombiner loop was put into operation on October 19. The efficiency of the platinized alumina catalyst was shown to be at least as good at 1000 psi as at atmospheric pressure. Although loop performance was normally quite smooth, two explosions interrupted operation. It is believed that such explosions can be avoided in the future.

The design of the dump valve test loop was completed, and construction was started late in December.

Some experiments to improve the efficiency of wire-mesh entrainment separators were run in a glass loop. The best performance was obtained by prewashing the entrainment-laden gas with pure water.

Vanes of a new design, which will provide higher rotational velocities and, therefore, a more stable gas void, were installed in the 5000-gpm gas separator.

A proposal from Allis-Chalmers for fabrication of a totally enclosed 500-gpm pump, featuring top maintenance and hydrostatic bearings, is being evaluated. Proposals were received from Allis-Chalmers and Westinghouse for fabrication and

testing at high temperature and pressure of totally enclosed 20-cfm gas circulators.

An ORNL 5-gpm pump, which had been operating on an endurance test, failed electrically after 6750 hr of operation because of deterioration of the stator winding insulation. The winding has been replaced.

Tubing for the HRT heat exchangers has been subjected to inspection by ultrasonic and high-frequency induced-eddy-current methods. Evaluation of tube-inspection methods is part of the Foster-Wheeler heat-exchanger contract.

After 290 hr of intermittent operation on water at 1000 psi and 250°C, the 4000-gpm loop was shut down to observe the effects of temperature cycling and to prepare it for operation with UO_2SO_4 solution. No observable change in leak rate was evident as a result of operation, dismantling, and reassembly.

Tests of a letdown valve in the slurry injection pump loop have demonstrated that thoria prepared by double calcination of the oxalate at 375 and 650°C is considerably less abrasive than either Ames or Lindsay slurry.

7. Development of Blanket-System Components

Sulfate, either as an impurity in ThO_2 itself or added as $Th(SO_4)_2$, was found to lower the pH of ThO_2 slurries in the presence of oxygen. This prevented excessive attack by the circulating slurries on type 347 stainless steel pumps, flow restrictors, and other components where high slurry velocities occur. A sulfate concentration of 3000 ppm appeared to be sufficient to lower the pH below 6.

Sulfate concentrations of about 10,000 ppm produced serious caking both in the loop proper and in the pressurizer of a 5-gpm circulating system.

Sulfate was found to be removed from ThO_2 by calcining at temperatures above about 800°C.

Inspection of parts of the piping from a system which had a total service of about 10,000 hr with $UO_3 \cdot H_2O$ slurries and water at 250°C and about 5000 hr with ThO_2 slurries at 250°C showed negligible attack, except in a few areas, and only a thin adherent film.

Agreement was obtained between earlier Brookfield viscometer results on pumped slurry and pipe-line pressure-drop data at room temperature. Some evidence of thixotropy was found.

Pressure-drop and heat-flow studies in an 18-in.-dia model of the blanket pressure vessel were completed with water at temperatures up to 100°C. It was found that the bulk of the blanket was at a uniform temperature below the outlet temperature and that a thin hot layer existed near the reactor vessel. Heat-transfer coefficients on the blanket side of the reactor vessel ranged from about 250 to 450 $Btu/hr \cdot ft^2 \cdot °F$, depending on the flow rate.

The blanket mockup was revised to remove the requirement that a side stream of the slurry be boiled.

An equation was derived to correlate data on the local void fraction in a vertical column of boiling liquid in terms of the size of the column, the properties of the liquid, the power input, and two system variables.

8. Metallurgy

Experimental welds involving several proposed design combinations have been evaluated to select a procedure for the final girth closure weld on the HRT pressure vessel, a carbon-steel sphere clad internally with type 347 stainless steel. The subcontractor has been authorized to proceed with weld-qualification tests on full-thickness clad material taken from the plates which are actually to be used in the pressure vessel, utilizing the following sequence of weld deposits: (1) type 347 weld metal in the root and groove up to a point about $\frac{1}{16}$ in. below the carbon steel–stainless steel interface, (2) two layers of type 308L stainless steel weld metal over the type 347 weld metal to a point approximately $\frac{1}{8}$ in. above the interface, (3) two layers of ingot-iron weld metal over the type 308L weld metal, and (4) type 7016 carbon-steel electrodes to completion of the weld.

A fully austenitic, modified, type 347 welding wire (composition H) containing added manganese has been used successfully in a number of weld tests following the Heliarc welding procedure of the HRP-2 specification. Experimental welds made on several tubular sections will be subjected to service testing in dynamic-corrosion test loops.

Efforts to establish an acceptable testing procedure for evaluating the stress-corrosion susceptibility of austenitic stainless steels in homogeneous reactor environments have resulted in the construction of equipment designed for direct loading of small-diameter wire specimens. This test procedure produces failure within a reasonable

period of time in an $MgCl_2$ environment known to produce stress-corrosion cracking; it will next be used for a study of the stress-cracking susceptibility in homogeneous reactor environments.

Evaluation of the influence of metallurgical factors on dynamic-corrosion behavior has included the study of variation of the ASTM grain sizes of standard austenitic stainless steels. Special alloys designed to produce essentially complete sigma-phase structures are also being studied. Equipment has been designed and constructed for the study of the effects of hydrogen on the properties of commercial zirconium, titanium, and their alloys and for the study of the role of oxide films on the rate of hydrogen absorption by these materials.

Impact tests on Zircaloy-2 specimens from the first in-pile corrosion loop run have been made, and the results have been compared with those for specimens exposed to similar environments out-of-pile, as well as those for unexposed control specimens. No significant changes in transition temperature resulted from the in-pile exposure; from this fact it is inferred that no embrittlement of the impact specimens took place.

The fabrication of the HRT Zircaloy-2 core vessel by the subcontractor is nearing completion. A description, along with illustrations of the fabrication procedures and specially developed equipment, is included in the body of the report.

Irradiation of impact specimens of carbon steel, similar to the material being used in the HRT pressure vessel, as well as a variety of other materials in which there is an interest, is being carried out in several tests at the MTR and LITR. For the most part the more significant irradiations are still in progress, but irradiation of one group of specimens in the HB-3 facility of the LITR has been completed and the impact testing is in progress. Specimens taken from the weld-qualification test plate, involving material identical with that being used in the HRT pressure vessel, will be available shortly, and a special effort will be made to accelerate the testing of these materials and to evaluate the results.

PART V. CHEMICAL ENGINEERING DEVELOPMENT

9. Slurry Fuel and Blanket Studies

The immediate objective of this program is the chemical development of a thorium dioxide slurry for use in the blanket of the HRT. This program includes the demonstration of slurry radiation stability and the acquisition of sufficient understanding of slurries to support the over-all effort and assure the success of the thorium blanket experiment. The work of this quarter was concentrated on the development of apparatus and techniques for laboratory-scale study and characterization of slurries, the irradiation of slurry samples in both the LITR and the ORNL Graphite Reactor, gas-recombination studies, and the preparation of fine-particle oxide.

A stainless steel bomb with a dash-pot stirrer designed for slurry irradiation in the LITR was successfully tested in the reactor. The bomb contained water and a gold wire to monitor the neutron flux. In an experiment in which an aqueous slurry of thorium oxide was irradiated for 115 hr in the LITR at 300°C, the stirrer ceased to operate some time after the first 24 hr of the run. Since this bomb has not yet been opened, it is not known whether the stirrer stopped because of changes in the slurry or because of mechanical failure.

In further irradiation studies in the ORNL Graphite Reactor, a thorium oxide slurry that contained 8% U^{235} and 1% copper as the mixed oxides was irradiated for ten days at 275 to 280°C. No gas pressure in excess of steam was observed, indicating that complete recombination of the radiolytic gas was occurring. Stirring became labored and ceased after 24 hr. The thorium-U^{235} mixed-oxide slurry (530 g of thorium, 40 g of U^{235}) irradiated previously was examined and found to be so viscous that a dilution with water was required before it could be poured from the bomb. Examination of a pure thorium dioxide slurry irradiated previously showed it to be apparently unaffected by the irradiation.

Gas-recombination studies were carried out with various pure thorium oxide preparations and thorium oxide slurries containing 0.001 to 0.09 *m* $CuSO_4$ plus 0.0025 *m* H_2SO_4. None of the pure thorium oxide slurries exhibited sufficient catalytic activity for reactor use. The catalytic activity of the slurries containing copper sulfate increased directly with copper sulfate concentration and temperature and inversely with the slurry concentration. The recombination rates obtained with thorium oxide slurries containing 0.09 *m* $CuSO_4$ plus 0.0025 *m* H_2SO_4 were more than sufficient to maintain the TBR blanket at

[redacted]

less than 2000 psi total pressure. The catalytic activity appeared to be associated mainly with the copper sulfate in solution.

10. Thermal Breeder Fuel Processing

Data obtained from loop A operation indicate that the solubility of neodymium sulfate is 0.02 to 0.03 g per kilogram of H_2O at 285°C in the fuel solution of a two-region thermal breeder reactor. This amount of neodymium in solution will contribute about 0.2% neutron poison to the reactor. In none of the three loop runs made with neodymium sulfate was a significant amount of insoluble neodymium found in the main circulating stream. Some of the neodymium sulfate precipitated on and adhered to hot metal surfaces in the loop. The remaining insoluble neodymium sulfate collected in stagnant and low-velocity regions of the loop.

Laboratory tests confirmed the tendency of rare-earth sulfates to precipitate on hot stainless steel and titanium surfaces. However, an insignificant amount of neodymium sulfate adhered to Zircaloy-2 surfaces which were in contact with solution containing neodymium sulfate at the same temperature during neodymium precipitation.

Studies with 0.25-in.-dia hydroclones for continuously removing suspended solids from the fuel indicated that such units will remove 1-μ particles with efficiencies of greater than 90%. The units were more efficient at higher feed pressures and with higher underflow ratios. The optimum length for a 0.25-in.-dia cone was determined to be about 1.5 in. The sizes of the feed inlet and overflow port areas did not appear to affect the efficiency over a reasonable range.

The current HRT fuel-processing flow sheet recommends the removal of suspended solids in a single stage of hydroclones and the drying and re-solution of the solids in the shipping container. The processing plant will be operated in conjunction with the reactor to demonstrate the feasibility of continuous fuel processing. Startup of the chemical processing plant is scheduled for April 1, 1956.

11. Plutonium-Producer Blanket Processing

In a series of experiments designed to study the adsorption of plutonium on materials of construction, a type 347 stainless steel container adsorbed 0.80 mg/cm^2 and two titanium vessels adsorbed about 1.0 mg/cm^2, with no indication that equilibrium had been reached. Plutonium adsorption on zirconium reached an equilibrium value of 0.05 mg/cm^2.

Precipitation of plutonium dioxide under simulated reactor conditions was rapid enough that the supersaturation in the plutonium-producer blanket is not expected to be greater than 0.3 mg of plutonium per kilogram of D_2O. When Pu(VI) was added to uranyl sulfate solution under simulated reactor conditions, more than 90% was reduced to Pu(IV) in 5 min.

12. Thermal-Breeder Blanket Processing

Complete dissolution of thorium dioxide can be accomplished in a reasonable time by refluxing in 30% excess 8 *N* HNO_3 containing 0.04 *N* HF. Attempts to use less acid resulted in incomplete dissolution.

13. Summary of Work of Vitro Laboratory

Approximately 99% of the iodine was removed from a simulated fuel solution by contacting the vapor above the solution with metallic silver. The capacity of zirconium phosphate cation exchanger for cesium at room temperature was shown to be 67 mg of cesium per gram of adsorber. Tests showed that uranium salts used to make up simulated fuel solutions for studying adsorption of tagged elements should be freshly extracted to eliminate interfering beta counts from UX_1 and UX_2.

PART VI. SUPPORTING CHEMICAL RESEARCH

14. Radiation Decomposition of Thorium Nitrate Solutions

Yields of hydrogen and nitrogen from the gamma-ray decomposition of thorium nitrate solutions have been determined and are compared with yields for decomposition by reactor radiations and fission fragments. The effects on the gas yields of total dose, ullage, and the initial presence of H_2, O_2, air, and N_2 are also discussed.

15. Inorganic Chemistry

Exploratory investigations of the adsorptive properties of inorganic materials in aqueous media have shown that a commercial zirconium oxide, pure zirconium phosphate, and pure ZrO_2 treated with phosphoric acid adsorb europium ion reversibly from HCl solutions. The sharpness of

[redacted]

the adsorption-elution curves resembles that of curves obtained with conventional ion exchangers. Pure ZrO_2 shows no significant adsorption. The capacity of the best adsorber, zirconium phosphate, is about 10% of that of commercial ion exchangers.

The dispersion of aqueous suspensions of finely divided oxide powders in the presence of various additives (e.g., dilute H_2SO_4) can conveniently be studied by making an adsorption column from a mixture of the oxide and 200-mesh glass beads, and observing the cloudiness or clearness of the effluent after solutions of the additives have been poured through the column.

16. Phase Studies of Aqueous Systems at Elevated Temperatures

The phase diagram for the system UO_2CrO_4-H_2O has been completed and will appear as a separate report. Studies of the system ThO_2-CrO_3-H_2O at elevated temperatures indicate that between 100 and 250°C too high a ratio CrO_3/ThO_2 is required for the solutions to be attractive as breeder blankets.

17. Homogeneous Reactor Analytical Development

Construction of a High-Radiation Level Analytical Facility is proceeding according to schedule. The contractor's work will be completed by April 1, 1955, and the laboratory will be equipped and ready for operation before July 1, 1955. This facility will serve the needs of the HRP development work and the HRT operation.

Progress in the development of the following analytical methods is reported:

1. ion-exchange separation of aluminum from homogeneous reactor solutions,
2. spectrophotometric determination of nickel in the presence of uranyl sulfate,
3. amperometric titration of halides in uranyl sulfate solutions,
4. determination of dissolved oxygen in uranyl sulfate solutions,
5. estimation of soluble impurities in thorium oxide,
6. determination of aluminum in the presence of thorium,
7. separation of zirconium from thorium solutions,
8. determination of titanium in thorium solutions,
9. determination of palladium in the presence of thorium oxide,
10. determination of sulfate in thorium oxide.

18. Concentration of Nitrogen-15

Laboratory studies of the Carbonate system (ammonia gas vs ammonium carbonate solution) have established the temperature dependence of the isotopic separation factor in the range 15.6 to 44.3°C. High-temperature column studies support this data and indicate an optimum operation temperature of approximately 30°C for the system.

An initial survey of a new system for nitrogen enrichment, proposed by T. I. Taylor and W. Spindel of Columbia University, has been made. This system (the Nitrox system) employs the exchange between gaseous NO and aqueous HNO_3 to produce isotopic separation.

Cost estimates based upon very optimistic criteria indicate that N^{15} can be produced with the Nitrox system for about 48% of the cost with the Carbonate system.

[redacted]

CONTENTS

SUMMARY vii

PART I. EXPERIMENTAL REACTORS

1. HOMOGENEOUS REACTOR TEST 3
   1.1 Project Status 3
      1.1.1 Reactor hazards report 3
      1.1.2 Status of construction 4
      1.1.3 Procurement 4
      1.1.4 Thermal shield for HRT 5
      1.1.5 Possible blast effects from rupture of HRT vessel 5
      1.1.6 Pressure rise in HRT equipment cell from reactor failure 6
      1.1.7 Peroxide precipitation in HRT fuel lines 6
   1.2 Design 7
      1.2.1 General design status 7
      1.2.2 Reactor vessel and core tank 7
      1.2.3 Auxiliary components 11
   1.3 Nuclear Calculations 13
      1.3.1 Safety considerations 13
      1.3.2 The HRT and the "walk-away" phenomenon 23
   1.4 Component Development 26
      1.4.1 Pump development 26
      1.4.2 Fuel and blanket pumps 30
      1.4.3 High-pressure feed pumps 31
      1.4.4 Heat exchanger 31
      1.4.5 HRT gas separator titanium sleeve 33
      1.4.6 Fluid flow in HRT pressurizer 33
      1.4.7 HRT dump test 33
      1.4.8 HRT mockup loop 33
   1.5 Controls and Instruments 36
      1.5.1 General design 36
      1.5.2 Component development and testing 36
      1.5.3 Valve development 37

PART II. THORIUM BREEDER REACTOR

2. CONCEPTUAL DESIGN 41
   2.1 Reactor Analysis 41
      2.1.1 Effect of major process variables 41
      2.1.2 Effect of changes in the nuclear constants 41
   2.2 Engineering Studies 44
      2.2.1 Immediate program 44
      2.2.2 Turbine plant study 44
      2.2.3 TBR plant optimization 46
      2.2.4 Equipment design considerations 51

PART III. CORROSION

3. PUMP-LOOP CORROSION TESTS 55
   3.1 Pump-Loop Operation and Maintenance 55
      3.1.1 Loop status 55

[redacted]

[redacted]

3.1.2 Heat-exchanger test 56
3.2 Results of Loop Tests 56
3.2.1 Introduction 56
3.2.2 Results 56
3.3 Sedimentation Rates of Thorium Oxide Slurries at Elevated Temperatures 83

4. RADIATION CORROSION 86

4.1 In-Pile Loop 86
4.1.1 Development and construction 86
4.1.2 LITR operations – in-pile loop corrosion test DD 88
4.1.3 Remote dismantling and inspection 99
4.1.4 Correlation of corrosion data 103
4.2 Bomb Tests 107
4.2.1 LITR operations 107
4.2.2 MTR in-pile experiment 115

5. LABORATORY CORROSION STUDIES 120

5.1 Corrosion of Precipitation-Hardening Stainless Steels by Simulated Reactor Environments 120
5.2 HRT Pool Water Corrosion Studies 121
5.3 Evaporator Test 123
5.4 Boiling Nitric Acid Specification Tests on HRT Stainless Steels 123
5.5 Development of Twin Strip Specimens for the Evaluation of Stress-Corrosion Cracking 123
5.6 Toroid Dynamic-Slurry Studies 126
5.6.1 Engineering 126
5.6.2 Test results 128

PART IV. ENGINEERING DEVELOPMENT

6. DEVELOPMENT OF FUEL-SYSTEM COMPONENTS 135

6.1 Recombiner Development 135
6.1.1 High-pressure recombiner loop 135
6.1.2 Thermal convection type of catalytic recombiner 135
6.2 Dump-Valve Test Loop 136
6.3 Low-Pressure Entrainment Separator Tests 136
6.4 5000-gpm Gas Separator 136
6.5 Small Reactor Components 137
6.5.1 500-gpm pump and 20-cfm gas circulators 137
6.5.2 ORNL 5-gpm pump 137
6.6 Development of Large Heat Exchanger 137
6.7 4000-gpm Loop 137
6.8 Slurry-Injection Pump Loop 139

7. DEVELOPMENT OF BLANKET-SYSTEM COMPONENTS 141

7.1 Slurry Engineering and Component Development 141
7.1.1 Slurry-circulation studies 141
7.1.2 Thermal decomposition of thorium sulfate 146
7.1.3 Pressure drop in slurry systems 146
7.1.4 Slurry component development 149
7.2 HRT Blanket Mockup 150
7.3 Boiling Studies 152

[redacted]

[redacted]

7.3.1 Vapor transport 152
7.3.2 Transient behavior 152

8. METALLURGY 153

8.1 Welding Development 153
8.1.1 Welding of 1-in. carbon-steel plates clad with type 347 stainless steel 153
8.1.2 Welding of type 347 stainless steel with fully austenitic filler metal 154
8.2 Physical Metallurgy of Corrosion 155
8.2.1 Stress-corrosion cracking of austenitic stainless steels 155
8.2.2 Dynamic corrosion of austenitic-stainless-steel weld specimens 157
8.2.3 Dynamic corrosion study of factors associated with grain size in wrought austenitic stainless steels 157
8.2.4 Effect of hydrogen on properties of zirconium and its alloys 158
8.2.5 Role of oxide films on rate of hydrogen absorption by zirconium and its alloys 158
8.3 Mechanical Testing of Titanium and Zirconium 159
8.3.1 Commercial titanium 159
8.3.2 Zirconium alloys (Zircaloy-2) 159
8.4 Metallurgical Engineering Service 160
8.4.1 Fabrication of HRT Zircaloy-2 core vessel 160
8.5 Effects of Radiation on Structural Metals and Alloys 162

PART V. CHEMICAL ENGINEERING DEVELOPMENT

9. SLURRY FUEL AND BLANKET STUDIES 173

9.1 Thorium Dioxide Slurry Irradiation Studies 173
9.1.1 Slurry irradiations in the LITR 173
9.1.2 Slurry irradiations in the ORNL Graphite Reactor 173
9.1.3 Development of facilities for slurry irradiation studies 174
9.2 Gas Recombination Studies 174
9.3 Laboratory Evaluation of Thorium Dioxide Slurries 177
9.3.1 Preparation of fine-particle oxide 178

10. THERMAL BREEDER FUEL PROCESSING 179

10.1 Rare-Earth Chemistry 179
10.1.1 Neodymium solubility 179
10.1.2 Rare-earth sulfate precipitation behavior in loop A 179
10.1.3 Rare-earth precipitation behavior in laboratory tests 183
10.2 Hydroclone Development 184
10.2.1 The 0.5-in.-dia hydroclone 185
10.2.2 The 0.25-in.-dia hydroclones 186
10.2.3 Effect of particle size on efficiency 188
10.3 HRT Chemical Plant 188
10.3.1 Off-gas disposal 190
10.3.2 Hazards 190
10.3.3 Schedule 191
10.4 Equipment Development 191

11. PLUTONIUM-PRODUCER BLANKET PROCESSING 192

11.1 Adsorption of Plutonium on Stainless Steel, Titanium, and Zirconium 192
11.2 Precipitation Rate of Plutonium Dioxide 192

[redacted]

[redacted]

11.3 Estimate of Pu^{240} Content of Product 194
11.4 Neptunium Chemistry 195

12. THERMAL-BREEDER BLANKET PROCESSING 196

12.1 Dissolution of Thorium Dioxide 196
12.2 Leaching of Thorium Dioxide 196

13. SUMMARY OF WORK OF VITRO LABORATORY 198

PART VI. SUPPORTING CHEMICAL RESEARCH

14. RADIATION DECOMPOSITION OF THORIUM NITRATE SOLUTIONS 201

14.1 Gamma-Ray Decomposition 201
14.2 Yield-vs-Dose Studies in Reactor-Irradiated Solutions 201
14.3 Effect of Ullage 202
14.4 Effect of Added Gases 202

15. INORGANIC CHEMISTRY 203

15.1 Adsorption of Rare Earths on Inorganic Materials 203
15.2 Peptization of Oxide Powders 204

16. PHASE STUDIES OF AQUEOUS SYSTEMS AT ELEVATED TEMPERATURES 205

16.1 The System Uranyl Chromate–Water 205
16.2 Preliminary Observations of the System ThO_2-CrO_3-H_2O 205
16.2.1 Experimental 205
16.2.2 Results 206

17. HOMOGENEOUS REACTOR ANALYTICAL DEVELOPMENT 207

17.1 High-Radiation-Level Analytical Facility 207
17.2 Ion-Exchange Separation of Aluminum from HRT Fuel 207
17.3 Spectrophotometric Determination of Nickel in the Presence of Sulfate 207
17.4 Amperometric Titration of Halides 207
17.5 Determination of Dissolved Oxygen in Uranyl Sulfate Solution 208
17.6 Analysis for Impurities in Thorium Oxide 208
17.7 Aluminum in Thorium Oxide 208
17.8 Zirconium in Thorium 208
17.9 Titanium in Thorium 208
17.10 Palladium in Thorium Oxide 208
17.11 Sulfate in Thorium Oxide 208

18. CONCENTRATION OF NITROGEN-15 209

18.1 Laboratory Studies of the Carbonate System 209
18.2 The Nitrox System 210
18.3 Economic Comparisons of the Carbonate and the Nitrox Systems 211

[redacted]

Part I

EXPERIMENTAL REACTORS

S. E. Beall

1. HOMOGENEOUS REACTOR TEST

1.1 PROJECT STATUS

S. E. Beall
J. J. Hairston, Jr. S. Visner
J. W. Hill, Jr. P. M. Wood
S. I. Kaplan

1.1.1 Reactor Hazards Report

A hazards report[1] was prepared for the Advisory Committee on Reactor Safeguards concerning the possibility of radioactive material escaping from the HRT and from its gas-tight enclosure. A summary of the safety philosophy and evaluation is repeated here.

This study indicated that the likelihood of escape is sufficiently small that the hazards to operating personnel and to the public compare favorably with normally accepted risks. The HRT, like its predecessor the HRE, is fueled with an aqueous solution of UO_2SO_4 which is circulated at high temperature and pressure but will operate at a maximum power of 10 Mw. Novel features include the complete reliance for safety on its large negative temperature coefficient, 2×10^{-3} $k_{eff}/^{\circ}C$, instead of on safety rods, the location of the reactor in a pit to facilitate underwater maintenance, and the gas-tight construction of the shield for the purpose of containing a major release.

The HRT is an experimental facility in the sense that several homogeneous reactor concepts will be tested. At the present time, three experiments are planned with three different blankets: a pure D_2O blanket to demonstrate long-term reliable operation and practical maintenance, a slurry of ThO_2-D_2O at high concentration to demonstrate the breeding of U^{233}, and a low enrichment but high concentration UO_2SO_4 solution in the blanket to demonstrate the production and separation of Pu^{239}.

The safety of the HRT was considered with reference to the equipment design and layout for the first experiment with the D_2O blanket. However, it now appears that only minor revisions in equipment will be required for the other experiments. Furthermore, the analysis of reactivity rates and power excursions was extended to cover a range of nuclear constants – critical fuel concentration, temperature coefficient of reactivity, and prompt neutron generation time – which apply to the reactor experiments with all three blankets. At this time, there does not appear to be any significant hazard associated with the HRT experiments now planned.

A major hazard would stem from the release of the fission products accumulated in the reactor. The hazard from the U^{233} and Pu^{239} which will be present in different experiments is relatively small. Activity could conceivably be released from the reactor vessels as a result of mechanical failure, corrosion, explosion of D_2 and O_2, or sudden reactivity increases. However, it was shown that the mechanical design is very conservative, that corrosion rates are low for normal operating conditions, and that explosions are unlikely to cause damage. Accidents were studied which would result in large rates of reactivity addition; none of the rates was large enough to cause rupture of the equipment walls which would release activity into the gas-tight shield. To reach the yield point of the pressure vessel – which is about one-half the ultimate strength – a reactivity step of 3.1% is required.[2] This step is equivalent to a reactivity rate of 2.5% when the initial neutron level is determined solely by the Po-Be source of 10^7 neutrons/sec, or a rate of 3.5% per second with the delayed neutrons and photo-gamma neutrons which are present one day after a shutdown from 5 Mw. The Zircaloy-2 inner tank might be endangered at a reactivity rate in excess of 0.85% per second. Although rates of reactivity addition are normally limited to 0.008% per second, very abnormal situations were examined also. For example, a major steam-line rupture could give a rate as high as 1.7% per second. However, the only accident which could conceivably cause a rupture of the outer pressure vessel and release the activity is one in which the entire fuel inventory in the high-pressure system is suddenly accumulated inside the reactor core as a result of separation of the fuel solution into two phases, one of which contains most of the uranium. Since the fuel temperature will always be below that for two-phase separation, this

[1] S. E. Beall and S. Visner, *HRT Summary Report for the Advisory Committee on Reactor Safeguards*, ORNL-1834 (Jan. 5, 1955).

[2] P. R. Kasten, *HRT Safety Considerations*, ORNL CF-54-9-226 (Sept. 30, 1954).

accident was shown to be highly unlikely; furthermore, the gas-tight liner of the shield would not be ruptured, even if such an accident did occur.

The gas-tight reactor shield with an all-welded steel liner serves as a second barrier to the escape of the radioactive material. The pit will normally be kept at the subatmospheric pressure of 7.5 psia to prevent leakage of activity to the building and also to limit the pressure rise from the release of high-temperature solution. The shield can withstand an internal pressure of 30 psig. This is greater than the peak static pressure which would result from the escape of hot solutions after a failure in the high-pressure reactor system, for example, simultaneous brittle failure of the reactor vessel and ruptures in the piping from the steam generators.[3]

The only imaginable accident which could result in breakage of reactor components as well as the gas-tight pit enclosure was the "brittle failure" of the pressure vessel.[4] So-called "brittle failure" would be a consequence of embrittlement of the pressure-vessel steel by fast-neutron bombardment. However, protection against the dynamic effects of pressure-vessel failure will be provided by a 1½- or 2-in.-thick spherical steel blast shield just outside the pressure-vessel walls.

Although every possible protection has been designed into the reactor and its shielded enclosure to prevent the escape of activity, the consequences of a major release from the enclosure were considered in detail. The hazard from contamination of the surface waters is identical to that reported for the hazards evaluation of the Oak Ridge Research Reactor. Under the most pessimistic conditions, a condition of over-tolerance in the drinking-water supply might exist as far downstream as Kingston (20.8 river miles).

A major release of the reactor contents to the atmosphere would take the form of a hot cloud because of the stored heat in the reactor solution. The chief hazard from exposure to the cloud would arise from the inhalation of the fission products. If 50% of the material in the reactor were released at night, the emergency maximum permissible exposure (MPE) based on 25 rep would be exceeded, at most, by a factor of 5. The exposure would actually be less than the MPE for distances up to 8.3 miles and also beyond 90 miles from the reactor site. By day, the exposure would never be above the emergency MPE. In the event of rain-out of the material in the cloud, the external total body radiation would exceed 25 rep/hr if the rain-out occurred at a distance less than 20 miles during the day and 120 miles at night.

1.1.2 Status of Construction

J. J. Hairston, Jr.

The construction contractor released to ORNL the control-room area of the reactor installation, and finishing work in preparation for placing conduit, lighting, and circuit breakers was begun. On January 30, the steel-lined reactor cell was filled with water and tested for leaks. Several small leaks were found at joints which had been prefabricated in the contractor's shop. Approximately two weeks will be required for repair and finishing before the cell is accepted by ORNL.

1.1.3 Procurement

S. I. Kaplan

Major purchasing for the reactor proper, exclusive of the steam system, is nearly complete. Except for one order of heavy-wall pipe fittings, a partial shipment of 1½-in. pipe, and part of the large-diameter welded pipe, all orders for construction raw materials placed prior to this quarter have been received. Delivery of the auxiliary steam-system components, including the high-pressure boiler, steam-killer, and feedwater pumps, is expected during the next quarter.

The following materials and equipment were requisitioned during the quarter:

Pipe, fittings, weld rod, etc.	$ 9,400 (approx)
Recombiner condensers	6,300
Power-system components	900 (approx)
	$16,600 (approx)

Construction of the following reactor items in the area shops is now proceeding: feed pumps, gas separators, dump-tank evaporators and vapor headers, cold traps, entrainment separators, flanges and gaskets for leak detection, and condensate tanks.

[3] P. M. Wood, *A Further Study of Pressure Rise in HRT Shield*, ORNL CF-55-1-3 (Jan. 3, 1955).

[4] P. M. Wood, *A Study of Possible Blast Effects from HRT Pressure Vessel Rupture*, ORNL CF-54-12-100 (Dec. 14, 1954).

A significant effort is being expended in "certifying" materials of construction to prevent the use of materials other than those specified.

All metallic construction materials are marked, in addition to the manufacturer's markings, with HRP identification after delivery. Small parts are being marked to denote the component to which they belong. Records of chemical composition and mechanical properties are being maintained for all critical material, and samples of all materials are preserved for possible future study.

1.1.4 Thermal Shield for HRT

P. M. Wood

The design requirements for the thermal shield surrounding the reactor vessel were investigated. The purposes of the thermal shield are to provide part of the biological shielding for personnel, to reduce the neutron and gamma fluxes in the equipment cell and hence reduce radiation damage to materials of construction in the cell, and to absorb most of the neutrons and gamma rays from the reactor in a location where the heat generated can be conveniently removed.

An operating power level of 10 Mw of core power with a natural uranyl sulfate blanket containing 355 g of uranium per kilogram of D_2O was chosen as a design basis.

The thermal shield was specified as a cylindrical 2-ft layer of concrete around the reactor, extending from the floor to the top surface of the pressure vessel, with a flat tray extending across the top of the reactor and containing a 1-ft thickness of steel punchings and water. With this shielding arrangement, the radiation dose rate above the 5-ft-thick barytes concrete roof plugs is expected to be 12 mrem/hr. The fast-neutron flux in the cell, outside the thermal shield, will be 7×10^9 neutrons/cm^2/sec, and the thermal flux will be 4×10^7 neutrons/cm^2/sec. The gamma-ray intensity will be 5×10^4 to 1×10^5 r/hr. The heat generation in the thermal shield will be 177 kw.

1.1.5 Possible Blast Effects from Rupture of HRT Pressure Vessel

P. M. Wood

Aqueous reactors containing large amounts of water (light or heavy) at high temperature and pressure constitute a severe blast hazard. In addition to the blast effects that might result from a sudden failure of the reactor vessel, there would be a release of millions of curies of radioactive fission products which would escape through any holes in the shield structure opened by the blast. Since the fast-neutron irradiation may have an embrittling effect on mild steel, it was suggested by E. C. Miller[5] that, when the safety features of the HRT are being designed, a brittle-explosive-failure of the pressure vessel be assumed as a distinct possibility.

The study[6] of the blast effects to be expected was approached by three methods: a comparison with the damage to be expected from the detonation of high explosives with equivalent energy release, a study of the dynamics of a steam expansion, and a review of the literature on boiler explosions.

The conclusion reached in all three approaches was that, although an unrestrained expansion of the high-temperature water in the HRT would probably do no serious damage, sufficient momentum could be imparted to the parts of the pressure vessel and thermal shield to demolish the cell structure.

Fragments of the pressure vessel could be expected to achieve velocities of 100 fps. A missile of 1400 lb or approximately one-twelfth of the pressure vessel traveling at this velocity would destroy the gas-tight structure of the top shield.

In order to prevent this severe damage to the reactor structure in the event of a pressure-vessel failure, a spherical steel blast shield 1.5 in. thick will be installed just outside the pressure vessel. The blast shield will have sufficient strength to contain the static pressure and to absorb the impact from the expanding reactor if the pressure vessel should fail. The blast shield may be constructed of austenitic stainless steel, which does not suffer radiation embrittlement.

The considerations of blast damage apply equally well to the heat exchangers, although there is little danger of embrittlement by radiation. Since each shell contains 2000 lb of water and weighs 13,000 lb, it will be enclosed in steel mesh blast nets.

---

[5] E. C. Miller, *Possibility of Brittle Pressure Vessel Failure*, ORNL CF-54-4-112 (April 16, 1954).

[6] P. M. Wood, *A Study of Possible Blast Effects from HRT Pressure Vessel Rupture*, ORNL CF-54-12-100 (Dec. 14, 1954).

1.1.6 Pressure Rise in HRT Equipment Cell from Reactor Failure

P. M. Wood

A study of the pressures to be expected in the HRT equipment cell in the event of a failure of the reactor vessel was made and reported.[7] This study was extended[8] to include the effect that the release of the contents of the heat exchangers, steam lines, and steam drums would have if the reactor ruptured.

To obtain an upper limit for the pressure rise that might be expected, the instantaneous release of the reactor fluids with no heat transfer to the cell walls was considered. The expansion of the fluid into the equipment cell was assumed to be adiabatic at constant internal energy, with perfect mixing of the steam and air in the cell. If the contents of the reactor at 300°C initial temperature were released, the cell pressure would be 20.8 psig. If the contents of the reactor and fuel heat exchanger, at 300°C, and the contents of the steam drum and steam piping, at their normal operating temperature of 244°C, were released simultaneously, the cell pressure would be 32.1 psig.

If the fuel heat exchanger were released through a broken pipe into the cell, there would be time for significant heat transfer to the cell walls. On the assumption that the reactor at 300°C would be released instantly and that the fuel heat exchanger at 300°C would be released through the 6-in. steam line, a maximum pressure of 22 psig would be attained in the cell. If the blanket heat exchanger were released through its steam line at the same time, a maximum cell pressure of 29 psig would be reached. Since the reactor and both heat exchangers are to be protected by blast shields designed to stop fragments, it is extremely unlikely that simultaneous failures will occur.

1.1.7 Peroxide Precipitation in HRT Fuel Lines

P. M. Wood

In the present HRT design, cooling jackets are specified for the dump and sampler lines. There is a danger that uranium peroxide may be precipitated in these lines if the highly radioactive fuel is cooled below 70°C within a few minutes after leaving the main circulating loop. Calculations were made to determine, as a function of temperature, the beta and gamma power densities which would cause peroxide to precipitate and also the power densities to be expected from the absorption of beta particles in the HRT fuel.

The chemistry of peroxide decomposition in uranyl sulfate solutions has been discussed, and a procedure for calculating permissible power densities has been reported.[9] The solubility of uranium peroxide was taken as 0.0039 *M*. The following value of *G* was used:[10] 0.40 molecule of D_2O_2 produced per 100 ev of beta or gamma radiation absorbed in a uranyl sulfate solution containing 10 g of uranium per kilogram of D_2O. Since the dump and sampler lines are small, it was assumed that all the gamma particles escape from the solution and that all the beta energy is absorbed.

It is evident from Fig. 1.1 that the HRT fuel solution cannot immediately be cooled below 70°C

[7] P. S. Pasqua, *Pressures in the HRT Shield Resulting from Rupture of Reactor*, ORNL CF-54-9-30 (Sept. 3, 1954).

[8] P. M. Wood, *A Further Study of Pressure Rise in HRT Shield*, ORNL CF-55-1-3 (Jan. 3, 1955).

[9] M. D. Silverman, G. M. Watson, and H. F. McDuffie, Reactor Sci. Technol. 3, No. 3, 43 (1953) (TID-2010).

[10] C. J. Hochanadel *et al.*, Reactor Sci. Technol. 3, No. 1, 32 (1953) (TID-2008).

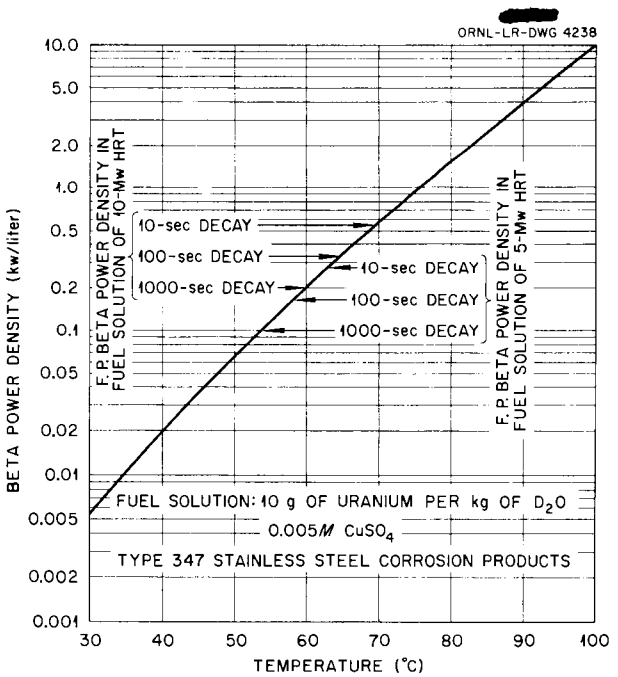

Fig. 1.1. Beta Power Density Which Will Cause Peroxide Precipitation in HRT Fuel Solution.

after removal from the main circulating loop without peroxide precipitation occurring if the operating power level is 10 Mw. During sampling, it will be necessary to maintain the isolation chamber temperature at approximately 80°C for 15 to 30 min after a sample is isolated. In order to prevent formation of uranium peroxide in the dump line, it may be necessary to apply a few pounds of steam pressure to the jacket on the line.

The peroxide buildup in the fuel flowing in the pulsafeeder feed pump line was also considered. If the fuel leaving the dump tanks is cooled to 50°C, 11 min would be required for the peroxide concentration to exceed the solubility. As the transit time from the dump tanks to the high-pressure loop is only 1 min, no peroxide should precipitate in this line.

1.2 DESIGN

R. B. Briggs

R. E. Aven	J. N. Robinson
R. H. Chapman	W. Robinson
H. N. Culver[11]	W. Terry
W. R. Gall	T. H. Thomas
J. E. Kuster[12]	R. VanWinkle
R. G. Pitkin[13]	F. C. Zapp

1.2.1 General Design Status

During the quarter ending January 31, 1955, design work was continued on equipment and piping layouts and details for the HRT. It is estimated that approximately 80% of the required design effort has been expended. Drawings for the reactor and auxiliary facilities are 50% complete, and those for the reactor cell and building are 95% complete. Process and instrument flow sheets are being combined, and final versions are being prepared for the reactor high-pressure and low-pressure core and blanket systems, the steam system, and the process water and emergency cooling system. Flow sheets are being developed for the waste disposal system and for services such as refrigeration, compressed air, etc. The most important flow sheets and equipment layouts have been presented in preliminary form in previous reports.[14–16] They will be included in future reports when revisions have been completed.

Designs for the HRT reactor vessel and core tank were approved for construction. Construction drawings were released for several more equipment items, leaving the pressurizers, several small heat exchangers, and the reactor vessel cooling system as the important equipment to be designed or approved.

1.2.2 Reactor Vessel and Core Tank

The designs for the reactor pressure vessel and core tank were completed by the Newport News Shipbuilding & Dry Dock Co. and have been approved for construction. An assembly of the vessels is shown in Fig. 1.2. While the design is basically the same as that described in a previous progress report,[16] changes were made in the diffuser for the core tank and in flange designs and nozzle attachments.

The core tank is a Zircaloy-2 spherical shell 32 in. in diameter and $\frac{5}{16}$ in. thick. The inlet nozzle to the sphere is a diffuser consisting of a 30-deg cone attached to a 90-deg cone which, in turn, is attached to the sphere. Nine perforated plates, each $\frac{1}{8}$ in. thick and having 55 to 60% free area, were installed in the diffuser by welding to the $\frac{3}{8}$-in.-thick wall. This design of the diffuser was found experimentally to be effective in obtaining a uniform expansion of a flow of 400 gpm of influent into the core.

The pressure vessel is a 60-in.-ID sphere to be made by welding together two hemispheres having 4-in.-thick carbon steel walls clad with 0.4 in. of stainless steel. Steel plate from which the hemispheres were formed is ASTM A212-52aT, Grade B, firebox quality steel manufactured in accordance with the ASTM A300-52T specification to obtain a low transition temperature as measured by impact tests. This treatment is expected to decrease the danger that fast-neutron damage might cause the steel to become brittle in the range of operating temperatures.

Special flanges were provided where the core inlet and outlet piping are connected to the pressure vessel. They were designed for operation at 2500 psi and 600°F; an allowable stress of

[11] On loan from TVA.

[12] On loan from Maxon Construction Co.

[13] On loan from Vitro Corp.

[14] R. B. Briggs *et al.*, *HRP Quar. Prog. Rep. Oct. 31, 1954*, ORNL-1813, p 6.

[15] R. B. Briggs *et al.*, *HRP Quar. Prog. Rep. July 31, 1954*, ORNL-1772, p 14.

[16] R. B. Briggs *et al.*, *HRP Quar. Prog. Rep. April 30, 1954*, ORNL-1753, p 22.

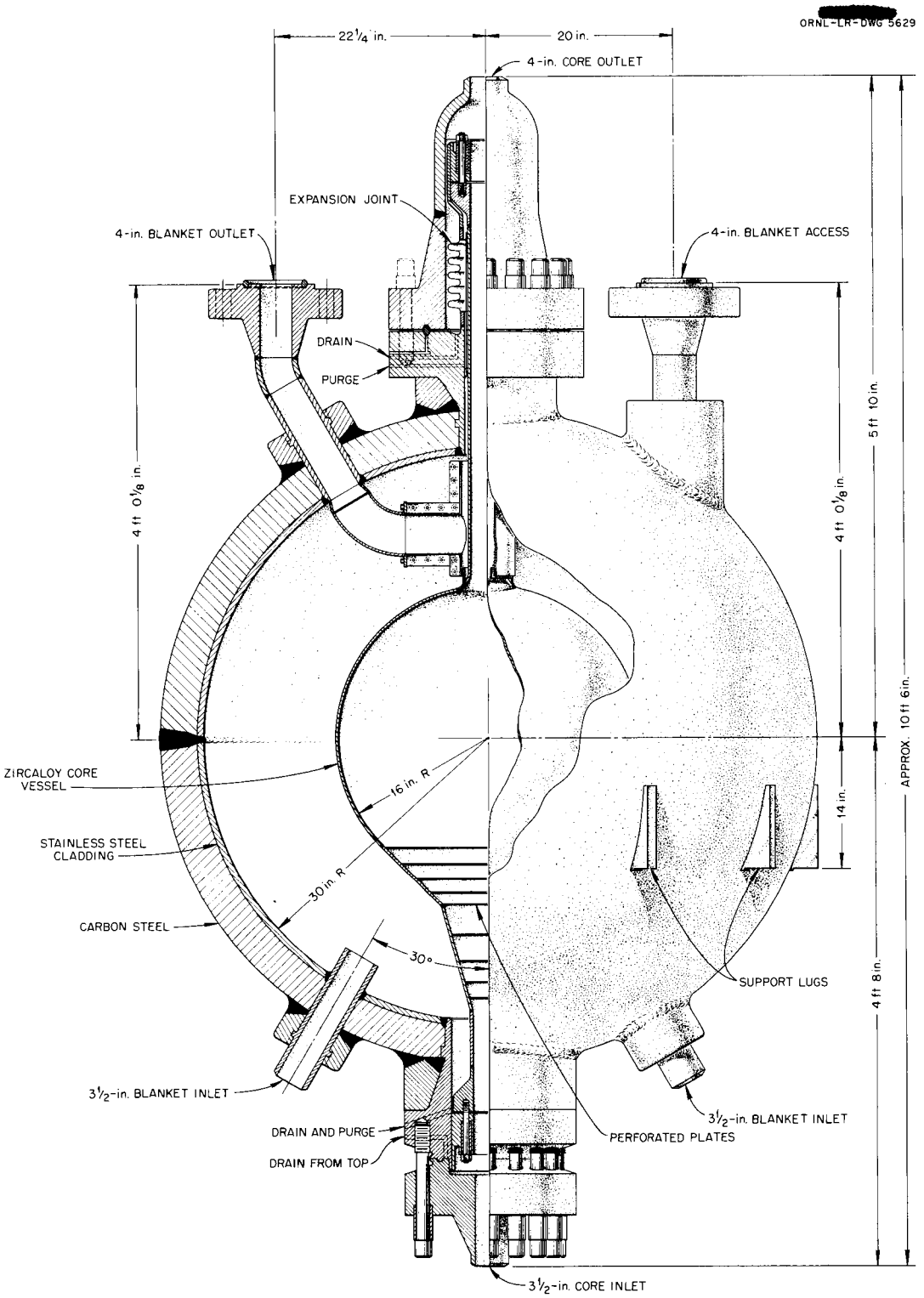

Fig. 1.2. HRT Pressure-Vessel Assembly.

11,200 psi [redacted] stress allowed for stainless steel flanges by the ASME Code for Unfired Pressure Vessels – was used. The connections permit access to the bellows expansion joint and to the Zircaloy-2–stainless steel connections before the system becomes highly radioactive. At the bottom of the vessel the flange will be seal-welded before the reactor is operated at power; consequently, the inlet piping cannot thereafter be replaced. A ring joint flange at the top will permit the piping to the gas separator and the pressurizer to be changed after the reactor has operated at power.

A prototype of the bellows was tested through 2500 cycles under representative temperature and pressure conditions with no evidence of failure. Another prototype will be cycled to failure in a later test.

A prototype of the zirconium-to-stainless-steel joint at top and bottom of the vessels was tested by thermal cycling between 200 and 572°F for 1000 cycles. The only gasket which remained leaktight after this test was a solid ring of Zircaloy-2, ¼ in. thick by ¼ in. wide. However, in order to make this gasket tight, bolt stresses between 60,000 and 90,000 psi were required. The bolts used were of 17-4 PH steel and had a yield strength of 160,000 psi (0.2% offset). Since these bolts will be exposed to fuel solution, it is desirable to reduce the stress to lower values to guard against stress corrosion effects. Stress corrosion tests are being conducted; alternate gaskets and bolting materials will be tested, and acceptable ones will be used if the 17-4 PH material proves to be unsatisfactory.

Nozzles through which the blanket fluid enters at the bottom and leaves at the top are to be attached to the vessel by a single weld at the inside surface of the vessel wall. Near the outer surface a bayonet-type mechanical attachment will be provided as a safety precaution to prevent the nozzle from becoming a projectile in event of failure of the weld. A prototype of this design was tested by thermal cycling the nozzle wall between 200 and 500°F, with the carbon steel portion of the wall maintained constant at 300°F. The joint was cycled 2000 times without damage.

Both bottom nozzles will contain special inserts which were designed so that fluid will sweep across the bottom of the tank to prevent ThO_2 from accumulating there when a slurry blanket is used. Fluid will leave through a single outlet at the top, which was designed to promote circulation and to prevent accumulation of slurry around the top of the core tank. The other top nozzle will be straight and vertical for use either as a spare connection or as an access hole for insertion of instruments or probes into the blanket space.

Stress analyses for the core and pressure vessels were essentially completed but have not been reported in detail. The major problem of the core tank is that of estimating the positive and negative pressure differences between core and blanket which will cause the vessel to split or to collapse. Values were calculated for the Zircaloy-2 tank, and experimental data were obtained for aluminum vessels in a full-scale mockup. It is now estimated that a core pressure 800 psi greater than the blanket pressure will be required to burst the core tank. A blanket pressure 400 psi greater than the core pressure will be required to collapse the tank.

Both pressure stresses and thermal stresses are considered to be important in the pressure vessel. Heat production data and a preliminary stress analysis have been reported.[16] The analysis of stresses in the carbon steel was extended to take into account the effects of the stainless cladding in reducing the heat production in the carbon steel by acting as a thermal shield and in effectively increasing the pressure acting against the carbon steel by virture of the greater coefficient of expansion of stainless steel. Calculations were made that include the range of material thicknesses obtained in the hemispheres which will form the vessel. One head varies in thickness from 3.6 to 4.7 in. of carbon steel with 0.5 in. of cladding, while the other varies from 3.7 to 4.9 in. of carbon steel with 0.5 in. of cladding.

Stresses calculated for the vessel are shown in Fig. 1.3. A fluid pressure of 2500 psi (the actual operating pressure is only 2000 psi) was used as a basis for the calculations, and the added pressure contributed by the cladding was calculated to be 780 psi at 600°F, resulting in an effective design pressure of 3280 psi. The heat generation assumed was that calculated for operation at 5 Mw with a D_2O reflector. Thermal stresses were reported for an insulated vessel and for a vessel with the outer surface cooled to the temperature of the

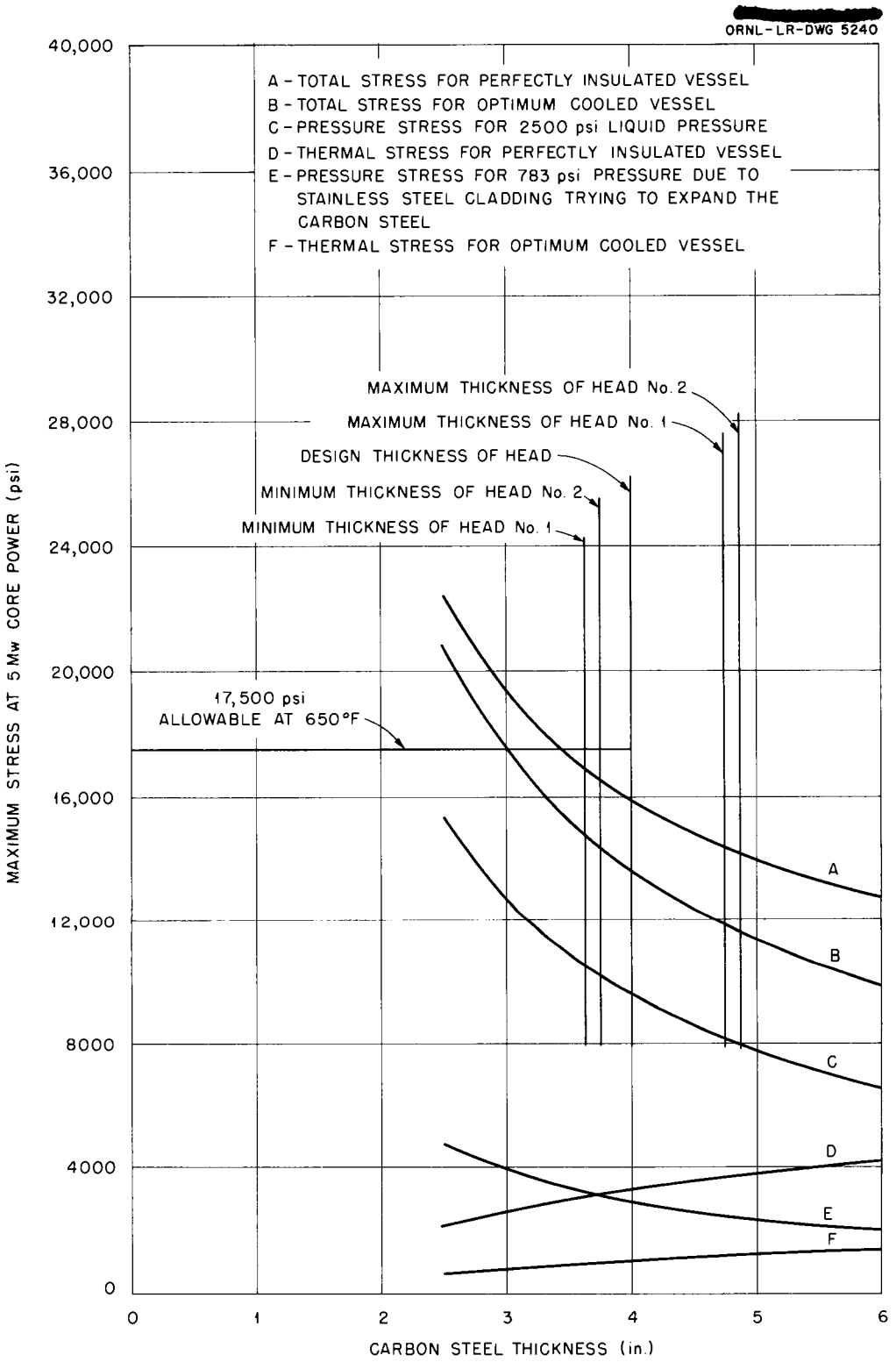

Fig. 1.3. Stresses in Carbon Steel Wall of HRT Pressure Vessel.

inner surface. The calculated stresses for operation at 5 Mw were within the 17,500 psi permitted by the ASME Code for Unfired Pressure Vessels. If the vessel is cooled properly, this is also true for operation at 10 Mw.

1.2.3 Auxiliary Components

Construction drawings were issued for several equipment items which were not reported previously.[17] They included the cold traps (items 9, 36, and 50), the purge pump head (item 23), the holdup tank (item 22), the transfer tanks (items 19 and 52), and the condensate tanks (items 14 and 37).

The cold trap is shown in Fig. 1.4. It was designed to cool 10 ft^3/hr of O_2 saturated with D_2O vapor from 130 to −20°F and to remove the heat released by radioactive decay of the gaseous fission products which pass through the trap. The resulting heat load will be 125 Btu/hr from cooling the gas and condensing and freezing the D_2O and will be 2400 Btu/hr from fission-product decay.

[17] R. B. Briggs *et al.*, *HRP Quar. Prog. Rep. Oct. 31, 1954*, ORNL-1813, Fig. 1.4, p 7.

[redacted]

[redacted]

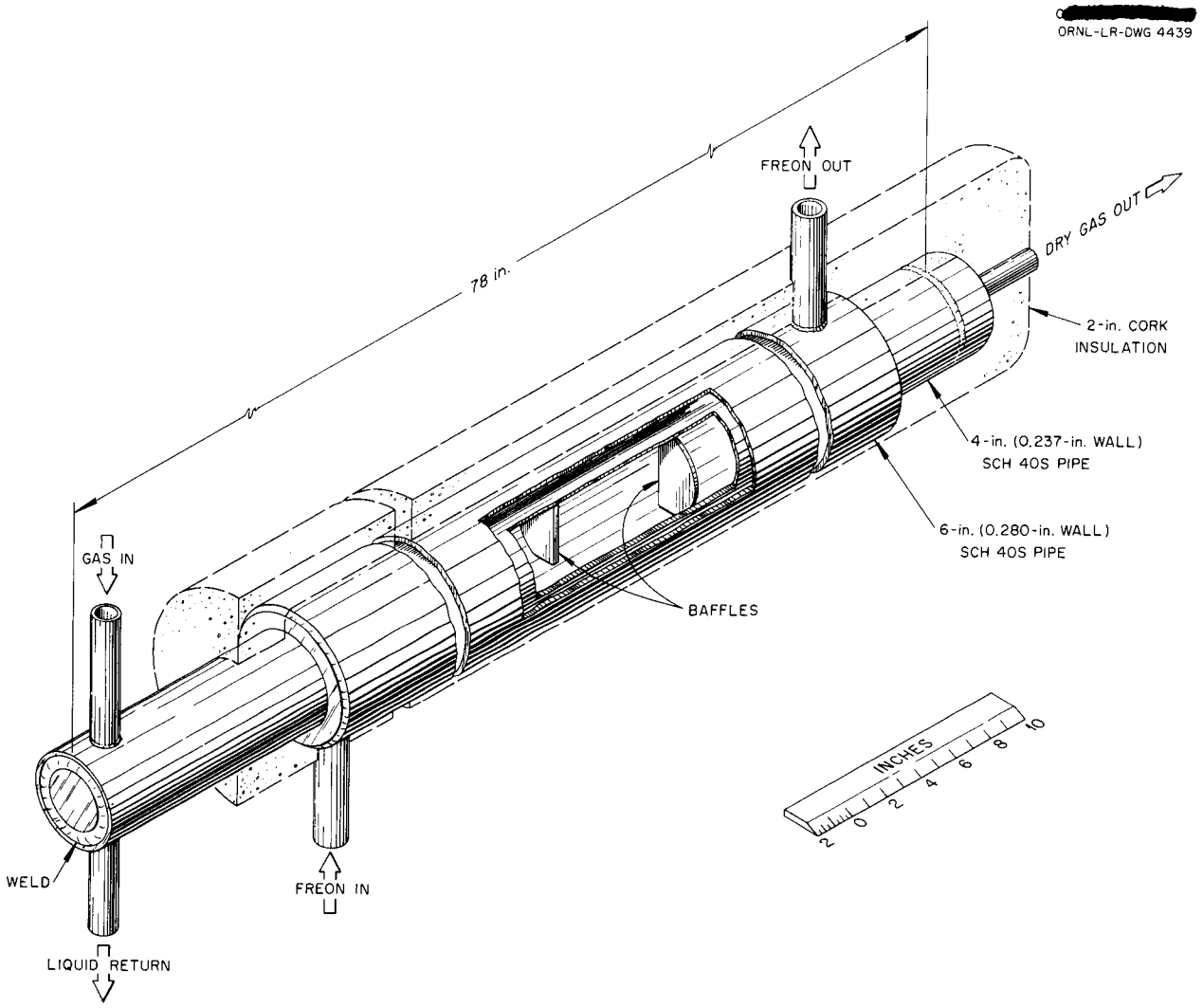

Fig. 1.4. Cold Trap.

Most of the latter heat will be generated in the pipe walls. Cooling will be achieved by evaporating Freon 12 in the outer jacket. The ends of the trap will be left uninsulated to prevent ice from plugging the inlet and exit lines. Baffles will be provided in the center of the trap to control convection circulation of the gas.

Figure 1.5 shows the assembly of the purge pump head. It is a diaphragm pump similar to the fuel and blanket feed pumps and was designed to pump 10 gph of D_2O from the low-pressure system into the core-system pressurizer, which will operate at 2000 psi. The drive unit is a standard Scott and Williams Hydropulse pump. A heavy-water leg will be provided between the rubber pulsators on the Hydropulse pump and the diaphragm of the purge pump head.

Construction drawings were also issued for the instrument thimble. An assembly of the thimble is shown in Fig. 1.6. Although it is similar in principle to that discussed in a previous report,[18] there are some changes in details. Lead shot and

[18] R. B. Briggs *et al.*, *HRP Quar. Prog. Rep. July 31, 1954*, ORNL-1772, p 14.

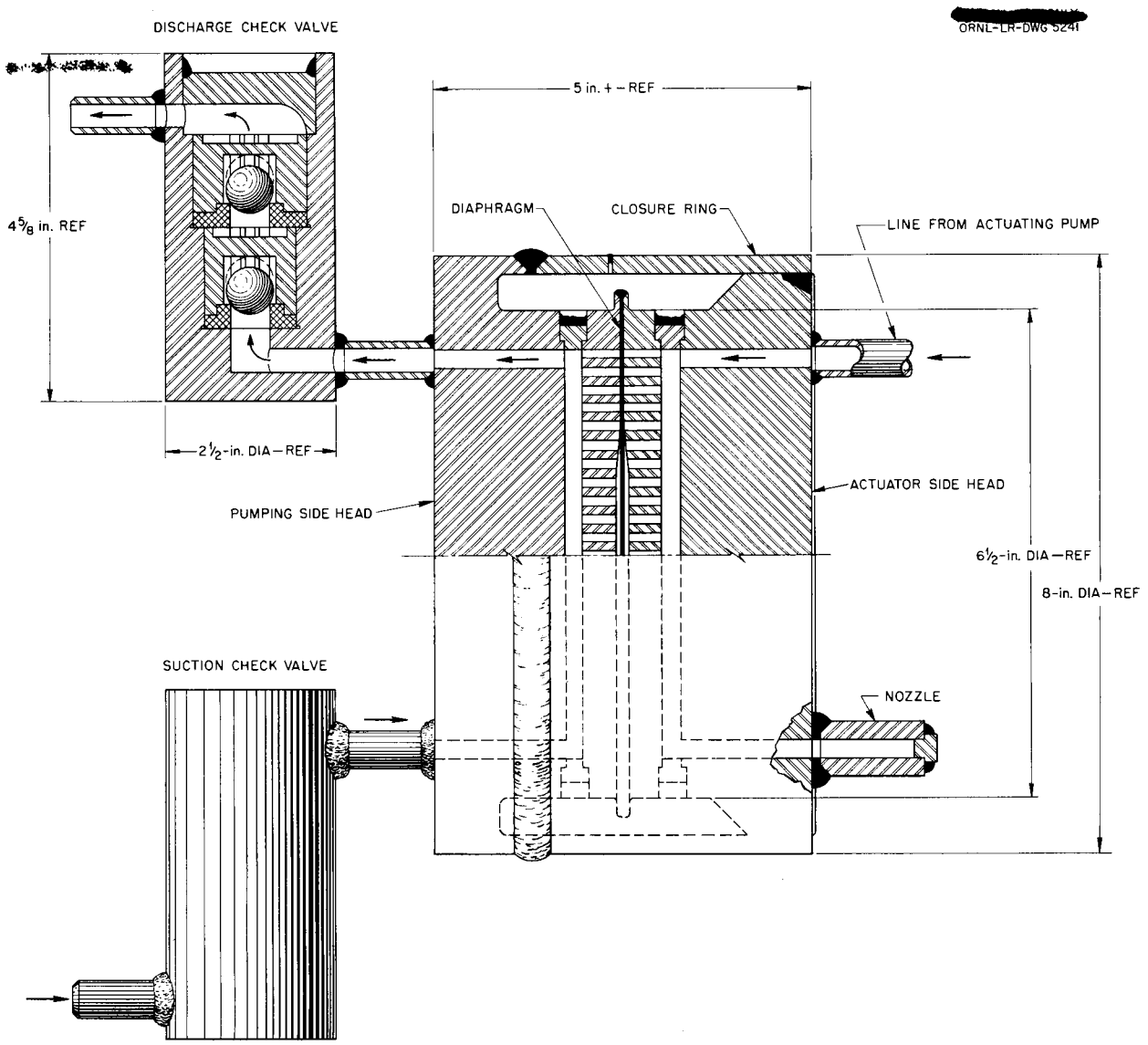

Fig. 1.5. Purge Pump Head All-Welded Assembly and Detail.

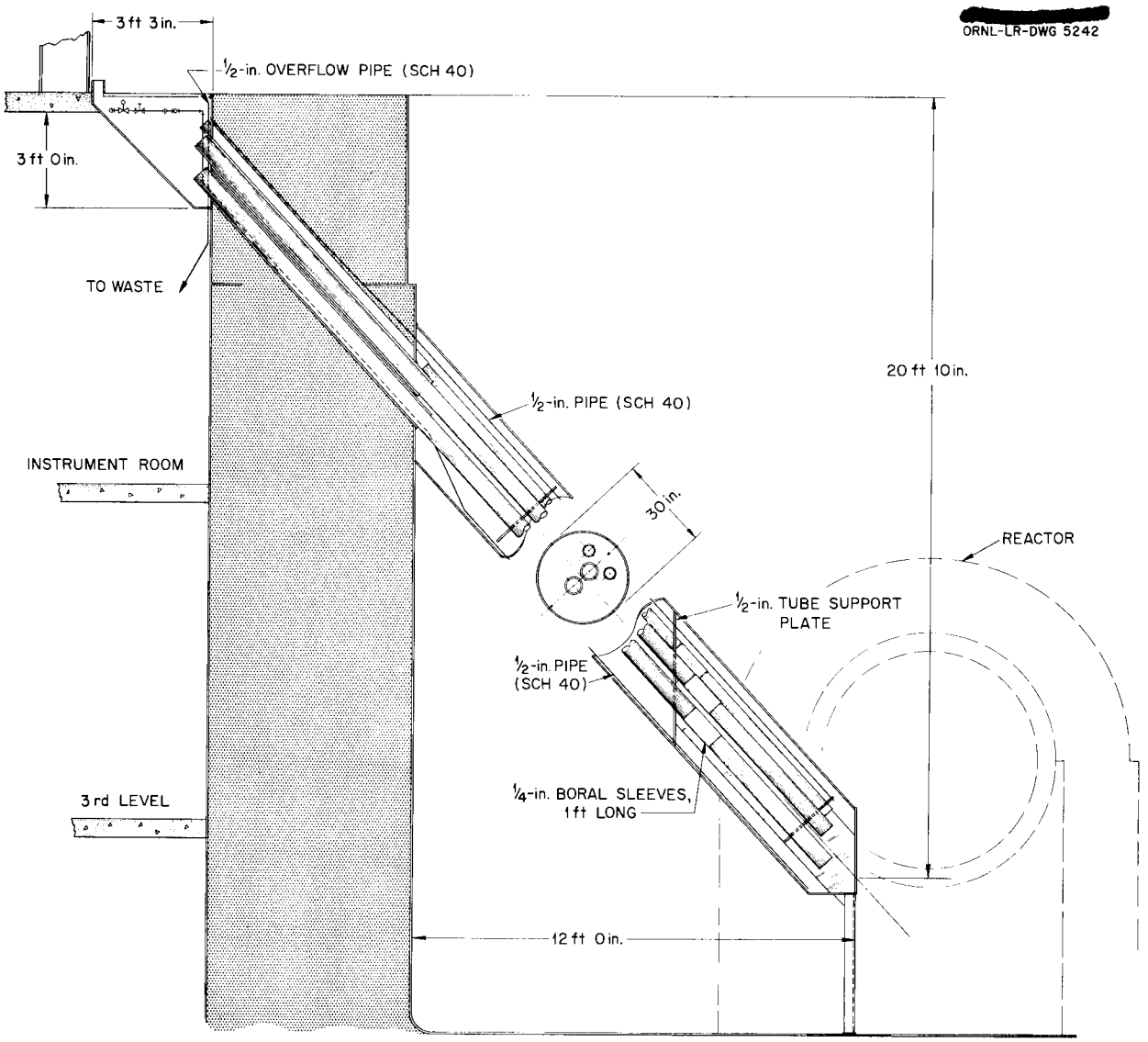

Fig. 1.6. Elevation – Instrument Tubes and Details.

water will be used as the shielding near the reactor; water alone will provide sufficient protection through most of the length.

1.3 NUCLEAR CALCULATIONS

M. C. Edlund

H. C. Claiborne, M. K. Hullings, L. Dresner, P. R. Kasten, T. B. Fowler, L. C. Noderer, M. Tobias

1.3.1 Safety Considerations

As was illustrated previously,[19] the pressure rise within the core vessel as a function of input reactivity gives a curve characteristic of the physical system. A parameter study was conducted with the aid of the Oracle to find the influence of particular parameters upon the maximum core pressure rise for a given reactivity addition.

The chosen parameter values are given in Tables 1.1 and 1.2. The Oracle results consist of the values of x, p, and t at the times when x and p have their maximum value and are given in Table 1.2. The results are plotted in Fig. 1.7

[19] M. C. Edlund, P. R. Kasten, and P. M. Wood, *HRP Quar. Prog. Rep. Oct. 31, 1954*, ORNL-1813, Fig. 1.13, p 21.

[redacted]

TABLE OF NOMENCLATURE

A = average cross-sectional area of piping between core and pressurizer, ft^2

b = rate of reactivity addition, sec^{-1}

C_2 = measure of effect of pressurizer volume upon core pressure rise, dimensionless

$F = \dfrac{\omega_b^2(1 + C_2) + \alpha_1 m_e + m_e^2}{\omega_b^2}$, dimensionless

$\dfrac{\partial k}{\partial T}$ = temperature coefficient of reactivity, $°C^{-1}$

L = length of piping between core and pressurizer surface, ft

m_e = equivalent value of m for a given ω_{np}^2 and ξ, sec^{-1}

m = instantaneous prompt reactivity addition divided by the average lifetime of prompt neutrons, sec^{-1}

n_f = velocity heads lost between core and pressurizer, dimensionless

p = rise in core pressure, psi

p_{max} = maximum rise in core pressure for a given reactivity addition, psi

p_0 = initial value of core pressure, psi

S = reciprocal volume heat capacity of core fluid, °C/kw-sec

t = time, sec

T_0 = initial average temperature of core fluid, °C

U_0 = initial average velocity of fluid in core exit piping, fps

v = normalized increase in velocity of fluid leaving core region, sec^{-2}

v_s = velocity of sound propagation in fluid, fps

V_c = volume of fluid in core region, ft^3 or liters

V_p = volume of pressurizing fluid in pressurizer, liters or ft^3

x = reactor power relative to initial power, dimensionless

x_{pc} = value of x when reactor is prompt critical

y = normalized rise in core fluid temperature, sec^{-1}

z = normalized change in fluid density, sec^{-1}

α_1 = normalized friction coefficient in core relief line, sec^{-1}

γ = effective value of fission neutrons which are delayed, divided by τ, sec^{-1}

γ_2 = conversion factor $(psi\text{-}sec)^{-1}$

γ_3 = conversion factor, sec^{-2}

ξ = rate of reactivity addition b, divided by τ, sec^{-2}

ρ = average density of core fluid, lb mass/ft^3

ρ_0 = ρ evaluated under initial conditions

τ = average lifetime of prompt neutrons, sec

ω_b^2 = (hydraulic system frequency times $2\pi)^2$, sec^{-2}

ω_n^2 = (nuclear system frequency times $2\pi)^2$, sec^{-2}

$\omega_{np}^2 = \omega_n^2 x_{pc}$

TABLE 1.1. GROUP PARAMETER VALUES

Group	Primary Parameters						Secondary Parameters*						
	ω_b^2 (sec^{-2})	C_2 (dimensionless)	α_1 (sec^{-1})	γ_3 (sec^{-2})	γ_2 [(psi-sec)$^{-1}$]	γ (sec^{-1})	τ (sec)	v_s (fps)	L (ft)	$\frac{\partial k}{\partial T}$ ($°C^{-1}$)	U_0 (fps)	V_p (liters)	n_f (dimensionless)
1	7400	0	14	555	0.0913	25	2×10^{-4}	2380	5	3.3×10^{-3}	15	∞	4.66
2	2560	0	14	555	0.265	25	2×10^{-4}	1400	5	3.3×10^{-3}	15	∞	4.66
3	3700	0	7	555	0.0913	25	2×10^{-4}	2380	10	3.3×10^{-3}	15	∞	4.66
4	1280	0	7	555	0.265	25	2×10^{-4}	1400	10	3.3×10^{-3}	15	∞	4.66
5	1850	0	3.5	555	0.0913	25	2×10^{-4}	2380	20	3.3×10^{-3}	15	∞	4.66
6	1850	0.4	3.5	555	0.0913	25	2×10^{-4}	2380	20	3.3×10^{-3}	15	24.2	4.66
7	640	0.4	3.5	555	0.265	25	2×10^{-4}	1400	20	3.3×10^{-3}	15	70	4.66
8	1280	0.2	7.0	555	0.265	25	2×10^{-4}	1400	10	3.3×10^{-3}	15	140	4.66
9	1280	0.4	7.0	555	0.265	25	2×10^{-4}	1400	10	3.3×10^{-3}	15	70	4.66
10	3700	0.2	7.0	555	0.0913	25	2×10^{-4}	2380	10	3.3×10^{-3}	15	48.4	4.66
11	3700	0.4	7.0	555	0.0913	25	2×10^{-4}	2380	10	3.3×10^{-3}	15	24.2	4.66
12	1850	0.2	3.5	555	0.0913	25	2×10^{-4}	2380	20	3.3×10^{-3}	15	48.4	4.66
13	640	0.2	3.5	555	0.265	25	2×10^{-4}	1400	20	3.3×10^{-3}	15	140	4.66
14	3700	0	10.5	155	0.0256	12.5	4×10^{-4}	2380	10	1.85×10^{-3}	15	∞	7.0
15	7400	0	10.5	155	0.0256	12.5	4×10^{-4}	2380	5	1.85×10^{-3}	15	∞	3.5
16	2620	0	10.5	155	0.0362	12.5	4×10^{-4}	2000	10	1.85×10^{-3}	15	∞	7.0
17	5240	0	10.5	155	0.0362	12.5	4×10^{-4}	2000	5	1.85×10^{-3}	15	∞	3.5
21	3700	0.1	10.5	155	0.0362	12.5	4×10^{-4}	2000	10	1.85×10^{-3}	15	97	7.0
22	7400	0.1	10.5	155	0.0362	12.5	4×10^{-4}	2000	5	1.85×10^{-3}	15	97	3.5
23	2620	0.1	10.5	155	0.0362	12.5	4×10^{-4}	2000	10	1.85×10^{-3}	15	137	7.0
24	2620	0.1	17.5	155	0.0362	12.5	4×10^{-4}	2000	10	1.85×10^{-3}	15	137	11.6
27	2620	0.1	10.5	109	0.0254	8.8	5.7×10^{-4}	2000	10	1.85×10^{-3}	15	137	7.0
28	2620	0.1	10.5	195	0.0453	8.8	5.7×10^{-4}	2000	10	3.3×10^{-3}	15	137	7.0
29	2620	0.2	10.5	109	0.0254	8.8	5.7×10^{-4}	2000	10	1.85×10^{-3}	15	69	7.0
30	2620	0	10.5	109	0.0254	8.8	5.7×10^{-4}	2000	10	1.85×10^{-3}	15	∞	7.0
31	2620	0.05	10.5	109	0.0254	8.8	5.7×10^{-4}	2000	10	1.85×10^{-3}	15	273	7.0
32	3700	0.05	10.5	109	0.018	8.8	5.7×10^{-4}	2380	10	1.85×10^{-3}	15	190	7.0
33	3700	0.05	10.5	620	0.102	50	1×10^{-4}	2380	10	1.85×10^{-3}	15	190	7.0
34	3700	0.05	10.5	62	0.0102	5	1×10^{-3}	2380	10	1.85×10^{-3}	15	190	7.0
35	3700	0.05	10.5	195	0.0321	8.8	5.7×10^{-4}	2380	10	3.3×10^{-3}	15	190	7.0
36	3700	0.05	10.5	19.5	0.00321	8.8	5.7×10^{-4}	2380	10	3.3×10^{-4}	15	190	7.0

*For all groups $\rho_0 = 52.5$ lb/ft^3, $p_0 = 2000$ psi, $\frac{1}{\rho}\frac{\partial \rho}{\partial T} = -2.92 \times 10^{-3}$/°C, $S = 7.63 \times 10^{-4}$°C/kw-sec, $T_0 = 280$°C, $V_c = 10.24$ ft^3, $A = 0.0667$ ft^2.

TABLE 1.2. RESULTS OF ORACLE CALCULATIONS FOR SPECIFIC CASES

Group*	Case	Variables			Oracle Results							
		m (sec^{-1})	ξ (sec^{-2})	ω_n^2 (sec^{-2})	$t_{x_{max}}$ (sec)	x_{max} (dimensionless)	$p(t_{x_{max}})$ (psi)	$t_{p_{max}}$ (sec)	$x(t_{p_{max}})$ (dimensionless)	p_{max} (psi)	p_{max} (psi) Calculated	m_e (sec^{-1})
1	A2	35	0	1.26×10^{-5}	0.530	5.53×10^{7}	34	0.521	5.36×10^{7}	36		
	A3	40	0	1.26×10^{-5}	0.473	7.5×10^{7}	54	0.468	7.4×10^{7}	55	65	
	A4	45	0	1.26×10^{-5}	0.427	9.9×10^{7}	84	0.425	9.9×10^{7}	84		
	A5	50	0	1.26×10^{-5}	0.390	1.29×10^{8}	122	0.391	1.29×10^{8}	122	148	
	A6	$-\gamma$	60	1.26×10^{-5}	1.184	9.33×10^{7}	75	1.181	9.29×10^{7}	75		
	A7	$-\gamma$	65	1.26×10^{-5}	1.125	1.04×10^{8}	88	1.123	1.04×10^{8}	88		
	A8	$-\gamma$	70	1.26×10^{-5}	1.073	1.15×10^{8}	102	1.073	1.15×10^{8}	102		
	A9	$-\gamma$	75	1.26×10^{-5}	1.027	1.26×10^{8}	117	1.028	1.26×10^{8}	117		
	A10	$-\gamma$	60	1.26×10^{-6}	1.235	1.11×10^{9}	97	1.235	1.11×10^{9}	97		
	A45	$-\gamma$	65	1.26×10^{-6}	1.174	1.24×10^{9}	114	1.176	1.23×10^{9}	114		
	A46	$-\gamma$	70	1.26×10^{-6}	1.120	1.37×10^{9}	131	1.122	1.37×10^{9}	132		
	A47	$-\gamma$	75	1.26×10^{-6}	1.074	1.50×10^{9}	151	1.076	1.50×10^{9}	152		
2	A25	35	0	1.26×10^{-5}	0.536	7.16×10^{7}	48	0.537	7.15×10^{7}	49		
	A26	40	0	1.26×10^{-5}	0.479	1.03×10^{8}	75	0.480	1.03×10^{8}	76	104	
	A27	45	0	1.26×10^{-5}	0.434	1.44×10^{8}	110	0.435	1.44×10^{8}	111		
	A28	50	0	1.26×10^{-5}	0.398	1.96×10^{8}	155	0.399	1.96×10^{8}	157	285	
	A29	$-\gamma$	60	1.26×10^{-5}	1.190	1.34×10^{8}	99	1.192	1.34×10^{8}	102		
	A30	$-\gamma$	65	1.26×10^{-5}	1.132	1.53×10^{8}	116	1.134	1.52×10^{8}	119		
	A31	$-\gamma$	70	1.26×10^{-5}	1.080	1.72×10^{8}	131	1.082	1.72×10^{8}	135		
	A32	$-\gamma$	75	1.26×10^{-5}	1.034	1.93×10^{8}	146	1.036	1.93×10^{8}	152		
	A33	$-\gamma$	60	1.26×10^{-6}	1.242	1.65×10^{9}	124	1.242	1.65×10^{9}	128		
	A34	$-\gamma$	65	1.26×10^{-6}	1.182	1.88×10^{9}	146	1.184	1.87×10^{9}	151		
	A35	$-\gamma$	70	1.26×10^{-6}	1.128	2.13×10^{9}	164	1.130	2.12×10^{9}	171		
	A36	$-\gamma$	75	1.26×10^{-6}	1.080	2.39×10^{9}	182	1.082	2.39×10^{9}	190		
3	A13	35	0	1.26×10^{-5}	0.530	5.82×10^{7}	45	0.519	5.55×10^{7}	50		
	A14	40	0	1.26×10^{-5}	0.473	8.08×10^{7}	78	0.467	7.94×10^{7}	81	107	
	A15	45	0	1.26×10^{-5}	0.428	1.09×10^{8}	124	0.425	1.09×10^{8}	125		
	A16	50	0	1.26×10^{-5}	0.391	1.45×10^{8}	186	0.392	1.45×10^{8}	186	263	
	A17	$-\gamma$	60	1.26×10^{-5}	1.184	1.02×10^{8}	110	1.182	1.02×10^{8}	110		
	A18	$-\gamma$	65	1.26×10^{-5}	1.126	1.14×10^{8}	130	1.124	1.14×10^{8}	130		
	A19	$-\gamma$	70	1.26×10^{-5}	1.074	1.28×10^{8}	152	1.074	1.28×10^{8}	152		

TABLE 1.2 (continued)

Group*	Case	Variables			Oracle Results						p_{max} (psi) Calculated	m_e (sec^{-1})
		m (sec^{-1})	ξ (sec^{-2})	ω_n^2 (sec^{-2})	$t_{x_{max}}$ (sec)	x_{max} (dimensionless)	$p(t_{x_{max}})$ (psi)	$t_{p_{max}}$ (sec)	$x(t_{p_{max}})$ (dimensionless)	p_{max} (psi)		
3	A20	$-\gamma$	75	1.26×10^{-5}	1.028	1.41×10^{8}	175	1.030	1.41×10^{8}	175		
	A21	$-\gamma$	60	1.26×10^{-6}	1.236	1.23×10^{9}	145	1.236	1.23×10^{9}	145		
	A22	$-\gamma$	65	1.26×10^{-6}	1.174	1.38×10^{9}	170	1.176	1.38×10^{9}	171		
	A23	$-\gamma$	70	1.26×10^{-6}	1.122	1.62×10^{9}	235	1.124	1.62×10^{9}	240		
	A24	$-\gamma$	75	1.26×10^{-6}	1.076	1.80×10^{9}	272	1.078	1.79×10^{9}	277		
4	A43	$-\gamma$	70	1.26×10^{-6}	1.133	2.98×10^{9}	297	1.134	2.97×10^{9}	303		
	A44	$-\gamma$	75	1.26×10^{-6}	1.086	3.39×10^{9}	327	1.088	1.37×10^{9}	343		
	A64	$-\gamma$	50	1.26×10^{-5}	1.344	1.30×10^{8}	130	1.357	1.16×10^{8}	142		
	A65	$-\gamma$	75	1.26×10^{-5}	1.040	2.66×10^{8}	269	1.056	2.03×10^{8}	319		
	A66	$-\gamma$	100	1.26×10^{-5}	0.873	4.60×10^{8}	445	0.890	2.97×10^{8}	567		
	A67	35	0	1.26×10^{-5}	0.540	8.86×10^{7}	87	0.550	8.46×10^{7}	91		
	A68	50	0	1.26×10^{-5}	0.403	2.70×10^{8}	274	0.418	2.07×10^{8}	324	614	
	A69	65	0	1.26×10^{-5}	0.325	6.61×10^{8}	622	0.342	3.78×10^{8}	815	2,650	
	A70	$-\gamma$	50	1.26×10^{-6}	1.401	1.63×10^{9}	164	1.415	1.41×10^{9}	184		
	A71	$-\gamma$	75	1.26×10^{-6}	1.086	3.38×10^{9}	336	1.102	2.44×10^{9}	410		
	A72	$-\gamma$	100	1.26×10^{-6}	0.912	5.83×10^{9}	546	0.930	3.33×10^{9}	720		
5	A37	35	0	1.26×10^{-5}	0.534	7.15×10^{7}	131	0.535	7.15×10^{7}	131		
	A38	40	0	1.26×10^{-5}	0.478	1.04×10^{8}	212	0.479	1.04×10^{8}	213	219	
	A39	45	0	1.26×10^{-5}	0.433	1.47×10^{8}	317	0.434	1.47×10^{8}	321		
	A40	50	0	1.26×10^{-5}	0.397	2.03×10^{8}	454	0.398	2.03×10^{8}	461	586	
	A41	$-\gamma$	60	1.26×10^{-5}	1.190	1.36×10^{8}	285	1.192	1.35×10^{8}	290		
	A42	$-\gamma$	65	1.26×10^{-5}	1.130	1.55×10^{8}	327	1.132	1.55×10^{8}	336		
6	A48	$-\gamma$	75	1.26×10^{-5}	1.038	2.39×10^{8}	643	1.052	1.92×10^{8}	737		
	A54	50	0	1.26×10^{-5}	0.401	2.38×10^{8}	638	0.414	1.96×10^{8}	728	934	
7	A52	50	0	1.26×10^{-5}	0.413	4.57×10^{8}	579	0.434	2.57×10^{8}	763		
	A53	$-\gamma$	75	1.26×10^{-5}	1.050	4.73×10^{8}	597	1.072	2.57×10^{8}	792	1,915	
8	A49	50	0	1.26×10^{-5}	0.404	2.88×10^{8}	305	0.421	2.10×10^{8}	369	710	
	A50	$-\gamma$	75	1.26×10^{-5}	1.041	2.89×10^{8}	302	1.059	2.06×10^{8}	372		

TABLE 1.2 (continued)

Group*	Case	Variables			Oracle Results							
		m (sec^{-1})	ξ (sec^{-2})	ω_n^2 (sec^{-2})	$t_{x_{max}}$ (sec)	x_{max} (dimensionless)	$p(t_{x_{max}})$ (psi)	$t_{p_{max}}$ (sec)	$x(t_{p_{max}})$ (dimensionless)	p_{max} (psi)	p_{max} (psi) Calculated	m_e (sec^{-1})
9	A55	$-\gamma$	75	1.26×10^{-5}	1.043	3.10×10^{8}	341	1.062	2.08×10^{8}	425		
	A60	50	0	1.26×10^{-5}	0.406	3.05×10^{8}	335	0.424	2.09×10^{8}	416	808	
10	A51	50	0	1.26×10^{-5}	0.395	1.70×10^{8}	317	0.403	1.59×10^{8}	336	414	
	A61	$-\gamma$	75	1.26×10^{-5}	1.032	1.68×10^{8}	315	1.041	1.56×10^{8}	335		
11	A56	50	0	1.26×10^{-5}	0.396	1.89×10^{8}	409	0.411	1.56×10^{8}	465	567	
	A57	$-\gamma$	75	1.26×10^{-5}	1.034	1.89×10^{8}	416	1.049	1.55×10^{8}	475		
12	A58	50	0	1.26×10^{-5}	0.399	2.20×10^{8}	547	0.410	1.94×10^{8}	604	759	
	A59	$-\gamma$	75	1.26×10^{-5}	1.036	2.18×10^{8}	540	1.047	1.92×10^{8}	598		
13	A62	50	0	1.26×10^{-5}	0.412	4.40×10^{8}	553	0.433	2.52×10^{8}	716	1,780	
	A63	$-\gamma$	75	1.26×10^{-5}	1.049	4.51×10^{8}	560	1.070	2.62×10^{8}	735		
14	C1a	$-\gamma$	32.5	3.53×10^{-6}	1.465	2.08×10^{8}	324	1.475	1.97×10^{8}	333	440	34.1
	C1b	$-\gamma$	37.5	3.53×10^{-6}	1.343	2.54×10^{8}	429	1.352	2.46×10^{8}	446	610	37.0
	C1c	$-\gamma$	42.5	3.53×10^{-6}	1.249	3.04×10^{8}	548	1.260	2.87×10^{8}	580	820	39.5
	C3a	$-\gamma$	37.5	3.53×10^{-2}	1.032	8.88×10^{3}	89	1.024	8.80×10^{3}	91	145	25.0
	C3b	$-\gamma$	42.5	3.53×10^{-2}	0.958	1.06×10^{4}	118	0.953	1.05×10^{4}	119	180	26.8
	C4a	$-\gamma$	37.5	3.53×10^{-4}	1.203	1.66×10^{6}	236	1.206	1.65×10^{6}	236	330	31.7
	C4b	$-\gamma$	42.5	3.53×10^{-4}	1.117	1.98×10^{6}	304	1.123	1.96×10^{6}	308	430	34.0
15	C1d	$-\gamma$	50	3.53×10^{-6}	1.133	3.16×10^{8}	331	1.138	3.12×10^{8}	337	470	43.5
	C1e	$-\gamma$	75	3.53×10^{-6}	0.902	5.58×10^{8}	746	0.912	5.13×10^{8}	808	1,200	54.0
	C3c	$-\gamma$	50	3.53×10^{-2}	0.870	1.21×10^{4}	69	0.860	1.19×10^{4}	72	100	29.5
	C3d	$-\gamma$	75	3.53×10^{-2}	0.690	2.10×10^{4}	175	0.690	2.10×10^{4}	175	260	38.0
	C4c	$-\gamma$	50	3.53×10^{-4}	1.014	2.14×10^{6}	180	1.013	2.14×10^{6}	180	240	37.0
16	C2a	$-\gamma$	32.5	3.53	0.874	21.1	10.5	0.830	20.3	11.1	17	13.0
	C2b	$-\gamma$	37.5	3.53	0.802	26.6	14.3	0.765	25.6	15.2	22	14.1
	C2c	$-\gamma$	42.5	3.53	0.745	32.5	19.0	0.714	31.5	20.1	30	16.0
17	C2d	$-\gamma$	50	3.53	0.679	40.7	12.4	0.647	38.9	13.5	22	18.2
	C2e	$-\gamma$	75	3.53	0.540	76.8	32.8	0.524	74.8	34.4	68	24.8

TABLE 1.2 (continued)

Group*	Case	Variables			Oracle Results						p_{max} (psi) Calculated	m_e (sec^{-1})
		m (sec^{-1})	ξ (sec^{-2})	ω_n^2 (sec^{-2})	$t_{x_{max}}$ (sec)	x_{max} (dimensionless)	$p(t_{x_{max}})$ (psi)	$t_{p_{max}}$ (sec)	$x(t_{p_{max}})$ (dimensionless)	p_{max} (psi)		
21	C6a	$-\gamma$	32.5	3.53×10^{-4}	1.313	1.49×10^6	289	1.326	1.43×10^6	301	390	29.3
	C6b	$-\gamma$	37.5	3.53×10^{-4}	1.205	1.81×10^6	357	1.219	1.71×10^6	376	482	31.7
	C6c	$-\gamma$	42.5	3.53×10^{-4}	1.120	2.15×10^6	437	1.134	2.01×10^6	463	620	33.8
22	C6d	$-\gamma$	50	3.53×10^{-4}	1.016	2.34×10^6	324	1.028	2.22×10^6	342	410	37.0
	C6e	$-\gamma$	75	3.53×10^{-4}	0.807	4.04×10^6	600	0.820	3.67×10^6	656	800	46.0
23	C7a	$-\gamma$	32.5	3.53×10^{-4}	1.315	1.60×10^6	273	1.330	1.52×10^6	287	390	29.4
	C7b	$-\gamma$	37.5	3.53×10^{-4}	1.207	1.97×10^6	341	1.224	1.82×10^6	367	510	31.6
	C7c	$-\gamma$	42.5	3.53×10^{-4}	1.122	2.37×10^6	420	1.139	2.15×10^6	459	680	34.0
	C8a	$-\gamma$	32.5	3.53×10^{-2}	1.130	8.44×10^3	138	1.148	8.11×10^3	143	190	23.0
	C8b	$-\gamma$	37.5	3.53×10^{-2}	1.037	1.035×10^4	170	1.053	9.96×10^3	176	236	25.0
	C8c	$-\gamma$	42.5	3.53×10^{-2}	0.963	1.24×10^4	207	0.978	1.19×10^4	216	300	27.0
24	C9a	$-\gamma$	32.5	3.53×10^{-4}	1.318	1.74×10^6	362	1.341	1.53×10^6	404	580	29.4
	C9b	$-\gamma$	37.5	3.53×10^{-4}	1.211	2.15×10^6	457	1.235	1.82×10^6	520	770	31.6
	C9c	$-\gamma$	42.5	3.53×10^{-4}	1.126	2.60×10^6	563	1.150	2.14×10^6	655	1,040	34.0
27	C11a	$-\gamma$	22.8	2.48×10^{-4}	1.501	1.54×10^6	271	1.519	1.46×10^6	285	370	24.8
	C11b	$-\gamma$	26.3	2.48×10^{-4}	1.382	1.87×10^6	337	1.401	1.74×10^6	359	480	26.8
	C11c	$-\gamma$	29.8	2.48×10^{-4}	1.287	2.23×10^6	410	1.306	2.05×10^6	443	600	28.5
	C15a	$-\gamma$	26.3	2.48×10^{-6}	1.548	2.84×10^8	528	1.570	2.48×10^8	592	780	31.0
	C15b	$-\gamma$	26.3	2.48×10^{-2}	1.180	1.02×10^4	176	1.204	9.67×10^3	186	225	21.0
28	C12a	$-\gamma$	22.8	4.44×10^{-4}	1.474	7.90×10^5	123	1.487	7.68×10^5	126	160	24.0
	C12b	$-\gamma$	26.3	4.44×10^{-4}	1.357	9.55×10^5	151	1.369	9.28×10^5	155	195	26.0
	C12c	$-\gamma$	29.8	4.44×10^{-4}	1.263	1.13×10^6	181	1.275	1.10×10^6	188	247	27.9
29	C13a	$-\gamma$	22.8	2.48×10^{-4}	1.504	1.67×10^6	368	1.536	1.41×10^6	414	500	24.8
	C13b	$-\gamma$	26.3	2.48×10^{-4}	1.384	2.02×10^6	435	1.414	1.71×10^6	499	610	26.8
	C13c	$-\gamma$	29.8	2.48×10^{-4}	1.290	2.41×10^6	520	1.318	1.99×10^6	595	730	28.5
30	C14a	$-\gamma$	26.3	2.48×10^{-4}	1.378	1.73×10^6	230	1.388	1.70×10^6	235	330	26.8
31	C14b	$-\gamma$	26.3	2.48×10^{-4}	1.380	1.80×10^6	282	1.394	1.74×10^6	295	400	26.8

TABLE 1.2 (continued)

Group*	Case	Variables			Oracle Results						p_{max} (psi) Calculated	m_e (sec^{-1})
		m (sec^{-1})	ξ (sec^{-2})	ω_n^2 (sec^{-2})	$t_{x_{max}}$ (sec)	x_{max} (dimensionless)	$p(t_{x_{max}})$ (psi)	$t_{p_{max}}$ (sec)	$x(t_{p_{max}})$ (dimensionless)	p_{max} (psi)		
32	C16a	$-\gamma$	35.1	8.04×10^{-7}	1.346	1.26×10^{9}	889	1.364	1.09×10^{9}	997	1,250	37.1
	C16b	36.2	0	8.04×10^{-7}	0.608	1.20×10^{9}	821	0.626	1.06×10^{9}	929	1,120	
	C16c	36.2	0	2.48×10^{-3}	0.386	3.88×10^{5}	826	0.404	3.41×10^{5}	929	1,120	
	C16d	27.0	0	2.48×10^{-6}	0.742	1.87×10^{8}	333	0.754	1.82×10^{8}	346	390	
	C16e	$-\gamma$	26.3	5.25×10^{-5}	1.438	9.21×10^{6}	359	1.449	8.95×10^{6}	369	450	28.1
	C16f	$-\gamma$	35.1	1.84×10^{-3}	1.101	2.68×10^{5}	368	1.113	2.60×10^{5}	380	480	28.5
	C16g	$-\gamma$	70.2	5.09×10^{-1}	0.595	1.03×10^{3}	401	0.607	9.96×10^{2}	415	560	29.8
	C16h	$-\gamma$	175.5	24.5	0.282	3.09×10	622	0.297	29.3	661		
	C16i	$-\gamma$	17.6	4.83×10^{-8}	2.111	9.79×10^{9}	348	2.122	9.51×10^{9}	357	440	27.9
33	C16j	$-\gamma$	250	5.47×10^{-7}	0.653	3.71×10^{10}	2505	0.648	1.72×10^{10}	3486	9,400	
	C16k	110	0	5.47×10^{-7}	0.231	4.66×10^{10}	2990	0.244	1.99×10^{10}	4350	21,600	
34	C16l	10	0	2.28×10^{-4}	1.333	2.38×10^{5}	72	2.732	1.03	99	76	
	C16m	$-\gamma$	5	2.28×10^{-4}	3.22	2.55×10^{5}	78				72	
35	C16n	27	0	5.25×10^{-5}	0.630	8.61×10^{6}	154	0.635	8.54×10^{6}	156	175	
	C16o	$-\gamma$	26.3	5.25×10^{-5}	1.435	8.96×10^{6}	161	1.445	8.81×10^{6}	165	198	28.0
36	C16p	27	0	5.25×10^{-5}	0.642	1.09×10^{7}	476	0.678	8.28×10^{6}	591	630	
	C16q	$-\gamma$	26.3	5.25×10^{-5}	1.451	1.16×10^{7}	520	1.488	8.77×10^{6}	651	750	28.0

*See Table 1.1 for group parameter values.

[redacted]

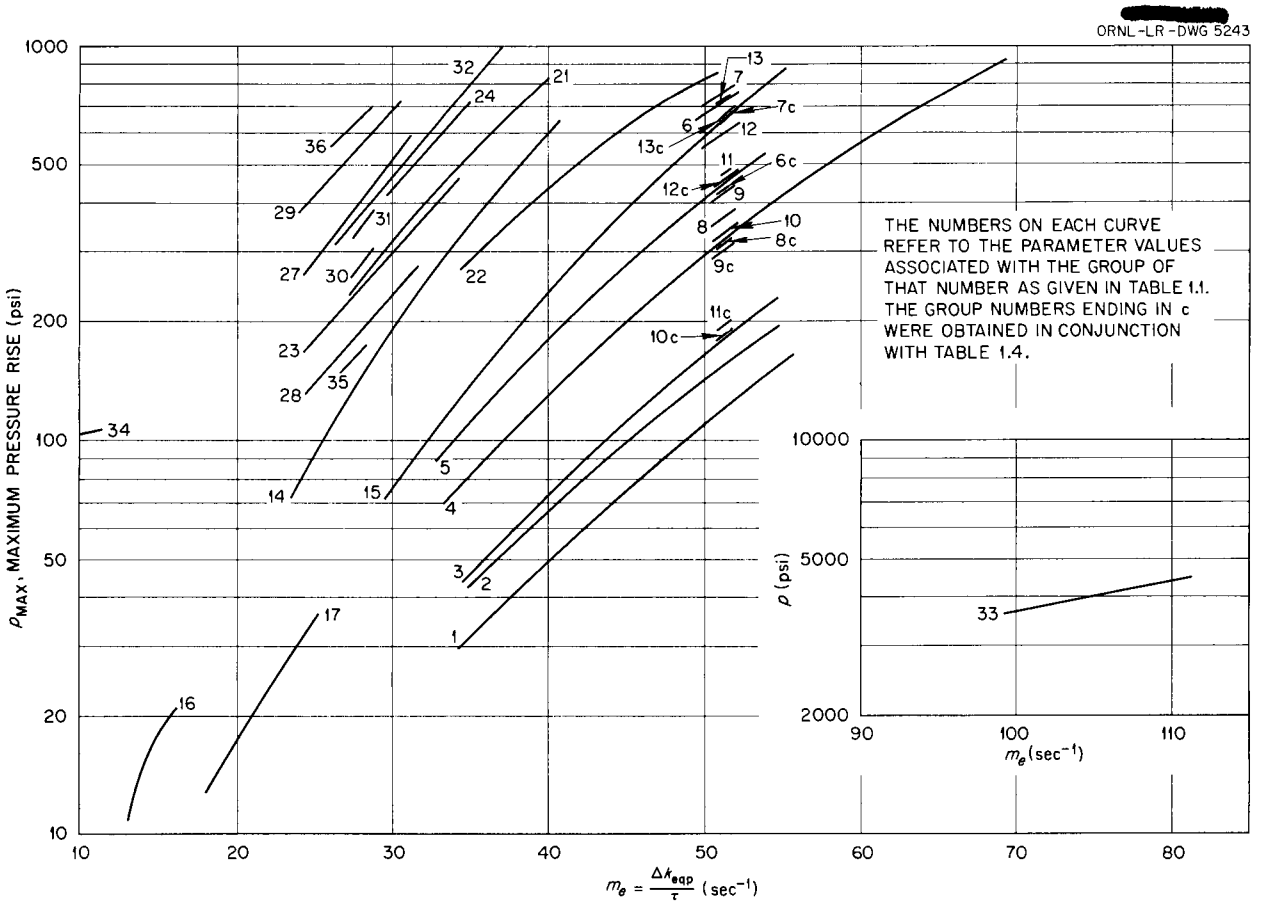

Fig. 1.7. Core Pressure Rise as a Function of Reactivity Addition for Various Physical Systems.

as p_{max} vs m_e for the various parameter values, where m_e is related to the rate at which reactivity is added, the average lifetime of prompt neutrons, and the modified nuclear frequency; m_e is practically independent of the particular physical system. In Figs. 1.8 and 1.9 are given the relations between m_e, ξ, and ω_{np}^2 for homogeneous reactor systems in general. After the value of m_e is known, the maximum core pressure rise can be obtained from the p_{max} vs m_e curve for a particular system. The values of m_e given in Table 1.2 were obtained from Fig. 1.8.

Table 1.3 gives the relation obtained between a particular parameter and the maximum core pressure. To use the relation it is necessary to know the maximum core pressure resulting from a given set of parameter values and a particular reactivity addition; the influence a parameter has upon the maximum pressure is then determined by inserting the desired parameter value in the appropriate parameter-pressure relation. A particular parameter-pressure relation does not appear to be fixed but to be a function of the other parameter values and the reactivity addition. However, the relations given in Table 1.3 are good approximations for parameter deviations about HRT values.

In addition to the Oracle results, Table 1.2 lists some calculated values of p_{max} obtained from the equation

$$(1) \qquad p_{max}\,(\text{calcd}) = \frac{m_e^2 F}{2\omega_b^2 \gamma_2}\left[0.385\, m_e + \alpha_1\left(1 + \frac{m_e^2 F}{4\gamma_3}\right)\right] + \frac{C_2 m_e}{\gamma_2}\,.$$

Equation 1 relates the maximum pressure to the sum of the maximum inertial and frictional resistances. The actual pressure rise does not occur when both inertial and frictional resistances are a maximum, and the fraction of a particular

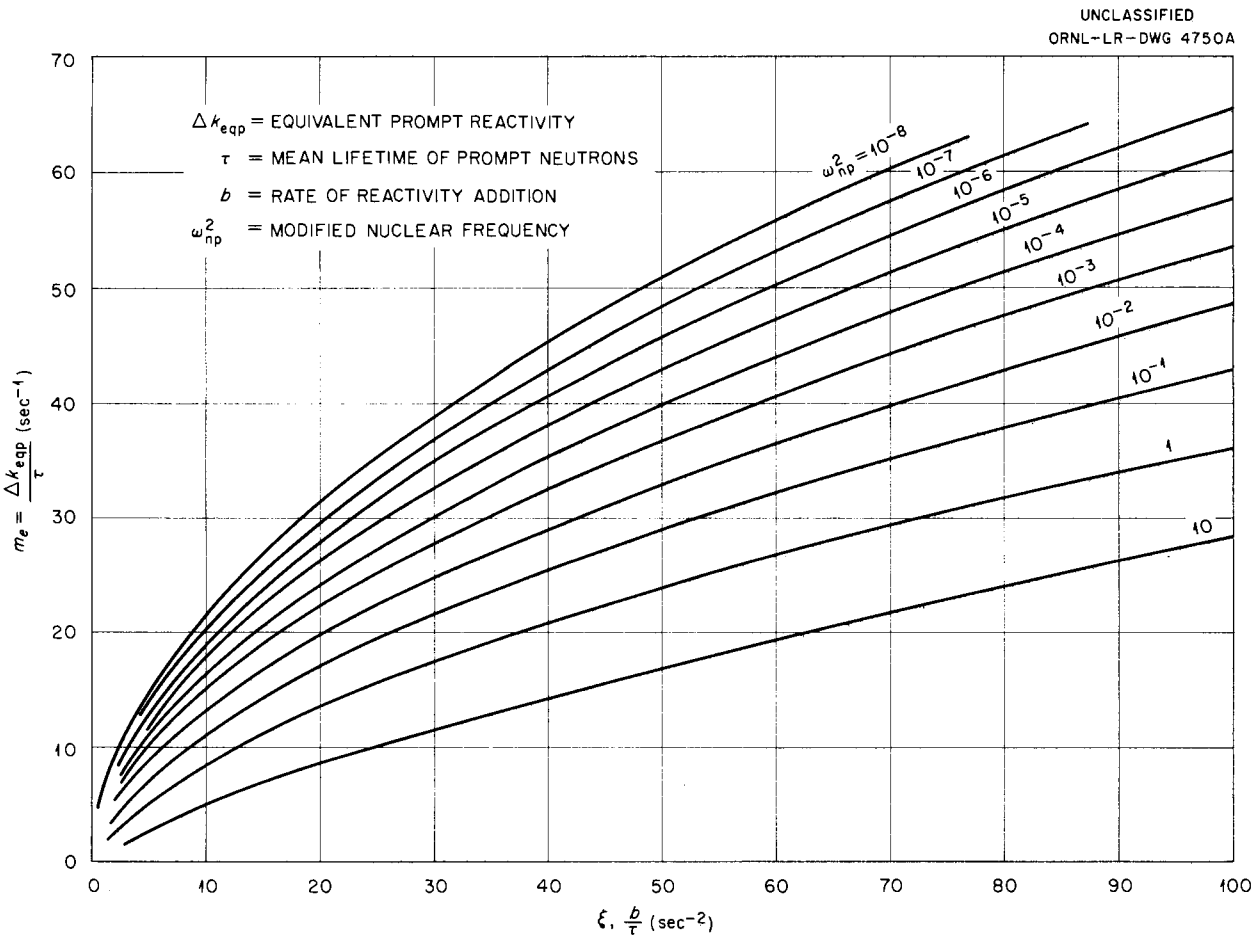

Fig. 1.8. Relation Between Equivalent Prompt Reactivity and Rate of Reactivity Addition.

resistance contributing to the maximum pressure rise is a function of the parameter values, so that Eq. 1 will not necessarily give the same maximum pressure-parameter relations obtained from Oracle calculations. However, the results indicate that Eq. 1 always overestimates p_{max} and that the overestimation increases with m_e and F. Thus design specifications based upon Eq. 1 are conservative.

The influence of a finite pressurizer volume upon the maximum pressure rise is illustrated in Table 1.4. The volume of the pressurizing fluid is inversely related to the value of C_2; so C_2 approaches zero only if the pressurizing volume becomes large. The relation between p_{max} and C_2 appears to be adequately given by Eq. 1; that is, if the pressure rise is known for a given value of C_2, the effect of C_2 upon p_{max} can be obtained from Eq. 1.

The equations used on the Oracle were those for an equivalent bare reactor system; namely,

(2) $\dot{x} = (m + \xi t + z)\, x + \gamma$,

(3) $\dot{y} = x - 1$,

(4) $\dot{z} = -v$,

(5) $\dot{v} = \omega_b^2 [z(1 + C_2) + \omega_n^2 y] - \alpha_1 v \left(1 + \frac{|v|}{2\gamma_3}\right)$,

(6) $p = \frac{1}{\gamma_2}(z + \omega_n^2 y)$.

Equations 2 to 6 indicate the parameters as m, ξ, γ, ω_b^2, C_2, ω_n^2, α_1, γ_3, and γ_2. However, Figs. 1.8 and 1.9 relate ξ and ω_n^2 to an equivalent value of m, designated m_e; also, insofar as safety calculations are concerned, the value of the de-

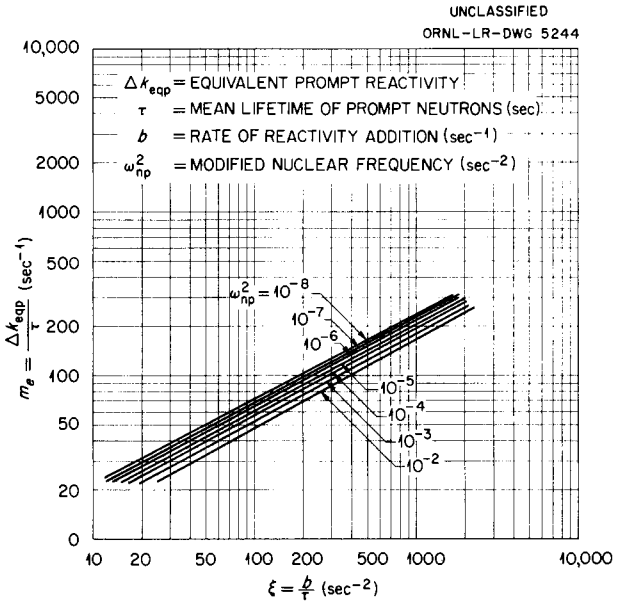

Fig. 1.9. Relation Between Equivalent Prompt Reactivity and Rate of Reactivity Addition for Large Values of ξ.

layed neutron fraction influences p_{max} to a negligible extent so long as reactivity is added as a linear rate function. The placement of the p_{max} vs m_e curve is therefore dependent only upon the values of ω_b^2, C_2, α_1, γ_3, and γ_2, which, in turn, are dependent upon the secondary parameters given in Table 1.2.

1.3.2 The HRT and the "Walk-Away" Phenomenon

A detailed analysis of the "walk-away" phenomenon with respect to the HRT is presented elsewhere.[20] The findings of that report and some additional results are summarized briefly here.

The walk-away phenomenon in the HRE was described[21] as a slow rise in reactivity produced by core concentration enhancement. This increase in concentration results when water is removed from the core as a result of radiolytic decomposition and accompanying vaporization at a rate faster than it is returned from the low-pressure system, causing an increase in power generation and, consequently, an increase in gas generation. This process continues until it is stopped by the operator. While it is slow, and therefore can be readily restrained, it is nevertheless a troublesome inconvenience.

The walk-away phenomenon was analyzed for the D_2O-reflected HRT by the use of linearized stability equations. Calculations were made at 5 and 10 Mw core power at several average core temperatures between 235 and 300°C. The reactor was assumed to operate (1) with that amount of copper which would allow the same decomposition gas production as operation at 1 Mw with no recombination or (2) with exactly enough copper to recombine the decomposition gas. As a check upon the validity of the calculations, similar methods were used for the case of the HRE without internal recombination, and the results agreed reasonably well with the observed performance of that reactor.

The calculations for the HRT indicate that it will be stable against walk-away at average core temperatures below 293°C at 5 Mw and below 273°C at 10 Mw if enough copper is used to recombine all the gas produced in excess of that corresponding to operation at 1 Mw. When just enough copper is used to recombine all the gas, the limiting temperatures are raised to 297°C at 5 Mw and 278°C at 10 Mw. If a surplus of copper is used so that decomposition gas is never produced, then the HRT will not walk away in the theoretical model used for these calculations.

For a given reactor power and recombination level, the calculations were performed to determine the largest values of the power removal temperature coefficient a (in w/°F) for which the system was stable for several different temperatures. (The power removal temperature coefficient a represents the change in heat removal rate in watts for a 1°F rise in average core temperature.) The maximum temperature of stable operation was then estimated by using an approximation to the actual value of a based upon the properties of the main heat exchanger. Curves of a vs temperature are displayed in Figs. 1.10 and 1.11. The steep curves are due mainly to the rapid decline in overpressure with increase in temperature. Little error is likely to be introduced in the estimate of the final limiting temperature by gross errors in estimating a. Under the assumptions and numbers used in the calculations, walk-away is not expected

[20] M. Tobias, *The HRT and the "Walk-Away" Phenomenon*, ORNL CF-54-12-206 (Dec. 28, 1954).

[21] S. E. Beall *et al.*, *HRP Quar. Prog. Rep. Jan. 31, 1954*, ORNL-1678, p 7–11.

TABLE 1.3. INFLUENCE OF SPECIFIC PARAMETERS UPON THE MAXIMUM CORE PRESSURE

Parameter Varied	Variation of p_{max}* with Parameter (near HRT values)	Remarks
$\left\lvert \frac{\partial k_e}{\partial T} \right\rvert$	$p_2 = p_1 \exp\left[480\left(\left\lvert\frac{\partial k_e}{\partial T}\right\rvert_1 - \left\lvert\frac{\partial k_e}{\partial T}\right\rvert_2\right)\right]$	Variation obtained by comparing groups 32, 35, 36 (exponent coefficient = 480), and groups 27 and 28 (exponent coefficient $\approx$ 500; changed v_s)
L	$p_2 = p_1 e^{0.18(L_2 - L_1)}$	Variation obtained by comparing groups 2, 4, 13c (exponent coefficient $\approx$ 0.11), groups 1, 3, 5 (exponent coefficient $\approx$ 0.09; increased v_s), groups 21c, 22c (exponent coefficient $\approx$ 0.14; changed τ, $\partial k_e/\partial T$), and groups 14, 15 (exponent coefficient $\approx$ 0.18; changed τ, $\partial k_e/\partial T$)
n_f	$p_2 = 0.85 \frac{n_{f_2}}{n_{f_1}} p_1$	Variation obtained by comparing groups 23 and 24
v_s	$p_2 = p_1 e^{1.18(v_{s_1} - v_{s_2})}$	Variation obtained by comparing groups 1 and 2 (exponent coefficient $\approx$ 1.14; L = 5), groups 4, 8c, 9c, 3, 10c, 11c (exponent coefficient $\approx$ 1.19; L = 10), and groups 7e, 13e, 6c, 12c, 5 (exponent coefficient $\approx$ 1.17, L = 20)
$V_p(C_2)$	Given by Eq. 1	See Table 1.4
τ	$p_2 = 0.7 \frac{\tau_1}{\tau_2} p_1$	Variation obtained by comparing groups 3 and 14, correcting group 3 for n_f and $\partial k_e/\partial T$; also groups 14 and 32, correcting group 32 for C_2, also groups 33, 34

*The subscript 1 refers to the original value of the parameter and the subscript 2 to the value for which the pressure rise is desired. The value p_1 is the core pressure rise for the physical system when the parameter has its original value.

in the HRT at the design average core temperature of 280°C.

Examination of the equations and the results indicates that the paramount cause of instability is insufficient overpressure. Also, increasing the fuel feed pump rate and increasing the ratio of the mass of solution held in the high-pressure system to that in the low-pressure system, as well as decreasing temperature, core concentration, and power, will increase reactor stability against walk-away. The use of copper recombination is seen to be essential. Without copper, the limiting average core temperature drops 30 to 40°F.

Calculations have been made for the HRT, producing gas at a rate corresponding to 1 Mw but operating at 5 and 10 Mw total power, to show the effect of some of the factors just mentioned. Figures 1.12, 1.13, 1.14, 1.15, 1.16, and 1.17 show the variation of the limiting a value with fuel feed pump rate, volume of the fuel in the low-pressure

TABLE 1.4. EFFECT OF PRESSURIZER VOLUME UPON CORE PRESSURE RISE

Group Comparisons	m_e	$C_2 = f\left(\frac{V_c}{V_p}\right)$	p_{max} (Oracle)	p_{max} Corrected to $C_2 = 0$ According to Eq. 1*
4	51.5	0	330	330
8	51.5	0.2	370	320 (Group 8c)
9	51.5	0.4	415	310 (Group 9c)
5	51.5	0	450	450
12	51.5	0.2	605	455 (Group 12c)
6	51.5	0.4	730	430 (Group 6c)
16	16	0	20.1	20.1
23	16	0.1	67.3	23.1
30	26.8	0	235	235
31	26.8	0.05	295	242
27	26.8	0.1	359	253
29	26.8	0.2	499	270
14	32.5	0	263	263
21	32.5	0.1	411	274
3	51.5	0	181	181
10	51.5	0.2	336	185 (Group 10c)
11	51.5	0.4	470	195 (Group 11c)
15	43.5	0	337	337
22	43.5	0.1	557	357

*Obtained by subtracting the pressure rise due to a finite pressurizer volume as given by Eq. 6, namely, the $C_2 m_e / \gamma_2$ term and the pressure rise due to change in F with change in C_2.

system (equivalent to varying the ratio of amount of fuel held in the high-pressure system to that in the low-pressure system), and rate of addition of pure heavy water to the high-pressure system. Additional calculations are in progress to show the effect of total pressure variation (i.e., overpressure). The figures show that the factors studied become increasingly important percentage-wise as the temperature rises and the stability declines. Of interest is the fact that the power removal temperature coefficient varies almost linearly with fuel feed pump rate and heavy-water feed rate. Another view of the relative value of the kinds of changes studied is shown in Figs. 1.10 and 1.11, where the limiting value of a vs T is plotted for high values of factors. It is seen, for example, that by increasing the fuel feed rate to 1.6 gpm it is possible to make the reactor as stable as when gas production was just suppressed by copper addition.

Evidently, walk-away could be prevented by automatic control devices which could change a to lower positive values or even negative values, if necessary, and such controls are a part of the HRT design. The study indicates, however, that inherent reactor properties, such as overpressure, can be adjusted to make homogeneous reactors stable against walk-away. Indeed, *any* procedure which acts to keep the core concentration from rising, such as by preventing radiolytic decomposition, by water replacement, or by lowering the rate at which water is removed from the high-pressure system, will restrain walk-away.

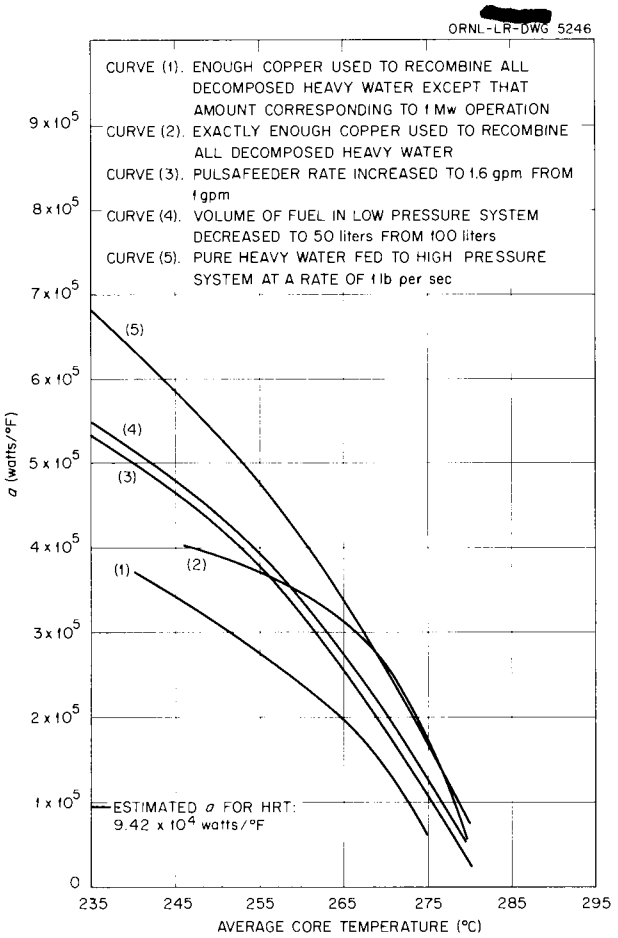

Fig. 1.10. Variation of Limiting Value of Power Removal Temperature Coefficient *a* in Watts Per Degree Fahrenheit vs Average Core Temperature for the HRT Operated at 10 Mw.

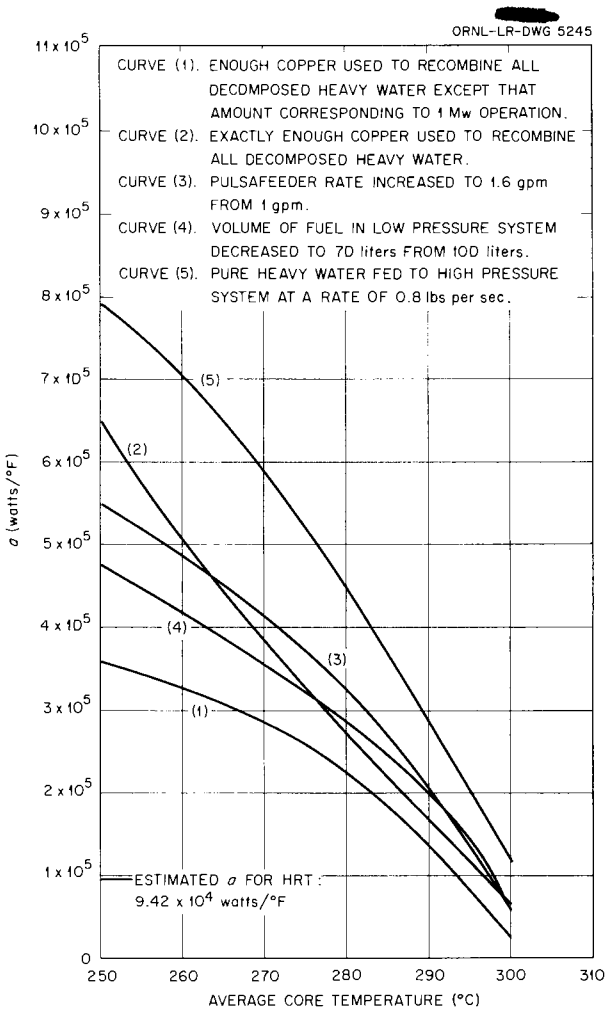

Fig. 1.11. Variation of Limiting Value of Power Removal Temperature Coefficient *a* in Watts Per Degree Fahrenheit vs Average Core Temperature for the HRT Operated at 5 Mw.

1.4 COMPONENT DEVELOPMENT

C. B. Graham

L. J. Bell, P. H. Harley, J. S. Culver, W. L. Ross, K. E. Estes, J. W. Skillern, C. H. Gabbard, I. Spiewak, L. F. Goode, D. S. Toomb, J. A. Hafford, R. E. Wascher

E. L. Youngblood

1.4.1 Pump Development

L. J. Bell, C. C. Hurtt, K. E. Estes, W. L. Ross, R. E. Wascher

Four of the five HRT-size pumps on order from Westinghouse have been received. Testing of the first 400A pump is described below. The second model 400A pump, which was designated for long-range pump development, was found to have a defective stainless steel pump casing. During welding of the pump suction nozzle to the test loop piping, cracks were discovered in the weld bevel of the nozzle. Subsequent examination, by Dy-check on the inside and x ray through the metal of the nozzle, disclosed numerous cracks or voids. The casing was returned to Westinghouse for further examination and repair or replacement. Similar examination of the other two pumps did not reveal defective material. The model 230A pump was disassembled and inspected, and its

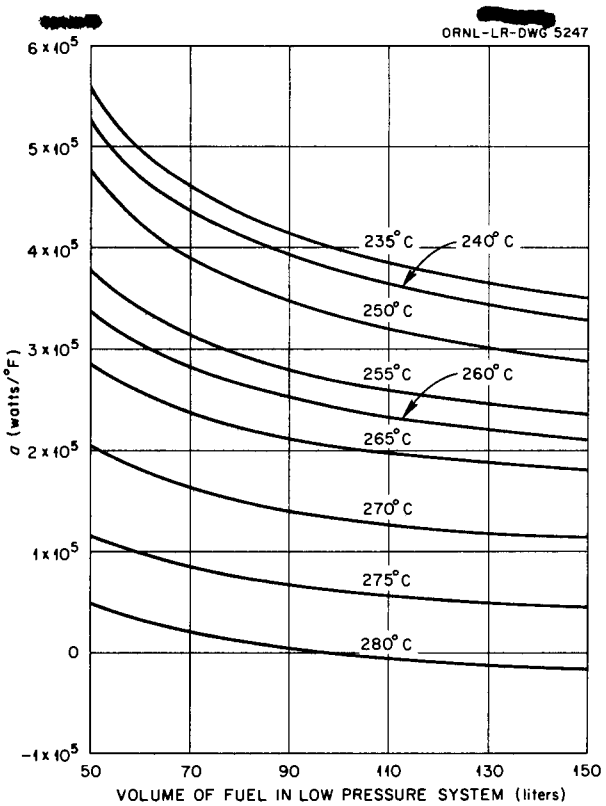

Fig. 1.12. Variation of Limiting Value of Power Removal Temperature Coefficient *a* in Watts Per Degree Fahrenheit vs Volume of Fuel in Low-Pressure System in Liters for the HRT Operated at 10 Mw at Various Core Temperatures. Enough copper was used to recombine all decomposed heavy water except that amount corresponding to 1 Mw operation.

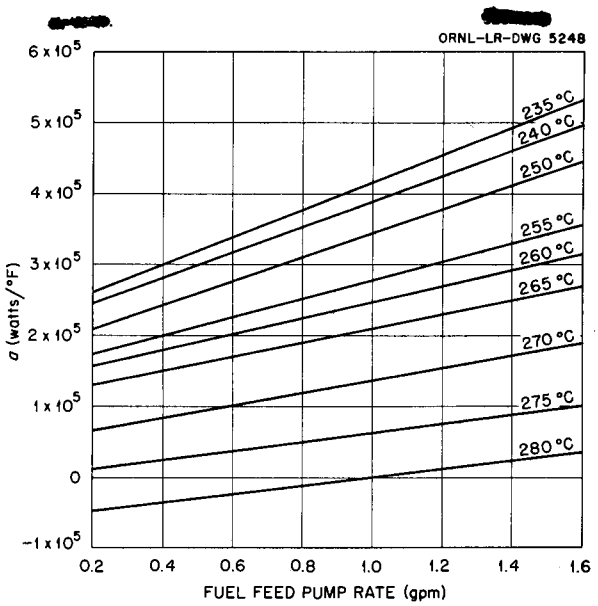

Fig. 1.13. Variation of Limiting Value of Power Removal Temperature Coefficient *a* in Watts Per Degree Fahrenheit vs Pulsafeeder Rate in Gallons Per Minute for the HRT Operated at 10 Mw at Various Core Temperatures. Enough copper used to recombine all decomposed heavy water except that amount corresponding to 1 Mw operation.

critical parts were measured, reassembled, and installed in the HRT mockup loop. The model 200A pump was received and turned over to the Engineering Research Group for operation on slurry. The fifth and last pump has been shipped.

The first Westinghouse 400A pump was installed and was operated for a short time with water. The test loop for the pump was described previously.[22] After it was checked for wear, the pump was put through 75 reduced voltage startups, 200 conventional starts and stops, and 20 startups with reverse rotation, when the rotation is switched to forward after a few seconds. With reverse rotation the pump delivered approximately 110 gpm, in comparison to the normal flow of 400 gpm. After this series of tests, the pump was dismantled. It was discovered that the shaft had been galled by the labyrinth seal in the thermal barrier or by a metal chip caught between the seal and the shaft. No other damage was observed. The two surfaces were dressed and the pump was reassembled. After the loop was chemically cleansed, it operated with water for 80 hr and then with a UO_2SO_4 solution containing approximately 10 g of uranium per kilogram of solution, 0.005 *m* $CuSO_4$, and 10 mole % excess H_2SO_4 for approximately 70 hr, when a bearing failure caused the loop to be shut down.

As shown in Fig. 1.18, the failure resulted in severe loss of the Graphitar, both locally and generally. The wear was sufficient to allow the stainless steel bearing collar to rub on the Stellite shoes of the Kingsbury thrust bearing. Figure 1.19 shows the resulting wear on the outer and inner edges of the Stellite shoes. The remaining shoe surfaces were quite smooth and had only a few burnish marks.

[22] W. L. Ross, L. F. Goode, and R. E. Wascher, *HRP Quar. Prog. Rep. July 31, 1954*, ORNL-1772, p 36–37.

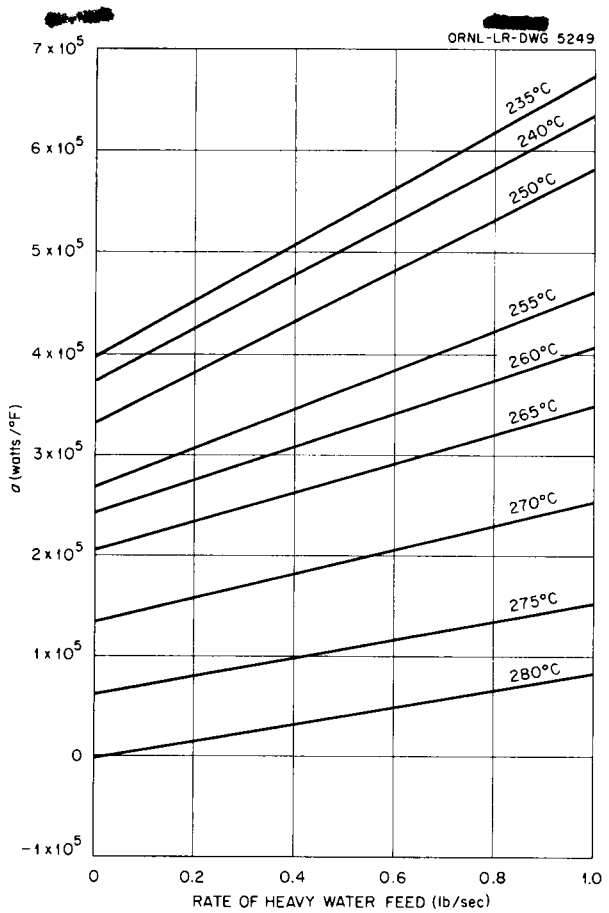

Fig. 1.14. Variation of Limiting Value of the Power Removal Temperature Coefficient *a* in Watts Per Degree Fahrenheit vs Rate of Heavy-Water Feed in Pounds Per Second for the HRT Operated at 10 Mw at Various Core Temperatures. Enough copper used to recombine all decomposed heavy water except that amount corresponding to 1 Mw operation.

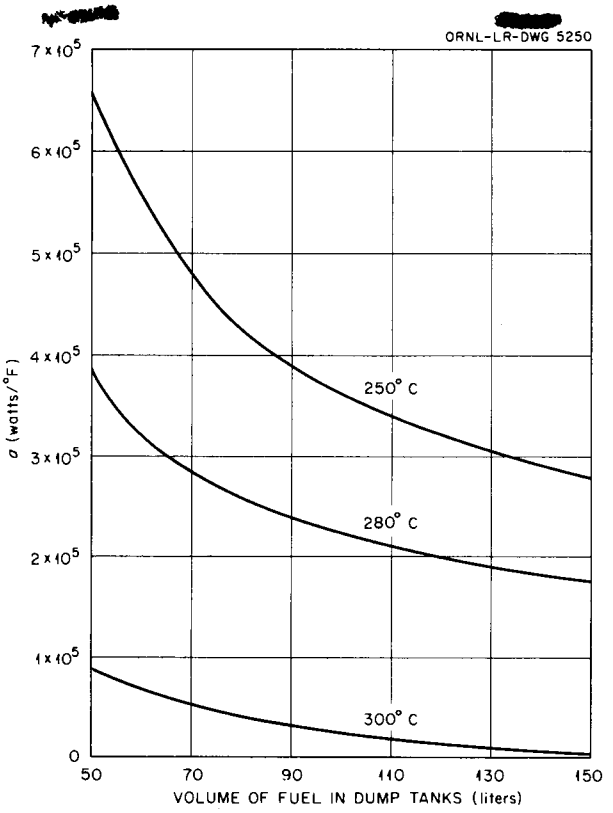

Fig. 1.15. Variation of Limiting Value of the Power Removal Temperature Coefficient *a* in Watts Per Degree Fahrenheit vs Volume of Fuel in Low-Pressure System for the HRT Operated at 5 Mw at Various Core Temperatures. Enough copper used to recombine all decomposed heavy water except that amount corresponding to 1 Mw operation.

In the central region of each shoe was what appeared to be a subsurface stain, observed as a dark area in Fig. 1.19. The reason for the bearing failure has not been definitely established. The three causes considered to be most likely are: gas in the bearing (lack of lubricant), defective Graphitar, and/or seizure of the shoes and Graphitar.

The pump rotor and Kingsbury thrust bearing were replaced with spares from the Westinghouse 400A pump No. 2. The loop was again started up with the UO_2SO_4 solution described above and was run about 522 hr at a temperature of 495° F and a pressure of approximately 1400 psi. At the end of the run, the temperature was raised to about 550° F and the pressure to 1600 psi in an attempt to attain an operating temperature of 572° F. Apparently more thermal insulation and/or more heaters will be needed on the loop to reach 572° F. The pump has now operated for a total of 679 hr.

Figure 1.20 shows the changes in concentration of uranium sulfate, copper sulfate, soluble nickel, and pH of the loop solution during the first 15 days of the run. The soluble nickel increased with time. Uranium, after a slight decrease in concentration at the start, appears to have leveled out to a constant value.

Examination of the pump parts after 679 hr revealed no significant corrosion, erosion, or wear.

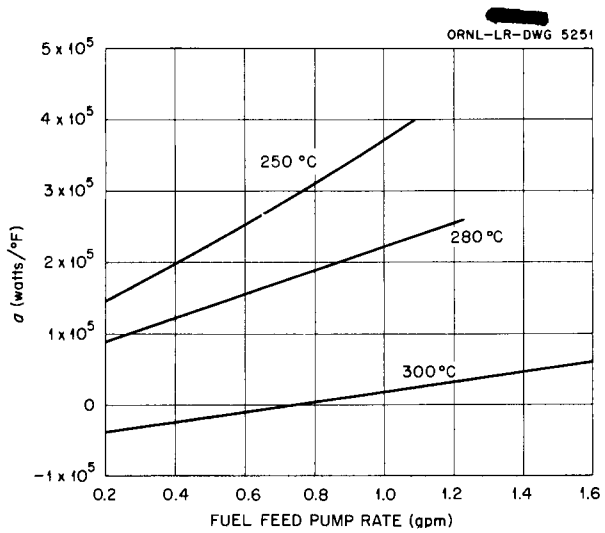

Fig. 1.16. Variation of Limiting Value of the Power Removal Coefficient *a* in Watts Per Degree Fahrenheit vs Pulsafeeder Rate in Gallons Per Minute for the HRT Operated at 5 Mw at Various Core Temperatures. Enough copper used to recombine all decomposed heavy water except that amount corresponding to 1 Mw operation.

All bearing surfaces appeared to be in very good condition and showed no measurable wear. The hubs of the pump impeller showed slight wear where the wearing rings had rubbed. The passive film apparently re-formed successfully, since no corrosion was observed. The shaft, including the section which goes through the seal rings of the thermal barrier, showed no wear. Also, the diffuser and scroll of the pump casing suffered no damage.

After the bearing failure, a thermocouple hole was drilled into the pump flange as shown in Fig. 1.21. Any gas-binding in the motor end of the pump should result in a change in temperature at the flange. The normal flow in the motor end of the pump can be seen in Fig. 1.21. The new thermocouple proved to be more sensitive than the original one at the top of the pump. A series of samples was withdrawn from the back end of the pump through a gage glass to check for gas; no gas was found under normal running conditions. No indication of gas was detected by the new thermocouple. When a sample was withdrawn from the motor chamber, hot fluid flowed into the chamber from the loop. This resulted in an immediate increase in temperature at the thermocouple.

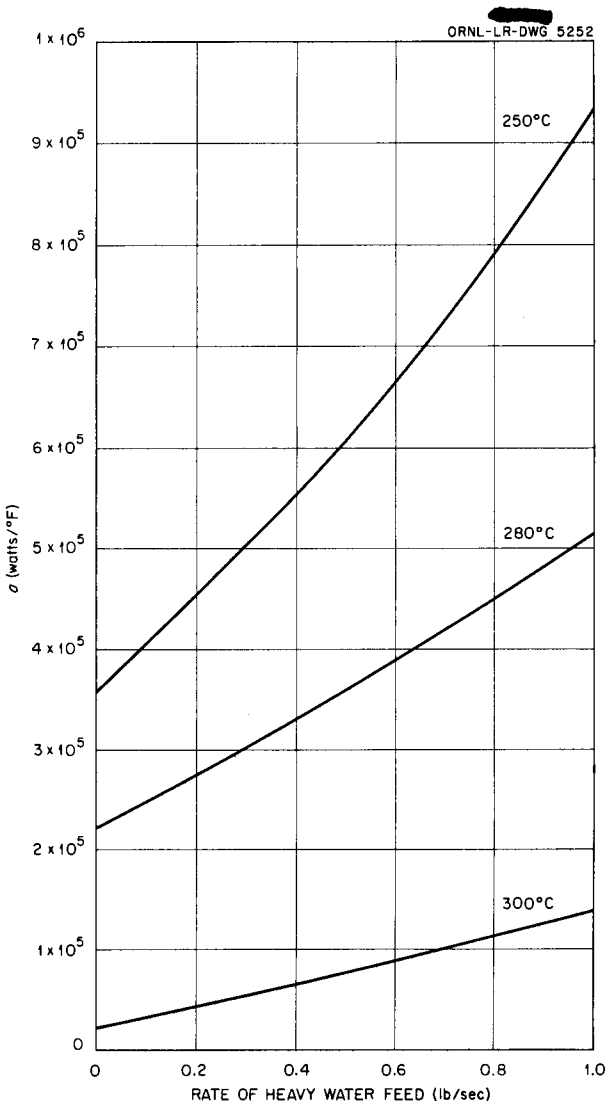

Fig. 1.17. Variation of Limiting Value of the Power Removal Temperature Coefficient *a* in Watts Per Degree Fahrenheit vs Rate of Heavy-Water Feed to the High-Pressure System in Pounds Per Second for the HRT Operated at 5 Mw at Various Core Temperatures. Enough copper used to recombine all decomposed heavy water except that amount corresponding to 1 Mw operation.

The difference of pressure between the back end of the pump and a pipe tap in the suction line of the pump was measured. It was discovered that the pressure in the suction line was higher by about $5\frac{1}{2}$ to 6 ft H_2O than the pressure at the

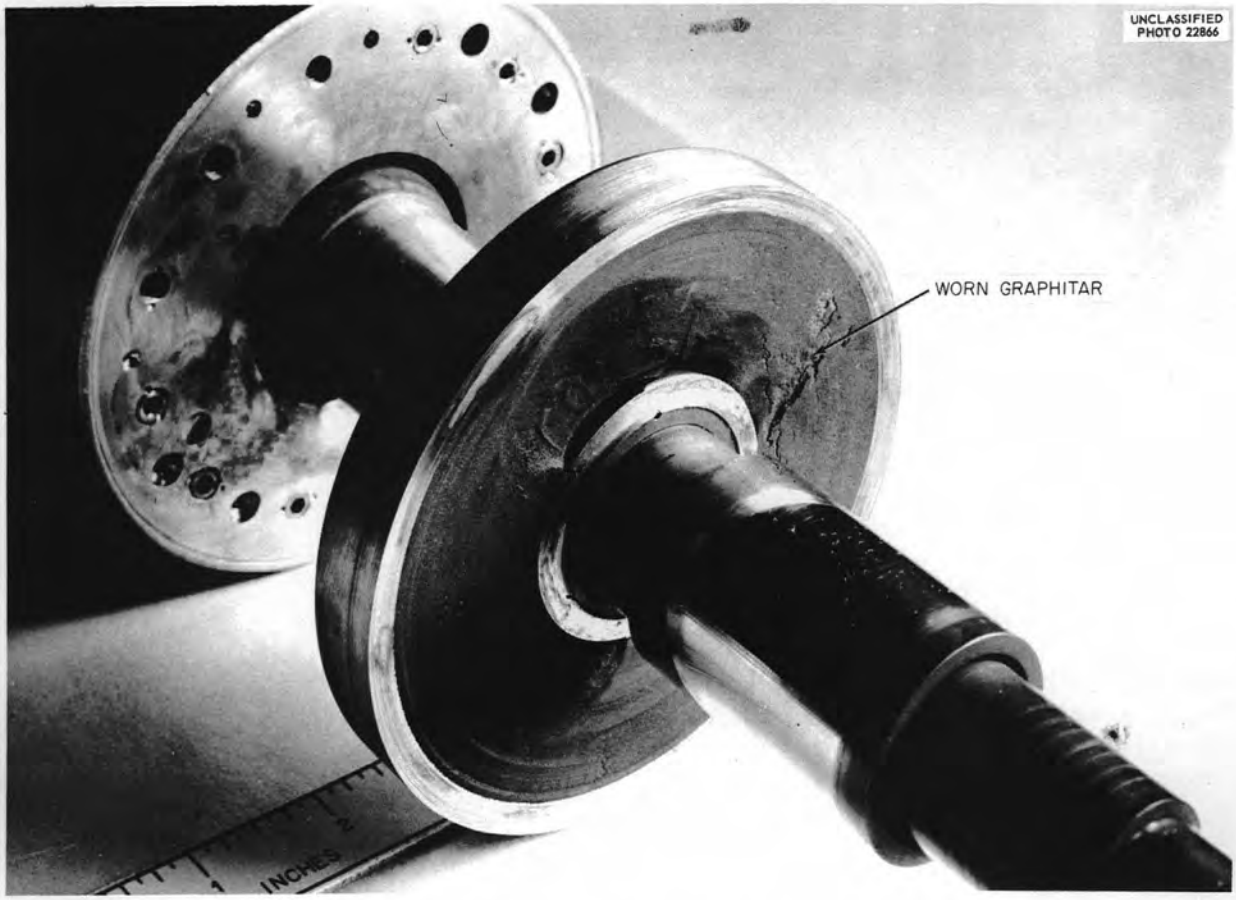

Fig. 1.18. Failure of 400A Thrust-Bearing Runner.

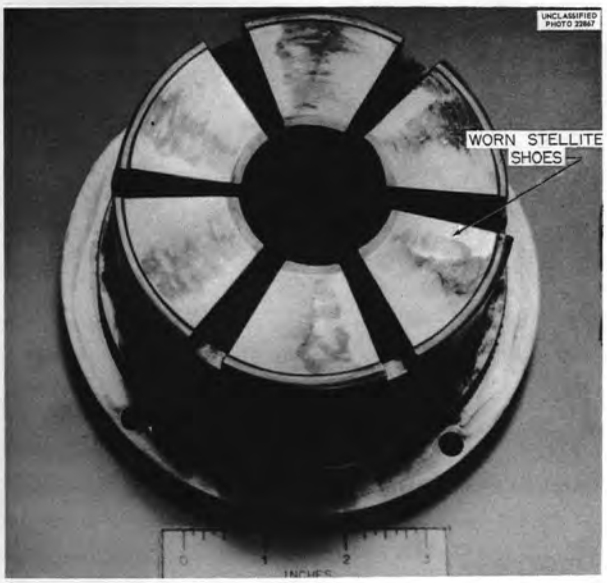

Fig. 1.19. Worn 400A Kingsbury Thrust Bearing.

back of the pump. It must be realized that this differential is dependent upon the clearance of the upper wearing ring and the balance parts of the impeller. This means that the back of the pump must be vented to a pressure lower than that of the operating loop.

1.4.2 Fuel and Blanket Pumps

L. J. Bell W. L. Ross
R. E. Wascher

Fabrication of one 230-gpm and one 400-gpm pump for the HRT is approximately 60% complete. Except for the substitution of stainless steel for a few titanium parts, ORNL specifications HRT-1028 and HRT-1005 will be followed in the first 230- and 400-gpm units. Fabrication should begin soon on an alternate of each of the above pumps with titanium metal for parts which are subject to high velocity and turbulence at temper-

ORNL-LR-DWG 5253

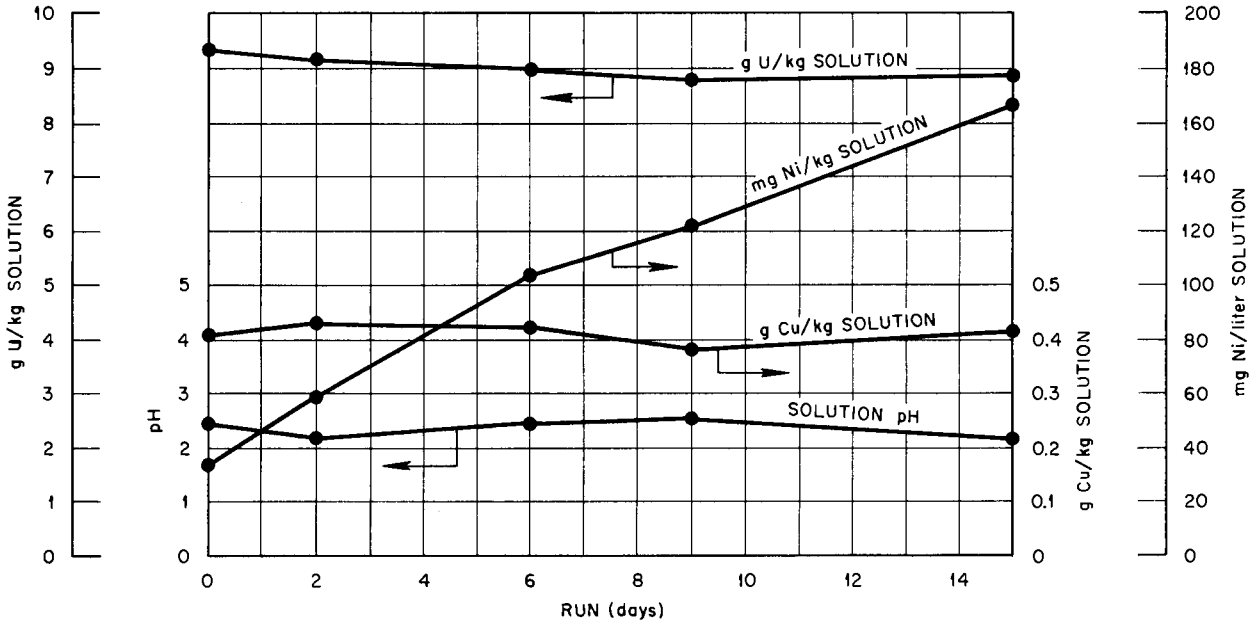

Fig. 1.20. Concentration Changes of UO_2SO_4 Solution.

atures above 212° F. The latter two will be built strictly according to the two specifications.

Samples of all materials used in the first two pumps were received. Certified papers on properties and on chemical analysis and nitric acid corrosion tests indicate that 20 items are acceptable for the intended service. Two items failed to pass the corrosion tests. Nine items do not have the proper papers or have not completed the required corrosion tests.

1.4.3 High-Pressure Feed Pumps

J. M. Baker J. S. Culver
E. L. Youngblood

The injection pumps in the HRT will combine HRE-type diaphragm pumping heads, of improved design, with a new hydraulic drive. They will have to feed both liquid and oxygen into the high-pressure system. The diaphragm heads are being built in the ORNL shops.

The hydraulic drive units and isolation systems for these pumps are being purchased from Scott & Williams, Inc. The hydraulic unit will be equipped with a variable volume pump, which will be controlled remotely by a positioned air cylinder. The oil pump is provided with an internal adjustment which limits the maximum output. Although the designs for the two are identical, the fuel pump can thus be set to deliver 0 to $1\frac{1}{2}$ gpm and the reflector pump to deliver 0 to $3\frac{1}{2}$ gpm.

The operating characteristics and limitations of the feed pumps are being determined in a system simulating reactor geometry and conditions. Tests are in progress to determine pump output as a function of suction temperature, suction pressure, and oxygen addition rate.

1.4.4 Heat Exchanger

L. F. Goode W. L. Ross

Fabrication of the HRT fuel and blanket heat exchangers at the Foster Wheeler plant in Carteret, N.J. is well along. The clad tube sheets, which were accepted on the basis of HRP specifications plus ultrasonic examination, are being welded to the steam drum shells. The raw forgings from which the heads are machined ($28\frac{3}{4}$-in. OD × 3-in.-thick type 347 stainless steel clad on 8 in. of carbon steel) passed ultrasonic examination and are undergoing specified HRP tests. All tubing which is scheduled for installation in the two units was accepted by ultrasonic and magnetic eddy

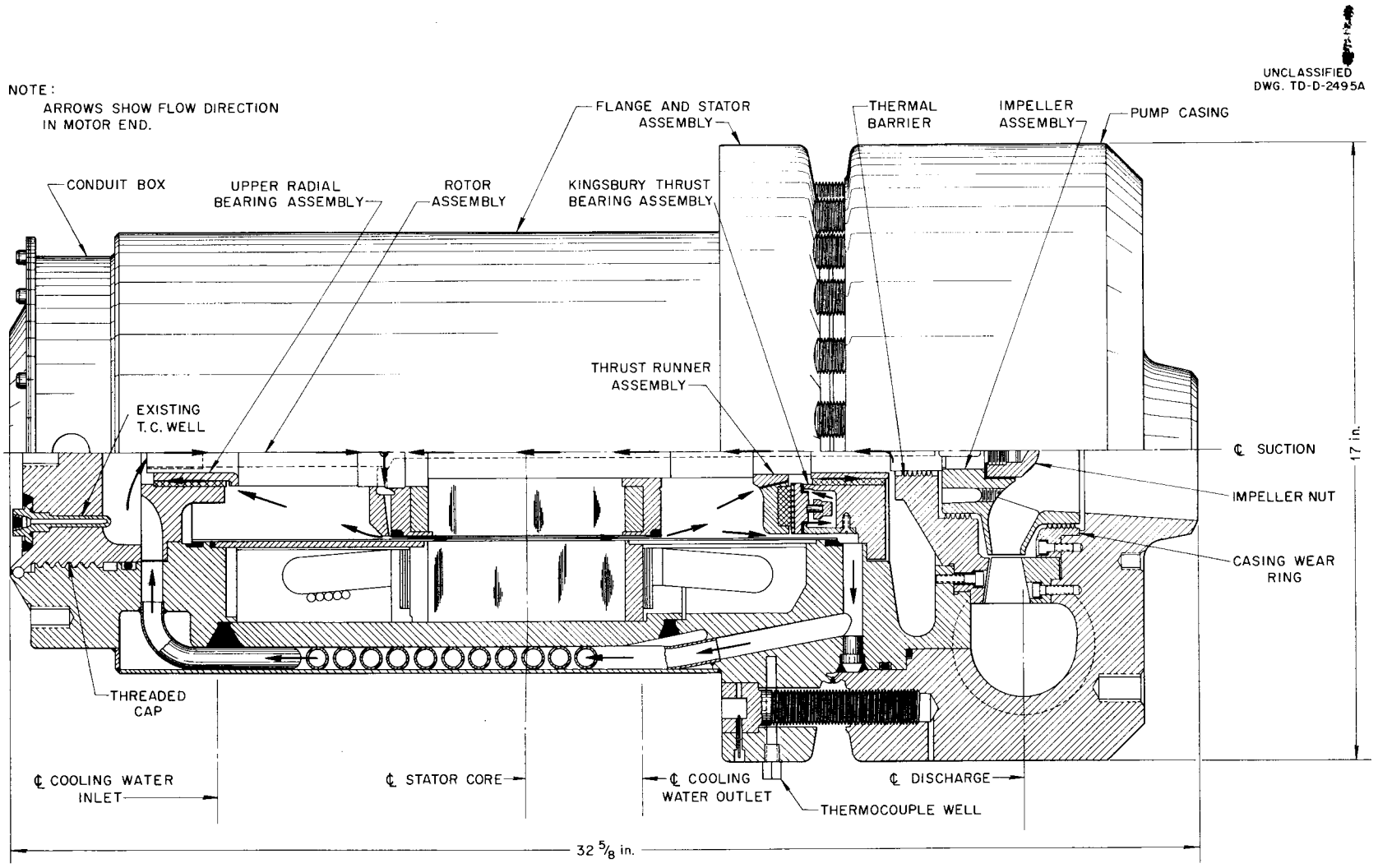

Fig. 1.21. 400A Centrifugal Pump.

current inspection methods. The tubing inspection is discussed in detail in Sec. 6.6.

A delay of about two weeks was experienced in obtaining the clad tube sheets. Therefore, the delivery date of the two exchangers is now tentatively set for March 31, 1955.

1.4.5 HRT Gas Separator Titanium Sleeve

J. A. Hafford J. W. Skillern
I. Spiewak

A titanium sleeve resembling that of the HRT gas separator was fabricated and thermal cycled inside a stainless steel pipe. The method of shrinking the sleeve into the pipe, with several weld-metal pads providing actual contact, was demonstrated to provide reliable contact at all temperatures up to 280°C. There was apparently no work-hardening or permanent set of the titanium after 21 thermal cycles between room temperature and 280°C.[23]

1.4.6 Fluid Flow in HRT Pressurizer

P. H. Harley I. Spiewak

Some experiments on the fluid flow in a model of the HRT pressurizer were reported previously.[24] A change in layout has made it necessary to modify the former arrangement of the pressurizer inlet so that it branches directly from a tee above the reactor core. This new arrangement (Fig. 1.22) was tested and was shown to work satisfactorily.[25]

[23] J. A. Hafford and J. W. Skillern, *Test of Titanium Sleeve in HRT Gas Separator*, ORNL CF-54-12-163 (Dec. 27, 1954).

[24] I. Spiewak and B. A. Hannaford, *HRP Quar. Prog. Rep. Oct. 31, 1954*, ORNL-1813, p 30–32.

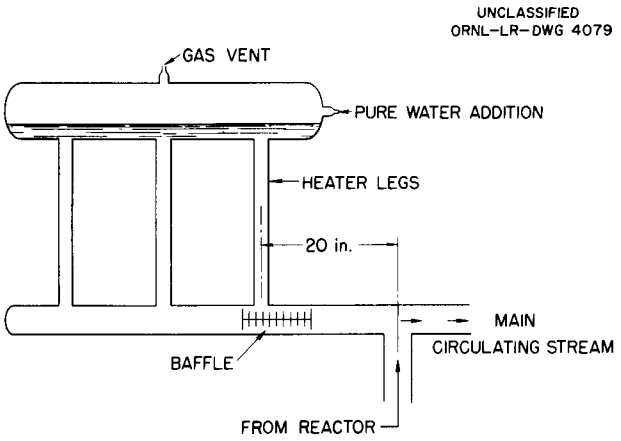

Fig. 1.22. HRT Pressurizer Flow Model.

A 3-gph flow of purge water to each leg was ample to prevent mixing between the heater legs and the main stream. However, a simple baffle was required to prevent main-stream turbulence from entering the heater legs.

The amount of gas collected in the new arrangement was quite low. With the baffle, gas at a rate of 0.3 cc/min was collected; without the baffle, no gas was collected. However, when the baffle was moved closer to the main stream, it intercepted a large eddy and sent considerably more gas into the pressurizer.

1.4.7 HRT Dump Test[26]

J. S. Culver S. R. West
C. H. Gabbard R. J. Lockett
D. S. Toomb

Construction of the first phase of the HRT dump test (Fig. 1.23), which involves the study of dumping from a single vessel, was completed. Two exploratory dumps were carried out successfully, and the system is now being operated in order to obtain fundamental data on flow rates and pressure gradients which might be expected when liquid is emptied from the reactor.

All material is on hand for the second phase of the test in which two concentric vessels will be dumped to simulate a simultaneous dump of the reactor core and blanket.

1.4.8 HRT Mockup Loop[27]

J. A. Hafford J. W. Skillern
A. L. Johnson I. Spiewak
D. S. Toomb

The construction of the HRT mockup is near completion (Fig. 1.24). The remaining work consists in connecting instrument lines and electrical wiring. The final component, the fuel feed pump, will be installed early in February.

The 3000-psi air compressor which provides gas to the loop for letdown was operated satisfactorily. A hydrostatic test of the 80-kw boiler system was carried out during the week of January 24. A final hydrostatic test of the high-pressure system will

[25] P. H. Harley, *Fluid Flow in HRT Pressurizer, Report No. 2*, ORNL CF-54-11-56 (Nov. 11, 1954).

[26] R. B. Briggs *et al.*, *HRP Quar. Prog. Rep. July 31, 1954*, ORNL-1772, p 23.

[27] C. B. Graham *et al.*, *HRP Quar. Prog. Rep. April 30, 1954*, ORNL-1753, p 44.

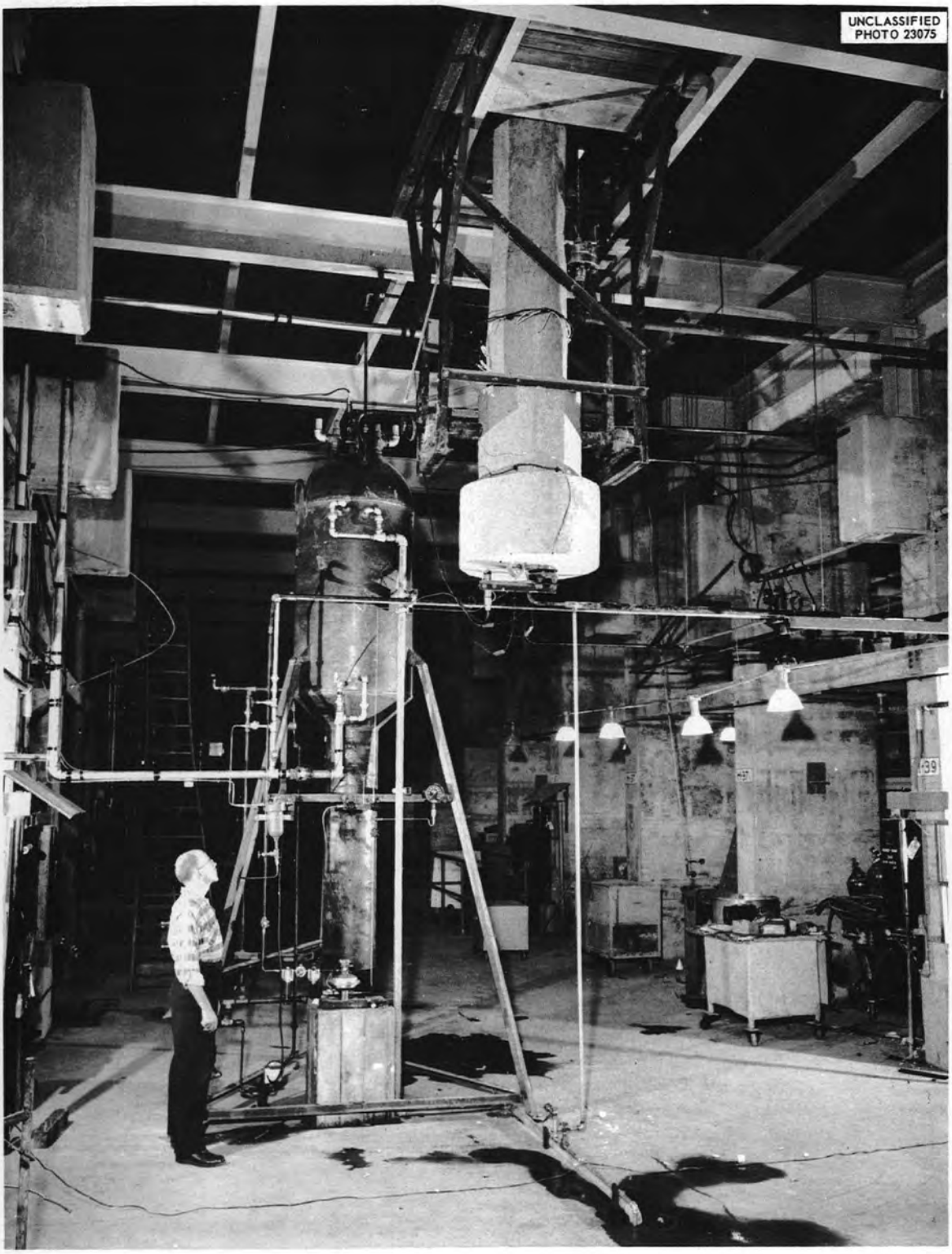

Fig. 1.23. HRT Dump Test.

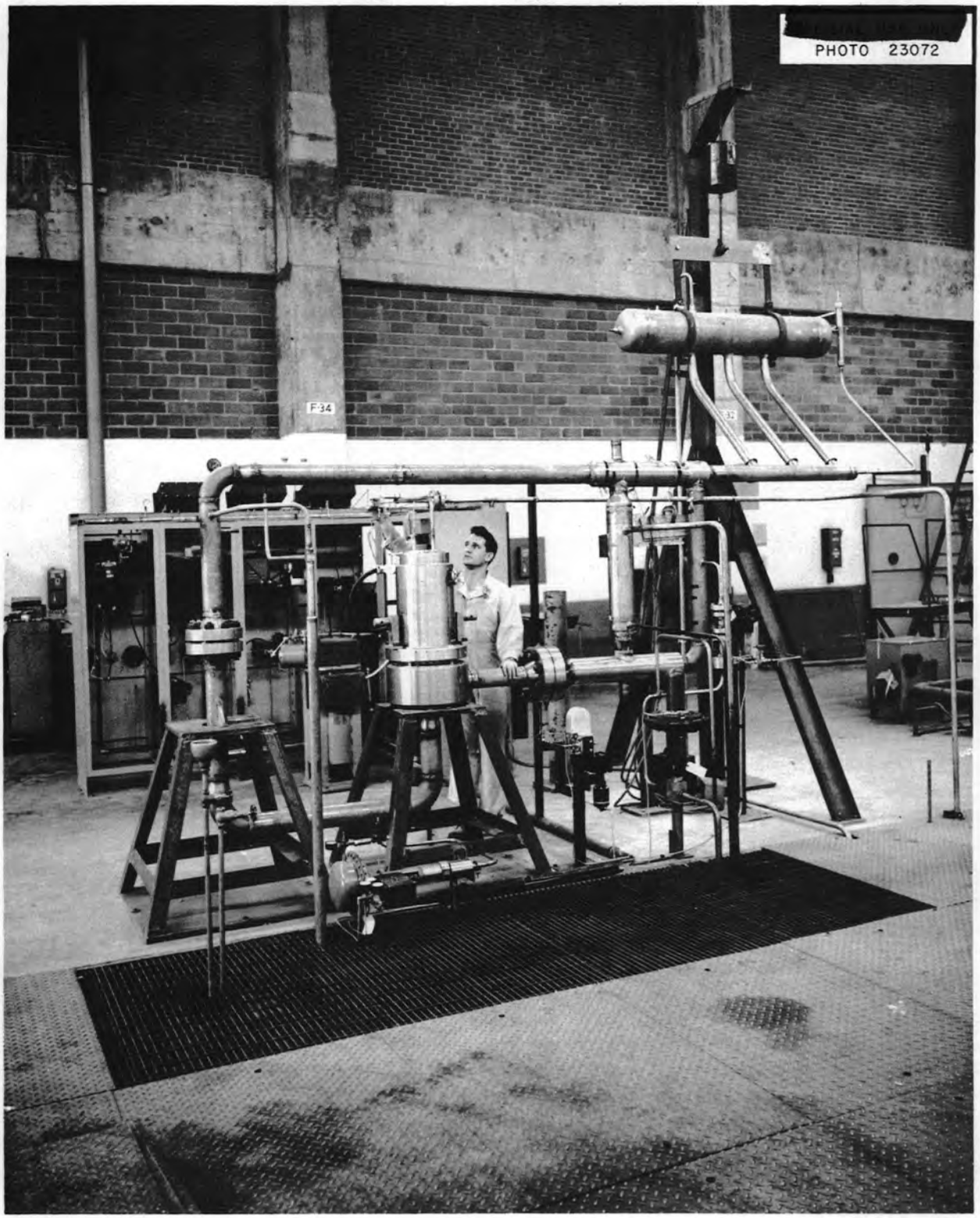

Fig. 1.24. HRT Mockup High-Pressure Loop.

fo[illegible] of the feed pump heads. The system will then be ready for operation.

1.5 CONTROLS AND INSTRUMENTS

W. P. Walker

M. C. Becker	R. L. Moore
A. M. Billings	R. F. Toucey
J. R. Brown	E. Vincens
J. C. Gundlach	K. W. West

1.5.1 General Design

In order to guarantee the leakage specification of the shield, air lines attached to the valves associated with high-pressure components will be blocked in the event of a rupture of these components. This will be accomplished either by solenoid valves, which will close upon pressure rise inside the shield, or by isolating pneumatic relays connected so as to vent to the instrument pits.

Design of the nuclear instrument thimble, through which the chambers for measuring reactor power will be inserted into the shield, was completed. Conduit layouts of the auxiliary instrument room and equipment in the reactor shield and below the control room were completed. A review of the procurement status shows that an expenditure of $80,000 has been committed, that $46,000 worth of equipment is out for bid, and that the total estimated to complete the procurement is $20,000. These give a total of $33,000 less than the original estimate of $179,000.

1.5.2 Component Development and Testing

(a) Electrical Pressure Seal. A pressure seal for electrical distribution into the reactor shield is required for the HRT to prevent the leakage of active gases into the control room area. A survey was made, and the seal manufactured by Stupakoff Ceramic & Mfg. Co., No. 95.0057, type V, was selected for ruggedness, current-carrying capacity, and ease of assembly. The manufacturer's rating for this unit is 450°F, 600 psi, and 30 amp. The HRT requirements are 140°F, 50 psi, and 25 amp. The following evaluation tests were performed on the seal:

1. pressure test, 300 psi H_2O, leaktight,
2. current test, 76 amp, 125°C rise,
3. temperature cycle test, 100°C instantaneous, leaktight,
4. leakage resistance throughout test, 7000 megohms,
5. impact test, 5 ft-lb shear, leaktight.

A sectional view of this seal is shown in Fig. 1.25.

(b) Thermocouple Pressure Seal. For the thermocouple seal, a packing gland type of seal has been selected for economy, accuracy of measurement, and ease of assembly. The requirement placed on this seal is leakage of less than 10^{-2} cc/min at 50 psi and 140°F for 20-gage Chromel-Alumel wire. Figure 1.26 shows the seal (manufactured by the Conax Corp.) with the lava insert that is crushed upon assembly.

Leakage with standard thermocouple wire (fiberglass braid on each wire, high-temperature varnished fiber-glass braid cover) proved to be excessive. Leakage with silicone-impregnated wire,

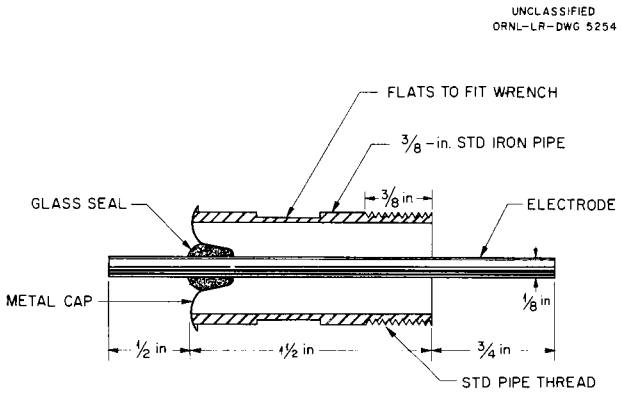

Fig. 1.25. Electrical Pressure Seal.

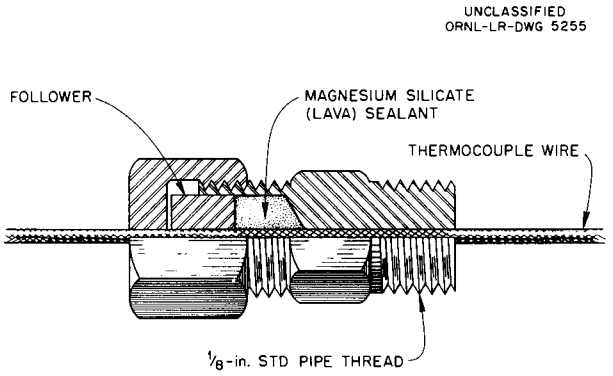

Fig. 1.26. Thermocouple Seal.

however, was satisfactory. The leakage test results are given below.

	100 psi of H_2O	Vacuum Leakage
Standard thermocouple wire	1 cc/min	30 cc/day
Silicone-impregnated wire	Leaktight	0.4 cc/day

The selected insulation is fiber-glass braid over phenol formaldyde enamel on each wire, with a silicone-alkyd copolymer varnish impregnated fiber-glass braid cover. Addition of enamel to each wire reduced the error encountered when the thermocouple wires were submerged in tap water. Supporting radiation tests on samples are in progress.

(c) Slow Startup of Westinghouse 400A Pump. In order to avoid adding excess reactivity at a high rate when the fuel circulating pump is started, it is necessary to ensure that the flow rate for the first minute of operation be as low as one-third of normal.

Two methods were investigated to reduce the flow rate: reduced voltage by the insertion of external resistance and reversed rotation of the pump.

The first method proved to be satisfactory for reducing the flow but had the disadvantages of requiring the pump to draw 200% current for the 1-min period and requiring the external resistance to be of 12-kw capacity.

The second method also proved to be satisfactory from the flow standpoint and to be much simpler electrically. The heat dissipation in the motor upon instantaneous reversal (the contactor time was 30 msec) was found to be 150% of normal starting dissipation and required 0.8 sec, compared with 0.55 sec, to complete. Additional tests will be performed to determine the effect of reversal on the pump thrust bearings.

(d) Process Monitoring. For process monitoring applications, the Jordan RAM system (manufactured by Jordan Electronic Mfg. Co., Inc.), shown in Fig. 1.27, was chosen. The remote unit contains an ionization chamber with an electrometer tube sealed inside and a remotely adjustable calibration source. The unit utilizes the logarithmic characteristic between grid current and plate current to cover a three-decade range. The external unit contains a meter with passive current-balancing circuits. Advantages of this unit are economy, simplicity, and physical size (4 × 4 × 6 in.). Stability tests indicate drifts up to 30% per week; however, the ability to calibrate the unit overcomes the disadvantage for process monitors in which orders of magnitude are the primary concern. In applications where detection causes the reactor to dump, dual units will be provided for increased reliability.

1.5.3 Valve Development

Further testing to develop a suitable bellows for the required ⅛-in. 2000-psi valve was performed.[28] Endurance tests of three Fulton-Sylphon bellows with ⅛-in. stroke at 250°C and 2000 psi were extended for periods in excess of 40,000 cycles before failure. These bellows are being incorporated in the ⅛-in. valve.

[28] J. N. Baird *et al.*, *HRP Quar. Prog. Rep. Oct. 31, 1954*, ORNL-1813, p 37.

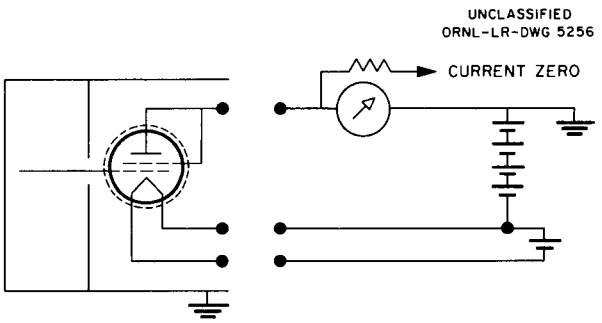

Fig. 1.27. Jordan Radiation Monitor.

Part II

THORIUM BREEDER REACTOR

J. A. Lane R. B. Briggs

2. CONCEPTUAL DESIGN

2.1 REACTOR ANALYSIS

M. C. Edlund
H. C. Claiborne M. Tobias

Investigation of the effects of major variables on the economics and characteristics of two-region thorium breeder-power reactors has been essentially completed. As reported previously,[1] the unit cost of electrical power is fairly insensitive to changes in the process variables.

The study of the effect of changes in the nuclear constants on the cost of electrical power has also been completed. The results show that the unit cost of electrical power is insensitive to rather large variations in these nuclear constants.

All results are for a three-reactor station supplying 375 Mw of electrical power at an assumed net station efficiency of 26%.

2.1.1 Effect of Major Process Variables

The results previously reported were based on an assumed cross section of 40 barns at 20°C for the group-3 poisons (fission-product poisons affected by chemical processing). As shown in Fig. 2.1, substitution of the latest cross-section estimate of 18 barns at 20°C causes the optimum poison level to shift from 7 to 6%. The net result is a cost reduction of about 0.1 mill/kwhr and a 0.01 increase in the breeding gain. Reducing the group-3 poison cross section by over a factor of 2 does not appreciably affect the optimum blanket thickness and optimum thorium concentration in the blanket for 5- and 6-ft cores (see Fig. 2.2).

Other than plant investment, the largest single cost is the inventory charge – nearly 1 mill/kwhr when values of 20 and 14 kw/liter are used for external power densities of the core and blanket systems, respectively. The effect of increasing these external power densities is shown in Fig. 2.3. Doubling the core external power density of 20 kw/liter gives a reduction in cost of 0.25 mill/kwhr, but doubling the blanket external power density of 14 kw/liter saves only 0.07 mill/kwhr. The savings realized from further increases in power density rapidly decrease.

For these calculations, it was assumed that no change in capital operating expense was necessary to achieve higher power densities. Consequently, probably only part of the indicated savings could be realized.

It is possible that engineering considerations will preclude core power densities appreciably over 100 kw/liter. It would then be necessary to increase the core size or to operate with a larger portion of the total power in the blanket. TBR type of reactors with 5- and 6-ft cores have power densities of about 200 and 122 kw/liter, respectively. In order to reduce the power density of the 5-ft core to 122 kw/liter, it would be necessary to operate with a U^{233} concentration in the blanket of about 12 g per kilogram of thorium. This would increase the cost of power to such a point that a 6-ft core would be more economical.

2.1.2 Effect of Changes in the Nuclear Constants

The principal conclusions presented in the previous HRP report[1] concerning the effect of changes in the nuclear constants have been substantiated.

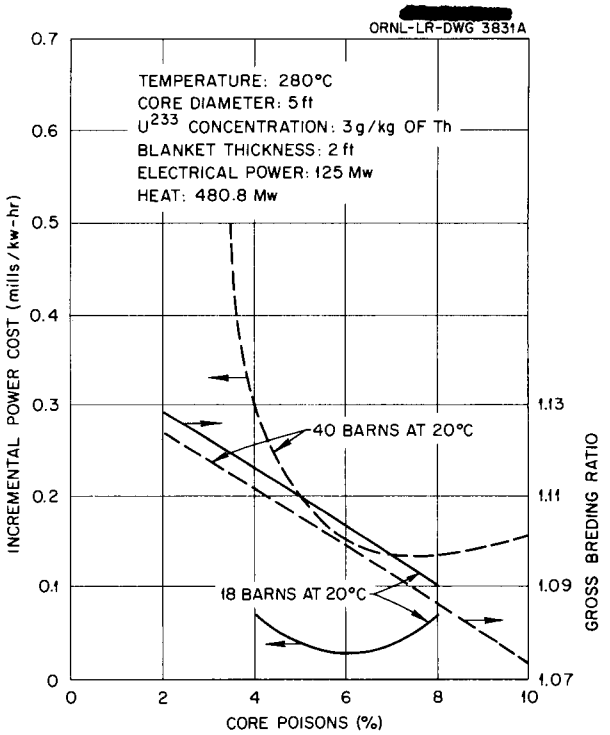

Fig. 2.1. Effect of Group-3 Poisons on Incremental Power Cost and Gross Breeding Ratio.

[1] M. C. Edlund *et al.*, *HRP Quar. Prog. Rep. Oct. 31, 1954*, ORNL-1813, p 44–47.

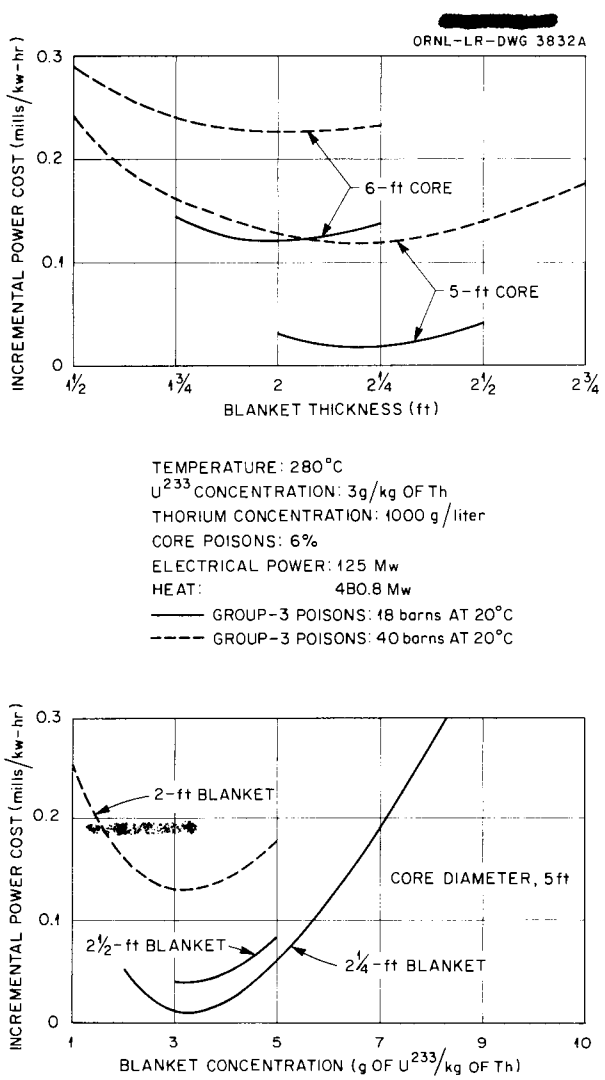

Fig. 2.2. Effect of Group-3 Poison Cross Section on Incremental Power Cost.

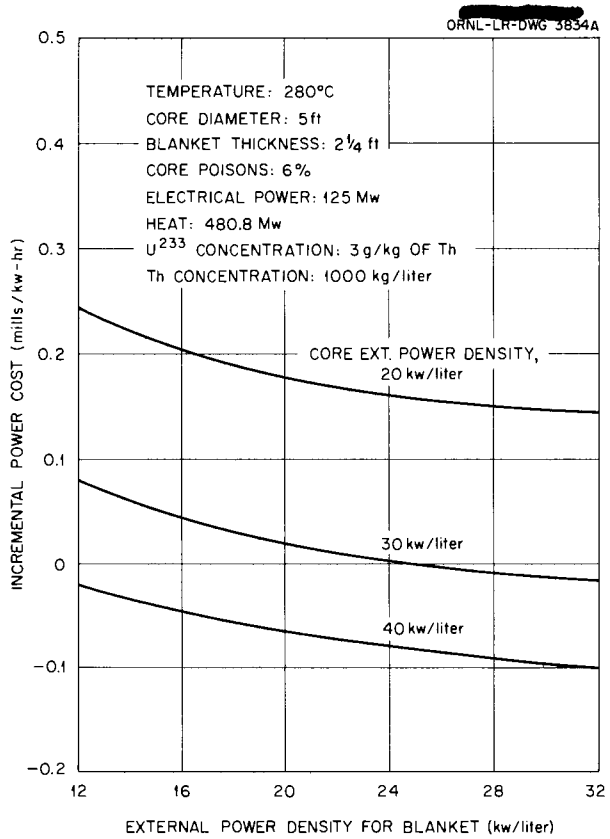

Fig. 2.3. Effect of External Power Densities on Incremental Power Cost.

Additional results which complete the study are presented in Table 2.1.

The most important cost increases were those produced by increases in the quantities τ_B, $\sigma_{a_{13}}$, and p_B and decreases in η. Increasing τ_B results in a rise in fast leakage at the expense of resonance capture in thorium, while all other neutron losses remain practically unaffected. Raising $\sigma_{a_{13}}$ causes protactinium absorption to rise at the expense of thorium capture, as well as a change in *core* isotope ratios leading to higher capture rates in U^{234}, U^{235}, and U^{236}. An increase in resonance escape probability, p_B, raises blanket power, increases leakage, depresses resonance capture, and increases thermal capture. A decrease in both resonance and thermal capture in thorium is the principal result of a decrease in $\eta(23)$ of 0.04 (1.7%).

Critical concentration was most strongly affected by τ_C, D_{2C}, and, naturally, η. A 50% rise in the first two produced a critical concentration increase of about 30%, while the 1.7% rise in $\eta(23)$ caused a 4.4% rise in the critical concentration. The breeding ratio was not significantly affected by changing either τ_C or D_{2C}.

No factor had a significant effect upon blanket processing except p_B, for which a decrease of 50% led to a 12% decrease in cycle time. The core Thorex cycle was affected mainly by the diffusion constants and τ_C; the greatest effect observed, produced by lowering D_{2C}, was a decrease of cycle time by about 134 days out of 337. However, no

TABLE 2.1. EFFECT OF SUBSTANTIAL CHANGES* IN THE NUCLEAR CONSTANTS**

Parameter, Standard Value	Parameter Deviation (%)	ΔC_T	ΔC_X	B	$B(G)$	$G(U)$
Extrapolation distance, 15.24 in.	−50	+0.03	−0.03	1.097	51.7	8.4
	+50	−0.01	+0.01	1.107	59.0	8.4
η, 2.32	−1.7	+0.10	−0.13	1.072	38.6	8.8
	+1.7	−0.12	+0.14	1.135	72.6	8.1
$\sigma_{a_{13}}$, 96.8	−50	−0.07	+0.08	1.124	66.3	7.8
	+50	+0.07	−0.09	1.086	45.7	9.0
τ_B, 212.4	−50	−0.09	+0.11	1.132	70.5	8.8
	−25	−0.02	+0.02	1.110	58.6	8.5
	+25	+0.02	−0.02	1.098	52.6	8.4
	+50	+0.10	−0.11	1.077	40.8	8.2
τ_C, 218	−50	−0.01	−0.02	1.099	52.8	6.7
	−25	0.00	0.00	1.103	55.1	8.0
	+25	+0.01	0.00	1.105	56.1	8.8
	+50	+0.03	+0.02	1.108	58.0	10.8
D_{1B}, 1.49	−50	−0.01	−0.01	1.101	54.0	7.5
	+50	+0.01	+0.01	1.106	56.4	9.0
D_{2B}, 1.173	−50	−0.01	+0.01	1.108	57.0	7.5
	+50	+0.03	−0.01	1.099	52.7	8.9
D_{1C}, 1.67	−50	−0.01	+0.02	1.107	57.1	9.5
	+50	0.00	−0.01	1.104	50.2	7.8
D_{2C}, 1.2304	−50	−0.02	−0.04	1.095	50.6	5.1
	+50	+0.03	+0.01	1.107	57.4	10.8
p_B, 0.56	−50	−0.05	+0.07	1.122	65.4	8.3
	+50	+0.08	−0.09	1.082	43.5	8.6
Combination case 1 (D's, τ's, and p high; extrapolation distance low)		+0.46	−0.41	1.004	1.22	15.4
Combination case 2 (D's, τ's, and p low; extrapolation distance high)		−0.22	+0.10	1.128	68.4	3.5

*The following properties were common to all the calculations performed:

Temperature, 280°C
W, grams of U^{233} per kilogram of thorium, 3
G_{02}, grams of thorium per liter, 1000
f_{pc}, poison fraction in core, 0.06
Reactor power, 480.8 Mw (125-Mw electrical output)
Core diameter, 5 ft
Pressure-vessel diameter, 9 ft
External power densities, kw/liter
Core system, 20
Blanket system, 14

**The symbols in column headings are defined as follows:

ΔC_T = incremental power cost, mills/kwhr,
ΔC_X = incremental credit for excess fissionable material produced, mills/kwhr,
B = breeding gain, atoms of fissionable material produced per atom of fuel burned,
$B(G)$ = net grams of fissionable material produced per day,
$G(U)$ = uranium concentration in core, grams of uranium per kilogram of heavy water.

significant changes were noted in either core or blanket chemical-processing costs.

2.2 ENGINEERING STUDIES

R. B. Korsmeyer
A. L. Gaines M. I. Lundin
P. N. Haubenreich R. G. McGrath[3]
M. C. Lawrence[2] C. L. Segaser
W. F. Taylor[4]

2.2.1 Immediate Program

Because of insufficient data, intelligent selection of a specific reactor design for detailed study is not possible at this time. Accordingly, the original program[5] has been modified to include preliminary investigation of four variants of the thorium breeder reactor with the hope that advances in technology will permit selection of one of them for further study later. With each of the four variants it was assumed that one or more of the fundamental engineering problems have been solved. They are given below.

(a) Case A – All Low-Pressure Recombination. The flow sheet, patterned after the HRT, will be based on the assumption that satisfactory letdown valves can be developed and that feed pumps will operate with great reliability over long periods of time.

(b) Case B – All High-Pressure Recombination. While layout and cost estimation of case A are in progress, the flow sheet will be revised on the assumption that safe and reliable high-pressure recombiners can be designed and will be utilized in both the core and blanket circulating systems. After completion of case A, the layout and cost estimation of case B will be undertaken.

(c) Case C – No External Recombination. During the layout of case B the flow sheet will again be revised on the assumption that all recombination will be accomplished internally in the core and blanket systems. It is believed that a method for removing iodine from the core and blanket fluids can be developed or, alternatively, that the penalty imposed by xenon poisoning can be offset by savings in investment or other operating charges. Any D_2 and O_2 that may appear as surplus will be recirculated until redissolved and recombined. After completion of case B, layout and cost estimation of case C will be undertaken.

(d) Case D – Boiling Blanket System. One of the above three schemes will be selected for a core system, and a boiling blanket system utilizing high-pressure recombination will be designed to go with it.

2.2.2 Turbine Plant Study

The cost influence of the larger turbine plant components and operating conditions for the first optimization of the TBR, sized to deliver 100 Mw of net electrical output per reactor (three reactors for the station), has been completed. The correlations developed are based on technical and cost data obtained from Westinghouse, General Electric, and Allis-Chalmers, largely through Pioneer Service & Engineering Co. Unit costs have been corrected as of 1954 by data from the *Handy Public Utility Construction Cost* (compiled and published by Whitman, Requardt & Assoc. and Benjamin L. Smith & Assoc.). Account numbers shown below refer to the Federal Power Commission uniform system of accounts.

(a) Turbine Plant Construction vs Steam Temperature. The collection of turbine plant costs vs steam temperature for dry and saturated steam at the throttle is shown in Fig. 2.4. The cost includes, for account 311, the turbine plant building with crane and normal fixtures and the screenhouse (prorated between boiler and turbogenerator on the basis of proportionate utilization of the total station building volume); for account 312, boiler feed system including heater and feed pumps and instruments and controls with panels and piping; for account 314, 100-Mw turbogenerator extras, support, condenser and auxiliaries, erection labor, and "other costs"; for account 315, accessory electrical equipment; for accounts 342 and 343, transmission plant; and for account 310, miscellaneous costs. The overhead and indirect charges are figured at an average of 13.3% of direct costs.

Comparison of Fig. 2.4 with corresponding data previously reported[6,7] will show a slight reduction

[2]On loan from General Dynamics Corp.

[3]On loan from Westinghouse Electric Corp.

[4]On loan from Pioneer Service & Engineering Co.

[5]M. C. Edlund *et al.*, *HRP Quar. Prog. Rep. Oct. 31, 1954*, ORNL-1813, p 43.

[6]R. B. Briggs, *Aqueous Homogeneous Reactors for Producing Central-Station Power*, ORNL-1642, Fig. 25 (May 4, 1954).

[7]J. D. Maloney, Jr., *Cost Estimates for Seven 200 Mw Turbine Plants for Operation with Nuclear Reactors at Various Steam Conditions*, ORNL-1387 (Dec. 23, 1952).

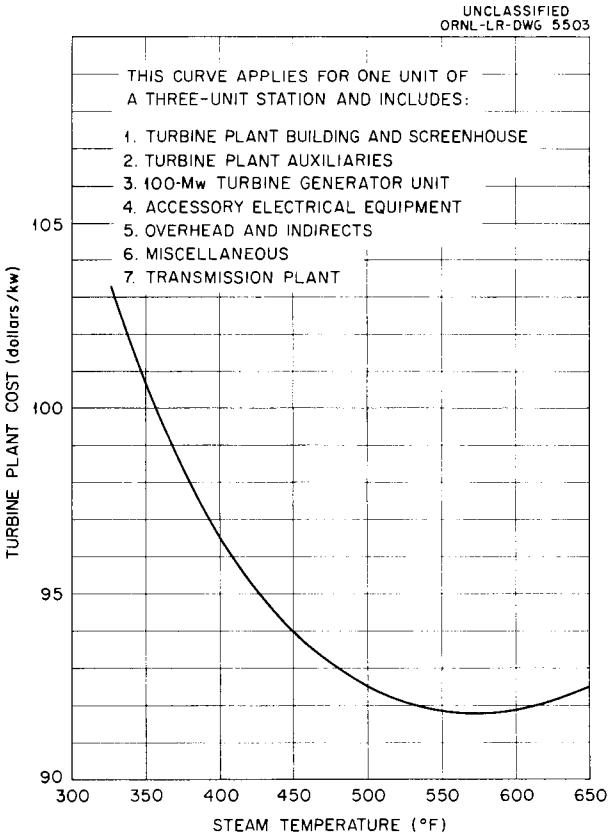

Fig. 2.4. Turbine Plant Cost vs Steam Temperature.

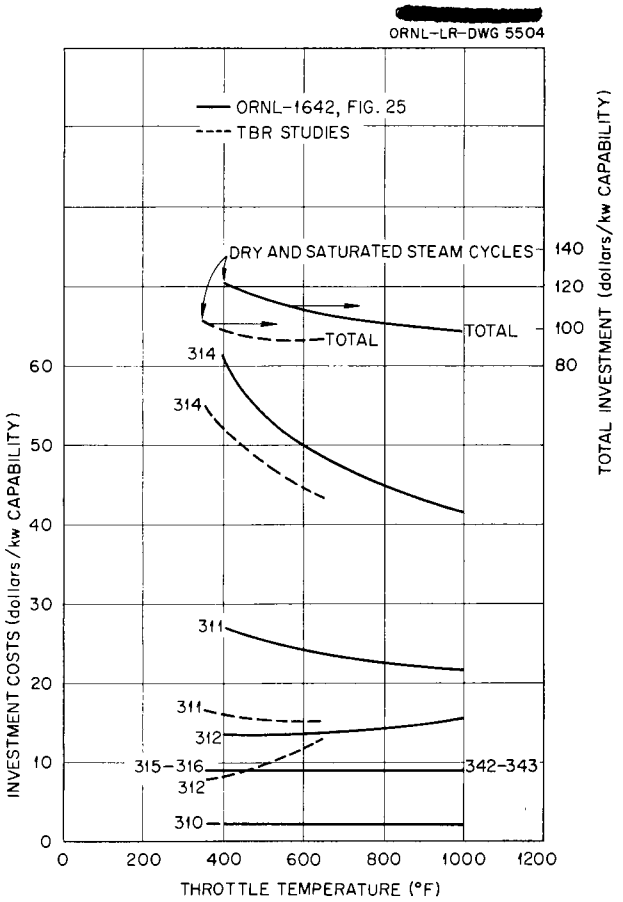

Fig. 2.5. Effect of Steam Conditions on Power-Plant Cost for 300-Mw Plant.

in the estimated turbogenerator investment with respect to accounts 311, 312, and 314. The lower estimate for account 311 results from a more reasonable prorating of the costs between the boiler plant and the turbogenerator plant. The lower estimate for the turbogenerator equipment (account 314) reflects the difference in the estimates presented in the Foster Wheeler–Pioneer Service report,[8] which is based on installation data for several stations in the 100-Mw range, and the extrapolation of the Johnsonville steam plant construction costs.[9] Since the feedwater heater and pumping costs comprise about 75% of account 312 and always increase with temperature and pressure, the effect of steam pressure on the cost is believed to be greater than indicated heretofore. At present more comprehensive cost data on feed pumps operating in the ranges pertinent to TBR operation are being sought. The estimates presented previously[10] are compared with the present estimate in Fig. 2.5.

(b) Turbine Cycle Efficiency vs Steam Temperature. The relation between turbine throttle flows and heat balance data for various dry and saturated steam cycles utilizing one moisture separator is shown in Fig. 2.6. The turbogenerators are 1800-rpm units exhausting at $1\frac{1}{2}$ in. Hg absolute and utilizing three stages of regenerative feedwater heating. The curve includes the feed enthalpy rise but has not been penalized for pumping power, inasmuch as the reactor heat load is to be determined on the basis of the estimated cycle efficiency in the optimization studies. A curve of net cycle

[8] R. M. Gould *et al.*, *A Survey of Reactor Systems for Central Station Power Generation*, NEA-5301 (Oct. 1953).

[9] J. D. Maloney, Jr., *Cost Estimates for Seven 200 Mw Turbine Plants for Operation with Nuclear Reactors at Various Steam Conditions*, ORNL-1387 (Dec. 23, 1952).

[10] R. B. Briggs, *Aqueous Homogeneous Reactors for Producing Central-Station Power*, ORNL-1642, Fig. 25 (May 4, 1954).

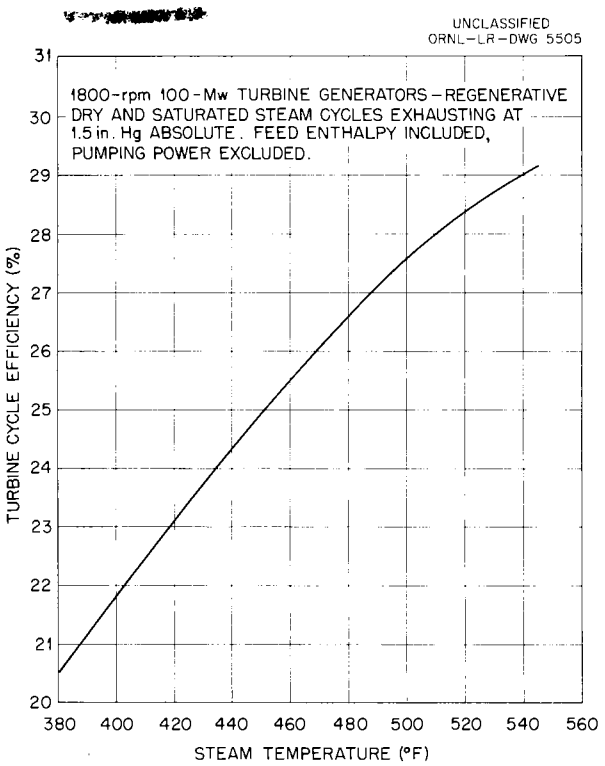

Fig. 2.6. Turbine Cycle Efficiency vs Temperature.

efficiency would therefore lie slightly below the one shown and increasingly so at the higher steam temperatures.

Since all details of heat economy could not profitably be considered for all steam temperatures, the curve undoubtedly indicates slightly lower efficiencies than can be achieved after a detailed investigation has been made of particular operating conditions (e.g., heat recovery from ejector steam), and such an investigation will be undertaken when operating conditions are selected for final design. The improvement expected, however, would increase the efficiencies shown by only about 1%.

A comparison with similar estimates[11,12] reveals that Fig. 2.6 shows a slightly lower efficiency, particularly at the lower steam temperatures, as a result of differences in estimated turbine efficiency in the lowest pressure stages. The data on which Fig. 2.6 is based were supplied by Westinghouse engineers currently studying the design of large, low-temperature turbines and are believed to be more realistic than data used heretofore.

(c) Turbine Plant Auxiliary Power vs Steam Temperature. The turbine plant auxiliary power includes all power necessary for feed pumps, circulating water pumps, condensate pumps and heaters, and separator drain and makeup requirements. The reactor power requirements are not included. The relation of the auxiliary power requirement to the steam temperature is shown in Fig. 2.7.

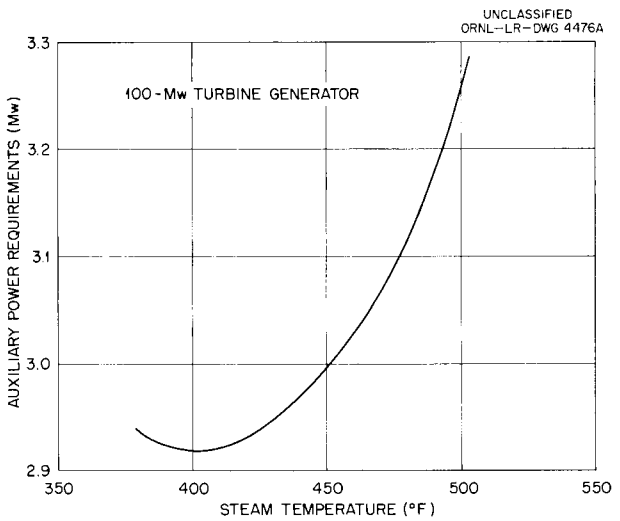

Fig. 2.7. Turbine Plant Auxiliary Power Requirements vs Temperature.

2.2.3 TBR Plant Optimization

(a) Core System. The characteristic data for the TBR presented in the last quarterly report[13] were used for calculating the relative annual charges associated with inventory, equipment cost, piping, pumping requirements, and turbine cycle efficiency for four average core temperatures, five steam temperatures, and four fluid velocities through the heat exchanger tubes. The core outlet temperatures were held at 300°C so that the steam temperature is related directly to the core inlet temperature. The family of curves relating incremental annual charges vs steam temperature is shown in Fig. 2.8.

[11] T. T. Shimazaki and C. H. Robbins, *Power Conversion in Nuclear Power Plants*, NAA-SR-278 (Aug. 15, 1954).

[12] N. A. Beldecos and A. K. Smith, *Comparative Performance of Turbine Generator Units in Saturated Steam Cycles*, WIAP-P-1 (July 1954) (ASME Paper 54-SA-65).

[13] R. B. Korsmeyer *et al.*, *HRP Quar. Prog. Rep. Oct. 31, 1954*, ORNL-1813, Table 2.4, p 51–52.

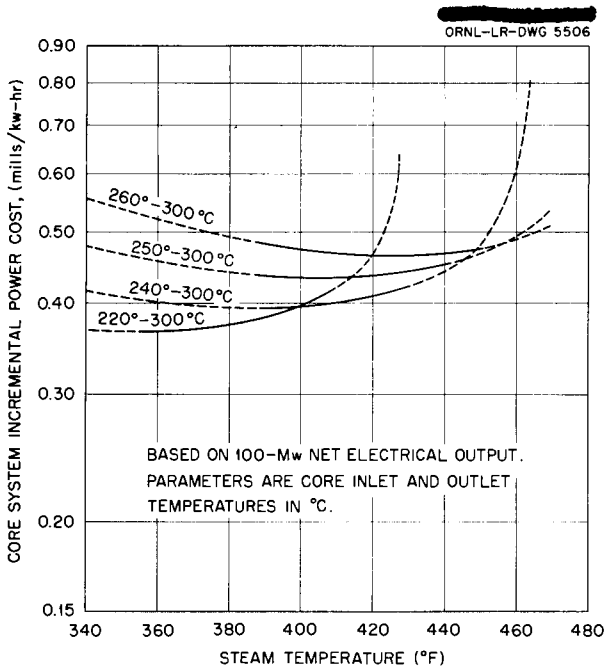

Fig. 2.8. Core System Incremental Power Cost vs Steam Temperature.

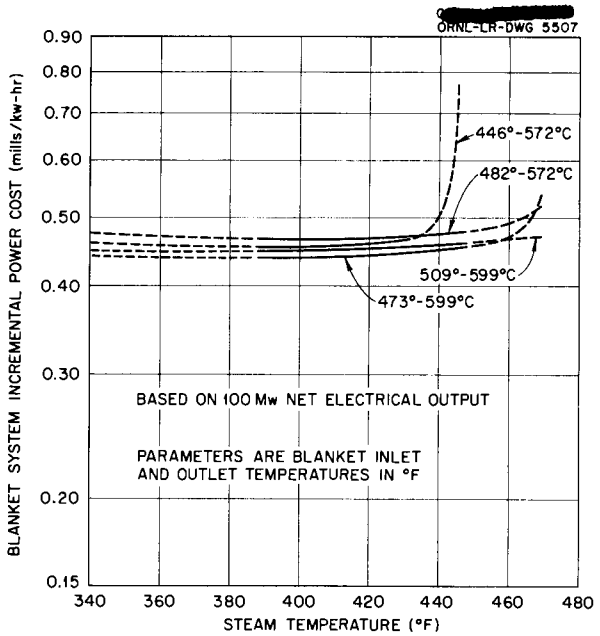

Fig. 2.9. Blanket System Incremental Power Cost vs Steam Temperature.

As seen in the figure, successively decreasing costs are obtained with decreasing core temperature, which relationship is true until very low thermal efficiencies are reached.

(b) Blanket System. A similar optimization of the blanket system was completed in which four combinations of inlet and outlet temperatures were examined, and the results are shown in Fig. 2.9. Unlike the core optimization, no particular restriction was placed on the blanket outlet temperature; the two outlet temperatures considered were 300 and 315°C. From Fig. 2.9 it is seen that the blanket variables do not have an appreciable influence on the plant optimization for reasonable approach temperatures in the heat exchanger.

(c) Over-all Optimization. Combining the core and blanket studies (Figs. 2.8 and 2.9) with the influence of steam temperature on turbogenerator investment (Fig. 2.4) gave the over-all plot shown in Fig. 2.10 of steam temperatures vs incremental operating cost for given core inlet temperatures. The curve for an average core temperature of 265°C (230°C inlet) was obtained by cross plot of the other data and reveals that the optimum combination is reached at this average core temperature and a steam temperature of about 410°F. Although not

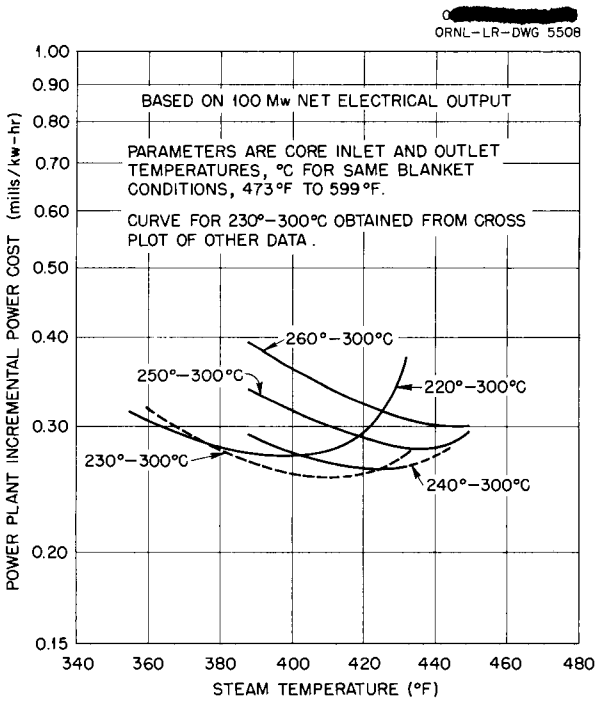

Fig. 2.10. Power Plant Incremental Power Cost vs Steam Temperature.

separately shown, Fig. 2.10 includes the influence of chemical processing, feed costs, inventory charges on fuel in storage, cost of D_2O makeup, and credit for excess U^{233} production. The cost of D_2O makeup was computed on the basis of 5% loss per year. The other items were obtained by interpolating and extrapolating the results of the Oracle study to obtain the values at the desired combinations of total power, specific powers, and temperatures. The data for the various core inlet-outlet temperature combinations are shown in Table 2.2.

(d) Corrosion Limitations. Since the optimum core inlet temperature and pipe velocity were outside the limit previously set from the standpoint of corrosion, the velocity and temperature limits were re-examined and were set at 35 fps and 250°C minimum. Inserting these limitations raised the optimum steam temperature to 436°F and penalized the operation by only $18,000 per year.

(e) Value of Heavy Water. A study has been completed to determine the possible reduction of total charges for the power plant if heavy water can be obtained for $20 per pound instead of $40 per pound. This study indicated that the reduction in annual costs may be about $145,000 for the lower value. Recalculation of the optimum velocities in the core and blanket pipe systems with the less expensive holdup charges indicated a reduction in (unrestricted) velocity of about 2 fps in each system (to about 38 fps in the core system and to about 27 fps in the blanket system). The effect on optimum steam temperature was negligible.

(f) Revision of Reactor Characteristics. The studies which were completed during the last quarter have resulted in changes in some of the characteristics of the TBR presented in the previous quarterly report. Characteristics of the reactor currently considered are summarized in Table 2.3. The steam temperature of 436°F, which was found to give the most economical power for the temperature restrictions placed on the core fluid, is considerably less than that assumed in previous studies. Because of the resultant decrease in thermal efficiency, the heat load is increased in order to hold the electrical output constant. However, the larger temperature difference between the reactor fluid and the steam results in smaller heat exchangers and reduced holdup. Changes in most of the other operating conditions are due to the higher power, lower holdup, and consequent higher specific power. In order to be consistent with the optimization calculations, the average temperature listed is the arithmetic average of the inlet and outlet temperatures. The mean power densities in the reactor are the average densities in the core and blanket regions. The power densities in the external systems are the ratio of heat removal rates divided by the volumes of fluid retained outside the reactor vessel.

(g) Influence of Cost Changes on Design Steam Temperature. Since the annual charges on the fixed investment are based on some rather arbitrary rules which may be changed in the future, the effect of large changes in the annual charges on the optimum steam temperature was investigated because the design of the entire turbogenerator plant is dependent on the steam temperature assumed. The effects of these changes are shown in Fig. 2.11, where the differential power cost is plotted vs steam temperature for the different accounting rules stated. The best information now available on the variation of power cost with steam temperature for the 275°C average core temperature

TABLE 2.2. POWER PLANT BASIC PARAMETERS vs CORE TEMPERATURE CONDITIONS

Core Temperature (°C)		Temperature of Minimum-Cost Steam (°F)	Steam Pressure (psia)	Turbine Cycle Efficiency (%)	Net Station Efficiency (%)	Core Heat Power (Mw)	Blanket* Heat Power (Mw)	Core Power Density (kw/liter)			Blanket Power Density (kw/liter)		
Inlet	Outlet							Reactor Core	Heat Exchanger	External System	Reactor Blanket	Heat Exchanger	External System
220	300	397	240	21.6	20.4	398	93	215	155	85	7.0	212	69
230	300	410	278	22.5	21.2	382	89	206	150	76	6.7	188	64
240	300	424	323	23.4	22.1	368	86	198	145	70	6.5	162	59
250	300	436	366	24.1	22.7	357	83	192	140	61	6.3	138	55
260	300	453	436	25.1	23.7	343	80	185	138	53	6.0	100	47

*Blanket temperature range fixed at 473 to 599°F.

TABLE 2.3. REACTOR CHARACTERISTICS FOR PRELIMINARY DESIGN OF A 300-Mw STATION

(Revised)

Net electrical capability per reactor, Mw	100
Steam temperature, °F	436
Steam pressure, psia	366
Turbine cycle efficiency, %	24.1
Net station efficiency, %	22.7
Reactor operating pressure, psia	2000

Item	Core	Blanket
Reactor Construction		
Material	Zircaloy 2	10% stainless-steel-lined carbon steel
Wall thickness, in.	0.5	5.0
Thermal shield thickness, in.		4.0
Space between shield and vessel, in.		1.0
Pipe connections	Concentric	Straight-through
Inside diameter	5 ft 0 in.	10 ft 5 in.
Blanket thickness		2 ft 3 in.
Volume, liters	1,855	13,200
Reactor Systems		
Operating temperature, °C (°F)		
Average	275 (527)	280 (536)
Inlet	250 (482)	245 (473)
Outlet	300 (572)	315 (599)
System volume, liters	7,700	14,700
Fluid composition	UO_2SO_4-D_2O-$CuSO_4$	ThO_2-D_2O-(U)
U^{233}	2.51 g per kg of D_2O	3.00 g/liter
U^{234}	2.23 g per kg of D_2O	0.19 g/liter
U^{235}	0.31 g per kg of D_2O	0.07 g/liter
U^{236}	3.54 g per kg of D_2O	0.00 g/liter
Uranium (total)	8.59 g per kg of D_2O	3.26 g/liter
Pa^{233}		1.34 g/liter
Thorium		1,000 g/liter
Inventory		
D_2O, kg	6,600	11,000
$U^{233} + U^{235}$, kg	18.7	45.1
Thorium, kg		14,700
Heat removal rate, Mw	358	82
Mean power density in reactor, kw/liter	193	6.2
Power density in external system, kw/liter	61	55

TABLE 2.3 (continued)

Item	Core	Blanket
Power density at surface of core tank, kw/liter	70.5	78
Thermal flux at core tank, neutrons/cm^2/sec	1.12×10^{15}	1.0×10^{15}
Total fission-product poisons, fraction	0.065	
Poison cross section, barns	18	
Gross breeding ratio		1.11
Net fissionable uranium produced, g/day		53.6
Total uranium produced, g/day		55.9
Circulation rate, gpm	26,200	4,400
Maximum fluid velocity, fps	35	21
G for D_2O decomposition, molecules of D_2O per 100 ev	1.67	
Rate of D_2 formation (no catalyst), lb-moles/sec	0.125	
Rate of O_2 formation (no catalyst), lb-moles/sec	0.062	
Gas in solution at outlet, g-moles/liter		
D_2	0.105	
O_2	0.052	
Volume of gas generated (no catalyst)		
At 300°C and 2000 psia, cfm (wet)	163	
At STP, cfm	3,970	
$CuSO_4$ concentration required for 100% recombination, g-moles/liter	0.005	
Fraction of total gas production (no catalyst) required to hold xenon poison to 1%	0.33	
Volume rate to hold xenon poison to 1% at 300°C and 2000 psia, cfm	54	
Chemical Processing		
Filtration cycle, days	1.0	
Thorex cycle, days	130	120
Processing rates		
Fluid (at reactor temperature), liters/day	58.3	126
Fluid (at room temperature), liters/day	44.8	100
$U^{233} + U^{235}$, g/day	141	386
Total uranium, g/day	430	410
Protactinium, g/day		168
Thorium, kg/day		126
Thorium feed rate, g/day		566
Cooling period to get $\leqq 3$ βw/liter, days	120	85
Thorex fissionable uranium inventory, kg	16.9	47.0
Thorex thorium inventory, kg		10,700

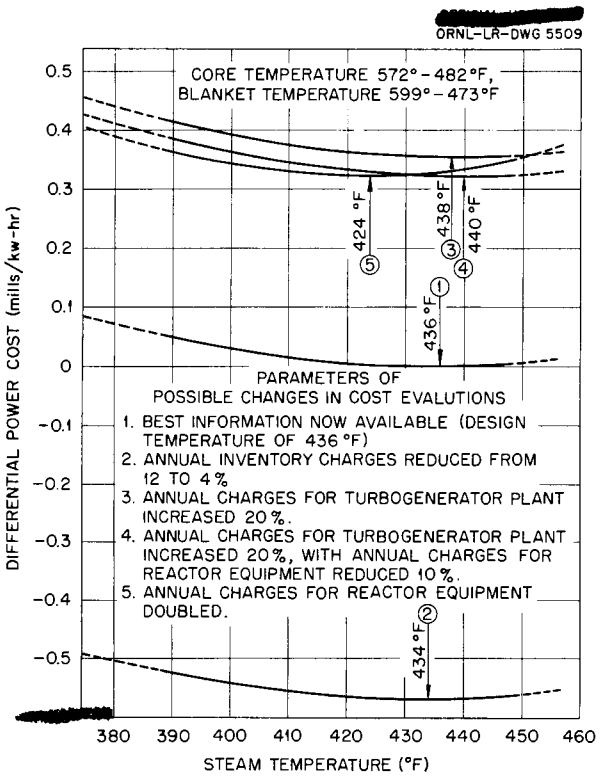

Fig. 2.11. Influence of Cost Changes on Design Steam Temperature.

and the 473 to 599°F blanket temperature span indicates a minimum cost at a steam temperature of 436°F, as previously reported. This is the norm against which the other minimia are compared. The extremes of the minimum steam temperature are obtained when the costs associated with the turbogenerator plant are increased 20% at the same time that the charge for installing the reactor equipment is decreased from 40 to 25% of the estimated equipment cost (a net change of 11% in the reactor equipment annual charges), which gives an optimum of 440°F, and when the annual charges associated with the reactor equipment are doubled, giving an optimum steam temperature of 424°F. Thus, a range of 16°F covers this wide variation in the cost of the components which may vary with steam temperature. No estimate of the cost of producing power from the TBR has yet been made, as the costs of items which do not vary with steam conditions have not been figured.

On the basis of this evaluation a steam temperature of 436°F will be used in the further refinement of the TBR design.

2.2.4 Equipment Design Considerations

(a) Core System Gas Separator. Calculations of the approximate size of the pipe line gas separator have been completed for the purpose of determining preliminary layout dimensions. The equations used in sizing the ISHR gas separator[14,15] were used to estimate the void length required for efficient separation. The forced vortex equation was used, and the inlet vane angle was assumed to be 45 deg. A hub-to-pipe diameter ratio of 0.43, based on the HRT design, was chosen. The required pipe size is 2 ft in inside diameter, and the void length is 11 ft. Under this condition the maximum fluid velocity does not exceed 35 fps. It may be desirable to utilize two separators in parallel rather than one larger and longer separator. However, the optimum combination of pressure drop and inventory holdup will need to be calculated.

(b) Core and Blanket Pressurizers. The time behavior of the TBR has been investigated by calculations on the Oracle for the purpose of establishing design specifications consistent with reactor safety. A total core pressure rise limited to 200 psi was examined, half of which was assigned to the compression of the gas in the pressurizer. Under this assumption the ratio of the core volume to the gas volume in the core pressurizer should not exceed 2, thus requiring a pressurizer volume of about 1000 liters. Also, the cross-sectional area of the core annular outlet pipe must be at least 3.1 ft^2 and the length of piping between core and pressurizer should not exceed 10 ft.

The combined blanket and core system has not been analyzed, but, on the basis of power densities and volumes in the core and blanket, the volume of the blanket pressurizer should also be about 1000 liters. A 14-in.-dia blanket outlet pipe appears to be adequate, and the distance between the blanket and pressurizer can be as great as 15 ft. Analysis of the combined core and blanket systems will be made in the future.

[14] J. O. Bradfute, *ISHR Gas Separator*, ORNL CF-52-5-235 (May 21, 1952).

[15] R. E. Aven, *Length of Gas Separator for ISHR*, ORNL CF-53-7-136 (July 21, 1953).

(c) Criticality of Uranyl Sulfate Solutions in Horizontal Cylinders. The criticality calculations described in another report[16] have been extended to cover the use of U^{233} as fuel in order to determine the safe limits for the diameter of the TBR dump tanks. The calculations were for long circular cylinders with a moderator of H_2O, D_2O, or a mixture of the two. Because the tanks must be safe when covered with water, the cylinders were assumed to have an infinite H_2O reflector. A layer of cadmium (or other poison) opaque to thermal neutrons was assumed to be present on the cylinders. Properties of the moderators are the same as those used in the HRT calculations.

The results are shown in Fig. 2.12. If all mixtures of H_2O and D_2O are considered to be possible, the envelope to the curves represents an upper limit to the safe concentration of U^{233}. Because of uncertainties in the calculations, the TBR dump tanks will be designed so that the maximum concentration possible will be substantially lower than the concentrations shown in the curves.[17]

(d) Heat Generation in the Reactor. The flux distribution for the power levels shown in Table 2.3 was determined by Oracle calculations and was found to be very similar to that reported previously.[18] From these data the heat generation per unit volume was calculated on the assumption that no gas phase is present in the reactor, and a plot of power density vs reactor radius is shown in Fig. 2.13. The heat generation in the ½-in.-thick core vessel wall from radiation absorption is estimated at 21 w/cm³. Removal of this heat under steady-state conditions at such a high rate indicates the probability of boiling next to the core vessel wall in spite of the over-pressure relative to the fluid bulk temperature.

[16] M. C. Edlund *et al.*, *HRP Quar. Prog. Rep. July 31, 1954*, ORNL-1772, p 32–33.

[17] P. N. Haubenreich, *Criticality Calculations for TBR Dump Tanks, TBR Design Memo No. 9*, ORNL CF-55-1-172 (Jan. 31, 1955).

[18] R. B. Korsmeyer *et al.*, *HRP Quar. Prog. Rep. Oct. 31, 1954*, ORNL-1813, Fig. 2.12, p 56.

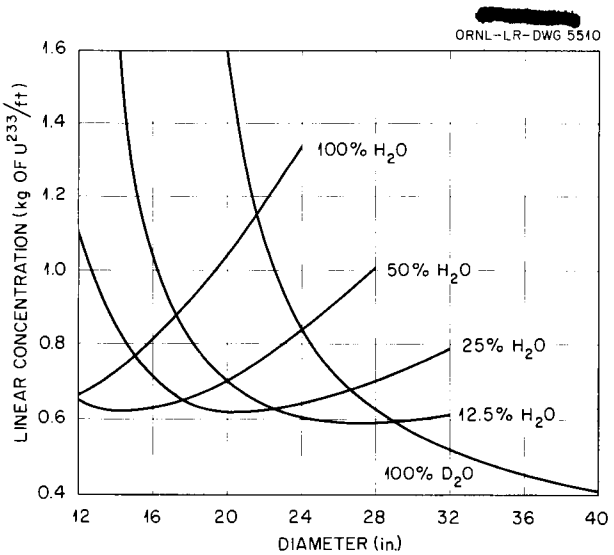

Fig. 2.12. Criticality of Cadmium-coated Cylinders of Infinite Length Containing U^{233} (H_2O-reflected, 20°C).

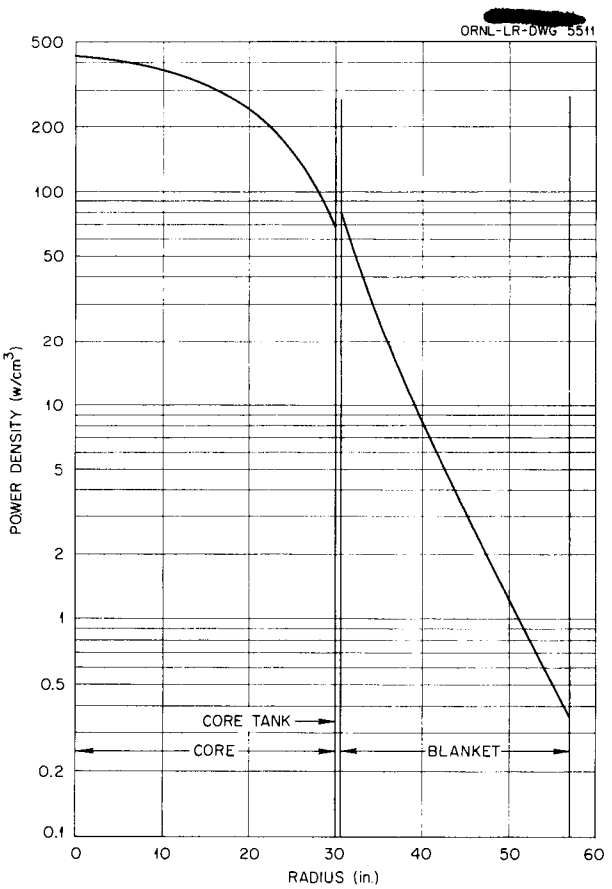

Fig. 2.13. Heat Production vs Reactor Radius.

Part III

CORROSION

E. G. Bohlmann

3. PUMP-LOOP CORROSION TESTS

J. C. Griess H. C. Savage
R. S. Greeley R. E. Wacker
S. A. Reed F. J. Walter

3.1 PUMP-LOOP OPERATION AND MAINTENANCE

H. C. Savage F. J. Walter

3.1.1 Loop Status

(a) Solution. Fourteen dynamic test loops are available for corrosion tests. At present, multipass[1] loops K, L, and M are being used to conduct long-term corrosion tests.

A series of runs with various concentrations of uranyl sulfate solutions at 320°C and 1700 to 1900 psig was completed in loop A during the past quarter. Loop A accumulated a total operating time of 6794 hr at 320°C. The loop operated very satisfactorily throughout this period, with no serious corrosion of either the pump or the loop. The loop and pump parts exposed to the circulating solution were of type 347 stainless steel. The pump impeller weight loss after the 6794 hr of operation was less than 1 g.

The Westinghouse 100A pump in loop G (all-titanium construction) is being operated at a reduced frequency, by means of a Louis Allis Co. motor-generator set, to reduce the pump output and thus the liquid velocity past the corrosion specimens, so that the corrosion of stainless steel can be studied at velocities below the critical velocity in the absence of appreciable chromate ions in solution. (The all-titanium loop does not contain chromium and other corrosion products which normally result from generalized attack in the type 347 stainless steel loops.) In the run now in progress the pump output has been reduced to approximately 20 gpm, which gives a bulk flow velocity of about 15 fps past the corrosion sample pins.

A series of runs was completed in loop H to determine the effect of cavitation on over-all corrosion rates, as well as the possible effect on the critical velocity. Detailed results of these runs are given in Sec. 3.2.

Loop N, which was specifically designed[2] for operation with high-concentration (>0.17 *m*) uranyl sulfate solutions, is now operating with 1.34 *m* uranyl sulfate solution at 275°C with approximately 1000 ppm of dissolved oxygen. Insofar as possible, points of potential high turbulence, such as sharp corners, elbows, and sharp edge restrictions, were eliminated in the design and construction of loop N to reduce the high rate of corrosion which normally occurs in these areas. The loop is made of type 347 stainless steel, with the exception of some special test sections. In addition to the smooth-flow design of the loop, the bulk velocity of the circulating solution in the 1½-in. sch. 80 pipe has been reduced to about 5.5 fps by reducing the pump speed with the Louis Allis motor generator.

(b) Slurry. The new slurry loop[3] which will replace loop C is 75% complete. Tests on a Plexiglas mockup of the sample barrel[4] for this loop were completed. The tendency for a vortex to form at the top of the barrel, where the fluid flows into the specimen holder, was checked by injecting air bubbles into water that was flowing through the barrel. The straightening vanes were adequate for preventing vortex formation.

The Plexiglas sample barrel was then installed in a glass loop containing thorium oxide slurry in an attempt to determine whether or not particles of thorium oxide would settle and pack in the bottom of the barrel. The pump was turned on until the slurry (~ 100 g of ThO_2 per kilogram of H_2O) was thoroughly mixed. When mixing was complete, the pump was turned off, and the thorium oxide particles in the sample barrel were allowed to settle to the bottom of the barrel. When the pump was turned on again, the 10- to 20-gpm circulation through the sample barrel resulted in sufficient flow and turbulence to resuspend all the settled particles.

[1] H. C. Savage, R. A. Lorenz, and D. Schwartz, *HRP Quar. Prog. Rep. March 31, 1953*, ORNL-1554, p 48, Fig. 29.

[2] H. C. Savage and F. J. Walter, *HRP Quar. Prog. Rep. April 30, 1953*, ORNL-1753, p 61.

[3] H. C. Savage, F. J. Walter, and R. M. Warner, *HRP Quar. Prog. Rep. Oct. 31, 1954*, ORNL-1813, p 63 and Fig. 3.2, p 66.

[4] *Ibid.*, p 65, Fig. 3.1.

3.1.2 Heat-Exchanger Test

The test heat exchanger described in a previous report[5] was installed in 100A loop K for long-term over-all heat-transfer-coefficient measurements at simulated HRT conditions. Loop K is operating at 300°C and 1500 psi with 0.04 *m* UO_2SO_4 containing 0.006 *m* H_2SO_4, 0.005 *m* $CuSO_4$, and approximately 1000 ppm of dissolved oxygen.

At the beginning of the present run, the over-all heat-exchange coefficient was 1200 to 1500 Btu/hr·ft^2·°F. After approximately 3000 hr of operation, the coefficient appeared to have decreased to 900 to 1000 Btu/hr·ft^2·°F. The preceding coefficients were calculated on the assumption that the properties of the uranyl sulfate solution are identical to those of water at the same temperature and are subject to confirmation of variables, such as flow rate, at the termination of the run.

3.2 RESULTS OF LOOP TESTS

J. C. Griess R. S. Greeley

3.2.1 Introduction

During the past quarter the major effort has been on the following problems: the determination of the corrosion resistance of a number of metals and alloys to uranyl sulfate solutions, particularly those alloys that have low resistance to corrosion at high uranyl sulfate concentrations; the evaluation of the importance of cavitation in regard to the phenomenon of critical velocity; the effectiveness of hexavalent chromium as a corrosion inhibitor; the completion of a series of tests at 320°C; and the initiation of a series of tests of very long duration.

3.2.2 Results

(a) General Corrosion Rates. It has been customary to report in tabular form the results of all tests with pin-type corrosion specimens, and in this report Table 3.1 gives the results obtained during the past quarter. As has been the case in all previous reports,[6–13] the corrosion rates are average rates for the entire exposure period and for the entire exposed portion of the pin. Generally, the rate of corrosion at low flow rates is high during the first 50 to 100 hr and then becomes low after a protective coating has formed. Also, it has been noted that the attack on a pin is not always uniform; frequently the pin will be heavily corroded in a few select areas, whereas the remainder of the pin may be only slightly corroded. Therefore the corrosion rates reported in Table 3.1 must be used with discretion. In any given run the results allow a comparison of one specimen with another, and in this respect the table is useful. However, at high flow rates, when a protective film does not form, the corrosion rate is constant and has quantitative meaning.

(b) Corrosion Testing in 0.06 *m* Uranyl Sulfate at 320°C. A series of runs totaling more than 5000 hr was completed in which 0.06 *m* uranyl sulfate containing 0.006 *m* sulfuric acid was circulated at 320°C (see runs A-67 through A-72 in Table 3.1). In each run both pin- and coupon-type corrosion specimens were exposed, and solution samples were withdrawn from the loop and analyzed chemically.

The rate of increase of nickel in the solutions indicated a generalized corrosion rate of 0.1 to 0.2 mpy for the entire system in all runs, and in each case the pH of the solution showed a slight decrease. The change in pH was due to the hydrolysis of uranyl ion and the formation of hexavalent chromium, both reactions producing hydrogen ions. The hydrolysis reaction was apparently very slow, since only in the three runs of longest duration was any uranium trioxide found in the loop. In each run the hexavalent chromium concentration of the solution was two to three times that of the nickel, indicating that the equivalent of all of the chromium originating from the corrosion process remained in solution. In fact, in some of the runs it appeared that the

[5] H. C. Savage, R. A. Lorenz, and D. Schwartz, *HRP Quar. Prog. Rep. Jan. 1, 1953*, ORNL-1478, p 62 and Fig. 26, p 63.

[6] J. C. Griess, J. M. Ruth, and R. E. Wacker, *HRP Quar. Prog. Rep. Jan. 1, 1953*, ORNL-1478, p 63.

[7] J. C. Griess and R. E. Wacker, *HRP Quar. Prog. Rep. March 31, 1953*, ORNL-1554, p 49.

[8] J. C. Griess and R. E. Wacker, *HRP Quar. Prog. Rep. July 31, 1953*, ORNL-1605, p 74.

[9] J. C. Griess and R. E. Wacker, *HRP Quar. Prog. Rep. Oct. 31, 1953*, ORNL-1658, p 45.

[10] J. C. Griess and R. E. Wacker, *HRP Quar. Prog. Rep. Jan. 31, 1954*, ORNL-1678, p 50.

[11] J. C. Griess and R. E. Wacker, *HRP Quar. Prog. Rep. April 30, 1954*, ORNL-1753, p 61.

[12] J. C. Griess, *HRP Quar. Prog. Rep. July 31, 1954*, ORNL-1772, p 60.

[13] J. C. Griess and R. S. Greeley, *HRP Quar. Prog. Rep. Oct. 31, 1954*, ORNL-1813, p 67.

TABLE 3.1. CORROSION RATES OF PIN-TYPE CORROSION SPECIMENS

Run No.	UO_2SO_4 Concentration (m)	Temperature (°C)	Time (hr)	Additions	Flow Rate (fps ± 10%)	Pin Material	Number of Pins	Corrosion Rate (mpy)		
								Minimum	Average	Maximum
A-67	0.06	320	977	800–1500 ppm O_2 0.006 m H_2SO_4	17	Type 304L SS (stainless steel)	4	0.92	0.98	1.0
						309 SCb SS	2	2.0	2.6	3.1
						347 SS	4	1.3	1.4	1.5
						Zircaloy-2	1		*a*	
						Platinum	1		0.03	
						Iodide titanium	1		*a*	
					66	304L SS	6	0.99	3.5	6.7
						309 SCb SS	3	4.2	4.3	4.5
						347 SS	6	2.8	20	46
						Zircaloy-2	2		*a*	
						Zirconium, crystal bar	2		*a*	
						Zirconium, 2.5% tin alloy	2		*a*	
						Iodide titanium	2		0.03	
						Titanium 75A	2		0.03	
A-68	0.06	320	495	800–1500 ppm O_2 0.006 m H_2SO_4	17	304L SS	3	1.1	1.3	1.3
						304L SS[b]	1		8.4	
						309 SCb SS	2	1.2	2.5	2.7
						347 SS	4	0.96	1.1	1.5
						Zircaloy-2	1		*a*	
						Titanium (3% Al + 5% Cr)	1		1.4[c]	
					66	304L SS	3	2.2	2.3	2.5
						304L SS[b]	1		18	
						309 SCb SS	3	2.7	3.7	5.0
						316 SS	1		4.2	
						322W SS[d]	1		2.3	
						329 SS	1		2.4	
						347 SS	3	2.6	2.9	3.4
						347 SS[e]	1		1.8	
						430 SS	2	0.96	1.2	1.5
						Iodide titanium	1		0	

TABLE 3.1 (continued)

Run No.	UO_2SO_4 Concentration (m)	Temperature (°C)	Time (hr)	Additions	Flow Rate (fps ± 10%)	Pin Material	Number of Pins	Corrosion Rate (mpy) Minimum	Average	Maximum
A-68	0.06	320	495	800–1500 ppm O_2 0.006 m H_2SO_4	66	Titanium 75A	1		*a*	
						Titanium 100A	1		*a*	
						Titanium 150A	1		0.65	
						Titanium (3% Al + 5% Cr)	1		1.1[c]	
A-69	0.06	320	200	800–1500 ppm O_2 0.006 m H_2SO_4	17	304L SS	4	2.2	3.2	3.7
						309 SCb SS	3	2.2	8.3	16
						318 SS	2	2.0	3.1	4.2
						347 SS	4	4.5	5.0	5.6
						Misco C	1		8.8	
					66	304L SS	6	4.0	5.4	6.5
						304 SS	3	6.8	7.3	8.0
						309 SCb SS	2	5.9	5.9	5.9
						318 SS	2	5.4	7.1	8.7
						329 SS	1		4.9	
						347 SS	7	6.5	8.1	13
						Misco Metal	1		31	
						Misco B	1		6.7	
						Misco C	1		11	
						Miscro 4	1		15	
						17-4 PH SS	1		3.4	
A-70	0.06	320	842	800–1500 ppm O_2 0.006 m H_2SO_4	17	304L SS	6	0.77	1.4	1.7
						309 SCb SS	2	4.4	4.4	4.4
						318 SS	1		3.1	
						347 SS	5	2.1	2.4	2.7
					66	304L SS	7	1.5	3.1	7.4
						309 SCb SS	4	3.2	4.3	5.6
						318 SS	2	3.5	6.7	9.8
						347 SS	14	2.0	4.2	10
						Titanium (3% Al + 5% Cr)	1[c]		0.95	

TABLE 3.1 (continued)

Run No.	UO_2SO_4 Concentration (m)	Temperature (°C)	Time (hr)	Additions	Flow Rate (fps ± 10%)	Pin Material	Number of Pins	Corrosion Rate (mpy) Minimum	Average	Maximum
A-71	0.06	320	300	800–1500 ppm O_2 0.006 m H_2SO_4	17	304L SS	5	2.2	3.0	4.3
						309 SCb SS	2	9.1	10	11
						347 SS	5	2.6	4.9	6.3
						347 SS[e]	2	5.3	5.7	6.0
					61	304L SS	6	3.7	9.9	21
						304L SS[e]	1		3.3	
						309 SCb SS	3	11	12	12
						316L SS	2	4.3	6.4	8.4
						347 SS	12	4.4	11	19
						347 SS[e]	2	4.2	4.4	4.6
						Titanium (2.5% Sn + 3% Al)	1		3.1[c]	
						Titanium (3% Al + 5% Cr)	1		4.0[c]	
A-72	0.06	320	2265	800–1500 ppm O_2 0.006 m H_2SO_4	17	304L SS	4	0.38	0.62	0.76
						309 SCb SS	2	2.1	2.2	2.2
						321 SS	1		1.0	
						347 SS	5	1.1	1.3	1.4
						347 SS[e]	2	1.2	1.4	1.5
					62	304L SS	3	0.80	1.1	1.2
						304 SS[e]	1		1.4	
						309 SCb SS	3	2.1	3.7	6.6
						316L SS	1		2.1	
						318 SS	1		1.5	
						321 SS	2	1.4	1.6	1.7
						347 SS	8	1.5	2.1	3.3
						347 SS[e]	2	1.4	1.8	2.1
						Zircaloy-2	3		[a]	
						Zirconium (2.5% Sn)	1		[a]	
						Titanium (2.5% Sn + 5% Al)	1		1.3[c]	
						Titanium 75A	1		0.1	

TABLE 3.1 (continued)

Run No.	UO_2SO_4 Concentration (m)	Temperature (°C)	Time (hr)	Additions	Flow Rate (fps ± 10%)	Pin Material	Number of Pins	Corrosion Rate (mpy) Minimum	Average	Maximum
B-50	0.17	250	205	1000–2000 ppm O_2	14	302B SS	2	8.2	8.7	9.1
						304L SS	2	9.8	11	13
						309 SCb SS	1		13	
						322W SS	1		8.2	
						322W SS[d]	1		9.8	
						347 SS	6	10	12	13
					74	302B SS	2	170	175	180
						304L SS	2	160	170	180
						309 SCb SS	1		160	
						322W SS	1		210	
						322W SS[d]	1		57	
						347 SS	7	150	180	240
B-51	0.17	250	200	1000–2000 ppm O_2	18	304L SS	4	16	23	27
						309 SCb SS	2	20	21	21
						347 SS	6	23	26	34
						Titanium 75A	1		/	
						Zircaloy-2	1		/	
					75	304L SS	4	140	150	160
						309 SCb SS	2	160	165	170
						347 SS	6	120	150	160
						Titanium 75A	1		0.31	
						Zircaloy-2	1		/	
D-36	0.17	200	286	500–1500 ppm O_2	15	302B SS	1		3.7	
				200 ppm Cr(VI)		304L SS	4	6.8	7.2	7.8
				as $K_2Cr_2O_7$		309 SCb SS	2	15	17	18
						347 SS	6	6.7	7.5	8.2
						Platinum	1		0	
					75	304L SS	4	21	27	40
						309 SCb SS	1		23	

TABLE 3.1 (continued)

Run No.	UO_2SO_4 Concentration (m)	Temperature (°C)	Time (hr)	Additions	Flow Rate (fps ± 10%)	Pin Material	Number of Pins	Corrosion Rate (mpy) Minimum	Average	Maximum
D-36	0.17	200	286	500–1500 ppm O_2 200 ppm Cr(VI) as $K_2Cr_2O_7$	75	347 SS	5	30	40	53
						Platinum	1		2.9	
D-37	0.17	200	492	500–1500 ppm O_2 200 ppm Cr(VI) as $K_2Cr_2O_7$[g]	15	302B SS	1		0.69	
						304L SS	4	2.2	2.5	2.7
						309 SCb SS	2	5.1	6.8	8.3
						321 SS	1		15	
						347 SS	6	7.5	11	13
					75	304L SS	4	44	45	46
						321 SS	1		94	
						347 SS	5	38	51	57
E-33	0.04	175	1111	500–1000 ppm O_2 0.006 m H_2SO_4	16	302B SS	1		12	
						304L SS	4	4.5	4.8	5.2
						309 SCb SS	2	2.8	3.1	3.3
						321 SS	2	4.3	4.5	4.6
						347 SS	5	5.4	5.6	5.9
					30	302B SS	1		9.2	
						304L SS	8	4.4	5.0	5.6
						309 SCb SS	4	3.1	3.2	3.3
						316L SS	4	5.2	5.6	6.3
						318 SS	1		6.6	
						321 SS	2	4.7	5.1	5.5
						347 SS	6	5.9	7.0	9.3
						347 SS[e]	2	4.6	4.8	4.9
					73	304L SS	4	5.6	6.2	7.2
						309 SCb SS	2	4.3	6.5	8.7
						318 SS	1		7.5	
						321 SS	2	6.6	7.7	8.7
						347 SS	4	6.2	7.4	10
						347 SS[e]	1		5.5	

TABLE 3.1 (continued)

Run No.	UO_2SO_4 Concentration (m)	Temperature (°C)	Time (hr)	Additions	Flow Rate (fps ± 10%)	Pin Material	Number of Pins	Corrosion Rate (mpy) Minimum	Average	Maximum
F-39	0.17	250	106	1000–2000 ppm O_2	13	304L SS	5	8.8	11	14
				200 ppm Cr(VI)		347 SS	6	17	18	18
				as $K_2Cr_2O_7$[b]		347 SS[e]	2	15	17	18
					74	304L SS	5	220	240	300
						347 SS	6	180	220	230
						347 SS[e]	2	230	245	260
F-41	0.17	250	604	0–50 ppm O_2	11	304L SS	3	6.0	8.4	9.8
F-42–F-45	0.04	250	total[i]	0–50 ppm O_2		309 SCb SS	3	9.5	11	13
						318 SS	2	9.4	10	11
						321 SS	2	8.2	9.6	11
						347 SS	4	11	14	16
F-46	0.17	250	200	1000–2000 ppm O_2	12	304L SS	3	13	15	18
				100 ppm chloride		347 SS	5	5.4	17	22
				as NaCl		Platinum	2	0.06	0.11	0.16
						Gold	2[j]	6.5	6.8	7.0
					74	304L SS	3	130	130	130
						347 SS	5	130	144	170
						Platinum	2	6.4	6.6	6.8
						Gold	2[j]	36	55	74
F-47	0.17	250	200	1000–2000 ppm O_2	12	304L SS	3	15	17	19
				200 ppm chloride		347 SS	5	14	16	25
				as NaCl		Platinum	2	0.52	0.52	0.52
						Gold	1[k]		37	
					74	304L SS	2	180	200	220
						347 SS	5	140	160	170
						Platinum	2	2.5	3.0	3.4
						Gold	2[j]		[l]	

TABLE 3.1 (continued)

Run No.	UO_2SO_4 Concentration (m)	Temperature (°C)	Time (hr)	Additions	Flow Rate (fps ± 10%)	Pin Material	Number of Pins	Corrosion Rate (mpy) Minimum	Average	Maximum
F-48	0.17	250[m]	200	1000–2000 ppm O_2 130 ppm iodide as KI	12	304L SS	3	16	19	23
						347 SS	5	17	20	23
						Platinum	2	0.30	0.38	0.45
						Gold	2[j]	0.93	0.95	0.97
					74	304L SS	5	150	160	170
						347 SS	5	140	170	190
						Platinum	2	1.8	2.0	2.2
						Gold	2[k]	2.0	2.1	2.2
F-49	0.17	250	50	1000–2000 ppm O_2 130 ppm iodide as KI	12	304L SS	3	89	93	95
						347 SS	5	86	92	100
						Platinum	2		[n]	
						Gold	2[j]	9.9	10	10
					74	304L SS	5	100	120	150
						347 SS	5	110	120	150
						Platinum	2		[n]	
						Gold	2[k]	9.7	9.9	10
H-39	0.17	250[m]	29	100–1000 ppm O_2	18	304L SS	5	110	110	120
						309 SCb SS	2	89	92	94
						321 SS	2	89	93	96
						347 SS	5	110	120	120
					64	304L SS	5	120	140	160
						309 SCb SS	2	110	120	120
						321 SS	2	100	120	140
						347 SS	5	110	120	140
H-40	0.17	250[m]	200	100–1000 ppm O_2	18	304L SS	5	40	54	75
						309 SCb SS	2	26	27	28
						321 SS	2	40	44	48
						347 SS	5	24	33	42

TABLE 3.1 (continued)

Run No.	UO_2SO_4 Concentration (m)	Temperature (°C)	Time (hr)	Additions	Flow Rate (fps ± 10%)	Pin Material	Number of Pins	Corrosion Rate (mpy) Minimum	Average	Maximum
H-40	0.17	250^m	200	100–1000 ppm O_2	64	304L SS	5	160	170	180
						309 SCb SS	2	160	170	170
						321 SS	2	160	170	180
						347 SS	5	150	160	170
H-41	0.17	250^m	400	100–1000 ppm O_2	17	302B SS	2	34	87	140
						304L SS	4	14	17	22
						309 SCb SS	2	11	14	16
						321 SS	2	18	21	24
						347 SS	4	14	17	20
					64	302B SS	2	300	330	360
						304L SS	4	140	150	150
						309 SCb SS	2	160	170	170
						321 SS	2	160	170	180
						347 SS	4	120	150	170
H-42	0.17	250^m	200	300–2000 ppm O_2	17	304L SS	4	19	26	38
						309 SCb SS	2	19	20	21
						321 SS	2	48	49	49
						347 SS	5	20	25	32
						Synthetic sapphire	1		18	
					64	304L SS	5	240	250	260
						309 SCb SS	2	270	280	280
						321 SS	2	220	220	220
						347 SS	5	160	230	270
H-43	0.17	250^m	200	100–1000 ppm O_2 90 psig He	18	304L SS	4	54	69	85
						309 SCb SS	2	27	28	28
						321 SS	2	56	72	88
						347 SS	5	33	43	49
						17-7 PH SS	1		19	

TABLE 3.1 (continued)

Run No.	UO_2SO_4 Concentration (m)	Temperature (°C)	Time (hr)	Additions	Flow Rate (fps ± 10%)	Pin Material	Number of Pins	Corrosion Rate (mpy) Minimum	Average	Maximum
H-43	0.17	250[m]	200	100–1000 ppm O_2 90 psig He	64	304L SS	4	140	150	160
						309 SCb SS	2	160	160	160
						321 SS	2	140	140	140
						347 SS	5	130	160	170
						17-7 PH SS	1		180	
H-44	0.17	250	200	5000–7000 ppm O_2	16	304L SS	4	43	45	49
						309 SCb SS	2	28	29	30
						321 SS	2	80	82	84
						347 SS	5	25	33	43
						347 SS[e]	1		130	
					64	304L SS	4	220	240	290
						309 SCb SS	2	260	270	270
						321 SS	2	200	220	230
						347 SS	5	210	230	240
						347 SS[e]	1		230	
H-46	0.17	250[m]	200	2000 ppm Cr(VI) as $K_2Cr_2O_7$	18	304L SS	2	2.0	2.2	2.3
						309 SCb SS	1		2.3	
						321 SS	1		2.3	
						347 SS	6	2.1	2.5	3.1
					64	304L SS	2	40	75	110
						309 SCb SS	2	16	49	81
						321 SS	2	170	200	220
						347 SS	5	150	190	220
H-47	0.17	250	200	2000 ppm Cr(VI) as $K_2Cr_2O_7$ 200 psig He (at room temperature)	17	304L SS	2	0.76	0.98	1.2
						309 SCb SS	2	0.34	0.55	0.76
						321 SS	2	0.68	0.72	0.76
						347 SS	8	0.08	0.60	0.76

TABLE 3.1 (continued)

Run No.	UO_2SO_4 Concentration (m)	Temperature (°C)	Time (hr)	Additions	Flow Rate (fps ± 10%)	Pin Material	Number of Pins	Corrosion Rate (mpy) Minimum	Average	Maximum
H-47	0.17	250	200	2000 ppm Cr(VI) as $K_2Cr_2O_7$ 200 psig He (at room temperature)	64	304L SS	2	160	170	170
						309 SCb SS	2	160	180	190
						321 SS	2	160	160	160
						347 SS	8	130	170	190
H-48	0.17	250	200	2000 ppm Cr(VI) as $K_2Cr_2O_7$ 200 psig O_2 (at room temperature) (1000–2000 ppm)	16	304L SS	2	1.7	1.8	1.9
						309 SCb SS	2	1.8	2.2	2.6
						321 SS	2	1.7	1.8	1.8
						347 SS	7	1.6	1.8	2.0
						Synthetic sapphire	1		1.6	
					64	304L SS	2	160	200	240
						309 SCb SS	2	190	230	260
						321 SS	2	210	260	300
						347 SS	8	180	290	310
H-50	0.17	250	200	1000–2000 ppm O_2	16	304L SS	2	12	13	14
						309 SCb SS	2	7.2	10	13
						321 SS	2	18	19	19
						347 SS	8	2.8	13	17
					64	304L SS	2	300	300	300
						309 SCb SS	2	350	350	350
						321 SS	2	250	260	260
						347 SS	8	240	280	300
H-51	0.17	250[m]	200	2000 ppm Cr(VI) as $K_2Cr_2O_7$	17	304L SS	2	1.7	1.7	1.7
						309 SCb SS	2	1.5	1.6	1.6
						321 SS	2	1.2	1.4	1.5
						347 SS	8	0.94	1.3	1.8
					64	304L SS	2	190	210	230
						309 SCb SS	2	210	220	220
						321 SS	2	260	300	340
						347 SS	8	130	260	400

TABLE 3.1 (continued)

Run No.	UO_2SO_4 Concentration (m)	Temperature (°C)	Time (hr)	Additions	Flow Rate (fps ± 10%)	Pin Material	Number of Pins	Corrosion Rate (mpy) Minimum	Average	Maximum
I-19	0.02	250	200	1000–2000 ppm O_2 0.005 m H_2SO_4	12	302B SS	2	8.2	9.0	9.7
						304 SS	1		3.1	
						304 SS[e]	2	1.9	3.2	3.4
						304L SS	2	2.0	2.3	2.6
						309 SCb SS	2	3.6	3.7	3.7
						310 SS	1		3.5	
						310S SS	1		3.1	
						316 SS[e]	2	3.2	3.3	3.3
						316L SS	1		3.0	
						318 SS	2	4.3	4.9	5.4
						321 SS	2	2.3	2.6	2.9
						322W SS	2	2.0	2.0	2.0
						322W SS[d]	2	2.6	2.6	2.6
						322W SS[o]	1		20	
						347 SS	3	2.7	2.9	3.1
						347 SS[e]	2	2.2	2.5	2.8
						410 SS	2	15	17	18
						410 SS[d]	2	16	17	17
						416 SS	2	14	14	14
						416 SS[d]	2	12	12	12
						420 SS	2	44	45	45
						420 SS[d]	2	19	20	21
						430 SS	2	4.8	5.0	5.2
						440-C SS	2	110	110	110
						440-C SS[d]	2	15	21	26
						443 SS	2	2.3	2.5	2.6
						446 SS	2	2.7	3.0	3.3
						17-4 PH SS	2	1.4	1.6	1.7
						17-4 PH SS[d]	2	1.4	1.6	1.7
						17-7 PH SS	2	1.5	1.6	1.6
						17-7 PH SS[d]	2	4.3	4.6	4.8
						Carpenter 20 SS	2	5.8	5.9	6.0

TABLE 3.1 (continued)

Run No.	UO_2SO_4 Concentration (m)	Temperature (°C)	Time (hr)	Additions	Flow Rate (fps ±10%)	Pin Material	Number of Pins	Corrosion Rate (mpy) Minimum	Average	Maximum
I-19	0.02	250	200	1000–2000 ppm O_2 0.005 m H_2SO_4	12	Carpenter 20 SS[e]	2	5.4	5.7	5.9
						Misco B	1		1.9	
						Miscro 4	2	8.8	8.8	8.8
						Stellite 1	2	23	24	25
						Stellite 3	2	24	24	24
						Stellite 6	2	26	29	31
						Stellite 25	2	35	38	40
						Stellite 98M2	2	16	19	22
						Worthite	2	4.9	5.1	5.3
						Worthite[e]	2	9.6	10	11
						Incoloy	1		3.8	
						Inconel	1		160	
						Inconel X	1		27	
						Inconel (low carbon)	1		88	
I-20	0.02	200	200	1000–2000 ppm O_2 0.005 m H_2SO_4	12	302B SS	2	13	14	15
						304 SS	1		7.3	
						304 SS[e]	2	7.1	7.4	7.6
						304L SS	2	7.1	7.4	7.7
						309 SCb SS	2	3.9	4.2	4.5
						310S SS	2	3.2	3.9	4.6
						316L SS	1		7.2	
						316 SS[e]	2	7.6	7.7	7.8
						318 SS	2	5.3	5.5	5.7
						321 SS	2	6.2	6.3	6.4
						322W SS	2	6.9	7.7	8.4
						322W SS[d]	2	7.8	8.3	8.8
						347 SS	4	7.1	8.0	8.9
						347 SS[e]	2	7.7	7.8	7.8
						410 SS	2	9.9	15	20
						410 SS[d]	2	19	21	22

TABLE 3.1 (continued)

Run No.	UO_2SO_4 Concentration (m)	Temperature (°C)	Time (hr)	Additions	Flow Rate (fps ± 10%)	Pin Material	Number of Pins	Corrosion Rate (mpy) Minimum	Average	Maximum
I-20	0.02	200	200	1000–2000 ppm O_2 0.005 m H_2SO_4	12	416 SS	2	7.4	13	18
						416 SS[d]	2	17	18	19
						420 SS	2	49	52	54
						420 SS[d]	2	25	26	27
						430 SS	2	11	12	13
						440-C SS	2	190	190	190
						440-C SS[d]	2	20	29	38
						443 SS	2	4.1	4.2	4.2
						446 SS	2	3.8	4.1	4.3
						17-4 PH SS	2	5.7	6.7	7.7
						17-4 PH SS[d]	2	8.1	8.3	8.5
						17-7 PH SS	2	5.8	6.2	6.5
						17-7 PH SS[d]	2	11	12	12
						Carpenter 20 SS	2	5.0	5.4	5.7
						Carpenter 20 SS[e]	2	5.9	6.0	6.0
						Misco B	1		6.0	
						Miscro 4	2	15	16	17
						Stellite 1	2	24	28	32
						Stellite 3	2	72	84	96
						Stellite 6	2	19	20	21
						Stellite 25	2	12	13	14
						Stellite 98M2	2	51	52	52
						Worthite	2	6.2	6.3	6.3
						Worthite[e]	2	16	17	17
						Incoloy	1		10	
						Inconel	1		140	
						Inconel X	1		15	
						Inconel (low carbon)	1		46	
I-21	0.02	300	200	1000–2000 ppm O_2 0.005 m H_2SO_4	12	302B SS	2	11	12	13
						304 SS	1		4.3	
						304 SS[e]	2	2.0	4.2	6.4

TABLE 3.1 (continued)

Run No.	UO_2SO_4 Concentration (m)	Temperature (°C)	Time (hr)	Additions	Flow Rate (fps ± 10%)	Pin Material	Number of Pins	Corrosion Rate (mpy) Minimum	Average	Maximum
I-21	0.02	300	200	1000–2000 ppm O_2 0.005 m H_2SO_4	12	304L SS	1		3.0	
						309 SCb SS	3	3.2	3.5	3.7
						310S SS	2	2.8	3.3	3.8
						316L SS	1		2.6	
						316 SS[e]	2	1.7	4.4	7.0
						318 SS	2	5.3	5.4	5.5
						321 SS	2	4.0	4.4	4.7
						322W SS	2	2.8	3.1	3.3
						322W SS[d]	2	3.3	3.9	4.4
						347 SS	4	3.9	4.2	4.8
						347 SS[e]	2	2.0	3.6	5.2
						410 SS	2	18	37	55
						410 SS[d]	2	31	35	39
						416 SS	2	24	30	36
						416 SS[d]	2	29	32	34
						420 SS	2	100	110	110
						420 SS[d]	2	44	46	47
						430 SS	2	19	20	20
						440-C SS	2	100	110	110
						440-C SS[d]	2	35	36	36
						443 SS	2	1.8	1.8	1.9
						446 SS	2	1.4	2.0	2.6
						17-4 PH SS	2	2.4	2.6	2.8
						17-4 PH SS[d]	2	4.4	4.7	4.9
						17-7 PH SS	2	2.6	2.7	2.8
						17-7 PH SS[d]	2	11	12	12
						Carpenter 20 SS	2	7.0	7.2	7.4
						Carpenter 20 SS[e]	2	7.6	7.7	7.7
						Misco B	1		5.3	
						Miscro 4	2	49	53	57
						Stellite 1	2	48	52	54
						Stellite 3	2	40	42	43

TABLE 3.1 (continued)

Run No.	UO_2SO_4 Concentration (m)	Temperature (°C)	Time (hr)	Additions	Flow Rate (fps ± 10%)	Pin Material	Number of Pins	Corrosion Rate (mpy) Minimum	Average	Maximum
I-21	0.02	300	200	1000–2000 ppm O_2 0.005 m H_2SO_4	12	Stellite 6	2	41	54	66
						Stellite 25	2	45	48	50
						Stellite 98M2	2	35	36	36
						Worthite	2	6.4	6.4	6.4
						Worthite[e]	2	11	13	14
						Incoloy	1		4.1	
						Inconel	1		300	
						Inconel X	1		47	
						Inconel (low carbon)	1		310	
I-22	0.06	200	200	1000–2000 ppm O_2 0.006 m H_2SO_4	12	302B SS	2	19	21	22
						304 SS	1		14	
						304 SS[e]	2	20	21	22
						304L SS	2	10	10	10
						309 SCb SS	2	6.5	6.8	7.1
						310S SS	2	5.0	5.2	5.3
						316L SS	1		10	
						316 SS[e]	2	11	12	12
						318 SS	2	7.7	8.0	8.2
						321 SS	2	9.2	9.2	9.2
						322W SS	2	15	15	15
						322W SS[d]	2	13	14	14
						347 SS	4	10	11	12
						347 SS[e]	2	11	15	18
						410 SS	2	26	28	30
						410 SS[d]	2	32	35	38
						416 SS	2	32	33	33
						416 SS[d]	2	38	39	39
						420 SS	2	74	78	82
						420 SS[d]	2	42	47	52
						430 SS	2	68	70	71
						440-C SS	2	240	250	250

TABLE 3.1 (continued)

Run No.	UO_2SO_4 Concentration (m)	Temperature (°C)	Time (hr)	Additions	Flow Rate (fps ±10%)	Pin Material	Number of Pins	Corrosion Rate (mpy) Minimum	Average	Maximum
I-22	0.06	200	200	1000–2000 ppm O_2 0.006 m H_2SO_4	12	440-C SS[d]	2	51	61	71
						443 SS	2	5.8	6.1	6.3
						446 SS	2	4.9	5.4	5.9
						17-4 PH SS	2	17	17	17
						17-4 PH SS[d]	2	17	18	19
						17-7 PH SS	2	13	13	13
						17-7 PH SS[d]	2	22	23	24
						Carpenter 20 SS	2	7.0	7.3	7.6
						Carpenter 20 SS[e]	2	6.6	7.2	7.8
						Misco B	1		9.1	
						Miscro 4	2	53	55	56
						Stellite 1	2	61	64	66
						Stellite 3	2	190	200	200
						Stellite 6	2	45	46	46
						Stellite 25	2	18	18	18
						Stellite 98M2	2	140	170	200
						Worthite	2	7.9	8.4	8.9
						Worthite[e]	2	28	29	30
						Incoloy	1		12	
						Inconel	1		110	
						Inconel X	1		29	
						Inconel (low carbon)	1		23	

[a]Showed slight weight gain; specimen did not form film of iron and chromium oxides.

[b]Pin chromized before exposure.

[c]Pin contained film of corrosion products that was not removed.

[d]Hardened by suitable heat treatment.

[e]Cast.

[f]Showed large weight gain due to deposition of iron and chromium oxides on the surface.

[g]Potassium dichromate added three times during the run to maintain the Cr(VI) concentration.

[h]Potassium dichromate added 8 hr after start of run.

[i]Same specimens used in runs F-41 through F-45.

[j]Gold foil 0.005 in. thick rolled loosely in shape of pin. Corrosion rates reported are probably too high since corrosion was assumed to occur on outer surface only.

[k]A gold wire of 0.3-cm dia served as the corrosion specimen.

[l]The high solution velocity destroyed the foil.

[m]Pressurizer at 285°C.

[n]Specimen covered with a thin gold plate and showed slight weight gain.

[o]Malcomized.

solution was actually leaching some chromium from the scale which had been formed on the loop walls during previous runs at lower temperatures.

The same stainless steel (type 347) impeller was used throughout the above series of runs, and no detectable weight change was observed. There were no changes in the appearance, and throughout this series the balance of the pump did not change.

The average corrosion rates of all types of steels can be seen in Table 3.1. Figure 3.1 shows the weight loss of 347, 304L, and 309SCb stainless steel pins as a function of time at a flow rate of 17 fps. The weight loss plotted represents the average weight loss of the number of pins listed in Table 3.1, and the vertical lines through the symbols represent the maximum spread in the weight loss. It is interesting to note that type 304L had the lowest initial weight loss and also the lowest residual corrosion rate; type 309SCb had the highest initial weight loss and the highest residual corrosion rate; and type 347 was intermediate. The 495- and 977-hr runs gave uniformly low results. All pins had thin, lustrous films.

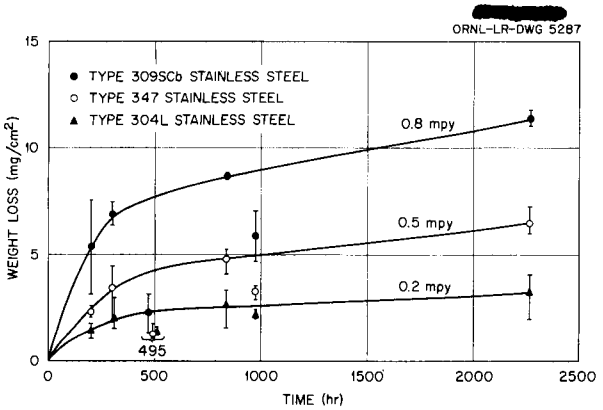

Fig. 3.1. Corrosion Rate of Stainless Steel Pins in 0.06 *m* Uranyl Sulfate Containing 0.006 *m* Sulfuric Acid at 320°C.

The pins that were exposed at 60 to 65 fps also had lustrous films that appeared to be identical with those formed at the lower flow rate. At the higher flow rate, the pins lost more weight during the first few hundred hours than did the pins at low flow rate, but the residual corrosion rates were nearly the same regardless of flow; however, the agreement among pins of the same alloy was poorer at the high flow than at the lower flow rate.

The coupons clearly indicated that at flow rates up to 100 fps the critical velocity was not attained. Regardless of flow rate all coupons looked alike, except the coupon exposed at the higher flow rate in run A-67. The high-velocity edge of this coupon was corroded appreciably, and the coupon lost an average of 65 mg/cm^2. However, in run A-72, in which the flow conditions were approximately the same as in run A-67 and the exposure time was more than twice as long, no heavy corrosion was visible and the last coupon lost 8 mg/cm^2.

In the above series of runs, as in all runs at 300°C or higher, there were no measurable amounts of iron and chromium oxides transported from one part of the system to another. Platinum retained its metallic luster, and the titanium pins showed interference colors characteristic of very thin titanium dioxide films; however, the titanium–3% aluminum–5% chromium and the titanium–5% aluminum–2.5% tin alloys showed higher corrosion rates than did the alloys of higher titanium content and had relatively heavy, brown films on their surfaces.

All Zircaloy-1 and Zircaloy-2 pins developed black films and showed slight weight gains. Only in run A-67 were two crystal-bar zirconium pins exposed; one pin developed a white oxide over what appeared to be a black oxide undercoat and showed a weight gain two and one-half times greater than that of any of the other zirconium pins; the other pin, machined from the same material, did not show the white oxide and gained very little weight.

In run A-67, specimens of Zircaloy-2, titanium, and type 347 stainless steel were placed in the gas phase of the pressurizer to determine whether the gas phase contained corrosive gases such as sulfur trioxide. None of the specimens showed any significant attack.

In run A-68 two chromized type 304L pins were exposed, one at high velocity and the other at low velocity. In each case the chromized pin lost six to eight times more weight than did the 304L pins which had received no surface treatment. The behavior exhibited by the chromized pins in this run was similar to that observed in other runs at 300°C or higher. On the other hand, chromized stainless steel has demonstrated a very high

degree of corrosion resistance to uranyl sulfate solutions in the range of 200 to 250°C. It appears that, at high temperatures, uranyl sulfate solutions containing oxygen are sufficiently strong oxidizing agents to oxidize chromium to the soluble hexavalent state at an appreciable rate, whereas at low temperatures the rate of oxidation is very slow.

(c) Long-Term Tests. During the past quarter three loops were started on runs proposed to last for essentially the life of the loop. The solution in each loop contained 0.04 *m* uranyl sulfate (10 g of uranium per liter of solution at room temperature), 0.006 *m* sulfuric acid, and 0.005 *m* cupric sulfate. In loop K the temperature of the solution is 300°C; in loop L, 200°C; and in loop M, 250°C.

Loop K has been in operation for more than 3000 hr. After 2865 hr of operation the run was interrupted, and the corrosion specimens were scrubbed and weighed. All pin-type corrosion specimens had complete coatings of a thin oxide, even though some of the pins had been exposed to flow rates as high as 37 fps. Practically all the pins showed only slight weight losses; the losses would have been somewhat greater, however, had the oxide coatings been removed. The average corrosion rates for type 347 stainless steel pins, which were typical of all austenitic stainless steels exposed at the four different flow rates, were: at 9 fps, 0.11 mpy; at 19 fps, 0.14 mpy; at 33 fps, 0.18 mpy; and at 37 fps, 0.26 mpy.

The increase in corrosion rate with increasing flow rate indicated by the data more likely resulted from the increased metal attack during film formation, such as was observed in runs A-67 through A-72 above, than from a real difference in the continuing corrosion rate after film had formed. Six pins which contained welds in their centers were exposed at 33 fps. These pins showed no selective attack on either the parent metal or the weld metal and had lost the same weight as was lost by the unwelded pins subjected to the same flow.

The coupons clearly showed that the critical velocity of the system was in excess of 50 fps. The coupon at high velocity showed a few triangular pits, which were unexpected. However, the bottoms of all the pits were completely covered with a black film – evidence that the pins were not actively corroding when the run was stopped.

After examination, all specimens were returned to their holders, and the holders were replaced in the loop in the same positions from which they had been removed. The test is being continued, and the same solution is being used that was in the loop at the end of the run.

Loop M has now been in operation for more than 2500 hr. The specimens in this loop were examined after 2306 hr of operation. All corrosion specimens in this loop had complete films and generally were similar in appearance to those from loop K. The average corrosion rates of the type 347 stainless steel pins were: at 10 fps, 0.07 mpy; at 19 fps, 0.08 mpy; at 35 fps, 0.11 mpy; and at 38 fps, 0.12 mpy. It should be remembered that these specimens were not defilmed, and hence the true corrosion rates were somewhat higher.

The coupons had a continuous, smooth, black film, and at the maximum velocity of 70 fps the critical velocity had not been reached.

All the specimens were returned to the loop after they were weighed, and the same solution that was in the loop when the run was terminated was added to the loop; the run has been resumed.

Loop L, in which the temperature is 200°C, has been in operation for only about 200 hr, and, to date, the specimens have not been examined.

From time to time the above three runs will be interrupted for examination of the corrosion specimens and the loop itself. The results of these examinations will be given in future reports.

(d) Cavitation and Gas-Bubble Tests. The term "critical velocity" has been given to that flow rate over the coupon-type specimens at which the corrosion rate shows a sharp increase. The increase in corrosion rate occurs because the protective film of corrosion products is prevented from forming or is torn off when the solution rushes over the surface. Cavitation or the formation and/or collapse of gas bubbles in regions of turbulence or a sharp change in velocity conceivably could cause local forces great enough to rupture the oxide film.

If gas bubbles (from dissolved oxygen or other gases) are formed by a pressure drop (Bernoulli effect) as the solution velocity increases in the channel of the tapered coupon holder, increasing the total pressure on the system should repress the bubble formation and give a higher critical velocity. Runs H-40 through H-43 were made with relatively low oxygen pressures and with the pressurizer temperature at 285°C to provide about 400 psi excess steam pressure. The loop temperature was always 250°C. Run H-44 was made

under isothermal conditions, and only oxygen pressurization was used. It can be seen in Fig. 3.2 that the critical velocity increased 5 to 10 fps in the steam over-pressure runs (run H-41 has been omitted from the figure for clarity, since it was a longer time duplicate of run H-40 and gave the same critical velocity). Since this increase is at best only slightly greater than the experimental error in determining critical velocity, further experiments, with higher steam pressures, should be performed. In an attempt to duplicate H-44, run H-50 was made, but the chromate-ion concentration of the solution increased rapidly, and therefore the critical velocity was greater than in any of the above-mentioned runs (see Sec. 3.2.2*e*).

The formation of gas bubbles should depend on the concentration of gas in solution. Run H-43 was made with a mixture of oxygen and helium and with the same total pressure as was used for run H-42. No change in critical velocity occurred; so only one curve is shown in Fig. 3.2. However, increasing the oxygen concentration significantly increased the high-velocity (film-free) corrosion rate, as is shown in Fig. 3.2 for runs H-40 (about 700 ppm O_2) and H-42 (about 2000 ppm O_2).

In the absence of dissolved gas, cavitation could be caused only by the formation and collapse of steam bubbles. Since for the same over-pressure the pressure drop required to produce steam bubbles in a steam-pressurized loop is much greater than that required to produce gas bubbles in a gas-pressurized loop, the critical velocity should be higher in the absence of dissolved gas. However, as can be seen in Fig. 3.2, the results of runs H-46, 47, 48, and 51, although not clear-cut, suggest that in the absence of dissolved gas the critical velocity is increased only slightly, if at all, over that in the presence of dissolved gases. In all

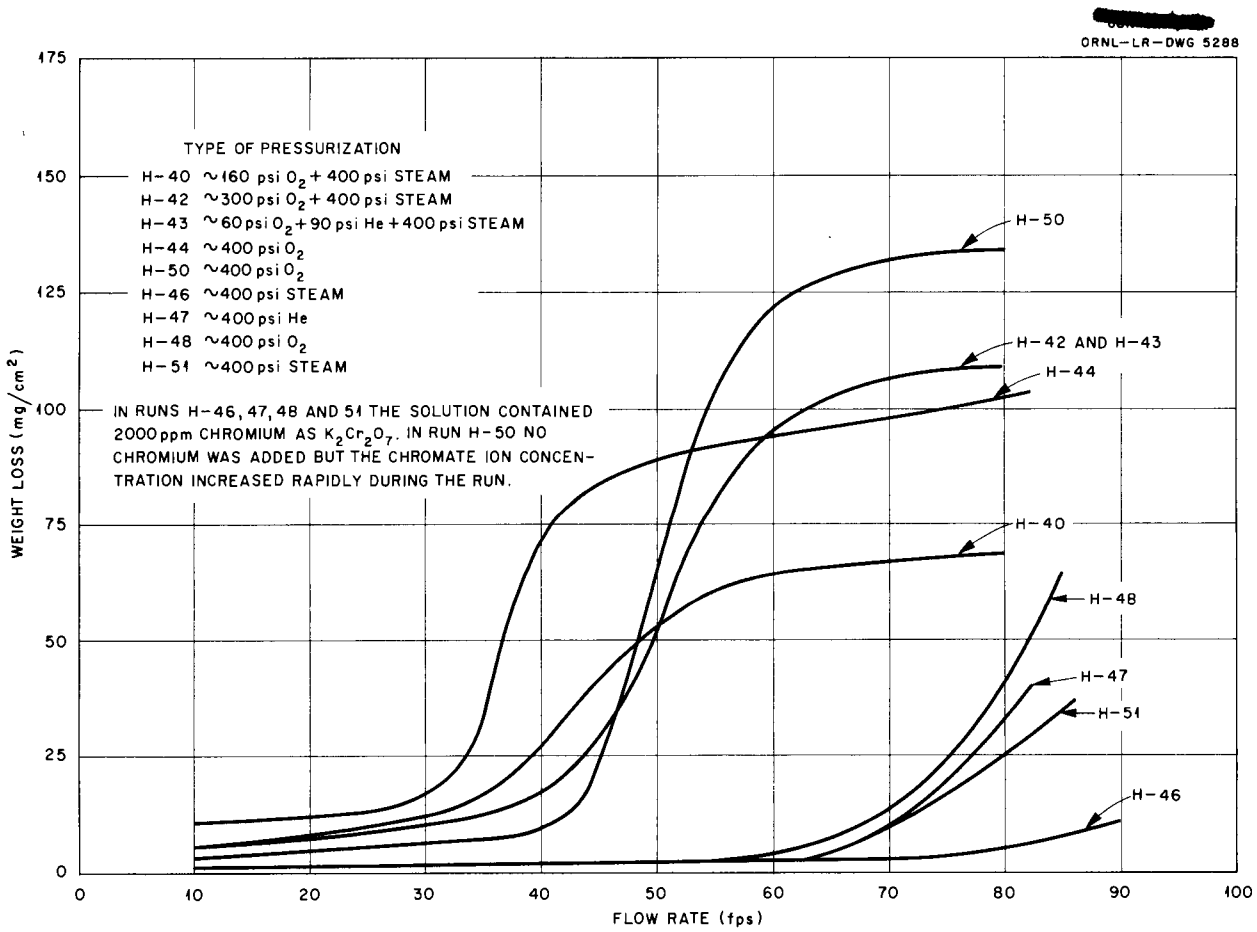

Fig. 3.2. Corrosion of Type 347 Stainless Steel in 0.17 *m* UO_2SO_4 at 250°C.

four runs about 2000 ppm of chromium as potassium dichromate was added as an oxidizing agent to prevent reduction and subsequent precipitation of the uranium. In runs H-46 and H-51 the loop was degassed and the system pressurized with steam (400 psi), but in run H-47 the system was pressurized with 400 psi helium and in run H-48 with 400 psi oxygen. No significant difference occurred between the run with helium and the one with oxygen, which indicates that, if there is an effect of dissolved gas, it is physical and not chemical.

In all the runs in which dichromate (2000 ppm of chromium as potassium dichromate) was used, the critical velocity was 30 to 40 fps higher than that in runs without added dichromate. This illustrates that the critical velocity is not solely (if at all) dependent on cavitation but must also be related to the character of the protective film and the strength of the bond between it and the underlying metal. Indeed, corrosion films of iron and chromium oxides usually build up on titanium, zirconium, and platinum pins exposed to solution velocities well above the critical velocity observed in the same test with stainless steel.

In summary, it appears possible that under the conditions of 0.17 *m* uranyl sulfate at 250°C the so-called "critical velocity" is influenced slightly by cavitation. It should be noted, however, that the critical velocity is very greatly increased by the presence of hexavalent chromium, and this fact makes the evaluation of a cavitation effect difficult. Any stainless steel system that contains uranyl sulfate and oxygen at high temperature will contain hexavalent chromium, whose rate of formation depends on many factors, including the previous history of the loop. While the data do not allow a firm conclusion, they do show clearly that when the system contains dichromate ions the nature of the protective coating is such that it is able to withstand higher flow rates.

The pin data obtained from the above runs are shown in Table 3.1, from which it can be seen that at low flow rates the addition of potassium dichromate to the solution had a pronounced effect in lowering the extent of corrosion. At high flow rates, however, the addition of dichromate intensified attack on film-free areas of the pins, thereby causing severe pitting. In runs H-40 through H-44 without dichromate, very nearly all the pin surface was corroded, and the average corrosion rates of the high-velocity pins as reported in Table 3.1 are meaningful. However, in runs H-46 through H-48 and H-51, in which potassium dichromate was added, a smaller percentage of each pin was corroded and penetration was greater. In these runs the average corrosion rates in Table 3.1 are deceptively low.

The high corrosion rates reported in Table 3.1 for run H-39 at 18 fps are due to the shortness of the run. As explained in the next section, samples at all velocities corrode at about the same high rate during film formation at the beginning of a run.

(e) Effect of Chromium(VI) on the Corrosion of Stainless Steel. In previous quarterly reports[14,15] the beneficial effect of dichromate ions on the corrosion of stainless steel was discussed. At that time it was shown that the introduction of only 200 ppm of hexavalent chromium to a 0.17 *m* uranyl sulfate solution before the start of a run had a marked influence on the critical velocity for stainless steel corrosion, as well as on the extent of corrosion during film formation below the critical velocity. Above the critical velocity the corrosion rate was greater in the presence of dichromate ions than in their absence. Other experiments in which the inhibitory action of Cr(VI) was demonstrated have been discussed in Sec. 3.2.2*d*.

Run F-39 was made in order to determine the effect of not having Cr(VI) present in the solution at the start of the run. For that reason the run was started with 0.17 *m* uranyl sulfate. Eight hours after the loop reached temperature, enough potassium dichromate was pumped into the loop so that the solution contained 200 ppm of Cr(VI). After the addition of the Cr(VI), the run was continued for an additional 98 hr, during which time the Cr(VI) concentration increased slightly. The results obtained from the coupon-type specimens are represented by curve B in Fig. 3.3. The runs represented by curves A and C were made under identical conditions of time, uranium concentration, and temperature; in one run (curve A), however, no Cr(VI) was added to the solution, whereas 200 ppm of Cr(VI) was added before the start of the other run (curve C). The data clearly show that the critical velocity was much higher when Cr(VI)

[14] J. C. Griess, *HRP Quar. Prog. Rep. July 31, 1954*, ORNL-1772, p 60.

[15] J. C. Griess and R. S. Greeley, *HRP Quar. Prog. Rep. Oct. 31, 1954*, ORNL-1813, p 67.

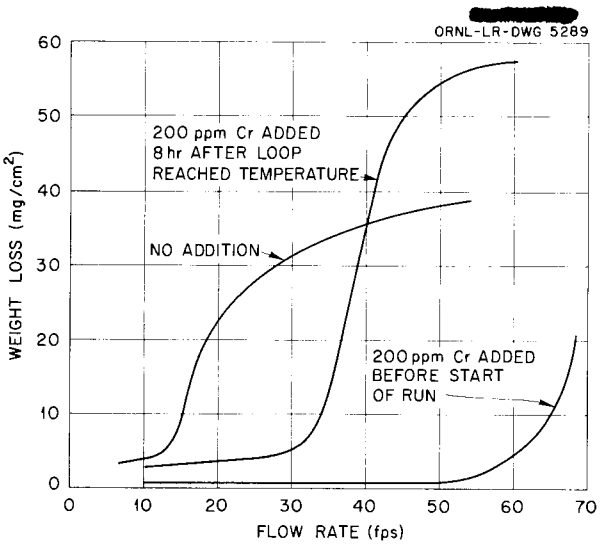

Fig. 3.3. Effect of Dichromate Ions on the Critical Velocity of Type 347 Stainless Steel. Conditions: 0.17 *m* uranyl sulfate, 250°C, 100 hr.

was added before the run was started than when it was added shortly after the run was started; however, the addition of chromium after the run had started gave a higher critical velocity than when no chromium was added. The difference between the height of curves A and B shows how the presence of Cr(VI) increased the rate of attack of the steel above the critical velocity. In the run represented by curve C, only the last coupon was corroded to any appreciable extent, and, even then, the coupon was nearly completely covered with scale.

A few observations of the appearance of coupons exposed to uranyl sulfate solutions for only short periods of time (usually less than 20 hr) indicated that all coupons developed thin films and lost the same weight regardless of the velocity with which the solution flowed past them. After longer periods under the same conditions, the coupons showed a typical critical-velocity effect. In other words, it may be that even at high flow rates a scale forms on all coupons and that after formation, and perhaps thickening, the film disintegrates beyond a certain flow rate, the value of which is determined largely by the uranium concentration and the temperature. The above results indicate that the presence of dichromate ions in the solution during the early stages of corrosion causes the initial film to be more protective or more adherent than the film formed when the solution does not contain the dichromate ions. Present plans call for a study of the corrosion of stainless steel as a function of velocity during the initial stages. Such a study may be helpful in an understanding of the factors associated with the critical-velocity phenomenon.

Two runs, D-36 and D-37, were made in order to determine whether dichromate ions would reduce the extent of corrosion of stainless steel in 0.17 *m* uranyl sulfate at 200°C. In run D-36, 200 ppm of chromium was added to the solution before the start of the run. After the run had reached temperature, the concentration of Cr(VI) decreased at a first-order reaction rate; after three days the concentration was only 100 ppm, and when the run was terminated after 286 hr the concentration was only 15 ppm.

Run D-37 was similar to D-36 except that a solution of potassium dichromate was pumped into the loop on three different occasions to maintain the Cr(VI) concentration between 50 and 200 ppm. As in run D-36, the hexavalent chromium concentration decreased at a first-order rate.

The results obtained from the corrosion specimens were not conclusive, but it appeared that at low flow the weight losses were slightly less than those occurring when no dichromate was present and that at high flow the weight losses agreed with those obtained under the same conditions without the dichromate addition.

It is interesting to note that, in a uranyl sulfate–stainless steel system which contains both oxygen and hexavalent chromium, oxygen serves as the oxidizing agent at temperatures of 250°C or higher, whereas at 200°C the hexavalent chromium serves partially as the oxidizing agent. Thus in a uranyl sulfate–stainless steel system the relative oxidizing power of oxygen and hexavalent chromium is to a large extent dependent on the temperature of the system.

The film formed in run D-37 was shown to be composed largely of a hydrous iron oxide, but it did contain a component which was not identifiable. In run H-46, discussed in Sec. 3.2.2*d*, the uranyl sulfate contained about 2000 ppm of Cr(VI), and an x-ray diffraction pattern of the oxide formed on the steel showed a very simple, but unidentifiable, pattern which was identical to a diffraction pattern of the unknown component from run D-37. Spectrographic analysis showed only iron and chromium to

be present in appreciable quantities, and chemical analysis showed the following weight per cent composition: Fe, 23.9; Cr, 19.7; Ti, 3.3; Ni, 0.6; U, 1.3; and SO_4, 1.9. The percentage of iron was lower than is usually observed, and the chromium concentration was higher. In a normal run without the Cr(VI) addition, the percentages are usually about 44 to 45 for iron and 4 to 10 for chromium.

(f) Corrosion of Gold and Platinum. Two runs were made in which sodium chloride was added to 0.17 *m* uranyl sulfate. In run F-46 the solution contained 100 ppm of chlorine, and in F-47, 200 ppm; both runs were made at 250°C. The prime purpose of these runs was to determine whether the presence of chloride ions in oxygenated uranyl sulfate solutions caused attack of gold and platinum. It can be seen from Table 3.1 that in run F-46 the platinum pins exposed at low flow were only slightly corroded, while at high flow rate the rate of attack was appreciable. In run F-46 the only gold specimens exposed to the solution were gold foil rolled into the shape of pins. At the high flow rate the gold foil was unable to withstand the flow, and the specimens were severely damaged. In fact, one of the specimens was torn to pieces, and small particles of gold were found attached to pins exposed at the high flow rates. At the lower flow rate the specimens were not damaged by the flow, and the gold was corroded at an average rate of 6.8 mpy. Gold, platinum, and type 347 stainless steel were placed in the gas phase of the pressurizer. At the completion of the run, examination of the specimens revealed no attack on any of the specimens located in the gas phase.

In run F-47, in which the chlorine concentration was 200 ppm, gold specimens showed a considerably heavier attack, the corrosion rate being as high as 37 mpy. The rate of attack on platinum was much lower than that for gold. At the lower flow the corrosion rate was 0.5 mpy, and at the higher flow, 3 mpy. Gas-phase specimens of gold and platinum showed no attack, but type 347 stainless steel was corroded; the specimens had numerous small, shallow pits.

In both runs F-46 and F-47 the stainless steel specimens in the solution showed pitting, which was most severe on the high-velocity pins in run F-46 (100 ppm of chlorine). In this case the pits were clearly visible without magnification, but the specimens exposed at lower flow rates showed no pitting when examined under low-power magnification. In run F-47 (200 ppm of chlorine) numerous small pits were found on all stainless steel specimens.

Runs F-48 and F-49 were made in order to determine the effect of iodide ions on the corrosion of gold and platinum. In each run the solution initially contained about 130 ppm of iodine, which was added as potassium iodide. In run F-48 the pressurizer temperature was 285°C and the loop temperature was 250°C. To keep oxygen in solution, steam from the top of the pressurizer was condensed and saturated with oxygen, and the condensate was returned to the loop through the rear of the pump. In this run the iodine concentration of the solution did not change during the run. Apparently the condensate dissolved any iodine vapor and returned it to the loop. In this run platinum, gold, and even stainless steel specimens exposed in the gas phase of the loop pressurizer showed no measurable attack. No pitting in solution or vapor was visible on the stainless steel even under high magnification. Both gold and platinum pins appeared to be attacked only slightly more than normal.

In run F-49 the loop was run isothermally and was pressurized with oxygen. The normal mixing line in which solution flowed through the pressurizer at a rate of about 2 gpm was used. Steam was not condensed in the pressurizer and was not returned to the rear of the pump as was done in run F-48. In run F-49 the iodine concentration of the solution decreased rapidly, and after one day the concentration of iodine in the system was 30 to 50 ppm. Gold and platinum specimens exposed in the gaseous region of the pressurizer showed no attack, but the type 347 stainless steel specimens were severely pitted. The run was terminated after 50 hr because the pressurizer rupture disc became so severely pitted that it leaked. The stainless steel specimens located in the pressurizer had numerous pits, some as deep as 8 mils.

The stainless steel specimens exposed in the solution were normal, and there was no evidence of pitting. The gold specimens were heavily attacked, the rate of penetration being about 10 mpy. The platinum pins became uniformly covered with a thin plate of gold and showed slight weight gains. This observation has not been made before, and the difference in behavior of gold and platinum

in runs F-48 and F-49 cannot be explained. That the thin yellow plate on the platinum pins was gold was verified by chemical analysis.

In conclusion, it appears that the presence of either iodide or chloride ions in uranyl sulfate systems will cause attack of both gold and platinum. However, the data presented in Table 3.1 for runs F-46 through F-49 are qualitative; the quantitative determination of the effect of iodide and chloride on the corrosion of gold and platinum would require a considerable number of runs.

In a previous quarterly report[16] the results of corrosion testing with gold-plated specimens were described. At that time it was shown that gold-plated stainless steel specimens, which had been plated in the usual manner by the use of a copper flash between the stainless steel and the gold, were not resistant to high-temperature uranyl sulfate solutions. Apparently the gold plate was porous, and the solution dissolved the copper flash, allowing the plate to flake off.

Recently the Los Alamos Scientific Laboratory plated some corrosion test specimens (coupons) for exposure in the 100A loops. The plating procedure was as follows:

1. a layer of nickel (~5000 atoms thick) from a nickel chloride flash bath,
2. a flash of silver about 0.1 mil thick,
3. three mils of gold from a gold cyanide bath containing a sulfonated oil as a smoothing agent,
4. heat cycle to 460°C,
5. pinhole-tested in ferricyanide bath.

Two type 347 stainless steel coupons plated by the above technique were exposed in runs B-50 and B-51. In each run the solution was 0.17 *m* uranyl sulfate circulated at 250°C. In each run one coupon was exposed in the velocity range of 20 to 35 fps, and the other coupon was exposed at the highest velocity possible, 50 to 80 fps. After run B-50 both coupons showed weight losses of less than 1 mg/cm^2, and there was no evidence of pinholes in the gold.

The same coupons were then exposed in run B-51; however, before run B-51 began, a small hole was drilled through the gold in the center of the coupon exposed at the lower flow rate to simulate a pinhole. Examination of the specimens after the run showed that both coupons had lost very little weight (<0.5 mg/cm^2) and that the small hole had become plugged with corrosion products, the removal of which revealed no selective attack of the steel and no evidence of the gold plate being undercut. In fact, both runs showed that the gold was completely nonporous and that should it be removed from a small portion of the surface no accelerated attack of the steel would be likely. That there is no apparent galvanic action between stainless steel and gold in uranyl sulfate solutions at 250°C has been reported before.[16]

(g) Corrosion Resistance of Selected Alloys. During the course of corrosion testing in the 100A loops, a number of different alloys were tested. All the results obtained prior to this report period have been presented in tabular form previously.[17–24] A considerable amount of testing on alloys other than the austenitic stainless steels was completed recently, and the results can be seen in Table 3.1, runs I-19 through I-23. In the following paragraphs an attempt will be made to summarize as briefly as possible the results of the tests to date on the alloys other than the type 18-8 austenitic stainless steels. All specimens were exposed in the unstressed condition. Table 3.2 gives the nominal chemical composition of the alloys.

(1) Type 322W Stainless Steel. Type 322W stainless steel can be precipitation-hardened. Pin-type specimens in both the annealed and the hardened condition were tested under several conditions. In the temperature range of 200 to 320°C both the hardened and the annealed specimens showed a corrosion resistance to all concentrations of uranyl sulfate as high as that of type 347 stainless steel. In all cases the attack was of a general nature, and after attack the surface

[16] J. C. Griess, *HRP Quar. Prog. Rep. July 31, 1954*, ORNL-1772, p 60

[17] J. C. Griess, J. M. Ruth, and R. E. Wacker, *HRP Quar. Prog. Rep. Jan. 1, 1953*, ORNL-1478, p 63.

[18] J. C. Griess and R. E. Wacker, *HRP Quar. Prog. Rep. March 31, 1953*, ORNL-1554, p 49.

[19] J. C. Griess and R. E. Wacker, *HRP Quar. Prog. Rep. July 31, 1953*, ORNL-1605, p 74.

[20] J. C. Griess and R. E. Wacker, *HRP Quar. Prog. Rep. Oct. 31, 1953*, ORNL-1658, p 45.

[21] J. C. Griess and R. E. Wacker, *HRP Quar. Prog. Rep. Jan. 31, 1954*, ORNL-1678, p 50.

[22] J. C. Griess and R. E. Wacker, *HRP Quar. Prog. Rep. April 30, 1954*, ORNL-1753, p 61.

[23] J. C. Griess, *HRP Quar. Prog. Rep. July 31, 1954*, ORNL-1772, p 60.

[24] J. C. Griess and R. S. Greeley, *HRP Quar. Prog. Rep. Oct. 31, 1954*, ORNL-1813, p 67.

TABLE 3.2. CHEMICAL COMPOSITION OF CERTAIN ALLOYS

Alloy	Composition (%)						Other Constituents (%)
	Cr	Ni	C	Fe	Si	Mn	
322W	17	7	0.07	Balance	0.05 max	0.5 max	0.70 min Ti; 0.20 Al
17-4 PH	16/18	3.5/5.0	0.05 max	Balance	1.0 max	1.0 max	4 Cu
17-7 PH	16/18	6.5/7.75	0.09 max	Balance	1.0 max	1.0 max	0.75/1/25 Al
Carpenter 20	20	29	0.07 max	Balance	1.0 max	0.75 max	2 Mo; 3 Al; 4 Cu
Warthite	20	24	0.07 max	Balance	3.5	1.0 max	3 Mo
Misco Metal*	19	38	0.5	Balance	1.5		
Misco B	25	13	0.25	Balance	1.5		
Misco C	29	10	0.25	Balance	1.5		
Miscro 4	13		0.07	Balance	1.5		
Inconel	11/15	Balance	0.15 max	10 max	0.5 max	1.0 max	0.2 Cu
Inconel X	14/16	Balance	0.08 max	7/9	0.55 max	1.0 max	0.2 Cu; 2.2/2.7 Ti; 0.4/1.0 Al; 0.7/1.2 Cb
Incoloy	19/22	32/36	0.1 max	Balance		1.5 max	
Stellite 1	29/33	0.5 max	2.2/2.7	3.0 max	1.5 max	0.5 max	9.5/13/5 W; 0.05/0.21 B; balance Co
Stellite 3	29/33	3.0 max	2.2/2.7	3.0 max	1.5 max	0.5 max	9.5/13/5 W; 0.05/0.20 B; balance Co
Stellite 6	26/31	3.0 max	0.9/1.4	3.0 max	1.5 max	1.0 max	3.5/6.0 W; balance Co
Stellite 98M2	27/31	3.0 max	1.8	4.5			16/19 W; 4.5 V; 0.8 Mo; balance Co
Haynes alloy 25	19/21	9/11	0.05/0.15	3.0 max	1.0 max	1/2	46/53 Co; 14/16 W
410	11.5/13.5		0.15 max	Balance	1.0 max	1.0 max	
416	12/14		0.15 max	Balance	1.0 max	1.25 max	0.60 max Zr or Mo
420	12/14		0.15 max	Balance	1.0 max	1.0 max	
430	14/18		0.12 max	Balance	1.0 max	1.0 max	
440-C	16/18		0.95/1.20	Balance	1.0 max	1.0 max	0.75 max Mo
443	18/23		0.20 max	Balance	1.0 max	1.0 max	0.90/1.25 max Cu
446	23/27		0.35 max	Balance	1.0 max	1.0 max	0.25 max N

*In all reports to date the designation for this material was Misco A. Actually, Misco A has never been tested in the 100A loops.

always remained smooth. At low flow rates type 322W steel developed black films, as does type 347, and, although the corrosion rate of the steel was not determined once the film had formed, the residual rate would probably be comparable to that for type 347 under the same conditions of test.

Only one test was made at a temperature lower than 200°C, and that was in 0.02 *m* uranyl sulfate at 100°C; the corrosion rate was less than 0.1 mpy. Further testing in the range of 100 to 200°C is in progress.

(2) Types 17-4 PH and 17-7 PH Stainless Steel. Both types 17-4 PH and 17-7 PH stainless steel alloys can be precipitation-hardened; in tests to date the two have shown similar corrosion resistance. In the annealed state both alloys showed practically identical corrosion resistance to uranyl sulfate solutions, and in the concentration range tested, 0.02 to 0.17 *m*, both demonstrated a corrosion resistance equal to that shown by type 347 stainless steel, at least at low flow rates. In the hardened condition both alloys had slightly less corrosion resistance to uranyl sulfate solutions, and type 17-7 PH was attacked to a somewhat greater extent than was type 17-4 PH; however, even in the hardened form both alloys exhibit a high degree of corrosion resistance and

may therefore be useful in reactor systems. The attack was uniform on both alloys; no pitting was observed. Both alloys are undergoing further testing (see also Sec. 5.1).

(3) Type 410 Stainless Steel. Both hardened and annealed type 410 stainless steel pins were tested under a few conditions. At low flow rates with 0.02 *m* uranyl sulfate the extent of attack of both the hardened and the annealed material was about the same, but was greater by a factor of 2 to 10 than that of type 347 stainless steel. The general appearance of the pins as removed from the loop indicated that film did not adhere well to the steel, and the surface of the steel, after it was defilmed, was rough. At 300°C in 0.02 *m* uranyl sulfate the hardened pins showed no pitting, but the annealed material had numerous small pits. The corrosion of type 410 stainless steel is such that it would not be suitable for use in uranyl sulfate solutions as dilute as 0.02 *m* and at temperatures of 200°C and higher. Tests in progress will determine its corrosion resistance at lower temperatures.

(4) Type 416 Stainless Steel. The behavior of type 416 stainless steel was very similar to that of type 410 stainless steel, and under nearly all conditions pin-type specimens showed nearly the same weight losses. However, under most conditions both the hardened and the annealed pins showed a tendency toward pitting, and in most cases the surface had numerous small pits after exposure. One test, in which an annealed pin was exposed to 0.02 *m* uranyl sulfate at 100°C, showed a corrosion rate of more than 300 mpy, which was considerably higher than that observed under the same conditions at 200 to 320°C. The corrosion resistance of type 416 stainless steel in uranyl sulfate solutions of all concentrations at all temperatures was so poor that the steel cannot be recommended for any part of a homogeneous reactor system contacting the fuel solution.

(5) Type 420 Stainless Steel. Relatively few tests have been run with type 420 stainless steel, but the tests have indicated that in 0.02 *m* uranyl sulfate in the temperature range of 200 to 300°C the corrosion rate is very high both with annealed and hardened specimens. In all cases the extent of corrosion of type 420 stainless steel was greater by a factor of 2 to 3 than that for either type 410 or 416. The extent of attack of the annealed steel was about twice that of the hardened steel. In one test with 0.02 *m* uranyl sulfate at 300°C the annealed steel developed numerous small round-bottom pits, but the pits were absent in the hardened material. Under most other conditions the attack was uniform, although some of the hardened pins showed some localized attack. In the temperature range of 200 to 300°C the extent of attack of type 420 stainless steel was very high. Further testing is in progress at lower temperatures.

(6) Type 430 Stainless Steel. In runs I-19 through I-22, type 430 stainless steel appeared to be less resistant to attack than did type 347 stainless steel. However, in a number of other runs, for example, A-68, type 430 stainless steel showed a corrosion resistance equal to that of type 347. At low flow, type 430 stainless steel pins develop a protective film under which the metal has always shown a very uniform type of attack. Only annealed pins were tested; the alloy is hardenable only by cold-working. Generally, at low flow in the concentration range of 0.02 to 0.17 *m* and at 200 to 320°C, the corrosion resistance of type 430 stainless steel was approximately equal to that of type 347 stainless steel. Tests are in progress to determine its corrosion resistance at lower temperatures.

(7) Type 440-C Stainless Steel. The results of the only testing completed to date with type 440-C stainless steel are included in Table 3.1, runs I-19 through I-22. Both the hardened and the annealed pins corroded extensively, but, as in the case of type 420 stainless steel, the hardened form had a much greater corrosion resistance than did the annealed form. In the annealed form the pins showed numerous round-bottom pits under all conditions; in the hardened form the pitting was absent, but the attack produced a very rough surface. Between 200 and 300°C at concentrations as low as 0.02 *m* uranyl sulfate the steel corroded so badly that it could be of no value to a reactor system. Tests at lower temperatures are in progress.

(8) Types 443 and 446 Stainless Steel. Although testing with types 443 and 446 stainless steel was not extensive, their corrosion resistance at low flow rates was equal to, or greater than, that of type 347 stainless steel. Further testing is in progress.

(9) Stellites. The Stellites that were tested are Nos. 1, 3, 6, 98M2, and Haynes alloy No. 25; most of the results obtained to date are shown in Table 3.1, runs I-19 through I-22. Generally, at the concentration of 0.02 *m* uranyl sulfate in the temperature range of 200 to 300°C, the attack on all the Stellites except Haynes alloy No. 25 was nonuniform, and the actual metal-penetration rate was even worse than the average corrosion rates given in Table 3.1. Large sections of the pins were unattacked, but other areas showed heavy, irregular attack. The Haynes alloy No. 25 pins did not develop film or scale in any case and corroded uniformly and apparently at a constant rate depending on the temperature and, to a lesser degree, on the uranium concentration. The corrosion of Haynes alloy No. 25 in 1.34 *m* uranyl sulfate was shown previously to be high and greatly dependent on the temperature.[25]

One other run in which the above Stellites were exposed was reported previously.[26] So that the results can be compared with those in Table 3.1, the conditions are repeated here: 0.02 *m* uranyl sulfate containing 0.005 *m* sulfuric acid at 100°C for 3600 hr. The observed corrosion rates for Stellites Nos. 1, 3, 6, 98M2, and 25 were 0.06, 1.3, 0.04, 1.0, and 0.06 mpy, respectively; the attack was uniform and the specimens did not change in appearance.

The results obtained to date clearly show that at temperatures of 200°C and higher all Stellites suffer corrosion to such an extent that they would be unusable under reactor conditions regardless of uranium concentration. Further testing in the temperature range of 100 to 200°C is in progress.

(10) Inconels. Most of the results of tests with the various Inconels are presented in Table 3.1, runs I-19 through I-22. It is obvious that Inconel X, Inconel, and low-carbon Inconel suffered heavy attack but that Inconel X had the highest corrosion resistance. Both the low-carbon Inconel and Inconel X were corroded in a very irregular manner, whereas Inconel, which suffered the heaviest attack, corroded in a very uniform manner. In these experiments none of the specimens was examined for intergranular attack.

In one other run in which 0.02 *m* uranyl sulfate containing 0.005 *m* sulfuric acid was circulated at 100°C, all the above alloys showed low corrosion rates, ranging from a few hundredths of a mil per year to a maximum value of 4 mpy. In that particular run it was noted that Inconel with a large grain size gave the highest rate, while the attack on the normal-grain-size material was less than 1 mpy. Inconel X, both annealed and age-hardened, showed corrosion rates ranging from 0.02 to 0.8 mpy.

Inconel diaphragms which were formerly used in the stators of 100A pumps generally were not satisfactory from a corrosion standpoint. Although under the conditions existing in the pumps the total corrosion was not great, the Inconel cans were penetrated by an intergranular attack. In view of such observations the wisdom of using Inconel diaphragms in pumps exposed to even the mildest conditions is doubtful.

(11) Carpenter 20 and Worthite Stainless Steel. Both Carpenter 20 and Worthite stainless steels developed films when they were exposed to uranyl sulfate solutions at temperatures of 200 to 300°C. Both steels generally suffered more attack than does type 347 stainless steel during the initial stages of corrosion, but, once a film formed, the residual corrosion rate appeared to be about the same as that of type 347 stainless steel. This difference was apparent at all temperatures and concentrations at which tests were conducted.

(12) Miscellaneous Alloys. Hastelloys C, F, and X have been tested only in 1.34 *m* uranyl sulfate at 250°C. Under these conditions the Hastelloy C pins were completely dissolved in less than 100 hr, and the others were very severely corroded. In one other run Hastelloy C pins were exposed to 0.02 *m* uranyl sulfate containing 0.005 *m* sulfuric acid at 100°C. Under these conditions the pins were free from visible attack, and a corrosion rate of less than 0.05 mpy was observed. No further tests on any of the Hastelloys were made.

Incoloy pins were examined only in runs I-19 through I-22 and in one run (see ORNL-1658, Table 8, run L-16) in which the conditions were the same as those for run I-19 but the exposure time was about four times longer. In the concentration range of 0.02 to 0.06 *m* and the temperature range of 200 to 300°C, Incoloy showed a degree of corrosion resistance comparable to that of type

[25] J. C. Griess and R. E. Wacker, *HRP Quar. Prog. Rep. March 31, 1953*, ORNL-1554, p 49.

[26] J. C. Griess and R. E. Wacker, *HRP Quar. Prog. Rep. April 30, 1954*, ORNL-1753, p 61.

347 stainless steel. The pins developed black protective coatings; when the scale was removed, the attack on the Incoloy was always very uniform.

(13) Cast Alloys. A relatively large number of type 347 cast stainless steel pins was exposed to uranyl sulfate solutions under various conditions. Generally, at both high and low flow rates, the cast alloy showed about the same corrosion resistance as was shown by the wrought steel. The only apparent difference observed between the two was in the critical velocity – the cast material appeared to have a lower critical velocity.

Pins made of cast 304, 304L, and 316 were not tested to the extent that cast 347 pins were, but from the existing data it is concluded that the corrosion resistance of the wrought and cast metals is about the same.

A few tests of cast Carpenter 20 (a material similar to Durimet 20) stainless steel showed that at low flow rates the cast alloy behaved in a fashion similar to that of the wrought steel. On the other hand, cast Worthite demonstrated a corrosion resistance considerably poorer than that of the wrought Worthite.

A series of four cast alloys supplied by the Michigan Steel Casting Company was tested. The alloys were designated as Misco A, B, and C and Miscro 4; their chemical composition can be seen in Table 3.2. It should be specifically noted that in previous reports[27–29] the designation Misco A has been incorrect. Those pins designated Misco A were actually Misco Metal, the composition of which is shown in Table 3.2. Misco A was never tested in the 100A loops. Misco Metal, which contains about 38% nickel, showed a low resistance to corrosion under most conditions. Misco B, which has a composition similar to that of type 309 stainless steel, showed a corrosion resistance similar to that of type 347 stainless steel. Misco C was tested only at 0.17 and 0.06 *m* uranyl sulfate concentrations at 250°C; under these conditions the corrosion resistance of the steel was approximately the same as that of type 347 stainless steel. Miscro 4 was examined under a number of conditions, but the results showed a high degree of inconsistency. For example, the results obtained in two different runs where the conditions were the same were 1 and 32 mpy. In the same runs the average corrosion rates of type 347 pins were 13 and 10 mpy, respectively. From the results in Table 3.1, runs I-19 through I-22, it is apparent that Miscro 4 was definitely inferior to type 347 stainless steel corrosionwise.

From the results obtained to date it can be concluded that, if it is desirable to use a casting, type 347 is as good as any other cast alloy from a corrosion-resistance standpoint, and may even be better. Types 304 and 316 are probably not greatly different from type 347, but only a limited amount of testing has been completed with these alloys. It should be emphasized that the critical velocity is probably lower on the cast stainless steels than on the wrought material, and this fact should be considered before using the steel.

3.3 SEDIMENTATION RATES OF THORIUM OXIDE SLURRIES AT ELEVATED TEMPERATURES

S. A. Reed

Tests were made to determine the sedimentation rates of thorium dioxide slurries at elevated temperatures. Approximate rates were determined at 250 and 300°C for three concentrations: 250, 500, and 1000 g of thorium oxide per liter.

The experimental technique consisted in sealing a known quantity of slurry in a quartz capsule 25 to 30 cm in length and 8 mm in diameter. The capsules were inserted in a vertical tube furnace and agitated by a mechanical vibrator. The apparatus is shown in Fig. 3.4. Each slurry sample was heated to the desired temperature and vigorously agitated for 30 min to obtain a uniform suspension. Agitation was then stopped, and settling was followed by means of a motion-picture camera. Rates were calculated by plotting the frames per second vs the change in slurry height. The results are shown in Table 3.3.

Slurries used in these tests were prepared from high-purity thorium dioxide and distilled water. The thorium dioxide was made by calcining purified thorium formate at 650°C for 4 hr. Chemical and spectrographic analyses indicated that less than 50 ppm of impurities was present. Traces of iron, calcium, and copper were the only impurities detected.

[27] J. C. Griess and R. E. Wacker, *HRP Quar. Prog. Rep. July 31, 1953*, ORNL-1605, p 74.

[28] J. C. Griess and R. E. Wacker, *HRP Quar. Prog. Rep. Oct. 31, 1953*, ORNL-1658, p 45.

[29] J. C. Griess and R. E. Wacker, *HRP Quar. Prog. Rep. Jan. 31, 1954*, ORNL-1678, p 50.

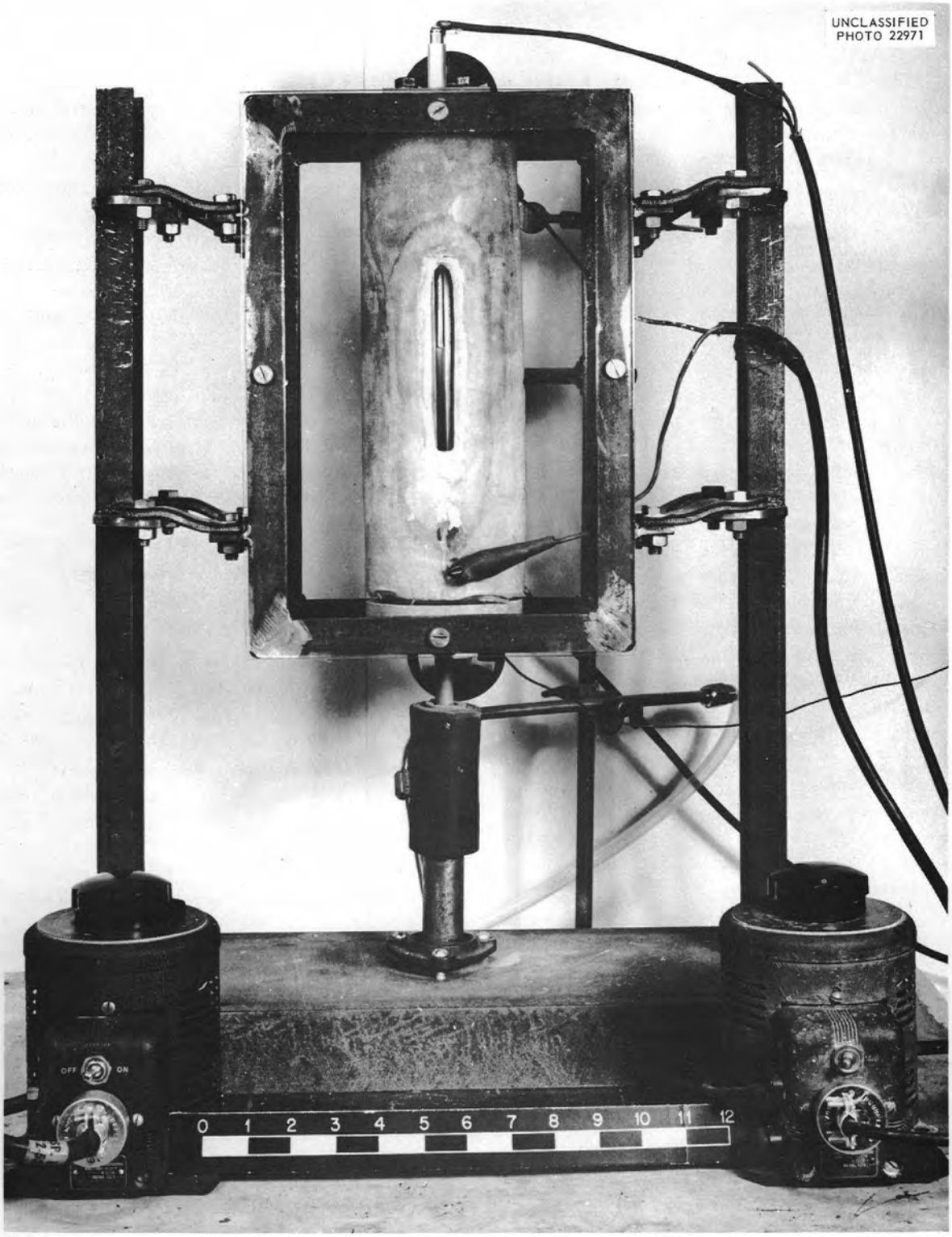

Fig. 3.4. Apparatus for Determining Sedimentation Rates of ThO_2 Slurries.

TABLE 3.3. SEDIMENTATION RATES OF ThO_2 SLURRIES AT 250 AND 300°C

Slurry Concentration (g of ThO_2 per liter)	Rate of Sedimentation (cm/sec)	
	250°C	300°C
250	0.24	0.28
500	0.14	0.18
1000	None*	None*

*No free settling was apparent. Although a measurable rate was observed, settling appeared to be in the compaction zone at all times.

It would appear from these data that in the concentration range where free settling occurs the change in sedimentation rate between 250 and 300°C could be explained on the basis of the change in viscosity of water alone. This assumption may not be valid, however, when the particles or agglomerates of thorium dioxide are surrounded by a lyosphere of water which could be effectively altered by a change in temperature or by the presence of impurities.

During tests made before the sedimentation rates were measured, several interesting phenomena were observed. While various slurry preparations were being heated from room temperature, a marked degradation of the larger agglomerates appeared to occur, particularly in the temperature range 150 to 180°C. As the heating proceeded to 250°C, the agglomerates continued to diminish in size but at a lesser rate. Visually, no change occurred between 250 and 300°C. Several slurries containing corrosion products, from loop tests, and slurries prepared in a laboratory blender at high shear rates were viscous and caked on the sides of the tubes at room temperature but moved freely at temperatures above 170°C. Slurries with high sulfate contamination (>5000 ppm), which were very viscous at room temperature, also flowed more readily at 250 to 300°C. However, those containing corrosion products, and especially sulfate, had a greater tendency to remain in the agglomerated state at elevated temperatures.

In all tests the phenomenon was reversible. When the temperature was gradually lowered, turbidity appeared in some preparations at a temperature as high as 180°C; the agglomerates grew rapidly on further cooling. The tube walls became coated, and the slurry returned to a viscous condition.

Settling-rate measurements are being continued and will be extended to include the lower temperature ranges, where extensive agglomeration occurs. Slurries made of other thorium dioxide preparations are also being investigated.

ACKNOWLEDGMENTS

The following groups contributed to the over-all program:

O. E. Menis, C. M. Boyd, R. G. Ball, R. E. Corcoran, M. L. Hubbard, I. B. Rukin, C. K. Talbott, N. M. Ferguson, W. R. Music, T. C. Rains, *et al.*, for analytical services to the Dynamic Loop and In-Pile Loop corrosion programs.

P. F. Thomason, *et al.*, for analytical services to the In-Pile Bomb test program.

U. Koskela, *et al.*, for analytical services to the In-Pile Loop and Bomb programs.

D. S. Toomb, J. A. Russell, *et al.*, for instrumentation for Loop and Laboratory test programs.

J. DeLorenzo, *et al.*, for instrumentation for In-Pile Loop and Bomb programs.

4. RADIATION CORROSION

G. H. Jenks H. C. Savage

W. N. Bley H. O. Day D. T. Jones M. D. Silverman
N. C. Bradley H. A. Fisch R. A. Lorenz H. H. Stone
S. F. Clark D. N. Hess J. R. McWherter R. M. Warner
W. E. Clark B. O. Heston A. R. Olsen W. C. Yee

4.1 IN-PILE LOOP

H. C. Savage G. H. Jenks

W. N. Bley J. E. Baker
N. C. Bradley R. A. Lorenz
D. T. Jones A. R. Olsen
R. M. Warner

4.1.1 Development and Construction

(a) HB-4 Mockup. In-pile loop assembly FF was completed during the past quarter. The circulating pump in this loop contains hardened type 17-4 PH stainless steel journal bushings instead of the Stellite 98M2 that was used in loop DD. The use of the 17-4 PH bushings will, as mentioned previously,[1] eliminates introduction of cobalt into the circulating solution. Loop FF contains Zircaloy-2 corrosion specimens in Zircaloy-2 holders in both the in-line and core positions and Zircaloy-2 impact specimens in the core position. All other components of the loop are type 347 stainless steel.

The initial testing of loop FF was essentially the same as that described previously[1] for loop DD. Approximately 224 hr of operation was accumulated on the loop in the in-pile mockup at Y-12 before the loop was installed in beam hole HB-4 in the LITR. After 82 hr of operation during the test period, it became necessary to replace the circulating pump because the screw holding the impeller to the rotor shaft broke off and allowed the impeller to loosen on the shaft and rub against the pump scroll. A new impeller screw, which has increased head thickness for additional strength, was tack-welded in place to prevent loosening. Screws of this type will also be used on future pumps.

Several interruptions to loop operation occurred due to water leakage at the silver-soldered connections in the loop and pump cooling-water lines passing through the loop and shield plug connector.[2] These leaks are believed to have resulted from poor silver-soldering procedures, which will be corrected.

In view of the initial difficulties with loop FF and as a final check of the loop assembly, the loop was run continuously for 123 hr at 250°C and 1000 psia with 0.13 *m* natural uranyl sulfate solution containing 0.031 *m* $CuSO_4$ and 0.0085 *m* (5 mole % excess) sulfuric acid. Operation during this period was entirely satisfactory. The loop was then charged with enriched uranyl sulfate solution (0.17 *m*) containing 0.031 *m* $CuSO_4$ as an internal catalyst for recombination of hydrogen and oxygen and 0.04 *m* (25 mole % excess) sulfuric acid. After 23 hr of satisfactory operation at 250°C and 1000 psia, loop FF, containing the enriched uranyl sulfate solution described above, was installed in beam hole HB-4 at the LITR for radiation-corrosion studies.

(b) Loop Package Testing. One in-pile development loop was used to test the modified 5-gpm in-pile circulating pump described in the following paragraphs. Two loops are now available and will be used to test proposed changes such as the use of a titanium or Zircaloy-2 core before the changes are incorporated in the in-pile loop assemblies to be inserted in HB-4.

(c) ORNL Pump for HB-4 Loop Package. The in-pile loop circulating pump now in use was designed by the REED Engineering Development Section. This pump has been described previously.[3,4]

Two of these pumps (Fig. 4.1), containing an all-metal (Stellite 98M2–Stellite 98M2) journal-bearing combination, have been built. One pump was operated for 140 hr with water at 250°C, and the other pump was operated for 140 hr with water at

[1] G. H. Jenks, H. C. Savage, *et al.*, *HRP Quar. Prog. Rep. Oct. 31, 1954*, ORNL-1813, p 88.

[2] G. H. Jenks, H. C. Savage, R. A. Lorenz, and D. T. Jones, *HRP Quar. Prog. Rep. April 30, 1954*, ORNL-1753, p 81-94.

[3] R. J. Kedl, T. H. Mauney, C. B. Graham, and W. L. Ross, *HRP Quar. Prog. Rep. Jan. 1, 1953*, ORNL-1478, p 58-59.

[4] G. H. Jenks, H. C. Savage, R. A. Lorenz, and D. T. Jones, *HRP Quar. Prog. Rep. April 30, 1954*, ORNL-1753, p 81-94.

[redacted]
ORNL-LR-DWG 5291

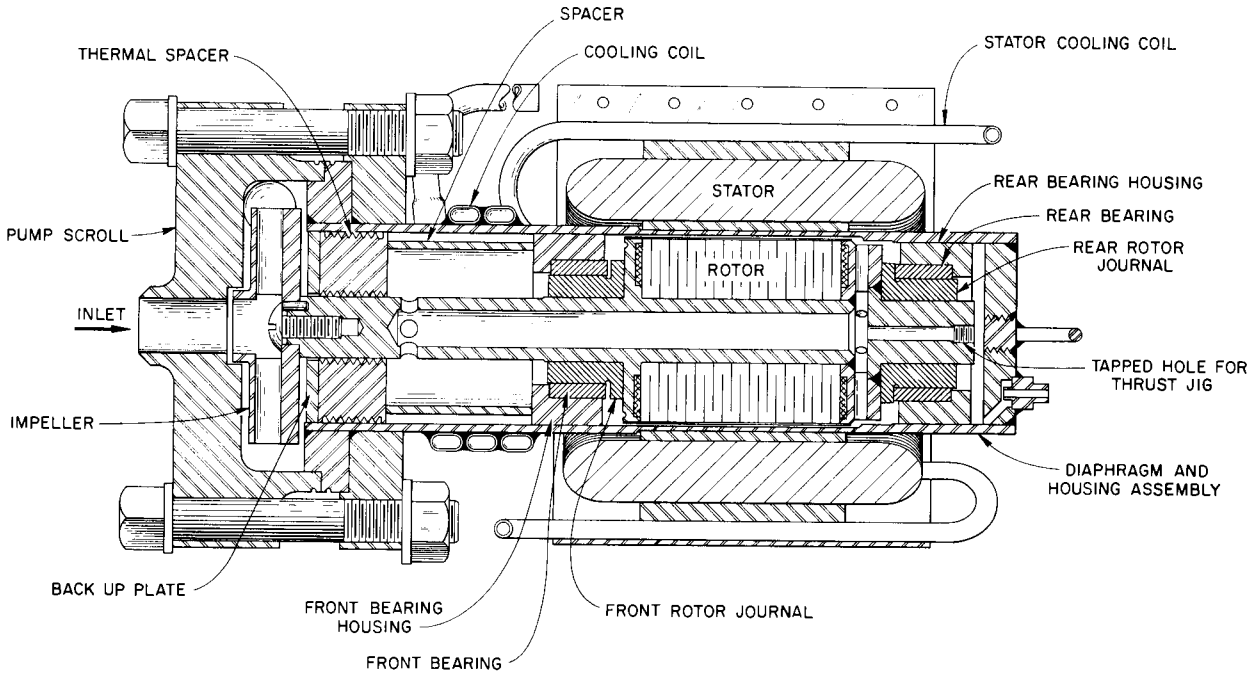

Fig. 4.1. Modified ORNL 5-gpm Pump for In-Pile Loop.

250°C followed by an operation of 100 hr with uranyl sulfate solution (0.17 *m*) at 250°C. No visible or measurable radial-bearing wear was observed in either case. However, some thrust-bearing wear (~0.010 in.) was found in the first pump, with a thrust load of less than 5 lb. Thrust-bearing wear of the second pump was negligible, with a thrust load of about 2 lb.

Similar runs with all-metal (Stellite 98M2) bearings in the present ORNL 5-gpm pump had been made previously. In one run (HT-8) bearing failure occurred after about 69 hr of operation. In another run of approximately 10 hr, excessive radial-bearing wear was noted.

The results of these tests indicate that some bearing improvement has been made with the modification described. One pump with "outboard" bearings is now being equipped with sintered aluminum oxide journals and bearings. The sintered aluminum oxide has shown excellent corrosion resistance to uranyl sulfate solutions, and preliminary tests of this material by the Mechanical Development Section at the K-25 plant indicate that it is an excellent bearing material. Until further tests are made on this pump, the second pump with "outboard" bearings will remain equipped with hardened type 17-4 PH stainless steel journal bushings and with Graphitar No. 14 bearings for use in an in-pile loop. This bearing combination has been satisfactory in the present pumps.

(d) Byron Jackson Pump. The Byron Jackson pump has been operated by the factory for approximately 40 hr at room temperature. During this time it was determined that the pump developed 41 ft of head at 5 gpm and that the performance curve is essentially flat to a flow rate of approximately 7.5 gpm. The temperature of the motor windings rose 42°C. The pump was then dismantled, and the aluminum oxide bearings, upon examination, showed no signs of wear. The pump was reassembled and operated at 2000 psi and 372°F for 1 hr. During this run the temperature of the motor windings rose 43°C. It was decided to have Byron Jackson complete this test in Oak Ridge on an existing loop. The pump has been shipped to ORNL.

(e) Allis-Chalmers Pump. On January 10, 1955 a purchase contract was negotiated with Allis-Chalmers for a 5-gpm pump. In the meantime, Allis-

Ch[redacted] completed machine work on all the parts for the pump and has sent these parts to ORNL for application of an oxide coating.

4.1.2 LITR Operations – In-Pile Loop Corrosion Test DD

(a) Introduction. An in-pile loop experiment which was designed to determine the effect of reactor radiations on the corrosion of stainless steel by uranyl sulfate solution at 250°C has been completed. The over-all experiment included: preparing the loop for operation and proving its satisfactory performance, exposing and operating the loop in hole HB-4 of the LITR, dismantling the loop, and examining the corrosion specimens and other portions of the loop for evidence of effects of the irradiation on corrosion.

(b) Preparation of Loop. The loop for this experiment was of the in-pile loop design described previously.[5] Details of the preparation for in-pile installation, together with pertinent details of construction, have been reported.[6] For convenience, some of this information is also repeated here.

[5] G. H. Jenks, H. C. Savage, R. A. Lorenz, and D. T. Jones, *HRP Quar. Prog. Rep. April 30, 1954*, ORNL-1753, p 81-94.

TABLE 4.1. LOOP VOLUMES AND OTHER SPECIFICATIONS

Loop volume (including pressurizer)	1505 cc
Pressurizer volume	520 cc
Flow rates	
(a) Pressurizer	6.6 cc/sec
(b) Core	5.7 gpm
Pump bearing material	Graphitar No. 14
Pump journal material	Stellite 98M2
System pressure checked at	1250 psi
Corrosion sample units	
(a) Specimen materials	Type 347 stainless steel
(b) In-line holder	Zircaloy-2 (No. 10)
(c) Core holder	Zircaloy-2 (No. 11)
(d) Minimum clearance	
(1) Core holder	0.044 in.
(2) In-line holder	0.046 in.
Impact sample units	
(a) Material	Zircaloy-2
(b) Identification numbers	2, 4, 6, 8, 10, 12, 14, 16

Constructional material for the loop was type 347 stainless steel. An ORNL 5-gpm canned-rotor pump was used to effect circulation. The loop contained two sets of stainless steel sample coupons, which were mounted in Zircaloy-2 tapered holders. It also contained a set of Zircaloy-2 impact specimens. The coupon holders were positioned in the loop so that, in HB-4, one set (core samples) was exposed to the maximum intensity of reactor radiations. The other set (in-line samples) was in a region of low radiation intensity. The set of impact specimens was located around the outside of the core sample holder, also in the field of high radiation intensity.

A summary of the loop and sample specifications is presented in Tables 4.1 and 4.2.

[6] G. H. Jenks, H. C. Savage, *et al.*, *HRP Quar. Prog. Rep. Oct. 31, 1954*, ORNL-1813, p 87-88.

TABLE 4.2. LOOP AREAS EXPOSED TO HIGH-TEMPERATURE SOLUTION

Component	Area Exposed (cm^2)
Stainless Steel	
Total main circulation lines (not including pump and core)	1553
Pressurizer	
Total 706 cm^2	
Area wetted when filled with 300 ml of solution	414
Pressurizer lines	300
Core (not including specimens)	445
Pump	
Scroll	272
Impeller	159
Samples	
Twelve core specimens	34
Twelve in-line specimens	34
	3211
Zircaloy-2	
Impact specimens	19
Core holder	162
In-line holder	162
	343

A summary of the loop operations which comprised part of the preparation is given in Table 4.3.

TABLE 4.3. SUMMARY OF PREPARATORY OPERATION

Time (hr)	Conditions
19.0	Distilled H_2O, 100 to 250°C
2.9	3 wt % tribasic sodium phosphate + N_2 (partial pressure 85 psi), 100°C
12.5	5 wt % HNO_3 + N_2 (partial pressure 85 psi), 100°C
12.4	Distilled H_2O + O_2 (partial pressure 70 psi), 250°C
84.9	Normal UO_2SO_4 (28 g of uranium per liter) + 0.031 *m* $CuSO_4$ + 0.0085 *m* H_2SO_4, 250°C, 70 psi O_2

Following the 85-hr operation with normal uranium, the loop was moved to the HB-4 site. There it was drained and flushed and recharged with a solution of the following composition, which was used for the in-pile operation: UO_2SO_4, 38.45 g of uranium per liter (U^{235}/total U = 0.888); $CuSO_4$, 0.031 *m*; H_2SO_4, 0.0085 *m*; CrO_3, 0.002 *m*.

(c) In-Pile Operation. The general operating conditions and procedures, the results, the corrosion indicated by nickel and oxygen data, and the performance of equipment are described in the following paragraphs.

(1) *General Operating Conditions and Procedures*

1. Exposure period

In-pile operation of the loop with enriched solution was for a period of 465 hr. The reactor operating schedule during this time is shown in Fig. 4.2. The reactor power levels during the initial operation were, chronologically, 0, 300 kw, and 1, 2, and 3 Mw. Further reactor operation after the initial period was at full reactor power of 3 Mw. The energy output of the LITR during the operation was 840 Mwhr, of which only 49 Mwhr was liberated at reactor powers below 3 Mw.

2. Temperatures

Design temperatures of 250°C in the main stream and 280°C in the pressurizer were maintained in the loop. The rotor region of the pump was at a temperature of about 70°C. These temperatures were maintained continuously during the in-pile operation, with the exception that on two occasions oxygen was added. On these occasions, the main stream and pressurizer temperatures were lowered to 185 and 215°C, respectively. Roughly, 2 hr was required for each addition. Control and measurement of temperature in the pressurizer were sufficiently precise that the uncertainty in relative values for the corresponding steam pressures was held to about ±1 psi. Control of temperature in the main stream was within ±1°C.

3. Excess oxygen

Excess oxygen was maintained in the loop at all times. As measured by the oxygen pressure in the pressurizer, the amount of excess was initially 70 psi. The corresponding pressure of dissolved oxygen in the main stream was 90 psi. During operation, the oxygen pressure decreased continuously as oxygen was consumed in oxidation of loop materials. Whenever the pressure had decreased to the neighborhood of (but not below) 25 psi, a volume of oxygen was added which was sufficient to return the pressure to the initial 70 psi. As mentioned previously, two additions were required during the in-pile operation.

The general method which was followed in adding a measured volume of oxygen to the loop has been described previously.[7] Accurate determinations of the oxygen pressure were made during each reactor shutdown. The determinations were carried out simply by measuring the temperature of the pressurizer and the total pressure. The difference between the value for the total pressure and the value for the steam pressure, which corresponded to the measured temperature, was taken as the value for the oxygen pressure. Gas pressures were also determined at regular intervals during reactor operation. However, the values thus obtained represented the pressure of excess oxygen plus the pressure of a 2:1 mixture of H_2 and O_2 formed in the radiolytic decomposition of water. The steady-state pressure of the radiolytic gas was small compared with that of the excess oxygen and remained fairly constant for long periods of operation. It was thus possible to obtain a fairly accurate value for the oxygen pressure at any time. Accurate determinations of the radiolytic gas pressure were made by observing the change in total

[7] G. H. Jenks, D. T. Jones, and R. A. Rosenberg, *HRP Quar. Prog. Rep. July 31, 1953*, ORNL-1605, p 102.

[redacted]

ORNL-LR-DWG 5292

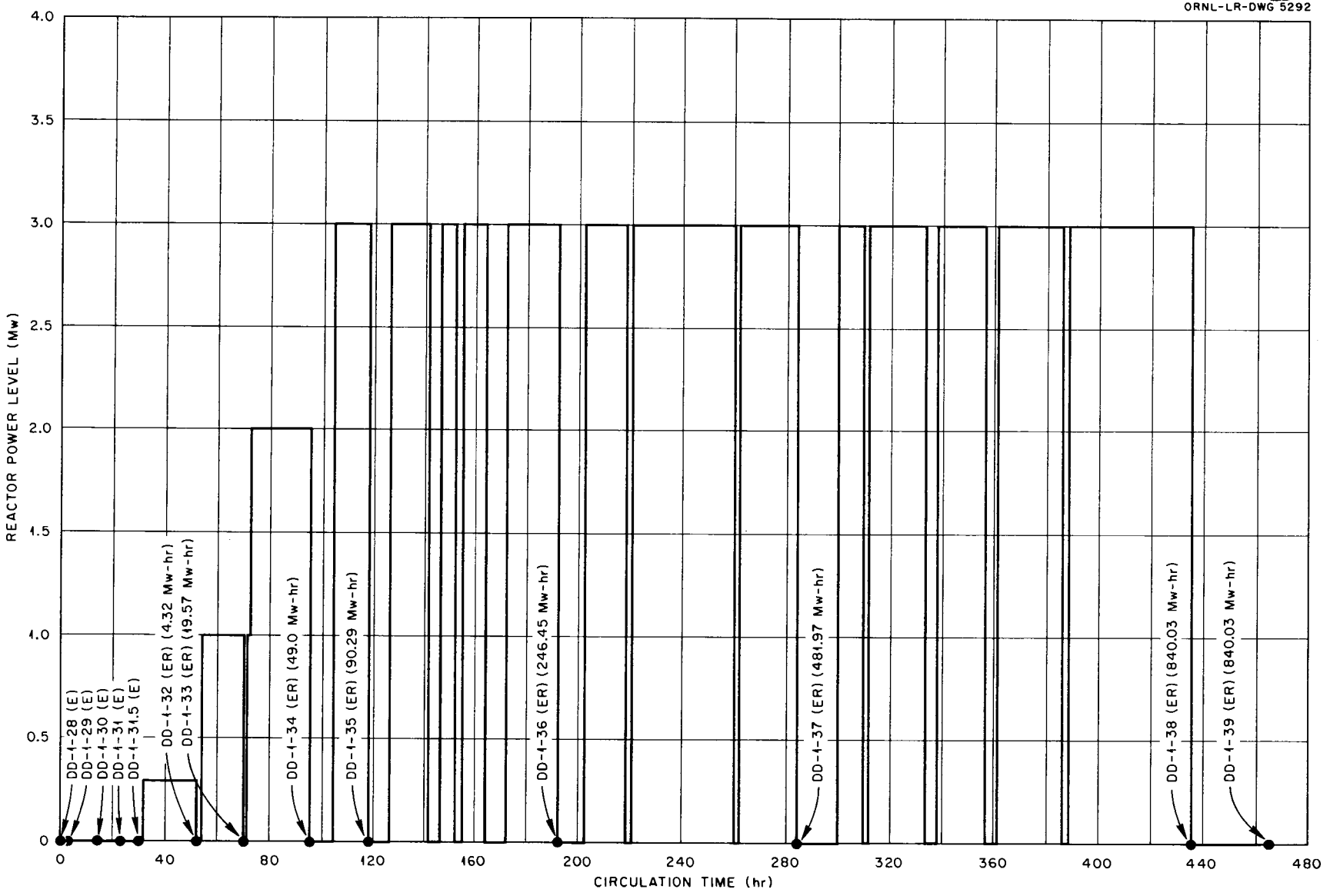

Fig. 4.2. Reactor Power Level During In-Pile Operation.

gas pressure at the times of reactor shutdown and startup.

The shutdown schedule during the operation is shown in Fig. 4.2.

4. Loop-solution sampling

Samples of loop solution were withdrawn during the enriched-fuel operation in accordance with the schedule shown in Fig. 4.2. These samples were subjected to chemical, spectrographic, and radiochemical analyses.

The sampling was carried out with the use of the loop sampling system.[8] With this system the solution is drawn from the loop through the drain line into a 4.5-ml tank, which is called the standard drain volume. From this tank the solution may be transferred into the fuel reservoir or into the sample tank.

Briefly, the procedure was to make two or three drain-line purges into the standard drain volume. Each was drained into the fuel reservoir. A sample was then collected in the tank and transferred to the sample tank. Two samples were taken on the occasion of each sampling. The second half of each sample was obtained after further purging of the drain line and standard drain volume. After the sample had been obtained, the standard drain tank and the sample lines were flushed with water and with nitrogen gas. The flush water was also drained into the fuel reservoir. Between sampling periods, the tank and lines were filled with N_2 at about 15 psi pressure. The loop liquid inventory was maintained and the drain line was flushed by forcing water into the loop from the thermal-expansion tank. This replacement of fuel with water resulted in a continuous dilution of solutes. By the end of the experiment, the UO_2SO_4 had been diluted to about 80% of the original concentration.

5. Fission power developed in loop solution

Determinations of the fission power that was developed in the loop solution were carried out in three different ways: measuring the difference between the electrical powers required to maintain loop temperatures when the reactor was at power and when it was shut down, analyzing the loop samples for total fissions, and monitoring the neutron flux at each core sample.

The solution analysis for total fission was carried out by the Analytical Chemistry Division. The method of analysis involved separation of cesium from the solution and comparison of the activity of this cesium with that of a total-fission standard.

The relative neutron fluxes which prevailed near each specimen were determined by measuring the relative quantities of the induced activity, Cr^{51}, in the different specimens after they were defilmed. A gamma-ray scintillation spectrometer was employed. Absolute values for the neutron fluxes at the different specimens were also determined from the induced chromium activities. They were determined by comparing the activities of the loop samples with the activity of a control sample which was irradiated in the ORNL Graphite Reactor for a known nvt.

6. Termination of operation

At the end of 465 hr of in-pile operation, the loop was drained and flushed with water. It was then withdrawn and transferred to the dismantling facilities in Building 4501. In order to drain the loop, the temperatures were lowered approximately 65°C from the operating temperatures, a pressure of 800 psi of nitrogen gas was applied in the pressurizer, and the solution was forced, by this pressure, through the drain line and into the fuel reservoir. Active gases from the loop were collected in the gas holdup tank. After the solution and gases were removed, the loop was evacuated and then filled with water. The water was circulated for approximately 10 min and then drained into the fuel reservoir. This flushing operation with water was repeated for a total of six flushings.

Before the loop was drained, the weight of solution in the fuel reservoir was measured, and the solution was sampled and removed. The weight was again measured and the solution sampled after the draining and flushings. These samples were analyzed for uranium, and a value was obtained for the total amount of uranium removed from the loop. After about a week of cooling, the solution in the fuel reservoir was transferred into the fuel removal tank and then to the Chemical Technology Division for storage. The gases in the gas holdup tank were vented, after cooling, into the pile off-gas system.

(2) *Results*

1. Solution analyses

a. Preparatory operation

The results of solution analyses during the preparatory operations are listed in Table 4.4.. The calculated total inventory for each constituent is listed in columns headed "Corr." These results

[8] G. H. Jenks, D. T. Jones, and R. A. Lorenz, *HRP Quar. Prog. Rep. Oct. 31, 1953*, ORNL-1658, p 68.

TABLE 4.4. ANALYSES OF SAMPLES FROM LOOP INVENTORY DURING PREPARATORY OPERATIONS*

Remarks	Sample No.	Total Circulation Time (hr)	Solution Withdrawn for Sample (ml)	H_2O Added After Sampling (ml)	Calculated Inventory Volume Before Sampling (ml)	Uranium		Sulfate		pH, Rep.	Copper		Cobalt		Nickel		Chlorine		Chromium		Iron		Aluminum		Manganese		Silicon	
						Rep. (mg/ml)	Corr.** (g)	Rep. (mg/ml)	Corr.** (g)		Rep. (μg/ml)	Corr.** (g)	Rep. (μg/ml)	Corr.** (mg)	Rep. (μg/ml)	Corr.** (mg)	Rep. (μg/ml)	Corr.** (mg)	Rep. (μg/ml)	Corr.** (mg)	Rep. (μg/ml)	Corr.** (mg)	Rep. (μg/ml)	Corr.** (mg)	Rep. (μg/ml)	Corr.** (mg)	Rep. (μg/ml)	Corr.** (mg)
Distilled H_2O, 100–250°C		19.0																										
3% TSP, 100°C, N_2 (85 psi)		2.9																										
5% HNO_3, original solution before charging to loop	DD-1-2	0									<1 (P)				(ND) (C)		<1 (T)		2 (C)		41 (C)							
5% HNO_3, 100°C, N_2 (85 psi)	DD-1-3	12.5									5 (P)		<1 (C)		12 (C)		<1 (T)		21 (C)		94 (C)							
	DD-1-4	12.5									9 (P)		10 (C)		15 (C)		<1 (T)		26 (C)		123 (C)							
	DD-1-5	12.5									3 (P)		8 (C)		11 (C)		<1 (T)		7 (C)		7 (C)							
Distilled H_2O, 250°C, O_2 (70 psi)	DD-1-12	12.4									(ND) (P)		(ND) (C)		(ND) (C)		<1 (T)		3 (C)		(ND) (C)							
	DD-1-13	12.4									(ND) (P)		(ND) (C)		(ND) (C)		<1 (T)		5 (C)		(ND) (C)							
Normal UO_2SO_4 solution before charging to loop	DD-1-1	0				28.5 (T)		15.5 (IE)		2.0	1907 (P)		(ND) (P)		(ND) (P)		(ND) (T)		1 (C)		10 (C)							
	DD-1-1(C)	0									1800 (S)				<4 (S)				<1 (S)				11.7 (S)		<1 (S)		2.3 (S)	
Charged solution to loop, 250°C, O_2 (70 psi)																												
Sample from main loop	DD-1-15	2	9	0	1109	26.6 (T)	29.5	15.5 (IE)	17.2	2.0	2050 (P)	2.27	(ND) (P)		8 (P)	9	<1 (T)	1	8 (C)	9	17 (C)	19						
Sample from behind pump	DD-1-16	2	9	1.2	1100	29.5 (T)	32.7	15.8 (IE)	17.6	2.0	1920 (P)	2.13	(ND) (P)		8 (P)	9	3 (T)	3	8 (C)	9	21 (C)	23						
Sample from main loop	DD-1-17	7	7	0	1092	28.3 (T)	31.0	16.2 (IE)	18.0	2.0	1960 (P)	2.17	(ND) (P)		22 (P)	24	<1 (T)	1	21 (C)	23	34 (C)	38						
Sample from behind pump	DD-1-18	7	7	0	1085	30.8 (T)	34.1	16.7 (IE)	18.5	2.0	1980 (P)	2.19	(ND) (P)		25 (P)	27	<1 (T)	1	16 (C)	18	26 (C)	29						
Sample from loop	DD-1-19	22	30	0	1078	28.4 (T)	31.5	15.5 (IE)	17.2	2.0	1950 (P)	2.17	19 (P)	21	90 (P)	97	3.7 (T)	4	5.8 (C)	7	4.3 (C)	5						
Sample from loop after shutdown at Y-12	DD-1-20	24	6	0	1048	28.3 (T)	31.4	16.2 (IE)	18.4	2.1	1760 (P)	1.97	(ND) (P)		77 (P)	84	<1 (T)	1	2.5 (C)	3	38 (C)	41	105 (S)	110	19 (S)	20	180 (S)	189
Loop inoperative about 20 hr between shutdown at Y-12 and startup at ORNL (inventory not removed from loop during this period)																												
Sample from main loop	DD-1-23	37.8	10	46.9	1042	27.3 (T)	30.4	16.6 (IE)	18.9	2.1	2150 (P)	2.37	(ND) (P)		85 (P)	92	5 (T)	5	25 (C)	27	30 (C)	32						
Sample from main loop using loop sampling procedure	DD-1-25	64.4	47.2	0	1049	25.7 (T)	29.1	16.9 (IE)	19.5	2.8	1900 (P)	2.15	163 (P)	172	131 (P)	142			34 (C)	37	90 (C)	96						
Sample from main loop after pump shutdown	DD-1-26	84.9	10	0	1032	28.2 (T)	32.6	15.5 (IE)	18.6	2.0	1960 (P)	2.26	125 (P)	138	123 (P)	138	8 (T)	9	46 (C)	50	19 (C)	25	2.9 (S)	9.6	15 (S)	17	19.2 (S)	31
Sample from loop inventory after removal from loop	DD-1-29	84.9			1012														69 (C)	73			198 (S)	207	25 (S)	27		

*Where no values are given, either an analysis was not requested or the analytical results were not reliable.

ND Not detected
C Colorimetric
T Titrametric
IE Ion exchange, volumetric
P Polarographic
G Gravimetric
S Spectrographic

**Amount present plus accumulated amount previously withdrawn as samples.

TABLE 4.5. ANALYSES OF SAMPLES FROM LOOP INVENTORY DURING ENRICHED-SOLUTION OPERATION*

Sample	Total Circulation Time (hr)	LITR Energy (Mwhr)	Inventory Volume at Time of Sample (ml)	Uranium		Correction Factor for Sample Dilution	Sulfate		pH	Copper		Cobalt		Nickel		Chlorine		Chromium		Iron		Aluminum		Manganese		Silicon		Specific Gravity
				Calc.*** (mg/ml)	Rep. (mg/ml)		Rep. (mg/ml)	Corr.** (mg/ml)		Rep. (μg/ml)	Corr.** (μg/ml)	Rep. (μg/ml)	Corr.** (μg/ml)	Rep. (μg/ml)	Corr.** (μg/ml)	Rep. (μg/ml)	Corr.** (μg/ml)	Rep. (μg/ml)	Corr.** (μg/ml)	Rep. (μg/ml)	Corr.** (μg/ml)	Rep. (μg/ml)	Corr.** (μg/ml)	Rep. (μg/ml)	Corr.** (μg/ml)	Rep. (μg/ml)	Corr.** (μg/ml)	
Orig. soln.	0	0		38.7	38.7 (G)		20.4 (IE)	20.4	1.80	1920 (P)	1920			(ND) (P)	(ND)	<1 (T)	<1	104 (C)	104	(ND) (C)	(ND)	17 (S)	17	<2 (S)	<2	41 (S)	41	1.043
DD-1-29(E)	2.4	0	1069	38.7	36.1 (T)	1.07	20.6 (IE)	24.7	2.00	1770 (P)	1930	(ND) (C)	(ND)	(ND) (C)	(ND)	1 (T)	1	73 (C)	79	(ND) (C)	(ND)	19 (C)	20	16 (S)	17	(ND) (C)	(ND)	
DD-1-30(E)	12.7	0	1081	37.6	31.0 (T)	1.21	17.0 (IE)	21.2	2.25	1520 (P)	1900	(ND) (C)	(ND)	(ND) (C)	(ND)	1 (T)	1	59 (C)	73	(ND) (C)	(ND)	9 (S)	11	12 (S)	15	9 (S)	11	
DD-1-31(E)	23.2	0	1060	37.8	33.9 (T)	1.12	19.7 (IE)	23.2	2.25	1820 (P)	2140	(ND) (C)	(ND)	(ND) (C)	(ND)	1 (T)	1	57 (C)	68	(ND) (C)	(ND)	12 (S)	13	11.5 (S)	14	145 (S)	163	
DD-1-31.5(E)	29.4	0	1078	36.3	31.2 (T)	1.16	18.7 (IE)	23.1 (IE)	2.00	1500 (P)	1850	(ND) (C)	(ND)	(ND) (C)	(ND)	1 (T)	1	54 (C)	67	(ND) (C)	(ND)							
DD-1-32(ER)	51.7	4.3	1070	36.1	33.3 (T)	1.09	18.8 (IE)	22.0	2.00	1610 (P)	1880	(ND) (C)	(ND)	(ND) (C)	(ND)	1 (T)	1	46 (C)	50	(ND) (C)	(ND)	3.4 (S)	3.7	5.6 (S)	7	11.4 (S)	13	
DD-1-33(ER)	72.6	19.6	1061	36.0	32.7 (T)	1.10	17.8 (IE)	21.4 (IE)	2.00	1610 (P)	1930	(ND) (C)	(ND)	(ND) (C)	(ND)	1 (T)	1	40 (C)	44			12 (C)	13					
DD-1-34(ER)	95.4	49.0	1052	35.8	29.7 (T)	1.21	16.5 (IE)	22.0	2.10	1420 (P)	1900	(ND) (C)	(ND)	(ND) (C)	(ND)	1 (T)	1	18 (C)	22									
DD-1-35(ER)	120.2	90.3	1044	35.4	26.9 (T)	1.32	17.0 (IE)	24.9	2.05	1430 (P)	2100	(ND) (C)	(ND)	79 (C)	105	1 (T)	1	3 (C)	4									
DD-1-36(ER)	192.9	246.5	1035	35.0	30.8 (T)	1.14	15.7 (IE)	20.6	2.20	1380 (P)	1820	87 (P)	100	143 (P)	167	1 (T)	1	15 (C)	17	23 (C)	26	21 (C)	25					
DD-1-37(ER)	289.0	482.0	1028	35.0	29.7 (T)	1.18	16.6 (IE)	22.7	2.60	1420 (P)	1950	142 (P)	171	277 (P)	336	1 (T)	1	15 (C)	18	17 (C)	21							
DD-1-38(ER)	435.5	840.0	1019	34.7	27.3 (T)	1.27	16.2 (IE)	23.9	2.60	1410 (P)	2090	121 (P)	160	368 (P)	483	<1 (T)	1	17 (C)	22	18 (C)	24	13 (C)	17					
DD-1-39(ER)	465.5	840.0	1010	34.5	32.1 (T)	1.08	17.9 (IE)	23.2	2.65	1550 (P)	2160	119 (P)	138	410 (P)	468	<1 (T)	1	42 (C)	45	28 (C)	32	13 (C)	15					

*Where no values are given, either an analysis was not requested or the analytical results were not reliable.

ND Not detected
C Colorimetric
T Titrametric
IE Ion exchange, volumetric
P Polarographic
G Gravimetric
S Spectrographic
E Enriched uranium
ER Enriched uranium, irradiated

**Analytical result corrected for dilution of sample and for amounts removed in previous samples.

***Analytical result corrected for dilution of sample.

are indicative of normal performance. A total of 137.6 mg of nickel entered solution during the UO_2SO_4 operation.

b. Enriched-solution operation

The results of solution analyses for constituents other than products of irradiation are listed in Table 4.5 and plotted in Fig. 4.3.

As stated previously, the volume of solution in the loop was maintained fairly constant by replacing with water the solution withdrawn during sampling. Calculated corrections for this dilution have been made for each constituent in order to obtain values for the amount which would have been present if dilution had not taken place. This

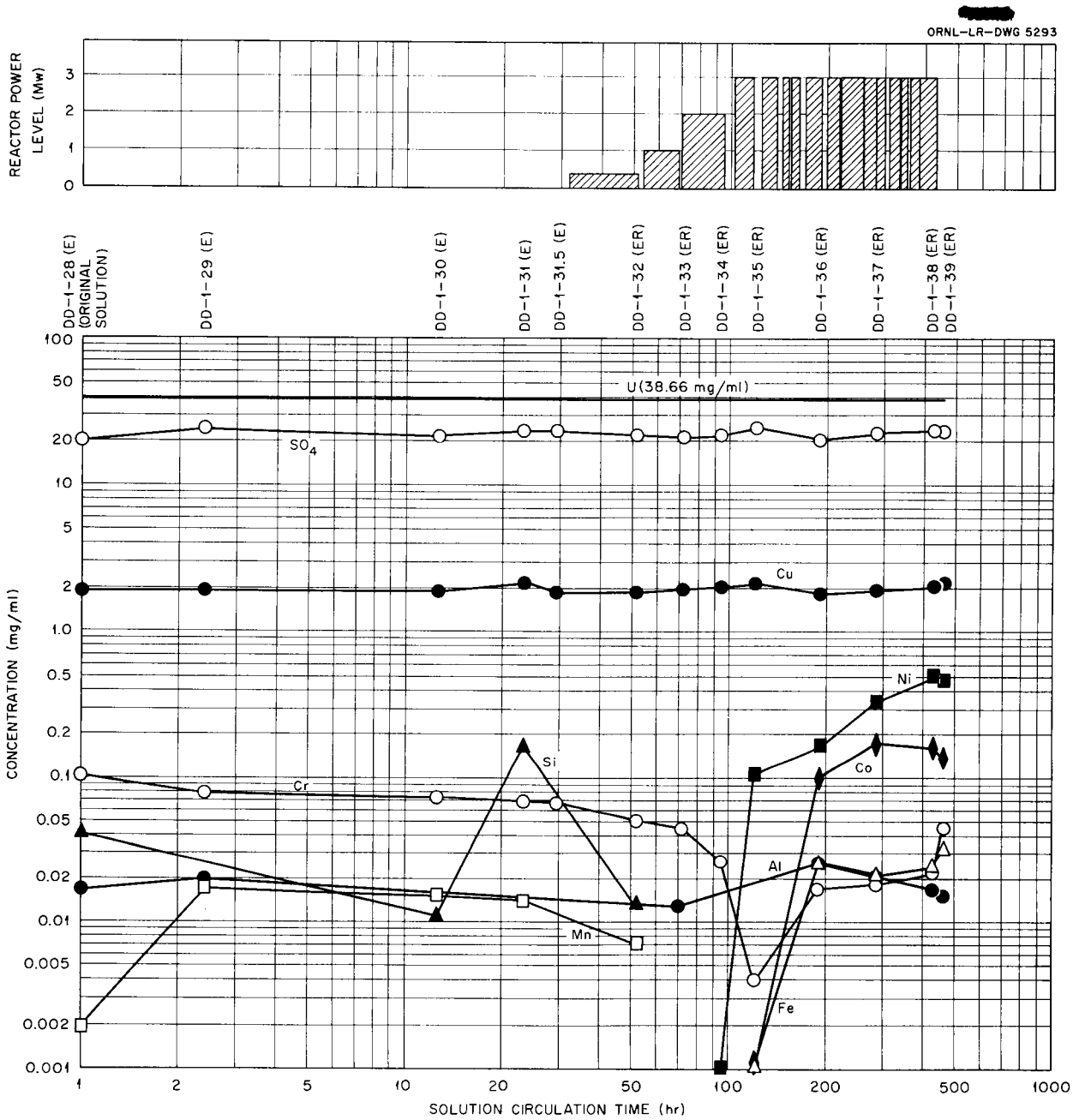

Fig. 4.3. Solution Analyses During In-Pile Operation.

correction was not applied to the chromium after irradiation was initiated, since the concentration of this element was then probably that of a steady state determined primarily by the oxidation-reduction characteristics at the time of sampling.

A further correction for dilution of sample contents was also found to be necessary. Analyses showed that each sample contained less than the calculated amount of uranium. The ratio of the calculated to the observed amounts ranged from 1.07 to 1.31. The correction for this dilution was obtained in each case by assuming that the calculated uranium concentration represented the true uranium concentration in the loop solution.

The validity of this assumption is supported by data described below, which, though uncertain, indicate fairly complete recovery of uranium from the loop. It is also supported by the fact that corrected values for the concentration of copper in solution were not consistently higher than the initial value. Neglecting the results of sample No. 39, which are anomalous in several respects, the average of the corrected values for copper is 2% greater than the initial value, and the maximum deviation from the average is ±7%. If precipitation of uranium had taken place while all the copper remained in solution, the corrected values for copper would have been higher than the initial value by a factor equal to the correction factor for sample dilution. Of course, the possibility is not eliminated that precipitation of a fraction of the uranium was accompanied by precipitation of an equal fraction of the copper. No corrections were applied to the measured values of pH of the samples.

2. Oxygen consumption

The results of oxygen depletion measurements are shown in Table 4.6. These data are from measurements made during reactor shutdown; hence no correction was required for a pressure of radiolytic gas.

3. Fission power in loop solution

a. Total-fission analyses

The results of solution analyses for total fissions are presented in Table 4.7. Values for the corresponding power from fission with the LITR at 3 Mw are also listed. These values were calculated from the analytical results with the use of a value of 200 Mev per fission. They are not adjusted to a common uranium concentration but, in each case, are average values of power from the start of irradiation to the time the sample was taken. The values for the latter portion of the operation are about

TABLE 4.6. OXYGEN CONSUMPTION IN LOOP

Remarks	LITR Energy (Mwhr)	Sample No.	Total Fuel Circulation Time (hr)	Δ Time (hr)	O_2 Volume at Time of Previous Sample (cc at STP)	O_2 Volume at Time of Sample (cc at STP)	O_2 Additions (cc at STP)	O_2 Consumed Since Last Sample (cc at STP)	Cumulative Amount of O_2 Consumed (cc at STP)
Enriched solution, no radiation	0	DD-1-28(E)	0	0	912	912		0	0
	0	DD-1-29(E)	2.4	2.4	912	912		0	0
	0	DD-1-30(E)	12.7	10.3	912	912		0	0
	0	DD-1-31(E)	23.3	10.6	912	912		0	0
	0	DD-1-31.5(E)	29.4	6.1	912	912		0	0
Radiation, Mw									
0.3	4.32	DD-1-32(ER)	51.7	22.3	912	912		0	
1.0	19.57	DD-1-33(ER)	72.3	20.6	912	906		7	7
2.0	49.00	DD-1-34(ER)	95.3	23.0	906	838		67	74
3.0	90.29	DD-1-35(ER)	120.0	24.7	838	642		197	271
3.0	246.45	DD-1-36(ER)	192.9	72.9	642	944	745	443	714
3.0	481.97	DD-1-37(ER)	292.4	99.5	944	528		416	1130
3.0	840.03	DD-1-38(ER)	434.8	142.4	528	713	788	603	1733
0	840.03	DD-1-39(ER)	465.5	30.7	713	607		106	1839

TABLE 4.7. TOTAL FISSIONS IN LOOP SOLUTION

Sample No.	Accumulated LITR Energy (Mwhr)	Inventory Volume at Time of Sample (ml at 25°C)	Calculated Uranium (mg/ml)	Total Fission per ml $\times 10^{-14}$		Fission Power in Loop Solution at 3 Mw (w)
				Analysis	Corrected for Dilution of Samples and Inventory	
DD-1-33(ER)	19.6	1061	36.0	3.32	3.71	534
DD-1-34(ER)	49.0	1052	35.8	8.28	10.2	583
DD-1-35(ER)	90.3	1044	35.4	15.4	20.8	640
DD-1-36(ER)	246.5	1035	35.0	42.0	49.2	550
DD-1-37(ER)	482.0	1028	35.0	60.9	74.3	421
DD-1-38(ER)	840.0	1019	34.7	103	134	433

20% below those for the first portion. This spread is probably representative of the uncertainty involved in this method of determining total fission, although some of the decrease with time can be accounted for by two factors: (1) The uranium concentration in the loop for sample 38 was 3.5% below that for sample 33. A difference in fission power of roughly the same percentage would then be expected between the operating periods represented by the two samples. (2) The fission standard which was employed contained only long-lived Cs^{137}, whereas the sample contained both Cs^{137} and 13-d Cs^{136}. The reported values for total fission are thus higher than the true values, and the amount by which they are higher is greatest for the earliest measurements. An approximate correction for the short-lived cesium was estimated for sample 34, with the result that the calculated value for the power was lowered from 583 to 490 w.

b. Electrical power

The difference between the electrical powers required to maintain loop temperatures with and without the reactor at power averaged about 560 w for the first half of the operating period and 530 w for the remainder. (These data are based on a rough calibration of the wattmeter used; a precise calibration will be made.) The ratio of these values is roughly equal to that for the average uranium concentration in solution during these periods. The values obtained from these measurements are not directly representative of the fission power, since gamma rays from the reactor contributed to heating in the core. It can be estimated that a net gain of 10% in power could result from absorption of reactor gamma rays and loss of fission gamma rays and neutrons.

From the results of the cesium analyses and electrical-power measurements, it appears to be probable that the fission power in the loop was between 400 and 500 w when the LITR was at 3 Mw.

If a value of 500 w in the core is assumed to be representative of the data, the average power density in the core solution was 1.7 w/ml with the reactor at 3 Mw. The average power density in the loop solution was 0.37 w/ml at operating temperature.

c. Induced activity in specimens

The results of the determination of the abundance of Cr^{51} in the various core specimens are presented in Table 4.8. The standard was a control specimen machined from the same stock used for the corrosion specimens. It was irradiated for 15 to 75 hr in a neutron flux of 6.30×10^{11} neutrons/cm^2/sec, and 173 hr elapsed between termination of exposure and counting. For the loop specimens, 912 hr elapsed between termination of loop operation and counting. Calculated values for the power density, which corresponds to the neutron flux at the surface of the specimens, are also tabulated. A uranium concentration of 36 mg/ml, 88.89% enriched, was a basis for the calculation.

4. Uranium balance

The amount of uranium initially charged to the loop was 41.49 g as given by the results of solution analyses and measurements of the volume of solution introduced.

TABLE 4.8. INDUCED CHROMIUM-51 ACTIVITY IN CORE SPECIMENS

Coupon Position	Defilmed Weight (g)	Cr^{51} Activity		Neutron Flux at 3 Mw (neutrons/cm^2/sec $\times 10^{-12}$)	Power Density at 3 Mw (w/ml)
		Counts/min per Coupon $\times 10^{-6}$	Counts/min per gram $\times 10^{-6}$		
A	1.7786	2.76	1.55	1.56	1.74
B	1.7913	2.45	1.37	1.37	1.53
C	1.8276	2.20	1.20	1.20	1.34
D	1.8272	1.93	1.06	1.06	1.18
E	1.8426	1.62	0.88	0.88	0.99
F	1.8521	1.44	0.78	0.78	0.87
G	1.8660	1.27	0.68	0.68	0.76
H	1.8481	1.11	0.60	0.60	0.67
I	1.9022	0.91	0.48	0.48	0.54
J	1.8795	0.76	0.40	0.40	0.45
K	1.9135	0.55	0.29	0.29	0.32
L	1.8832	0.53	0.27	0.27	0.30
Standard coupon	1.8876	1.17	0.62	0.63*	

*Known flux in ORNL Graphite Reactor.

TABLE 4.9. URANIUM RECOVERED FROM LOOP

Source	Solution Weight (g)	Specific Gravity	Solution Volume (ml)	Uranium Concentration (mg/ml)	Weight of Uranium (g)
Sample purges, flushes to weigh tank	6420	1.0	6420	0.83	5.30
Solution drained from loop and loop rinses to weigh tank	7965	1.0	7965	4.84	38.55
Loop samples sent to laboratory			35.80	32.1–36.1	1.12
Total recovered					44.97
Total charged					41.50
Material balance					108.4%*

*The discrepancy appears as a result of irreproducibility in the calibration of the weigh tank.

Data obtained in the determination of the weight of uranium removed from the loop are shown in Table 4.9. The weight of solution in the weigh tank was established by calibration of the weighing equipment with a known weight of water. The value of 1.0 listed for the specific gravity of weigh tank solutions is an assumed value. The fact that the resulting value for the total weight of uranium removed is 8% greater than the value for the charged weight points to an uncertainty of at

least 8% in the combined results of weight measurements and sampling of tank solutions, and of chemical analyses for uranium. However, it seems probable from the results that uranium recovery from the loop was fairly complete.

5. Radiolytic gas pressures

The steady-state pressures of radiolytic gases which were observed under irradiation were in the range 6 to 8 psi – roughly equal to the pressure predicted from out-of-pile studies of the catalytic activity of copper in the system.[9] Data from these pressure measurements have not been systematized and correlated, but will be reported later.

6. Fission products in loop solution

Data from the analyses of loop-solution samples for various fission products have not been correlated. These data will be reported later.

(3) *Corrosion Indicated by Nickel and Oxygen Data.* Values for corrosive penetration have been calculated which correspond to the amount of nickel found in the different samples and to the oxygen depletion data. It was assumed in these calculations that all steel surfaces in contact with high-temperature solution corroded uniformly and that steel surfaces in the cool rotor region of the pump did not corrode. It was also assumed that oxygen was consumed in the oxidation of steel only. The calculated values are shown in Fig. 4.4 and are plotted against the circulation time. Other quantities of interest are shown on additional scales. The oxygen data indicate a greater amount of corrosion than was indicated by the nickel data. This difference is not unexpected, since the loop contained Zircaloy-2 and since the pump was equipped with a Stellite-Graphitar bearing combination. These materials contained no nickel but undoubtedly consumed some oxygen. It is interesting that both the oxygen and nickel data indicate negligible corrosion during the operation at LITR powers below 3 Mw. The indicated corrosion rate increased sharply and then dropped some and remained fairly constant after the reactor power was raised to 3 Mw. The over-all corrosion rate based on nickel and circulation time is 1.6 mpy.

[9] G. H. Jenks, H. C. Savage, *et al.*, *HRP Quar. Prog. Rep. July 31, 1954*, ORNL-1772, p 84.

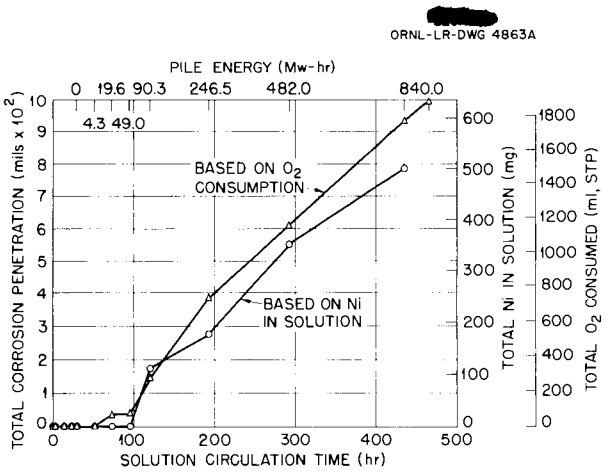

Fig. 4.4. Over-All Corrosive Penetration.

(4) *Performance of Equipment.* With a few minor exceptions, the performance of the loop, operating equipment, and instruments was satisfactory. The major exception to satisfactory performance was the neutron shutter, which was inoperable throughout the exposure. The shutter assembly was removed after the experiment had been in progress for about a week. It was found that excessive corrosion had resulted in a freezing of the shutter movement. Fortunately, the location at which the shutter had frozen corresponded to the open position for the experimental hole.

4.1.3 Remote Dismantling and Inspection

(a) Dismantling. The loop was dismantled in the remote cell in Building 4501, and portions were transferred to the Solid State Building hot cells for further machining and inspection. These portions included the core, the in-line sample holder, the pressurizer, the pressurizer heater, a portion of the line including the sample-line filter, and the pump.

Equipment performance in the remote cell was highly satisfactory. In addition to the operations which fell within the planned scope of the cell, it was possible to carry out two other operations. First, normal extraction of the loop from the loop jacket was prevented by a water line within the jacket. This line was successfully cut within the jacket without damage to the loop. This interference with normal extraction has been designed out of future assemblies. Second, the remote facility was used to free the front flange of the pump by cutting the bolts and seam weld. Since opening the pump is a lengthy operation in the Solid State cells, the operation in the remote cell represents a valuable improvement in the dismantling procedures. The cell was readily decontaminated after use.

Operations in the Solid State cells were, in general, satisfactory, although minor difficulties with the machine tools and particularly with the new remote manipulator more than doubled the time necessary for final sectioning and inspection.

(b) Results of Inspection and Evaluations. (1) *Qualitative.* In general, the surfaces in all portions of the loop, with the exception of the forward or high-flux portion of the core, were covered with a very dark, dull scale. The nearly stagnant area on the outside of the in-line holder and the high-velocity areas of the pump impeller and housing were covered with the same dull, black film.

The appearance of the pump and in-line holder and specimens is illustrated in Figs. 4.5, 4.6, and 4.7. There was no apparent localized attack.

The films from wetted areas of the pressurizer, as well as those from vapor-phase portions, were similar to those in other portions of the loop. However, they were somewhat browner than those in the loop. The demarcation line on the wall between solution- and vapor-phase regions became less and less distinct from the inlet to the outlet of the pressurizer. The film was darker at the outlet than at the inlet.

Obvious changes in film appearance were observed in the core. At the rear of the core, that is, the core region exposed to the least flux, the film had the same dull, black appearance that it did in the rest of the loop. From the rear toward areas of higher flux exposures, the nature of the film gradually changed. It appeared to become thinner, harder, and glossier. The forward third of the core was covered with a film which had the appearance of a very glossy, baked, black enamel. The film on the core cap had this appearance and a slightly blistered appearance in addition. However, it is likely that this blistered appearance resulted from the character of the surface before exposure. Some of the stock of end caps from which this core cap was drawn have the same blistered appearance. The surfaces of the cap and core walls are shown in Figs. 4.8 and 4.9.

The Zircaloy-2 impact specimens and Zircaloy-2 sample holder also exhibited differences as their locations in the core varied. The Zircaloy-2 surfaces in the low-flux areas were covered with a

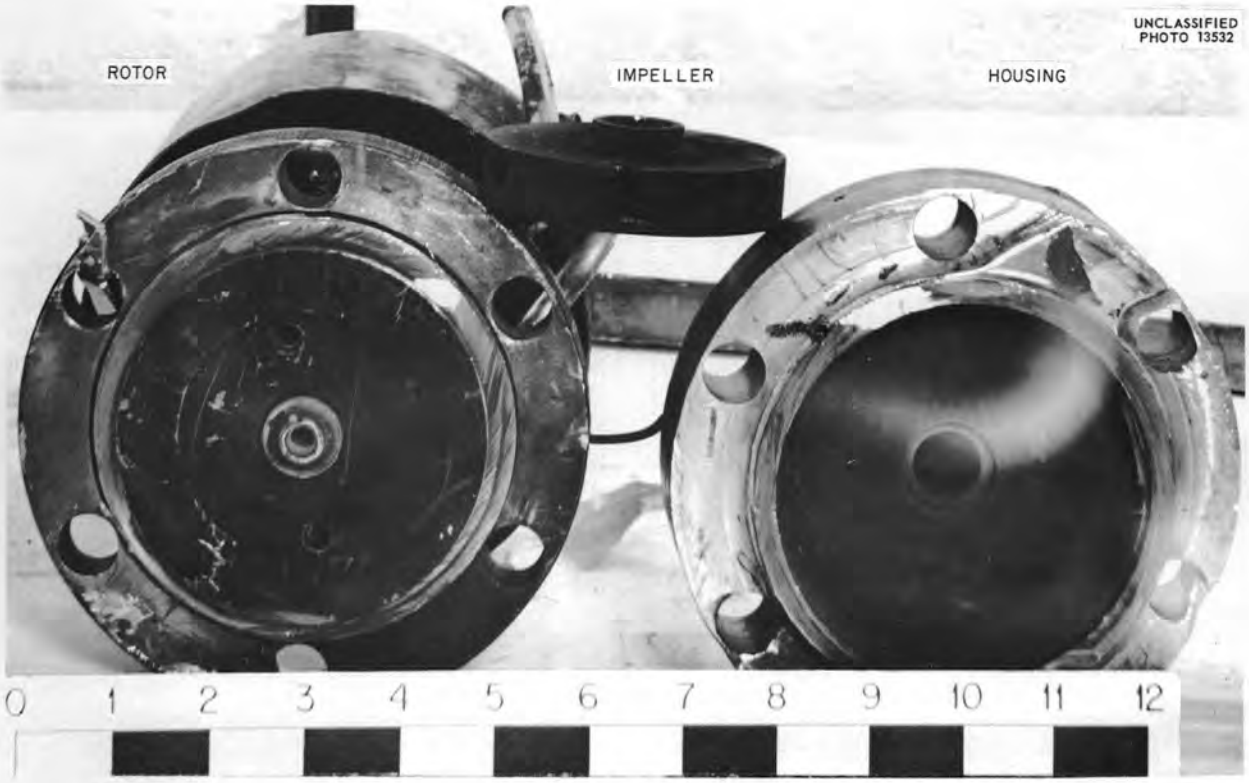

Fig. 4.5. HRP In-Pile Loop DD Pump.

Fig. 4.6. HRP In-Pile Loop DD In-Line Coupon Assembly Before Defilming.

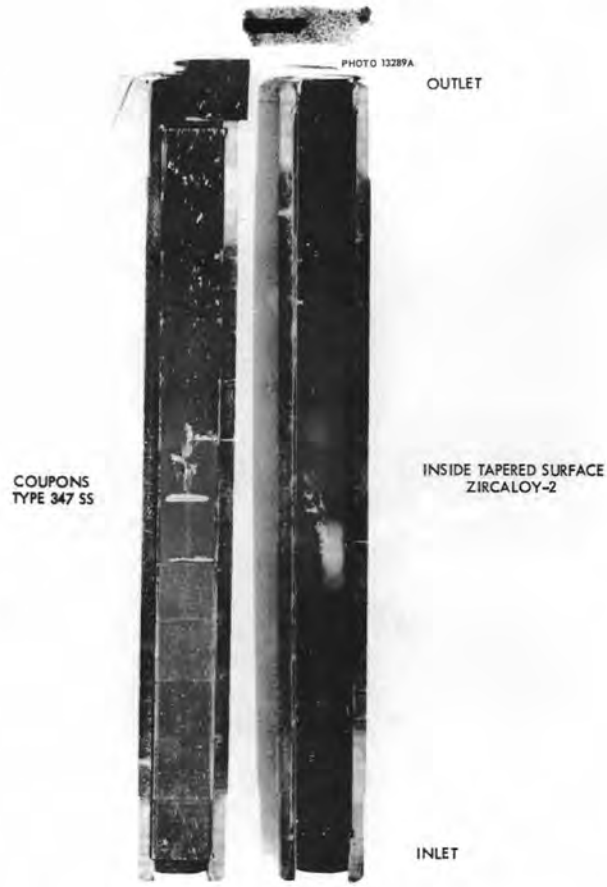

Fig. 4.7. HRP In-Pile Loop DD In-Line Coupon Assembly Before Defilming.

heavy, black film, which gradually changed to a brown color and became thinner, until the surfaces in the high-flux regions appeared to be completely free of film. The original fine machine marks were visible at the high-flux end of the Zircaloy-2 holder. The stainless steel specimens in the core were also covered with film which varied in appearance as did that on the core walls. No evidence was apparent of a velocity effect on the character of film on the specimens. The appearances of the specimens and holder are somewhat deceptively illustrated in Figs. 4.10 and 4.11. In these photographs, the glossy, black surfaces of the steel specimens which were in the highest flux appear to be light in color.

Sections from the pressurizer, the pressurizer heater, the pipe at the pump outlet, and the core cap were transferred to the Metallographic Section of the Solid State Division for examination. The Zircaloy-2 impact samples were transferred to the HRP Metallurgy Group for testing and evaluation.

Both the in-line specimens and the core specimens were defilmed, inspected visually, and weighed. Figure 4.12 is a group photograph of the defilmed core and in-line coupons. Figures 4.13 through 4.19 are magnified photographs of the individual coupons. Only two typical in-line coupons are included, while all the coupons from the core assembly are shown. In both cases, the flow pattern is from position A through position L, with the high-velocity region, approximately 50 fps, on the trailing edge of position G and the leading edge of position H. The sides of core coupons B through D, which were encased and apparently

[redacted]

CORE CAP WITH SPIDER IN PLACE

CORE CAP ALONE

Fig. 4.8. HRP In-Pile Loop DD Core Cap.

protected by the holder, stand in relief above the exposed surfaces. For coupon A, approximately 60% of the encased area was attacked to the same degree as the exposed areas. This additional attacked area has been treated as exposed area in the data, and the calculations are listed in Table 4.10.

Corrosion of the core coupons appeared to start with shallow pits, which apparently grew laterally until, in the case of the coupons in highest flux, the entire surface was removed. The orientation of the pits along machine marks may indicate some effect of work-hardening. This is being examined metallographically.

A further comment involves the defilming characteristics of the coupon. Since all coupons were defilmed cathodically in an inhibited sulfuric acid solution, the ease with which these films were removed is indicative of their protective nature. Every coupon from the core holder defilmed readily in 3 min at the normal current density of 20 amp/dm^2; only the last five coupons, which were exposed to the lowest fluxes, showed any electrode effect. The electrode effect is the result of a momentary anodic reaction of the coupon caused by the voltage drop across the film. The result of this anodic reaction is a shiny area adjacent to the contact points. All the in-line coupons showed some electrode effect, and each required from 10 to 15 min for defilming. Even after the application of voltage for this long period, the in-line specimens were not so completely defilmed as the core specimens.

(2) *Quantitative.* Sample-weight data for in-line and core specimens, with calculated values for corrosive penetration, are presented in Table 4.10; descriptions of the defilmed-surface appearance and other pertinent information are also included.

No correction has been applied to the values in Table 4.10 for the corrosion which occurred during the loop operation with normal solution. If corrosion of loop and specimens during the initial operation is assumed to have been uniform, the penetration of the specimens as given by nickel accumulation data was 0.02 mil. Inclusion of this penetration in the calculations would lower the 465-hr rate values by 0.4 mpy. The 280-hr values would be lowered by 0.6 mpy.

[redacted]

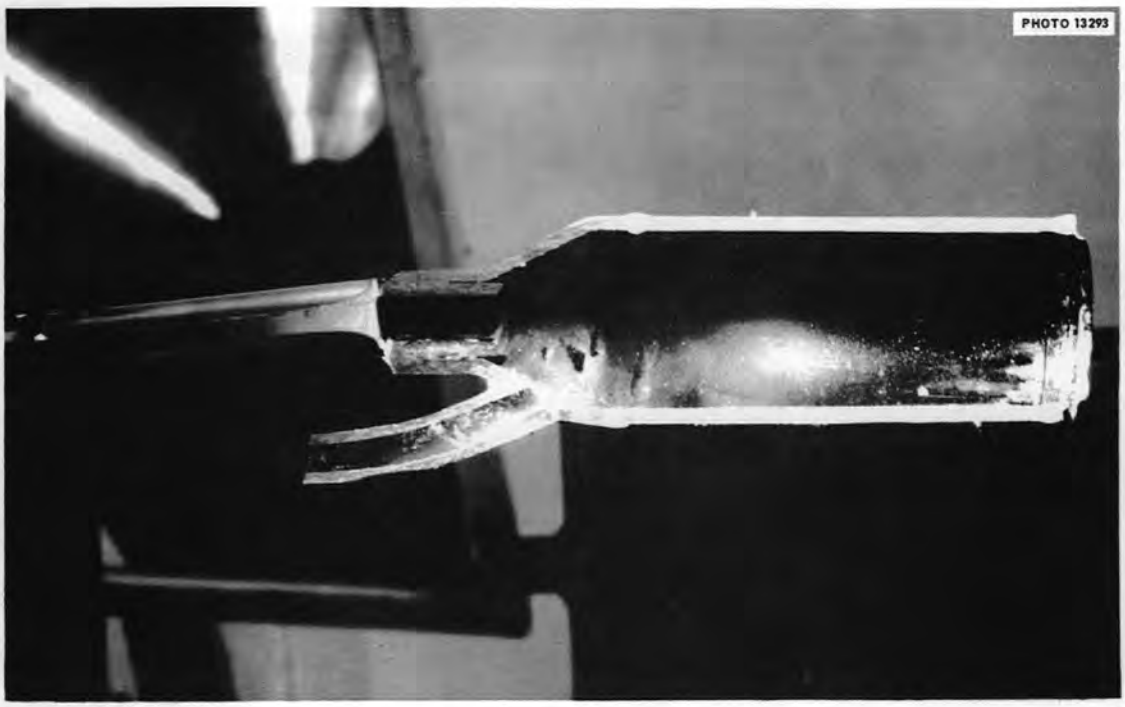

HIGH FLUX REGION

Fig. 4.9. HRP In-Pile Loop DD Core Section.

Weight-loss data for the core specimens are shown in Fig. 4.20 and are plotted against the neutron flux to which the specimen was exposed when the LITR was operating at 3 Mw. Determination of these fluxes was described in Sec. 4.1.2*c*. The letter adjacent to each point identifies the sample position. The number in each case is the value for solution velocity (in fps) past the leading edge of the specimen. An examination of the data by the Mathematics Panel produced the following relationship between these variables:

$$\log \text{penetration } (100 \times \text{mils}) = 0.791 - 0.21X_1 + 0.603X_2 - 0.0885X_2^2 + 0.0237X_1X_2 \quad ,$$

where X_1 = velocity, fps, and X_2 = power density, kw/liter.

(c) Corrosion-Examination Facility. This facility is scheduled for completion by the first of March, later than the anticipated schedule as a result of procurement delays on the cutting bridge and delays in delivery of the manipulators.

4.1.4 Correlation of Corrosion Data

As a basis for comparison between the nickel and weight-loss data, the following data from the experiment are reviewed:

1. The total amount of nickel which analyses showed to be in solution during the experiment was 629 mg – 137 mg from the preparatory operation and 492 mg from the enriched-solution operation, indicating, on the assumption that the percentage of nickel in the steel is 10.5, an oxidation of 5.990 g of steel.

2. The weight losses of the core specimens totaled 0.598 g.

3. The average weight loss for the in-line specimens was 1.55 mg/cm^2.

4. Visual inspection of the pressurizer indicated little difference in corrosion between surfaces which were in the vapor portion and surfaces in the liquid portions, in spite of the previously mentioned change in appearance between inlet and outlet. The degree of corrosion in the pressurizer appeared to be at least as great as that in the loop outside the core.

5. The rotor region of the pump has not been inspected, but, since the temperature of this region was below 100°C at all times, it is assumed that corrosion of steel was negligible.

TABLE 4.10. CORROSION DATA FOR STAINLESS STEEL CORROSION SPECIMENS

Sample No.	Position	Exposed Coupon Area (cm^2)	Flow Velocity Leading Edge (fps)	Initial Weight (g)	As-Removed Weight (g)	Defilmed Weight (g)	Weight Loss (mg)	Corrosion Penetration (mils)	Corrosion Rate* (mpy) 465 hr	Corrosion Rate* (mpy) 280 hr	Defilmed-Surface Appearance
Core holder No. 11											
436 A	A	3.25	9.7	1.8985	1.7827	1.7786	119.9	1.81	34.0	56.7	Exposed surface heavily attacked; clamped edges partially protected
437 A	B	2.80	11.3	1.8852	1.7952	1.7913	93.9	1.65	31.1	51.6	Exposed surface heavily attacked; clamped edges partially protected
438 A	C	2.80	13.7	1.9166	1.8310	1.8276	89.0	1.56	29.4	48.8	Exposed surface heavily attacked; clamped edges partially protected
439 A	D	2.80	17.1	1.9072	1.8297	1.8274	79.8	1.40	26.4	43.8	Exposed surface heavily attacked; clamped edges partially protected
440 A	E	2.80	22.9	1.9104	1.8454	1.8426	67.8	1.19	22.4	37.2	~70% of the exposed surface shows shallow pits; clamped edges protected
441 A	F	2.80	35.8	1.9111	1.8555	1.8521	59.0	1.04	19.6	32.6	~50% of the exposed surface shows shallow pits; clamped edges protected
442 A	G	2.80	41.5	1.9039	1.8694	1.8660	37.9	0.66	12.4	20.7	~20% of the exposed surface shows shallow pits; clamped edges protected
443 A	H	2.80	50.5	1.8674	1.8525	1.8481	19.3	0.34	6.4	10.6	~10% of the exposed surface shows shallow pits; clamped edges protected
444 A	I	2.80	28.2	1.9138	1.9115	1.9022	11.6	0.20	3.8	6.3	Some very shallow pitting of exposed surfaces
445 A	J	2.80	19.9	1.8872	1.8947	1.8795	7.7	0.14	2.6	4.4	Machining marks quite clear; no apparent pitting
446 A	K	2.80	15.2	1.9201	1.9303	1.9135	6.6	0.12	2.2	3.8	Machining marks quite clear; no apparent pitting
447 A	L	3.00	12.1	1.8884	1.8990	1.8832	5.2	0.08	1.5	2.5	Machining marks quite clear; no apparent pitting

TABLE 4.10 (continued)

Sample No.	Position	Exposed Coupon Area (cm^2)	Flow Velocity Leading Edge (fps)	Initial Weight (g)	As Removed Weight (g)	Defilmed Weight (g)	Weight Loss (mg)	Corrosion Penetration (mils)	Corrosion Rate* (mpy) 465 hr	Corrosion Rate* (mpy) 280 hr	Defilmed-Surface Appearance
In-line holder No. 10											
448 A	A	3.00	9.4	1.9194	1.9277	1.9164	3.0	0.05	0.9	1.6	Machining marks clearly visible; some very thin, black film remaining; no pitting
449 A	B	2.80	10.9	1.8910	1.9004	1.8885	3.5	0.06	1.1	1.9	Machining marks clearly visible; some very thin, black film remaining; no pitting
450 A	C	2.80	13.2	1.9092	1.9191	1.9025	6.7	0.12	2.2	3.8	Machining marks clearly visible; some very thin, black film remaining; no pitting
451 A	D	2.80	16.5	1.9191	1.9340	1.9172	1.9	0.03	0.6	0.9	Machining marks clearly visible; some very thin, black film remaining; no pitting
452 A	E	2.80	22.1	1.8991	1.9096	1.8949	4.2	0.07	1.3	2.2	Machining marks clearly visible; some very thin, black film remaining; no pitting
453 A	F	2.80	34.6	1.8898	1.8995	1.8833	6.5	0.11	2.1	3.4	Machining marks clearly visible; some very thin, black film remaining; no pitting
454 A	G	2.80	40.1	1.8902	1.8982	1.8848	5.4	0.09	1.7	2.8	Machining marks clearly visible; some very thin, black film remaining; no pitting
455 A	H	2.80	48.8	1.9035	1.9122	1.9007	2.8	0.05	0.9	1.6	Machining marks clearly visible; some very thin, black film remaining; no pitting
456 A	I	2.80	27.2	1.8823	1.8904	1.8794	2.9	0.05	0.9	1.6	Machining marks clearly visible; some very thin, black film remaining; no pitting
457 A	J	2.80	19.2	1.9113	1.9161	1.9055	5.8	0.10	1.8	3.1	Machining marks clearly visible; some very thin, black film remaining; no pitting
458 A	K	2.80	14.7	1.9142	1.9200	1.9100	4.2	0.07	1.3	2.2	Machining marks clearly visible; some very thin, black film remaining; no pitting
459 A	L	3.00	11.7	1.9054	1.9116	1.9001	5.3	0.08	1.5	2.5	Machining marks clearly visible; some very thin, black film remaining; no pitting

*Two corrosion rates are presented: total operation 465 hr and radiation time with 3 Mwhr equivalent to 1 hr.

[redacted]

PHOTO 13290

Fig. 4.10. HRP In-Pile Loop DD Core Coupon Assembly Before Defilming.

[redacted]

PHOTO 13291

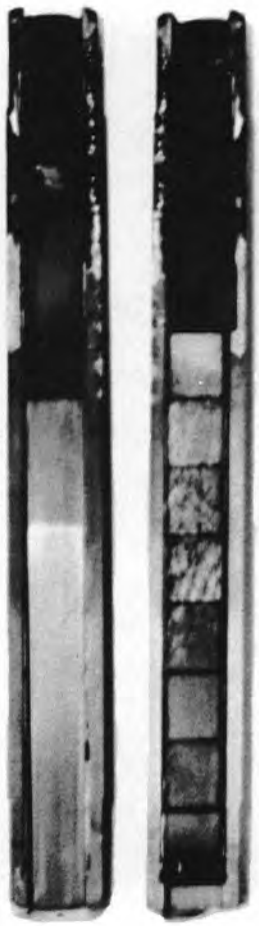

Fig. 4.11. HRP In-Pile Loop DD Core Coupon Assembly Before Defilming.

If it is now assumed that other steel surfaces in the loop, excluding the core specimens but including the pressurizer and the walls of the core, corroded uniformly and at an average rate equal to that of the in-line specimens, the predicted value for the amount of steel oxidized is 5.998 g. This value includes the 0.598 g which came from the core specimens. It is in excellent agreement with the value of 5.990 g which was indicated by chemical analysis.

An important point in this result is the suggestion that the walls of the core corroded no faster than surfaces in the unirradiated portion of the loop. Preliminary results of metallographic examination by members of the Solid State Division also indicate only moderate attack of the core wall.

If it is true that the core walls were corroded a moderate amount only, then the excessive corrosion of the core specimens can be explained only by assuming a strong but complex effect of velocity, or an interaction of some type between the steel and the Zircaloy-2 holder under irradiation, or a combination of both effects.

A corollary result of this picture of the data is the conclusion that corrosion in unirradiated portions of the loop was accelerated a small but sensible amount during exposure.

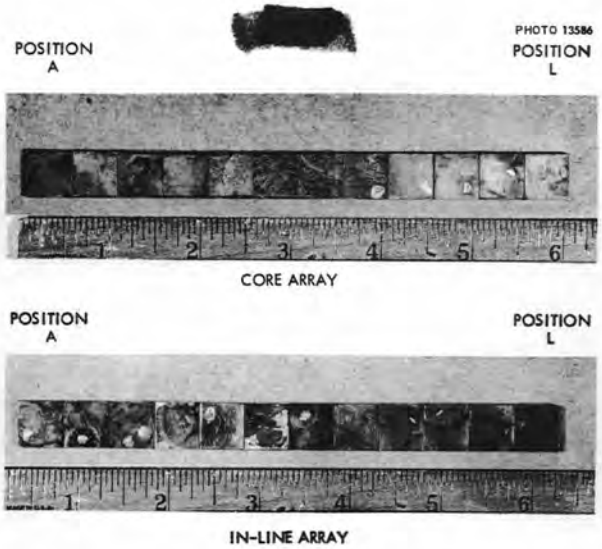

Fig. 4.12. HRP In-Pile Loop DD Corrosion Coupon Arrays After Defilming.

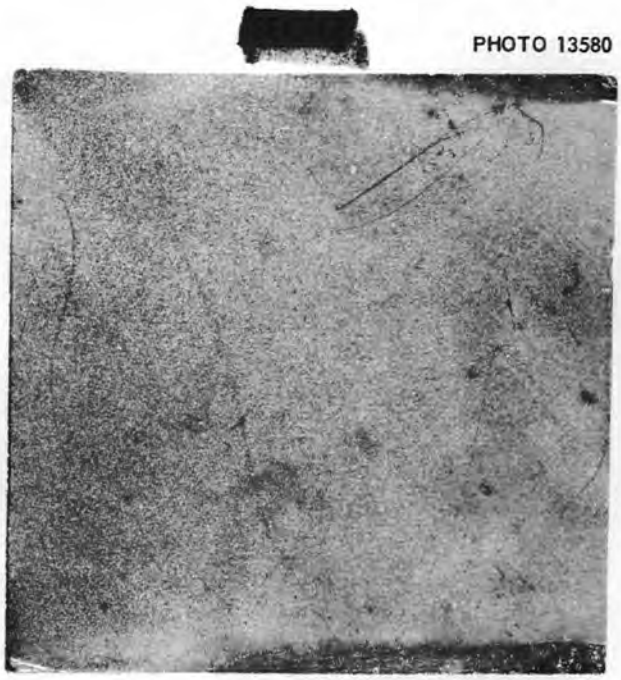

COUPON 436-A (POSITION A)

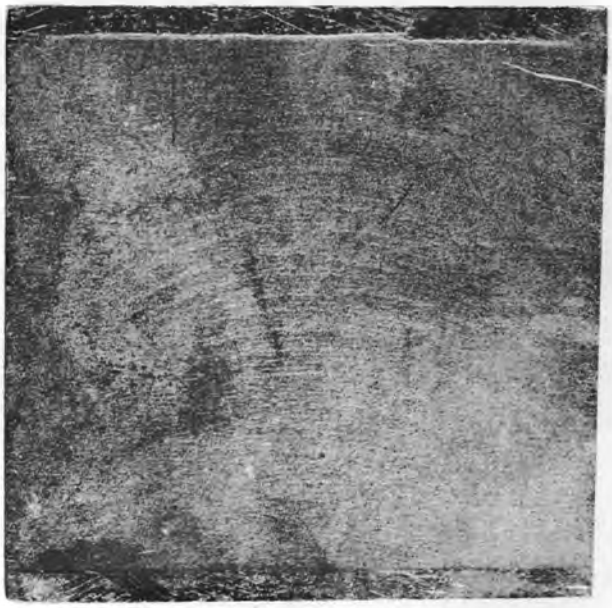

COUPON 437-A (POSITION B)

Fig. 4.13. Defilmed Type 347 Stainless Steel Corrosion Coupons from the Core Holder of In-Pile Loop DD.

4.2 BOMB TESTS

G. H. Jenks

A. L. Bacarella	D. T. Jones
W. E. Clark	J. R. McWherter
R. J. Davis	M. D. Silverman
H. O. Day	H. H. Stone
G. Eckerd	K. S. Warren
D. N. Hess	L. F. Woo
H. A. Fisch	W. C. Yee

4.2.1 LITR Operations

(a) Introduction. Studies of the effect of irradiation on the corrosion of Zircaloy-2 by uranyl sulfate solutions continued. Three in-pile exposures were completed in hole HB-6 at the LITR. Because the corrosion rates observed in the out-of-pile experiments were so extremely low, no further out-of-pile studies on Zircaloy-2 are planned except for those designed to serve as comparison bases for in-pile experiments when the experimental conditions have been rather drastically altered. One such out-of-pile experiment, H-56, is now in progress.

The effect of irradiation on the corrosion of titanium by uranyl sulfate is also under investigation. One in-pile experiment, H-76, utilizing a titanium system is now in progress.

[redacted]

PHOTO 13582

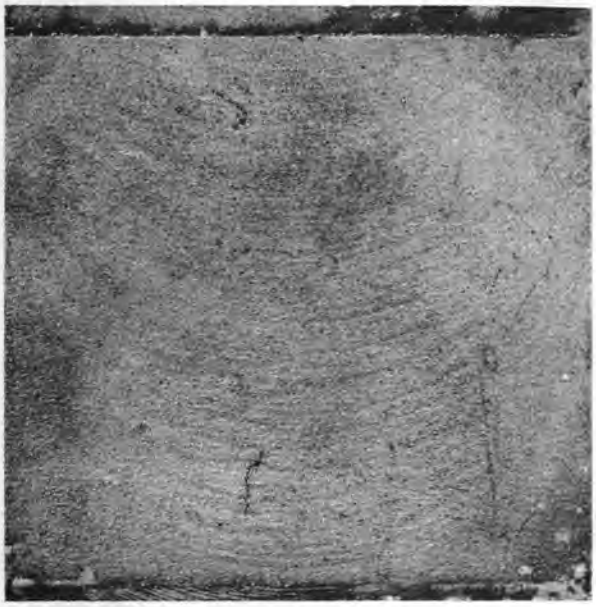

COUPON 438-A (POSITION C)

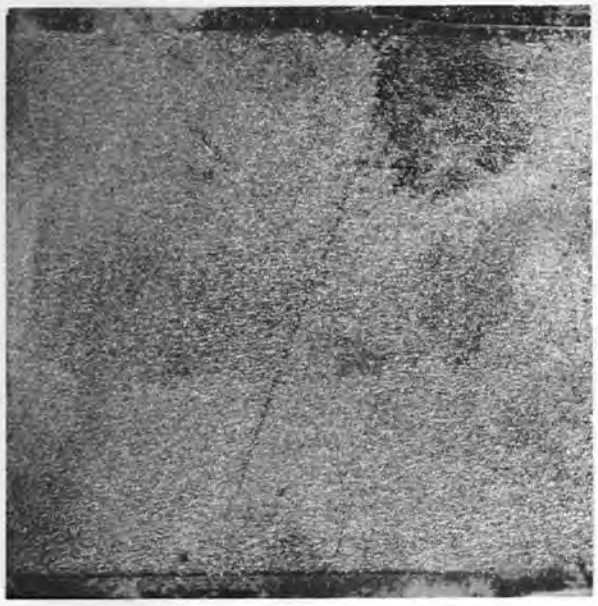

COUPON 439-A (POSITION D)

Fig. 4.14. Defilmed Type 347 Stainless Steel Corrosion Coupons from the Core Holder of In-Pile Loop DD.

[redacted]

PHOTO 13584

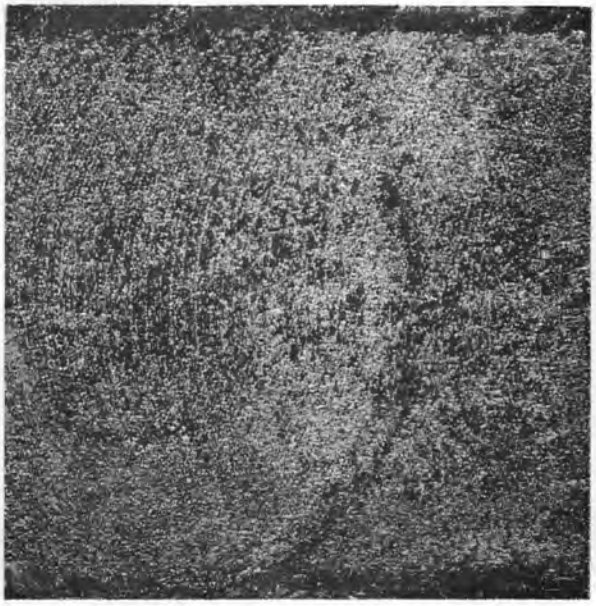

COUPON 440-A (POSITION E)

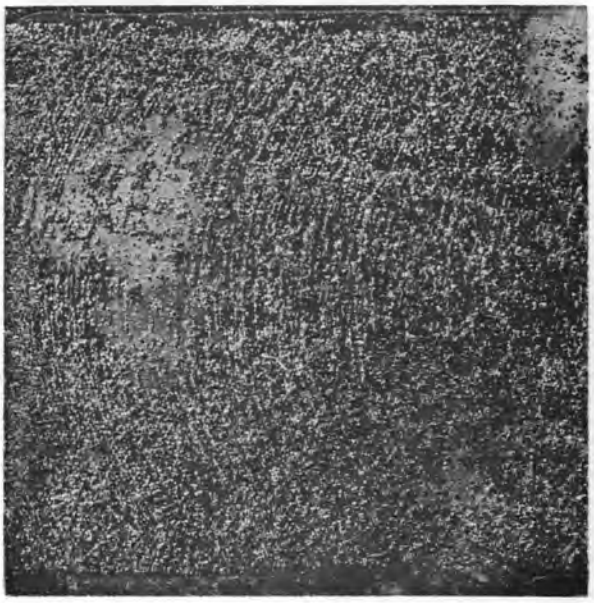

COUPON 441-A (POSITION F)

Fig. 4.15. Defilmed Type 347 Stainless Steel Corrosion Coupons from the Core Holder of In-Pile Loop DD.

[redacted]

PHOTO 13583

COUPON 442-A (POSITION G)

COUPON 443-A (POSITION H)

Fig. 4.16. Defilmed Type 347 Stainless Steel Corrosion Coupons from the Core Holder of In-Pile Loop DD.

[redacted]

PHOTO 13581

COUPON 444-A (POSITION I)

COUPON 445-A (POSITION J)

Fig. 4.17. Defilmed Type 347 Stainless Steel Corrosion Coupons from the Core Holder of In-Pile Loop DD.

[redacted]

PHOTO 13587

COUPON 446-A (POSITION K)

COUPON 447-A (POSITION L)

Fig. 4.18. Defilmed Type 347 Stainless Steel Corrosion Coupons from the Core Holder of In-Pile Loop DD.

[redacted]

PHOTO 13585

COUPON 449-A (POSITION A)

COUPON 454-A (POSITION G)

Fig. 4.19. Defilmed Type 347 Stainless Steel Corrosion Coupons from the In-Line Holder of In-Pile Loop DD.

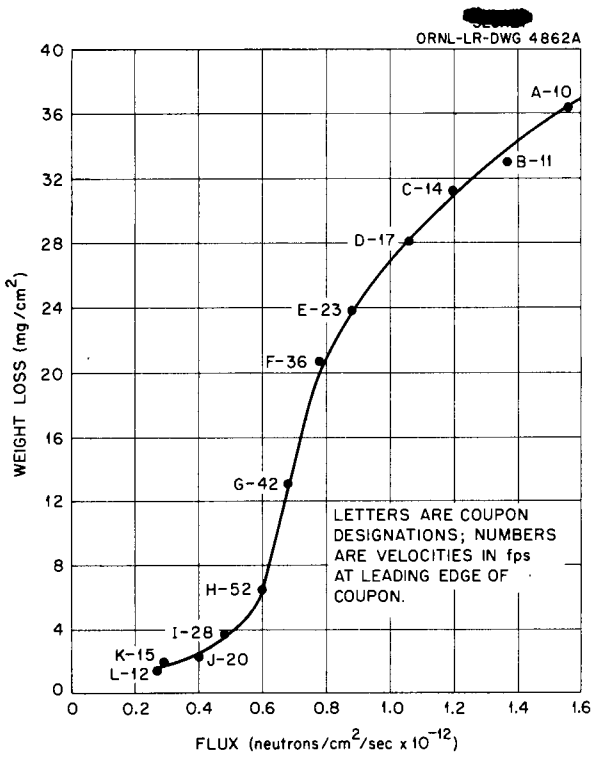

Fig. 4.20. Weight Losses for Type 347 Stainless Steel Core Sample Coupons vs Neutron Flux at Coupon Position.

Out-of-pile experiments are being carried out in stainless steel systems in order to determine the effect on corrosion rates of (1) pressurizing the system directly with oxygen gas rather than by the thermal decomposition of hydrogen peroxide, (2) the copper sulfate which is added to catalyze the recombination of the radiolytic hydrogen and oxygen gases, and (3) galvanic effects resulting from contact between untreated specimens with noble metals and with stainless steel specimens ennobled by pretreatment.

In general, the methods, techniques, and equipment employed have been reported previously.[10,11] The method of pressurizing the bomb with oxygen, however, was changed. With the exception of experiment H-60, the bombs in all experiments reported here were pressurized directly with oxygen by the use of a micrometer injector designed for that purpose. The injection method has the advantages of allowing the initial oxygen pressure to be determined accurately and of permitting the zero corrosion point to be determined more exactly than has been possible in the past. The use of oxygen instead of peroxide is also desirable in that it eliminates the precipitation of uranyl peroxide in the early stages of an experiment and, in stainless steel systems, eliminates the possibility of the reduction of chromate by peroxide. Some difficulties were encountered at first in the use of the injector, and, in consequence, the results obtained in certain out-of-pile experiments are in question. These difficulties have since been overcome.

All in-pile corrosion rates given in this report are based on LITR operating time at a power level of 3 Mw.

(b) Zircaloy-2. The Zircaloy-2 from which the bombs and pins were fabricated was from three different stocks, as indicated in Table 4.11.

TABLE 4.11. ANALYSES OF ZIRCALOY-2 STOCK

Element	Weight Per Cent		
	H-Series Bomb Stock	Z-Series Bomb Stock	Pin Stock
Sn	1.1	1.24	1.24
Cr	0.08–0.10	0.02	0.016
Ni	0.06	0.051	0.051
Fe	0.16	0.094	0.24*
Al	0.23*	0.035	0.09
H_2	0.0023	0.0004	0.0013
O_2	0.0026	0.001	0.0013
N_2	0.0010	0.001	0.001
C		0.010	0.017

*Spectrographic analysis gave 0.01–0.1%.

(c) In-Pile. The experimental conditions and data for the in-pile experiments are listed in Table 4.12, and the data are plotted in Fig. 4.21, with total corrosion values as ordinates and reactor energy in units of 3 Mw as abscissas. In HB-6 this power level corresponds to a neutron flux of 4.77×10^{12} neutrons/cm²/sec. Each bomb contained four pins of Zircaloy-2. The uranium used in all experiments was 93% U^{235}. Each bomb was

[10] C. H. Secoy *et al.*, *HRP Quar. Prog. Rep. April 30, 1954*, ORNL-1753, p 139.

[11] G. H. Jenks *et al.*, *HRP Quar. Prog. Rep. Oct. 31, 1954*, ORNL-1813, p 82.

TABLE 4.12. SUMMARY OF IN-PILE CORROSION STUDIES, NOVEMBER 1, 1954, TO JANUARY 10, 1955

Bomb No.	Material	Solution (m)	Exposure Temperature (°C)	Days Exposed[a]	Corrosion Rate (mpy)[b]	
					Pin Data	O_2 Data
H-60	Zircaloy-2	0.158 UO_2SO_4 0.019 $CuSO_4$ 0.040 H_2SO_4	250, 275	13.4	6.6	6.4 at 250°C 11.6 at 275°C
Z-1	Zircaloy-2	0.165 UO_2SO_4 0.011 $CuSO_4$ 0.040 H_2SO_4	280	5.9	c	12.3
Z-2	Zircaloy-2	0.165 UO_2SO_4 0.011 $CuSO_4$ 0.040 H_2SO_4	280	4.6	11.4	12.4
H-76	Titanium-75A	0.177 UO_2SO_4 0.021 $CuSO_4$ 0.046 H_2SO_4	250	Experiment continuing		

[a]LITR operating time at 3 Mw.
[b]Based on LITR operating time at 3 Mw.
[c]Data not yet available.

pressure-tested before use, filled with solution, pressurized with oxygen, and pretreated out-of-pile as has been described previously.[10,11] Each experiment is described in more detail below.

(d) H-60. The purpose of experiment H-60 was to test the effect of excess sulfuric acid (0.04 m) on the corrosion rate of Zircaloy-2 in a solution 0.16 m in uranyl sulfate (approximately 40 g of uranium per liter) and 0.019 m in copper sulfate. The over-all corrosion rate at 250°C amounted to 6.4 mpy. This indicates an approximate decrease of 30% in corrosion rate compared with the 9.6 mpy obtained in experiment H-58, which was made under the same experimental conditions and with the same solution without free acid. During the latter part of H-60 the temperature was allowed to rise to 275°C, at which point the corrosion rate was found to be about 11.6 mpy.

The increase in radiolytic gas pressure indicated a loss of 21% of the copper during the 250°C portion of the experiments and a loss of an additional 47% during the 275°C portion, leaving only 32% of the copper active at the end of the experiment.

As was previously noted, H-60 was pressurized with oxygen by means of hydrogen peroxide decomposition.

(e) Z-1 and Z-2. Experiments Z-1 and Z-2 were duplicate experiments designed to confirm the positive temperature coefficient of the corrosion rate indicated by the latter part of experiment H-60. In order to keep the pressure of radiolytic gases at approximately the same steady-state value as that observed in H-60, the more rapid rate of recombination at 280°C was counterbalanced by decreasing the concentration of copper sulfate to 0.011 m. Since thin-walled bombs were used, a large excess pressure of oxygen was not deemed to be safe, and consequently both runs were of relatively short duration. Because of the small number of experimental points, the rates obtained cannot be considered to be exact, although the two runs checked extremely well. The data indicate an over-all

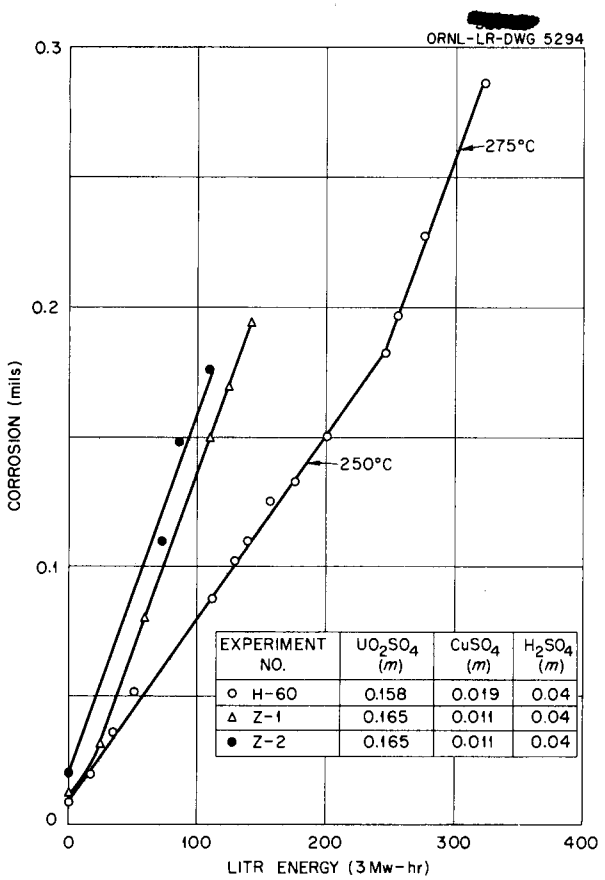

Fig. 4.21. In-Pile Corrosion of Zircaloy-2 and Titanium.

corrosion rate of about 12 mpy for both experiments. Comparison of this corrosion rate with that obtained at 250°C in H-60 indicates a temperature coefficient of roughly 0.2 mpy/°C between 250 and 280°C. A similar calculation, based on the 275°C values obtained during the latter part of H-60, gives approximately the same coefficient.

The increase in radiolytic gas pressure in Z-1 indicated a loss of 23% of the copper from the solution.

(f) Film Data. In the past, film data on Zircaloy-2 have been limited to weight gained by the metal, since no method has been available for stripping the corrosion film without attacking the metal underneath. Generally, the weight gain agreed reasonably well (to within 10–20%) with the overall corrosion calculated from oxygen decrease, but in the case of H-59 the pin-weight data were anomalously high, indicating a corrosion rate of about 35 mpy, compared with an oxygen rate of 9.0 mpy. The development of a film-stripping technique as described below resolved the discrepancy in favor of the oxygen data by indicating a rate of 6.8 mpy.

The high activity of the irradiated film has made it impossible to obtain detailed information as to film structure, but even a superficial macroscopic examination reveals striking differences between the irradiated film and the film formed outside of radiation: the latter is thin, dark, and extremely adherent both in the wet and dry states, but the irradiated film is tan and flakes off readily if allowed to dry. After drying, the major portion of the film can be stripped by cathodic treatment in a 5% sulfuric acid solution. Although the stripping is apparently never quite complete, this behavior contrasts sharply with the behavior of the out-of-pile film, which cannot be stripped by any known treatment without appreciable attack on the underlying metal.

Since the one experiment, H-60, indicated that the addition of excess sulfuric acid substantially diminishes the corrosion rate at 250°C, the possibility is suggested that at least part of the high corrosion rates observed is due to the inclusion in the film of hydrolyzed uranium and copper compounds. Observed losses of copper from the irradiated solutions have been as high as 60% of the initial amount present, and precipitates containing uranium and small amounts of copper have been found in the bomb at the conclusion of an experiment. Data from film analyses are not at present sufficiently complete to determine whether or not the corrosion rate can be correlated with the amounts of impurities in the film. The only satisfactory film analysis obtained thus far was on film from run Z-2, which gave the following:

Element	Per Cent
U	3.4
Fe	1.8
Cu	0.7
SO_4	7.4
Mn and Sn	Not detectable

Film data from H-60 will not be available because the pin strip sample was lost during the analysis. The bomb from Z-1 has not been opened; consequently, film and solution data are not yet available from this experiment.

(g) Solution Analyses. Analyses of solutions and precipitates from in-pile Zircaloy-2 experiments H-59, H-60, and Z-2 are listed in Table 4.13. Material balances have been made on the basis of these analyses, but the results of such balances are of questionable value. In Z-2, for example, the total uranium recovered amounts to about 110% of that originally present.

In H-59 the loss of copper determined from the material balance agrees well with that determined from radiolytic gas pressure, while in H-60 the indicated loss is 58% vs 68% from radiolytic gas pressure. Radiolytic-gas-pressure data from Z-2 and cesium data from Z-1 are not presently available.

(h) Out-of-Pile. Experiment H-56, which employs a Zircaloy-2 bomb and a solution 0.15 *m* in uranyl sulfate, 0.01 *m* in copper sulfate, and 0.5 *m* in sulfuric acid, is now in progress. The results of corrosion for the first six days indicate a probable

TABLE 4.13. SOLUTION AND PRECIPITATE ANALYSES

Experiment	pH		Constituent	Total Weight of Constituent (mg)		Precipitate (mg)
	Original Solution	Final Solution		Original Solution	Final Solution	
H-59	2.22	2.39	U	374.0	348.0	0.328
			Cu	11.9	8.2	0.003
			H_2SO_4	None		
			Total SO_4	171.0	150.0	0.539
			Ni		0.130	
			Cr		0.002	*
			Zr		0.344	3.480
			Sn		*	*
H-60	1.28	1.5	U	196.0	182.0	0.430
			Cu	6.85	3.92	0.052
			H_2SO_4	22.8		
			Total SO_4	113.4	103.3	0.417
			Ni		0.075	
			Cr		0.015	
			Zr		1.26	2.40
			Sn		*	*
Z-2	1.40	1.4	U	190.0	208.0	0.330
			Cu	3.28	2.50	0.021
			H_2SO_4	3.90		
			Total SO_4	101.4	110.6	0.384
			Ni		*	
			Cr		0.017	
			Zr		1.92	2.00
			Sn		*	

*Not detected.

leveling-off of the corrosion rate at about 0.2 mpy. An in-pile experiment with a similar solution is planned for HB-5 as soon as this facility becomes available.

(i) Titanium. Experiment H-76, which has been in progress for four weeks, consists of an all-titanium system and a solution which is 0.177 *m* in uranyl sulfate, 0.021 *m* in copper sulfate, and 0.046 *m* in sulfuric acid. Data obtained thus far indicate a corrosion rate of approximately 2 mpy under irradiation. Data from analysis of the 75A titanium used in the bomb and in the pins are presented in Table 4.14.

TABLE 4.14. ANALYSIS OF TITANIUM STOCK

Element	Weight Per Cent	
	Bomb Stock	Pin Stock
Al	0.038	0.021
Cr	0.001–0.01	Not detected
Fe	0.16	0.31
Mg	0.001–0.01	0.001–0.01
Mn	0.01–0.1	0.01–0.1
Si	0.01–0.1	0.01–0.1
V	0.01–0.1	0.01–0.1
W	<0.013	<0.013
H_2	0.016	0.009
N_2	<0.0005	<0.0005
[redacted]		
O_2	0.0023	0.0038

(j) Power-Density Calculations. Power densities in the bomb solutions for experiments H-59, H-60, and Z-2 were calculated from the measured neutron flux in hole HB-6 and also from an analysis of fission-product cesium as explained in the last report.[12] The results from the cesium analysis would be expected to be slightly high, since the method assumes the presence of only 37-y Cs^{137}, whereas some 13-d Cs^{136} was actually present as well. This source of error will be eliminated by recounting the samples after the short-lived isotope has decayed. As can be seen from Table 4.15, the power densities calculated from cesium analysis are anomalously low in the case of H-59 and Z-2.

[12]G. H. Jenks *et al.*, *HRP Quar. Prog. Rep. Oct. 31, 1954*, ORNL-1813, p 82.

TABLE 4.15. CALCULATED POWER DENSITIES AT 3 Mw

Experiment	Power Density (w/ml)	
	From Flux	From Cesium Analysis
H-59	11.0	7.9
H-60	5.7	5.9
Z-1	5.6	
Z-2	5.6	5.4
H-76	6.3	

Cesium analyses for Z-1 and H-76 are not yet available.

(k) Stainless Steel. No in-pile experiments were carried out on stainless steel during the past quarter. Data from current out-of-pile experiments not yet completed indicate the following:

1. In the absence of added chromate, systems pressurized with oxygen gas showed the same corrosion rates as those in which hydrogen peroxide was used. No experiments with added chromate have yet been run to check the effect of possible chromate reduction on the corrosion rate.
2. The presence of 0.1 *m* copper sulfate in 0.15 *m* uranyl sulfate solution does not increase the corrosion rate.
3. Stainless steel pins in platinum-lined bombs and in pretreated stainless steel bombs initially showed higher corrosion rates than did similar pins in untreated stainless steel bombs. In the pretreated stainless steel bomb the pin corrosion eventually leveled off at 0.10 to 0.15 mpy after two days, while in the platinum-lined bomb the corrosion rate continued at about 0.35 mpy after seven days.

(l) Additional Experimental Facilities. The HB-5 experimental facility in the LITR was put into operation in January after considerable delay stemming from fabrication difficulties and a bomb failure which resulted in the necessity of replacing some contaminated equipment.

A facility to open and unload the bombs was designed, and drawings were sent to the shops. Completion of this facility is scheduled for March 1, 1955.

4.2.2 MTR In-Pile Experiment

Contingent on the availability of an angular beam hole, an HRP rocking-bomb corrosion experiment

is scheduled to be inserted in the MTR during the latter part of April or the first part of May.

Tentative specifications covering the initial experiment are as follows:

Bomb material	Zircaloy-2
Corrosion pin material	Zircaloy-2
Internal volume of bomb, cc	6
Design pressure, psi	4000
Design temperature, °C	300
Volume of solution at 300°C, cc	4.5
Solution, grams of U as UO_2SO_4 per kilogram of D_2O	10
Enrichment, %	93.2
Catalyst	$CuSO_4$
Approximate thermal flux, neutrons/cm^2/sec	2×10^{14}
Specific power at 300°C, kw/liter	57
Oxygen pressure at 300°C, psi	1200

The bomb for the MTR experiment will be similar to the bomb shown in Fig. 4.22. The corrosion pins will be mounted in a rack around the central thermocouple well. A capillary tube will extend from one end of the bomb to a Baldwin cell at the face of the reactor for pressure measurements.

In order to make accurate oxygen-pressure measurements, it will be necessary to decrease the thermal neutron flux by a factor sufficient to permit 99% recombination. To reduce this flux, the experiment will be retracted into a cadmium shield. To minimize the diameter of this shield, the longitudinal axis of the bomb will be mounted in line with and rocked on the center line of the beam hole, as shown in Fig. 4.23, rather than perpendicular to the beam-hole center line as in similar experiments at the LITR.

The heat generation as a result of gamma absorption in the high-flux region of the beam hole will be about 5 w/g. For this reason, the bomb and its cooling-water jacket will be small. They will be housed in a 1½-in.-dia hermetically sealed can which increases to a larger diameter at the face of the reactor to encase the Baldwin cell and vent valve. This can will be rocked around its longitudinal axis on bearings in a concentric shielding plug, water filled and cooled in the beryllium and graphite region, which will house the previously mentioned cadmium shield.

The experiment will be equipped with a safety mechanism which will automatically retract the bomb into the cadmium sleeve in the event of unsafe operating conditions.

An experiment was conducted to determine the temperature difference between the solution and bomb wall as a function of the heat flow per unit area and the rate of rocking. A bomb with a central heating element as shown in Fig. 4.24 was inserted in an air-cooling jacket and filled with a volume of water sufficient to occupy 75% of the bomb volume at 250°C. The bomb was pressurized

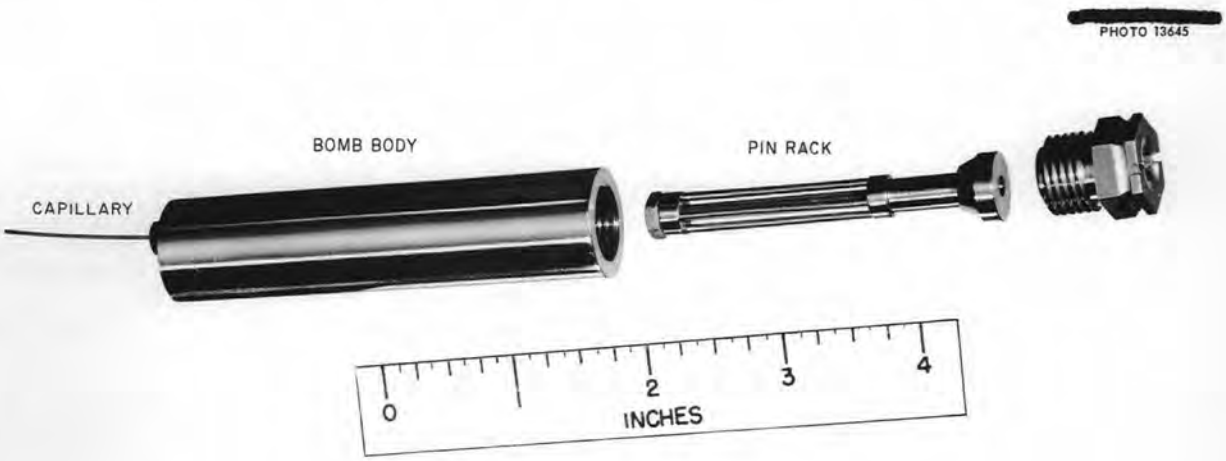

Fig. 4.22. MTR Experiment Bomb.

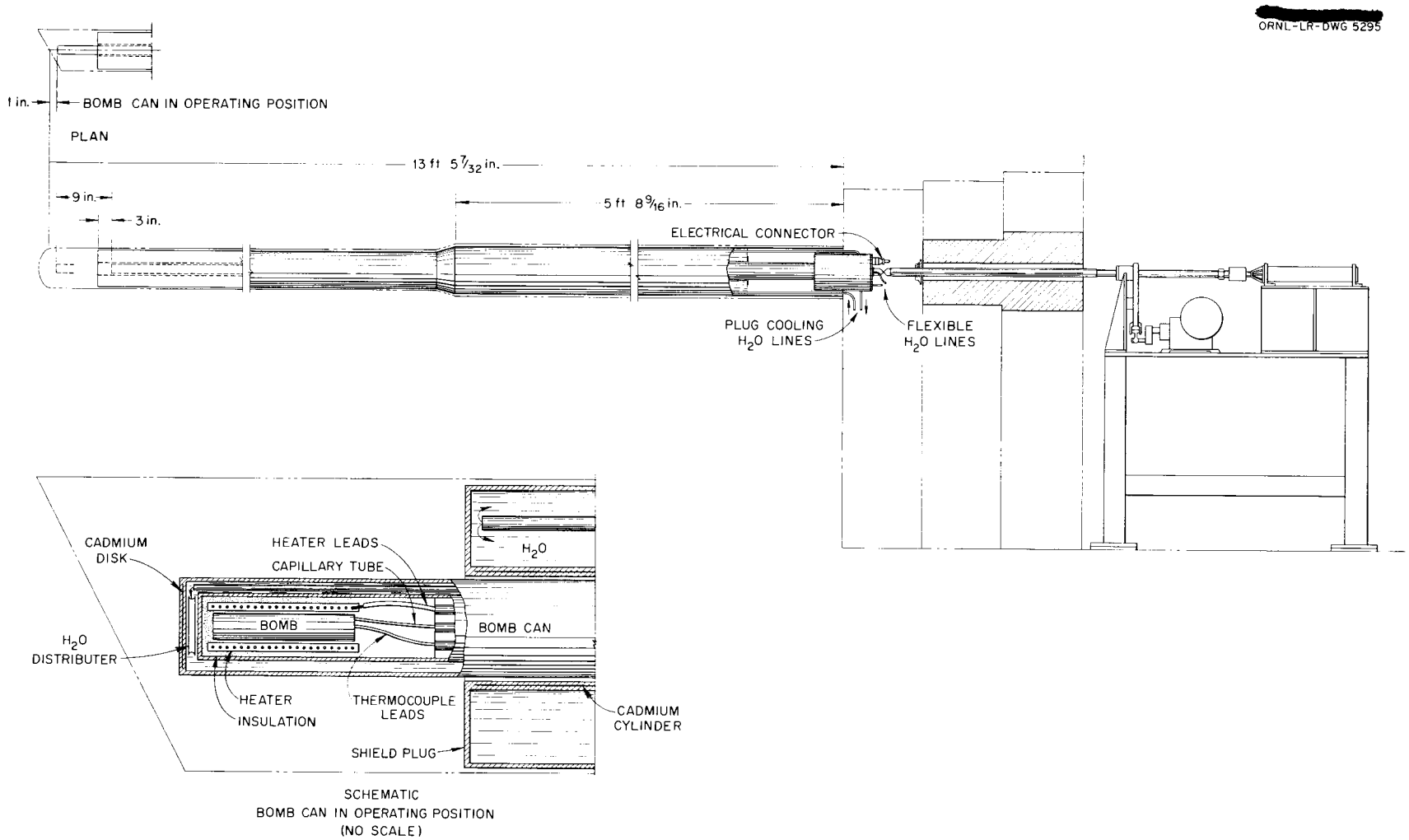

Fig. 4.23. Rocking Bomb for Hole HB-3 of the MTR.

at room temperature with 500 psi of helium. The bomb wall was maintained at 250°C, while the heat flow and rocking rates were varied. The bomb was rocked two ways, around its longitudinal axis and perpendicular to its longitudinal axis. The effect of heat flow, rocking rate, and type of rocking are shown in Fig. 4.25. At rocking rates above 8 cpm, perpendicular rocking appears to be slightly better than rocking around the center line. The heat flow in the MTR experiment will be 10 w/cm^2. Extension of the curves in Fig. 4.25 indicates that the temperature difference between the bomb wall and the solution will be about 35°C in the MTR at a rocking rate of 16 cpm around the longitudinal axis of the bomb. An experiment is planned to determine the effect of this thermal gradient on corrosion.

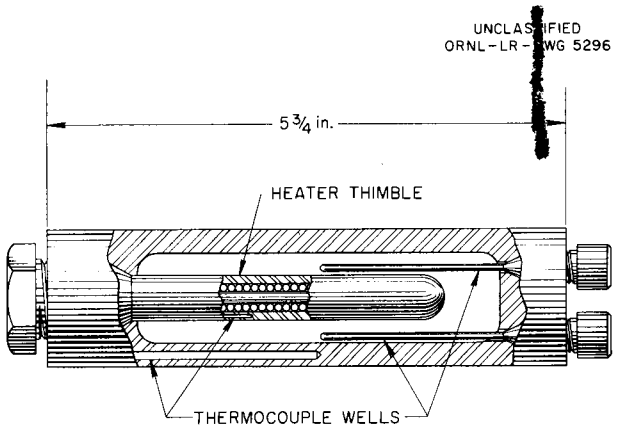

Fig. 4.24. Experimental ΔT Bomb.

[redacted]

ORNL-LR-DWG 5297

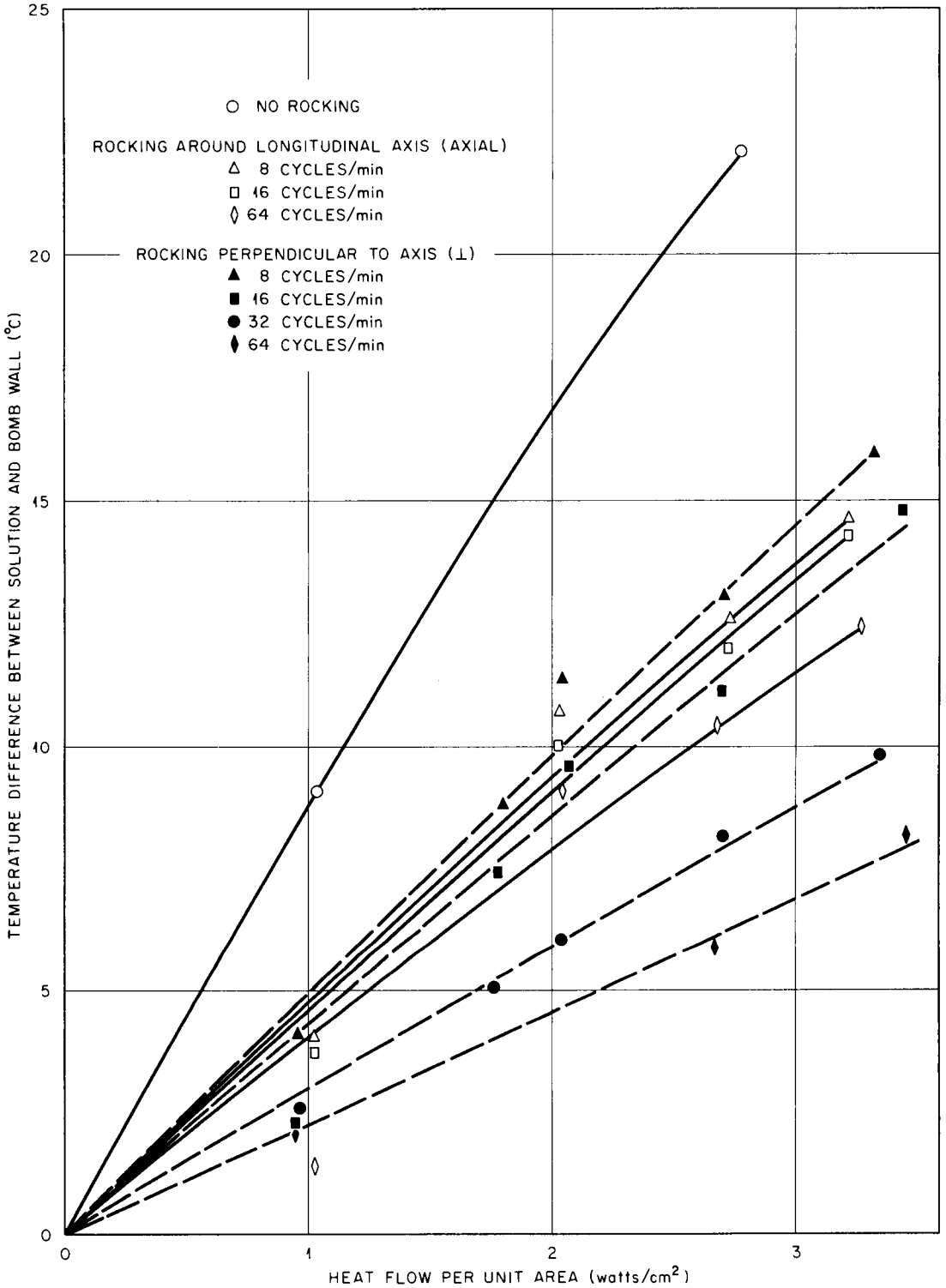

Fig. 4.25. Effect of Heat Flow and Rocking on ΔT.

5. LABORATORY CORROSION STUDIES

E. L. Compere G. E. Moore
J. L. English H. C. Savage
R. M. Warner

5.1 CORROSION OF PRECIPITATION-HARDENING STAINLESS STEELS BY SIMULATED REACTOR ENVIRONMENTS

J. L. English E. L. Compere

The precipitation-hardening stainless steels, particularly types 17-4 PH and 17-7 PH, have appeared to be attractive for a number of uses in the Homogeneous Reactor Project because of the hardness (Rockwell C-40 to 45) after heat treatment, with accompanying high strength, and because of indications of good corrosion resistance. Therefore type 17-4 PH (Cr 17%, Ni 4%, Cu 4%) has been used as a canned-rotor-pump bearing material in some in-pile loops and has been proposed as a high-temperature, high-stress bolt material for the fuel-contacting joint between the HRT core and pressure vessel. It was consequently desirable to examine these materials more closely, particularly in the hardened condition. Several degrees of hardness may be obtained by suitable heat treatment. Current results on unstressed, unwelded, fully hardened specimens are discussed below.

Wafer specimens of 17-4 PH and 17-7 PH stainless steel have been exposed in both annealed and fully hardened conditions to various typical simulated reactor solutions, as indicated in Table 5.1.

TABLE 5.1. CORROSION OF PRECIPITATION-HARDENING STAINLESS STEELS BY SIMULATED REACTOR ENVIRONMENTS

(Current values, undefilmed; most tests continuing)

Solution	Duration (hr)	Average Corrosion Rates (mpy)			
		Annealed		Fully Hardened	
		17-4 PH	17-7 PH	17-4 PH	17-7 PH
100°C, with Aeration					
Distilled water	600	0.02	Weight gain	0.005	Weight gain
5% HNO_3, not aerated	1000	0.5	0.2	5–12 (accelerated*)	28
0.02 *m* UO_2SO_4 + 0.005 *m* H_2SO_4	500	0.07	0.04	1 (cracks)	3 (blisters)
0.17 *m* UO_2SO_4	1000	0.07	0.05	0.5	0.2
	1900	0.1		0.08	
	700		0.06		17 (blisters)
1.3 *m* UO_2SO_4	1000	0.1	0.1	32 (accelerated,* cracks, pits)	2
250°C, with 150 psi Oxygen					
Distilled water	600	Weight gain	Weight gain	Weight gain	Weight gain
0.17 *m* UO_2SO_4	600	0.2	Weight gain	0.2	Weight gain
	1000	0.4 (defilmed)			
1.3 *m* UO_2SO_4	600	0.12	0.7		
	200			20 (accelerated,* pits)	41
300°C, with 150 psi Oxygen					
0.02 *m* UO_2SO_4 + 0.005 *m* H_2SO_4	600	Weight gain	0.05	2	0.1

*Corrosion rate increases with time.

The results given in the table are current results, as the tests are being continued. The following conclusions have been drawn: The materials appear to be more easily corroded in the fully hardened condition than in the annealed condition. Eruptive blisters were observed on fully hardened type 17-7 PH (Cr 17%, Ni 7%, Al 1%) stainless steel after it was boiled for 1300 hr in dilute uranyl sulfate. A photograph of one of these specimens is shown in Fig. 5.1.

In several cases, cracks were observed in fully hardened type 17-4 PH stainless steel exposed to boiling aerated dilute uranyl sulfate solution. These cracks appeared on both sides of the wafer specimen in a long line about $\frac{1}{8}$ in. below numerals which had been punched on the specimen edge. They may have been caused by residual stresses occurring as a result of the punching. One of the cracks is shown in Fig. 5.2.

More rapid corrosion also occurs on the fully hardened materials in 1.3 *m* UO_2SO_4 both at 100 and 250°C, becoming quite severe on some specimens.

In general, the precipitation-hardening steels appear to be less attractive in the fully hardened condition than they are in the annealed condition in these solutions.

5.2 HRT POOL WATER CORROSION STUDIES

E. L. Compere

The plan to fill the HRT pool with water for maintenance has introduced the question of corrosion of various reactor materials by the pool water. Among the undesirable effects of such

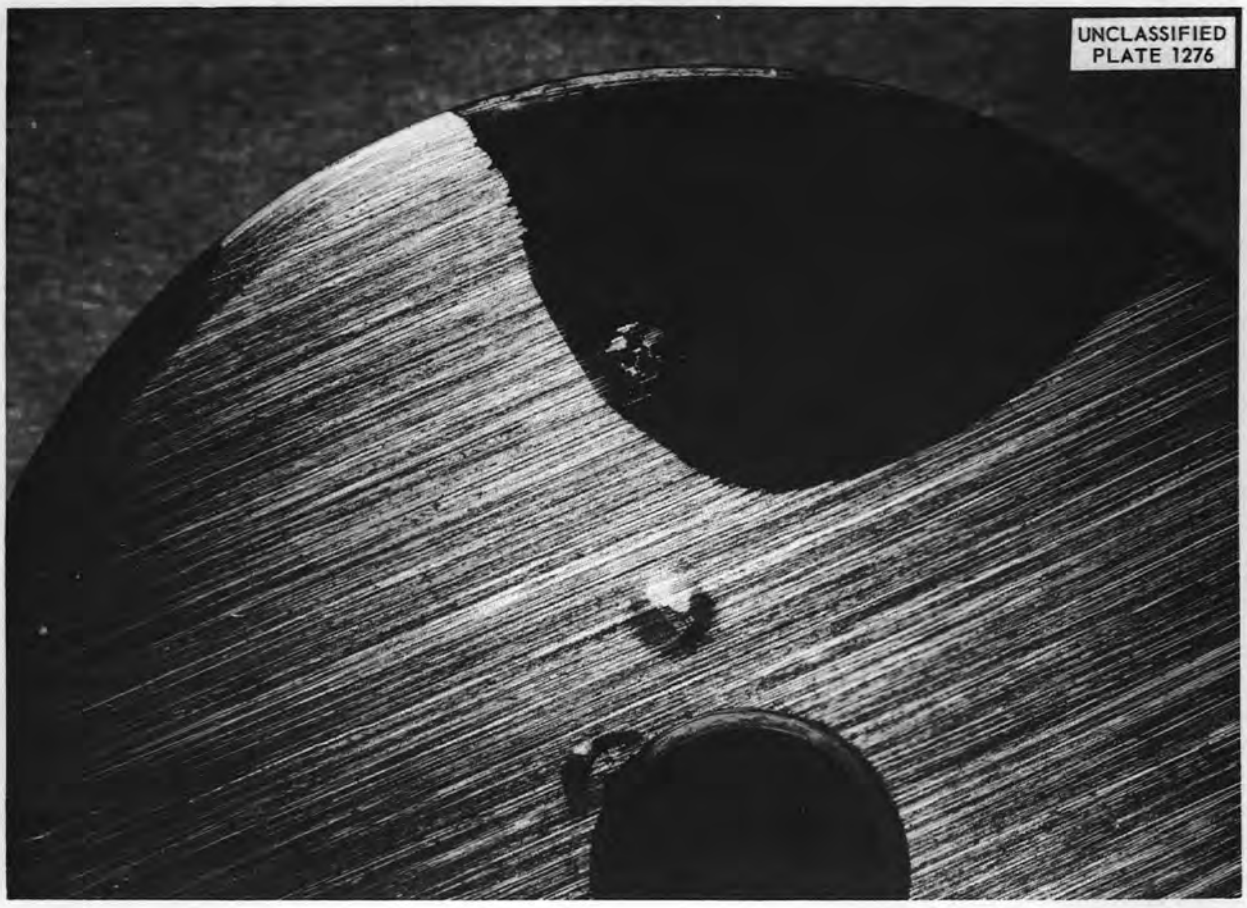

Fig. 5.1. Blisters on Fully Hardened Type 17-7 PH Stainless Steel After 1300 hr Boiling in Aerated 0.02 *m* UO_2SO_4 with 0.005 *m* H_2SO_4. 7X.

Fig. 5.2. Cracks on Fully Hardened Type 17-4 PH Stainless Steel After 1000 hr in Boiling Aerated 0.02 *m* UO_2SO_4 with 0.005 *m* H_2SO_4. 8X.

corrosion might be damage to materials with possible subsequent failure, freezing together of mechanical joints by crevice attack, and the deterioration of pool visibility because of increased turbidity and lowered light-reflecting ability.

Experiments have been carried out in which carbon steel, type 347 stainless steel, aluminum, copper, yellow brass, lead, magnesium, zinc, and galvanized steel, alone and in contact couples with carbon steel and stainless steel, were exposed to Oak Ridge aerated tap water, with and without various inhibitors, at room temperature for periods of 10 to 15 days. The results of these experiments are summarized in Table 5.2. Results of a seven-week exposure in the HRE storage pool are also reported.

In uninhibited tap water (test C-98) the most serious attack was on carbon steel. The attack occurred at a rate of 2 to 4 mpy and was accompanied by voluminous rust. This rust would be expected to deposit on most surfaces and would result in much loss in reflecting power. The experience in the HRE storage pool (test C-99) leads to similar conclusions. Zinc and galvanized steel were pitted, and magnesium was heavily corroded.

The use of 122 ppm sodium metasilicate as an inhibitor (test C-102) led to a colorless but somewhat turbid solution, with substantial attack on the magnesium, zinc, and galvanized specimens. Other materials were practically free of attack.

The attack on galvanized steel in all cases was on the coating, leaving the steel unattacked.

The use of a high-concentration sodium chromate inhibitor (test C-101) (3100 ppm Na_2CrO_4) resulted, as was expected, in no attack, no turbidity, and no deposits on the tank bottom. However, the

concentration was recognized as being unduly high, and an experiment (test F-35) in which 50 ppm sodium chromate was used is under way and has run 150 hr. A small amount of sodium silicate and sodium hexametaphosphate was included in this test, and some slight attack, presumably due to the silicate, has appeared on zinc and galvanized steel. Also, some slight attack in the crevice only was noted on aluminum-brass, aluminum-copper, and copper–carbon steel couples. A stressed flange-bolt assembly has also been exposed to this medium for 8 hr per day during this period and has been allowed to dry in air the remainder of the time. The only observed attack was trivial rust spots in some of the threads. The tank has remained clear (light yellow) and free from any "crud."

Sodium nitrite, less concentrated sodium chromate, and other inhibitors will be investigated in order to find the most desirable inhibitor. However, on the basis of the above tests, it is apparently quite desirable to inhibit the HRT pool water. The inhibitor should be added with the water.

Chromium-molybdenum alloy steel stud bolts (ASTM-A 193-52aT grade B7), $\frac{5}{8} \times 6\frac{1}{2}$ in., and carbon steel hex nuts (ASTM-A 193-53 grade 2H) from the stock purchased for use with HRT flanges were exposed to aerated tap water at room temperature for three and six weeks, respectively, after they were stressed to 20,000 psi in a sleeve and washer assembly. This exposure was to simulate immersion in the HRT pool during maintenance periods. A voluminous general coating of rust resulted. After defilming, corrosion rates were found to be 2 to 4 mpy, with no localized attack. Exposed bolts required 45 to 50 ft-lb of torque to loosen the nut, while unexposed bolts required 55 ft-lb of torque to loosen the nut. The major effect of this degree of corrosion would probably be that the rust would lower the visibility in the pool. Inhibition of the pool water would be expected to mitigate this effect.

5.3 EVAPORATOR TEST

J. L. English

Stress specimens of type 347 stainless steel have been exposed to boiling uranyl sulfate solutions contained in a steam-heated small-scale evaporator[1] for a total of 2022 hr. The specimens, of the three-point, constant-strain type,[2] were stressed at 20,000 psi and were exposed in duplicate to the solution and vapor phases. The first 1500-hr exposure was made in 0.17 *m* UO_2SO_4; the remaining time, 522 hr, was accumulated in a solution of 0.04 *m* UO_2SO_4 containing 0.005 *m* $CuSO_4$ and 10 mole % excess H_2SO_4.

There have been no indications of accelerated corrosion attack on the type 347 stainless steel as the result of the applied stress. The specimens have remained bright, lustrous, and completely free from cracking. Corrosion rates, based upon the as-scrubbed weight losses for the complete stress assemblies, were nearly negligible and ranged between 0.01 and 0.04 mpy for the solution and vapor-phase exposures.

The tests are being continued, and the specimens are scheduled for examination at 500-hr intervals.

5.4 BOILING NITRIC ACID SPECIFICATION TESTS ON HRT STAINLESS STEELS

J. L. English E. L. Compere

All type 347 stainless steels are required by HRT specifications to pass a standard boiling 65% nitric acid test, which serves as an indication of the general quality of the metal, the sensitivity to heat effects and welding, and the adequacy of columbium stabilization. Usually these tests are performed by the vendor, but, when they were not made, the tests were performed at ORNL. In particular, many of the stainless steel items destined for fabrication by Westinghouse into the 400A pump have been tested (over 50 items); a few items have not passed the specification, and the appropriate persons have been notified.

5.5 DEVELOPMENT OF TWIN STRIP SPECIMENS FOR THE EVALUATION OF STRESS-CORROSION CRACKING

E. L. Compere

Although stress-corrosion cracking of type 347 stainless steel, titanium, or Zircaloy-2 in contact with uranyl sulfate solutions has not been observed, the seriousness of the consequences of failure demands that their freedom from susceptibility to this type of attack be demonstrated. The acceptability of other materials proposed for high-stress

[1] E. L. Compere and J. L. English, *HRP Quar. Prog. Rep. July 31, 1954*, ORNL-1772, p 94–95.

[2] A. C. Jealous, *Thorex Information Meeting Summary, October 19 and 20, 1954*, ORNL CF-54-11-145, p 48 (Nov. 26, 1954).

TABLE 5.2. EFFECT OF INHIBITORS ON CORROSION OF REACTOR MATERIALS[a] BY OAK RIDGE WATER AT ROOM TEMPERATURE

	Medium				
	Tap Water, Aerated (Test No. C-98)	HRE Storage Pool, Tap Water (Test No. C-99)	Silicate Inhibited Tap Water, Aerated (Test No. C-102)	Heavily Inhibited Tap Water, Aerated (Test No. C-101)	Inhibited Tap Water, Aerated (Test No. F-35)
Inhibitor, ppm	None	None			
Na_2CrO_4				3100	50
Na_2SiO_3			122		4
$Na_6P_6O_{18}$			306		26
H_3PO_4			86		
pH, original	6.3		7.2	7.8	7.6
Duration, hr	213	1196	336	360	150 (in progress)
Pool appearance	Heavy turbid rust deposit on pool bottom		Colorless but slightly turbid; bottom clean	Clear yellow; bottom clean	Clear yellow; bottom clean
Materials showing slight or no general attack	SS; SS/SS; Cu; Cu/SS; B; B/SS; Al	SS; SS/SS; Al; Cu; Cu/SS; B; B/SS; Pb	Cu; Cu/CS; Cu/SS; Pb; Pb/CS; Pb/SS; B; B/CS; B/SS; CS; CS/CS; CS/SS; SS; SS/SS	All	Pb; Pb/CS; Pb/SS; CS; CS/CS; CS/SS; SS; SS/SS; Al; Al/CS; Al/SS; Cu; Cu/SS; B; B/CS; B/SS
Moderate attack	CS; CS/CS; CS/SS; Cu/CS; B/CS; Pb; Pb/CS; Pb/(SS)[b]	CS; CS/CS; CS/(SS)[b]	Al; Al/(CS);[b] Al/(SS);[b] (localized)		Zn; Zn/(CS);[b] Zn/(SS);[b] GvS; GvS/(CS);[b] GvS/(SS);[b] (Mg not included)
Substantial attack	Mg; Mg/CS; Mg/(SS)[b]	Cu/CS; B/CS; Pb/CS; Mg; Mg/CS; Mg/SS	Zn; Zn/(CS);[b] Zn/(SS);[b] GvS; GvS/(CS);[b] GvS/(SS);[b] Mg; Mg/(CS);[b] Mg/(SS)[b]		

TABLE 5.2 (continued)

	Medium				
	Tap Water, Aerated (Test No. C-98)	HRE Storage Pool, Tap Water (Test No. C-99)	Silicate Inhibited Tap Water, Aerated (Test No. C-102)	Heavily Inhibited Tap Water, Aerated (Test No. C-101)	Inhibited Tap Water, Aerated (Test No. F-35)
Moderate or greater crevice attack	(Al)[b]/CS; Al/(SS);[b] GvS/(CS);[b] GvS/(SS)[b]	Al/CS; Al/(SS);[b] Pb/(SS)[b]			Al/B;[c] Al/Cu;[c] Cu/CS[c]
Moderate or more pitting	Zn; Zn/CS; Zn/SS; GvS	Zn; Zn/CS; Zn/SS; GvS; GvS/CS; GvS/SS			

[a]CS – carbon steel
SS – type 347 stainless steel
Al – aluminum
Mg – magnesium
Zn – zinc
Cu – copper
B – brass
Pb – lead
GvS – galvanized steel

[b]Material in parentheses not attacked.
[c]Only slight crevice attack.

service in contact with reactor fluids, for example, the precipitation-hardening stainless steels, must also be demonstrated. A compact, easily fabricated, inexpensive type of stressed specimen was developed for evaluating the sensitivities of such materials to stress-corrosion cracking.

The proposed specimen consists of twin strips of metal, drilled and bolted together at each end and stressed over a short rod fulcrum in the center. In the experimental development of this specimen, the strips were of type 347 stainless steel sheet, $3\frac{1}{2} \times \frac{1}{2} \times \frac{1}{16}$ in., and a $\frac{1}{2}$-in. section of $\frac{3}{32}$-in. type 347 stainless steel welding rod served as the fulcrum. Stress was applied by tightening the bolts and, originally, was evaluated by strain gages. Subsequently, it was found that with a fixed metal thickness the strain (and stress) was substantially the same on both sides and could be reproduced to within about 10% by tightening the bolts to a measured deflection of the strips past snugness.

The specimen size was selected so that the strips could be cut from any materials larger than $\frac{1}{2}$-in. rod, $\frac{1}{16}$-in. steel, or $\frac{1}{2}$-in. sch. 40 pipe. Furthermore, the size was convenient for use in small autoclaves or other cramped locations. Failure of a specimen would result in a change from a parenthesis-like shape to a triangular shape and thus could be easily discerned even if the specimen were covered with a film which might obscure the observation of cracks. A specimen which has failed is shown in Fig. 5.3.

Some of the specimens were exposed at 40,000 psi of stress, to boiling 42% magnesium chloride solution.[3] Various polishing techniques were used on the edges. They were bolted with type 303 stainless steel bolts. The stresses applied and the time required to break one of the strips are given in Table 5.3. It will be noted that the results are, generally, in good agreement with values read from a chart in the *Corrosion Handbook*. This indicates that a specimen of this design gives results consistent with previous experience with this kind of corrosion attack both as regards stress and environment. The type of surface finish appeared to have little effect.

It is planned to use type 347 stainless steel in such specimens to explore the stress-corrosion tendencies of various reactor environments, including possible in-pile loop tests, and to use the specimen type for evaluating other materials, such as hardened type 17-4 PH stainless steel, exposed to various reactor environments.

5.6 TOROID DYNAMIC-SLURRY STUDIES

5.6.1 Engineering

R. M. Warner H. C. Savage

A 20-toroid rotator,[4] designed for the study of corrosion under dynamic conditions, has been installed. The relatively inexpensive circular pipe toroids (see Fig. 5.4) permit rapid evaluation of a large number of corrosion variables. This is particularly important in the thorium oxide slurry studies when the various oxide preparations and the effects of additives are being evaluated.

[3] M. A. Scheil, "Stress Corrosion Cracking in Stainless Alloys," p 174–182 in *Corrosion Handbook* (ed. by H. H. Uhlig), Wiley, New York, 1948.

[4] G. E. Moore and E. L. Compere, *HRP Quar. Prog. Rep. Oct. 31, 1954*, ORNL-1813, p 102.

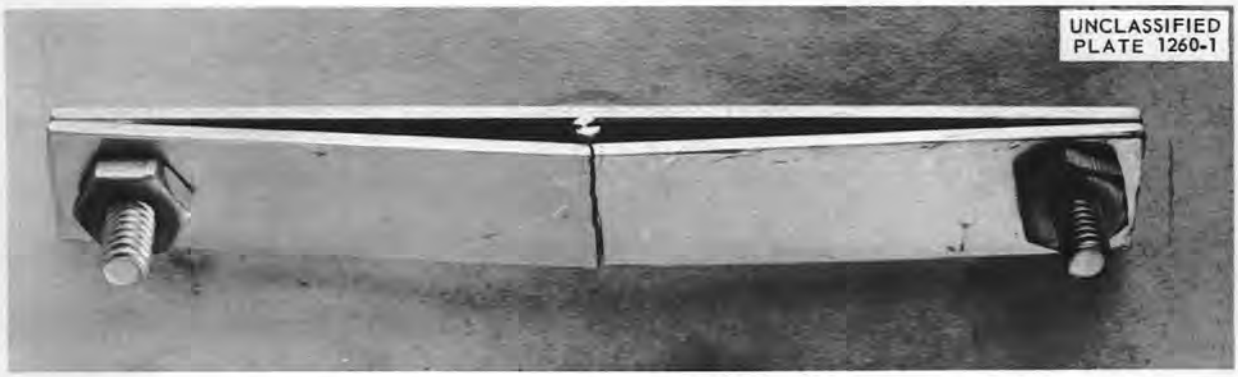

Fig. 5.3. Twin-Strip Stress Specimen of Type 347 Stainless Steel, Exposed to Boiling 42% Magnesium Chloride Solution. Failed in interval 24 to 45 hr.

TABLE 5.3. TWIN-STRIP, STRESSED SPECIMENS OF TYPE 347 STAINLESS STEEL EXPOSED TO BOILING 42% MAGNESIUM CHLORIDE SOLUTION

Finish	Stress (psi)	Time Interval in Which Break Occurred (hr)
Edges polished	33,000	45–65
Edges polished	42,000	24–45
Radiac cutoff wheel	40,000	10–15; 15*
Radiac cutoff wheel, then metallographic polish	40,000	10–15; 5–10
Radiac cutoff wheel, then electropolished	40,000	15–20; 20*
**	33,000	50–100
**	40,000	15–25

*Bolt heads of type 303 stainless steel broke at this time, relieving stress and stopping test; specimens were cracked at this point but not completely broken.

**For finish, see p 176 of *Corrosion Handbook* (ed. by H. H. Uhlig), Wiley, New York, 1948.

During the past quarter the 20-toroid rotator has been operated intermittently for approximately 60 hr to test the performance of the completed assembly. Approximately 40 hr of this time was accumulated with a furnace temperature of 250°C, while the remainder was at room temperature. With the exception of several minor mechanical adjustments, the over-all performance of the rotator was satisfactory. However, longer periods of continuous operation at the elevated temperature will be necessary to evaluate such factors as bearing wear and furnace serviceability. This phase of the testing will be conducted simultaneously with the use of the rotator in obtaining corrosion data.

The following capabilities and limitations of the 20-toroid rotator can be presented as the result of the performance testing. With the present mechanical arrangement the rate of rotation of the toroids may be adjusted and maintained at a value of ±5 rpm over a range of 850 to 1650 rpm, thus providing liquid velocities of 22 to 43 fps in the circular toroids. The furnace is capable of heating from room temperature to 250°C in approximately 15 min when utilizing approximately 75% of its total heat capacity. However, this is the temperature of the ambient air inside the rotator enclosure; the fluids in the toroids require approximately 1 hr to reach 250°C. Temperatures as high as 350°C can easily be attained.

The design of the 20-toroid rotator requires that the furnace heating elements be controlled by a stationary thermocouple positioned in the ambient region of the furnace near the toroids. Furthermore, this stationary thermocouple provides the only means of temperature measurement which can be used while the toroids are rotating. Since the temperature of the solutions is probably higher than that of the furnace ambient because they generate additional heat by flowing inside the toroids, an attempt is being made to obtain data which will correlate these two temperatures as a function of the rpm of the rotator. Based on the assumption that the temperature at the outer sides of the toroid walls is the same as that of the solution flowing inside, thermocouples have been tack-welded to them and terminate at jacks fastened to the rotating shaft outside the furnace enclosure. More accurate solution-temperature measurements can be made when the newly designed toroid thermocouple wells become available. After a period of operation sufficient to establish a temperature equilibrium condition between the solutions in the toroids and the furnace ambient, the motor will be shut off and the rotator stopped by applying a braking force on the rotating drum. The temperature of the ambient region of the furnace and of the outside wall of the toroid will be read simultaneously. While these data will not provide the exact correlation of the temperatures which exist during rotation, it is assumed that they will be within the limits of accuracy required for the future corrosion studies to be performed with this machine.

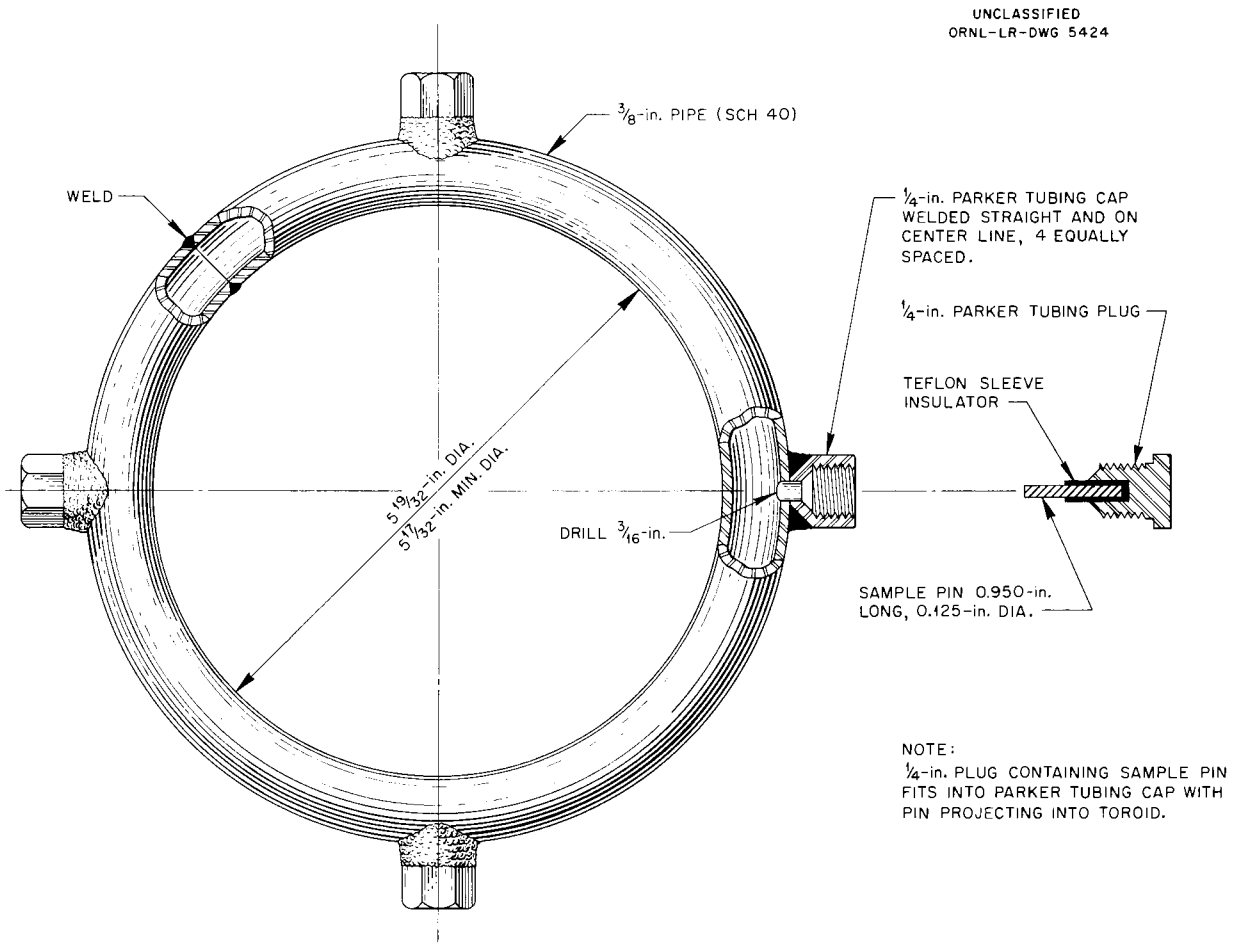

Fig. 5.4. Circular Pipe Toroid.

During the past quarter four additional four-toroid rotators[5] have been fabricated, installed, and placed in operation.

Improvements in the operation of the four-toroid rotators included the use of two Calrod heaters, bent in 6-in.-dia circles, instead of resistance wire to heat and maintain the toroids at the required operating temperature. Test runs indicated that the Calrods perform satisfactorily as heaters and are far more durable than the wound resistance wire. Also, thermocouple wells (which replace one of the four sample-pin holders in each toroid) have been designed and tested. While their use reduces the number of sample pins per toroid from four to three, they provide a more accurate measurement of the temperature of the solution than would be provided by a thermocouple tack-welded to the outside wall of the toroid. In addition, thermocouple failure during rotation is greatly reduced, and complete disassembly of the toroid bundle for thermocouple replacement is eliminated.

5.6.2 Test Results

G. E. Moore E. L. Compere

(a) Introduction. As indicated last quarter,[4] the detection of differences in the corrosion behavior of thoria slurries under selected standard conditions may find use in quality control and in evaluating the effect of process variables during production of thorium oxide. It was shown that slurries prepared from thorium oxide from two different sources (Ames and Lindsay No. 7) yielded significantly different corrosion results with type

[5]E. L. Compere and G. E. Moore, *HRP Quar. Prog. Rep. April 30, 1954*, ORNL-1753, p 109.

347 stainless steel under the test conditions. Additional experiments have now expanded the comparison to include thoria slurries from four sources: Ames, Lindsay batches Nos. 7 and 8, and the pyrohydrolyzed, 900°C fired material. These slurries were circulated in type 347 stainless steel toroids at 26 fps velocity over the temperature range 200 to 300°C with oxygen or inert gas atmospheres. Pin corrosion specimens of type 347 stainless steel, titanium (75A), and Zircaloy-2 were inserted in a circulating slurry whose concentration was varied from 100 to 2275 g of thorium per kilogram of water.

The corrosion rates of these metals over the range of temperature, slurry concentration, and blanket gases were generally less than 4 mpy. However, it was found possible to distinguish between some slurries from different sources on the basis of their corrosion of type 347 stainless steel.

The corrosion results so far obtained have been summarized in Table 5.4. The results are based on weight data of the sample pins inserted into the circulating slurry and are expressed as the $mg/dm^2/day$ (mdd) gain (+) or loss (–). The type 347 stainless steel specimens were electrolytically defilmed, whereas the results for titanium and Zircaloy-2 are based on as-removed, scrubbed weights. The weighing error was extimated to correspond to about ±4 mdd in most cases.

The slurries were prepared by adding a weighed amount of the as-received thorium oxide to an amount of distilled water calculated to yield the desired concentration. The calculated concentration generally agreed to about ±10% with that obtained by chemical analysis. Chemical analyses of these oxides are summarized in Table 5.5.

Oxygen was introduced into the system by the thermal decomposition of hydrogen peroxide added as a 30% solution; the resulting oxygen pressure was calculated at the operating temperature. For those experiments in the absence of oxygen, the vapor space above the slurry was swept out with either helium or nitrogen gas before the system was closed.

The recorded average temperature as determined by iron-constantan thermocouples welded to the toroid walls varied by approximately ±10°C about the desired nominal temperature. In the only run in which the wall temperature has so far been determined, it was about 7°C higher than the slurry temperature as determined by a thermocouple introduced into the slurry in a thermowell.

(b) Comparison of Thoria Slurries. The experimental conditions which were selected for the comparison of the slurries were as follows: 500 g of thorium per kilogram of water, 250°C, 26 fps relative velocity, and about 85 psi oxygen pressure (at 250°C). The corrosion results obtained on the type 347 stainless steel sample pins are summarized in Table 5.6, together with pertinent statistical values for the comparison.

Table 5.6 readily shows that the corrosion behavior of the two Lindsay materials is similar and that their corrosion rates are greater than those obtained for both the Ames and the pyrohydrolyzed thorium oxides. These last oxides are seen to show quite similar corrosion behavior under the test conditions.

The variance in these data was analyzed by means of the t-test, and the conclusions were the same. Lindsay No. 7 was not significantly different from Lindsay No. 8 in corrosion behavior under the test conditions, nor was the Ames significantly different from the pyrohydrolyzed. However, the Ames oxide gave results significantly lower than those of both Lindsay materials, while the pyrohydrolyzed oxide was statistically distinguishable from only the Lindsay No. 7. No statistically significant difference was found between the pyrohydrolyzed and the Lindsay No. 8 thorium oxides. The 95% confidence level was used to establish the significance of the difference in the means.

Table 5.6 also illustrates the good degree of reproducibility in corrosion results obtained in toroids under a selected set of conditions. The results with Ames slurry, for example, were obtained from eight runs in four different toroids over a nine-week period. The Lindsay No. 8 results show greater dispersion than the others; this is due to the presence of two values which are greater than the mean by a factor of 3. There appears to be no reason to exclude these values from consideration at the present time, however.

In addition to the corrosion results obtained with the slurries from these four different sources under the selected conditions as just described, vast differences in physical and handling properties were observed, particularly during the course of the studies discussed in the following section. Small amounts of the Ames thorium oxide

TABLE 5.4. SUMMARY OF SAMPLE-PIN CORROSION RESULTS OF TYPE 347 STAINLESS STEEL, TITANIUM (75A), AND ZIRCALOY-2 BY THORIUM OXIDE SLURRIES AT 26 fps RELATIVE VELOCITY IN STAINLESS STEEL TOROIDS

Slurry Source	Nominal Slurry Concentration (g of Th per kg of H_2O)	Nominal Temperature (°C)	Gas*	Rate of Pin Weight Change, Type 347 Stainless Steel, Defilmed				Rate of Pin Weight Change, As-Removed, Scrubbed			
								Titanium-75A		Zircaloy-2	
				Number of Pins	Values or Arithmetic Mean ($mg/dm^2/day$)	Standard Deviation	95% C.I. of Mean (±)	Number of Pins	Values or Range ($mg/dm^2/day$)	Number of Pins	Values or Range ($mg/dm^2/day$)
Ames	100	250	O_2	4	+0.2	4.7	8.6	2	+1 +19	2	+3 +17
	200	250	O_2	5	−0.2	1.9	2.6	2	+19 +25	1	+11
			He	4	−2.7	1.1	1.9	0		0	
	500	250	O_2	28	−1.4	2.7	1.1	2	0 +3	2	0 +1
			He or N_2	6	−12	5.2	6.0	1	+3	1	0
		300	O_2	1	−6			1	0	1	+14
	1000	250	O_2	4	−5.1	6.4	11.7	2	+17 −3	2	0 +8
			He	2	−70 −72			1	+16	1	+19
Pryohydrolyzed, 900°C fired	500	250	O_2	4	−3.6	1.5	2.7	2	0 0	2	0 −1
		300	O_2	2	−5 −6			1	+2	1	−2
	1000	250	O_2	2	−5 −6			1	−1	1	−1
	1300	250	O_2	2	−5 −6			1	−1	1	−2
Lindsay No. 8	100	200	O_2	2	0 −1			1	−1	1	−1
		250	O_2	2	−2 −3			1	−13	1	+2
		300	O_2	2	−3 −4			1	+2	1	+7
	500	200	O_2	2	−9 −10			1	0	1	−1
			N_2	2	−6 −10			1	−1	1	0
		250	O_2	12	−10.4	10.0	6.6	4	0 to −6	4	0 to −11
			N_2	6	−10.0	9.6	11.0	1	−2	1	−2
		300	O_2	8	−29.5	7.9	7.1	4	−8 to −26	3	+2 to −14
			N_2	2	+9 −17			1	−22	1	−28
	1000	200	O_2	2	−13 −13			1	−2	1	−1
		250	O_2	8	−32.6	15.7	14.0	4	−6 to −16	4	+1 to −8
		300	O_2	4	−28.0	3.0	5.5	2	−14 −15	2	+1 −3
	2275	250	O_2	2	−140 −164			1	−29	1	−14
Lindsay No. 7	500	250	O_2	16	−10.0	4.0	2.2	0		0	

*64 to 111 psi O_2 at temperature, or inert gas blanket.

TABLE 5.5. AVERAGE ANALYZED COMPOSITION OF SEVERAL THORIUM OXIDE SLURRIES

	Ames	Pyrohydrolyzed, 900°C Fired	Lindsay No. 8	Lindsay No. 7
Slurry, mg per g of Th				
Th (mg per g of slurry)	321	321	255	277
Fe	0.02	0.03	<0.02	<0.02
Ni	<0.02	0.02	<0.02	<0.02
Cr	<0.01	0.01	<0.02	<0.01
Cu	0.84[a]		<0.04	<0.04
Al		1.2[b]		
SO_4^{--}	0.08[c]	5.0[d]	<0.04[e]	0.14
pH	8.30	4.1	9.9	8.90
Supernatant liquid				
pH	6.40	4.2	7.0	7.0
Cl, ppm	5	6	<5	4
Specific conductance, 10^{-5} mhos/cm	7.5	21	1.6	1.4

[a]Oxide was sieved through copper screen.
[b]Aluminum vessels used in preparation of oxide.
[c]Two analyses at other slurry concentrations gave 6.7 and 6.0 mg of SO_4^{--} per gram of thorium.
[d]Analysis at concentration of 470 mg of thorium per gram of slurry gave 6.4 mg of SO_4^{--} per gram of thorium.
[e]Analysis at concentration of 460 mg of thorium per gram of slurry gave 0.05 mg of SO_4^{--} per gram of thorium.

TABLE 5.6. CORROSION OF TYPE 347 STAINLESS STEEL BY SLURRIES OF THORIUM OXIDE FROM SEVERAL SOURCES IN STAINLESS STEEL TOROIDS

Concentration: 500 g of thorium per kilogram of water
Temperature: 250°C
Relative velocity: 26 fps
Pressure: 85 psi of oxygen (at 250°C)

Slurry Source	Number of Pins	Arithmetic Mean of Corrosion Rate ($mg/dm^2/day$)	Standard Deviation	95% Confidence Range of Mean
Ames	28	−1.4	2.7	−0.3 to −2.5
Pyrohydrolyzed, 900°C fired	4	−3.6	1.5	−0.9 to −6.3
Lindsay No. 8*	12	−10.4	10.0	−3.8 to −17.0
Lindsay No. 7	16	−10.0	4.0	−7.8 to −12.2

*Includes certain highly divergent values.

were found to adhere strongly and uniformly to the pin specimens; in at least one case the oxide was estimated to be about 2 μ thick. The oxide appeared as a hard, transparent deposit that could be removed as a dirty white powder when scratched with a sharp tool but was fairly resistant to the ordinary stainless steel electrolytic defilming solution (Rhodine inhibited, 5% by weight sulfuric acid at 75°C for 3 min). In addition, at the concentration level of 1000 g of thorium per kilogram of water, the Ames slurry could not be poured from the toroids at the end of the runs (about 120 hr duration).

The Lindsay No. 8 slurry at a concentration of 1000 g of thorium per kilogram of water and the pyrohydrolyzed thorium oxide slurry even at a concentration of 1300 g could both be poured from the toroids after they had been circulated for about 120 hr. The Lindsay No. 8 poured more readily than the pyrohydrolyzed, which may have been only 20 to 50% removed by pouring. At the concentration level of 2275 g of thorium per kilogram of water, Lindsay No. 8 could not be poured at the conclusion of that experiment.

Some difficulty was experienced in handling the pyrohydrolyzed thorium oxide slurry at room temperature even before its circulation, particularly at the concentration of 1000 g of thorium per kilogram of water. Under these conditions the slurry could not be kept suspended for even very short periods of time, with the result that the liquid was transferred during the operations, leaving the solids caked along the glass pipet walls, in polyethylene transfer bottles, etc.

The behavior of the pyrohydrolyzed thorium oxide slurry at the above concentration level was observed in the apparatus shown in Fig. 3.4, Sec. 3.3. At 200°C the slurry appeared to be similar to slurries from other sources, but at 250°C it gave a settled slurry volume larger by about one-third than most other slurries. The same observation was made at 300°C. Throughout this operation the slurry did not cake on standing and was easily dispersed.

None of these oxides was observed to maintain a dispersed slurry for any appreciable length of time after the approximately 120 hr or more of circulation. Varying degrees of "creaminess," settling rates, and wetting abilities were observed, but these observations have been only qualitative.

(c) Temperature, Slurry Concentration, and Blanket Gas Effects. Table 5.4 shows that, for slurries of thorium oxide from four sources circulating in stainless steel toroids at 26 fps relative velocity, within the concentration range of 100 to 1000 g of thorium per kilogram of water, with temperatures from 200 to 300°C, and in the presence and absence of oxygen, the average corrosion rates of type 347 stainless steel were generally less than about 20 mdd (~4 mpy). Titanium (75A) and Zircaloy-2 generally show (undefilmed) corrosion rates of even smaller magnitude, although there are fewer data for these materials.

The dispersion and the general low level of the corrosion rates make it difficult at the present time to establish trends in the corrosion behavior of these materials as the temperature, slurry concentration, and blanket gas are varied. Slurries of Ames and pyrohydrolyzed oxides show little effect on the corrosion rates of these metals within the above limits, although the data are rather limited at the present time. The results on type 347 stainless steel with Lindsay No. 8 slurries perhaps show some trends: increased rates with increased slurry concentration and with increased temperature seem to be indicated, at least over a part of the ranges investigated.

Three toroids, fabricated of titanium instead of type 347 stainless steel, were put into service during the course of these experiments. Two of them leaked because of poor seating surfaces of the Parker-type closures. The third toroid gave corrosion results on type 347 stainless steel and titanium pins indistinguishable from those obtained in type 347 stainless steel toroids under identical experimental conditions.

Part IV

ENGINEERING DEVELOPMENT

J. A. Lane

6. DEVELOPMENT OF FUEL-SYSTEM COMPONENTS

C. B. Graham

J. S. Culver
D. M. Eissenberg
L. F. Goode
J. A. Hafford
B. A. Hannaford
P. H. Harley
R. J. Kedl
W. L. Ross
J. A. Russell
J. G. Smith
I. Spiewak
W. H. Stahlheber
W. E. Stapf[1]
D. S. Toomb
L. R. Weissert[1]
E. L. Youngblood

6.1 RECOMBINER DEVELOPMENT

D. M. Eissenberg
J. A. Russell
P. H. Harley
J. G. Smith
I. Spiewak

6.1.1 High-Pressure Recombiner Loop

On October 19, the high-pressure recombiner loop[2] was put into operation. After preliminary runs at 100 and 500 psi, the system was operated for 34½ hr at the normal operating conditions: 1000 psia, 250°C, 0.55-cfm total flow, and 3 mole % H_2. Helium was used as the diluent in these runs; the O_2 concentration varied between about 1.5 and 6%. The recombination efficiency was measured.

With the exception of a few minor flash backs during cold startups, the system operated very smoothly. However, on November 18 a detonation occurred which blew the rupture discs and damaged some of the tubing in the lines between the electrolytic cells and the circulating loop. The detonation was probably caused by some catalyst particles, which had been dislodged by a flash back and transferred into the undiluted stoichiometric gas-addition line.[3]

A search is being made for a catalyst less fragile than the Baker platinized alumina pellets, which crumble very readily. Platinized alumina pellets fired at 1600°C for increased strength were inefficient as a catalyst. The same was true of platinum-plated copper wire mesh. Commercially available platinized stainless steel catalyst is on order and will be tested.

During a routine shutdown on January 6, another explosion temporarily interrupted the operation. Because of an operational error, the catalyst beds were wetted, and, as a result, an explosive mixture accumulated in the recirculating loop. This mixture was ignited, probably by a dry spot on the catalyst. The resulting explosion, starting at 300 psi, shattered only the 3000-psi rupture discs. It is believed that future explosions can be avoided.

The conclusions which have been reached as a result of the recombiner loop operation are as follows:

1. The efficiency of platinized alumina catalyst at high pressures is at least as good as at low pressures. Above 350°C, the reaction rates, which can be quite high, are determined by mass transfer of reactants from the main stream to the catalyst surface. For example, H_2-to-water conversions of about 90% have been observed in a 1-in.-deep bed at a space velocity of 3.3×10^6 per hour.

2. To prevent flash backs it is necessary to preheat some of the catalyst surface so that at least part of the recombiner is dry at all times.

3. Structural material for the catalyst bed support and in the immediate vicinity of the bed should be type 347 or other stabilized stainless steel. Metallographic examination of type 304 stainless steel wire mesh through which flash backs occurred revealed a considerable amount of intergranular carbide precipitation.

6.1.2 Thermal Convection Type of Catalytic Recombiner

A system has been proposed which utilizes the heat of recombination to circulate hydrogen, oxygen, and diluent through a catalyst bed. The recirculating rates must be rapid enough to maintain subexplosive conditions at all times. The most desirable feature of this system is the elimination of a mechanical gas-circulating device.

A low-pressure unit is being designed for the first phase of experimental testing (Fig. 6.1). The low-pressure-drop catalyst bed of platinized stainless steel wire is mounted at the bottom of the chimney. Metered hydrogen and oxygen are introduced into the steam diluent in the annular space surrounding the chimney. The H_2O produced in

[1] On loan from The Babcock & Wilcox Co.

[2] C. B. Graham *et al.*, *HRP Quar. Prog. Rep. April 30, 1954*, ORNL-1753, p 53–54.

[3] D. M. Eissenberg, *Recombiner Loop Detonation*, ORNL CF-54-12-78 (Dec. 13, 1954).

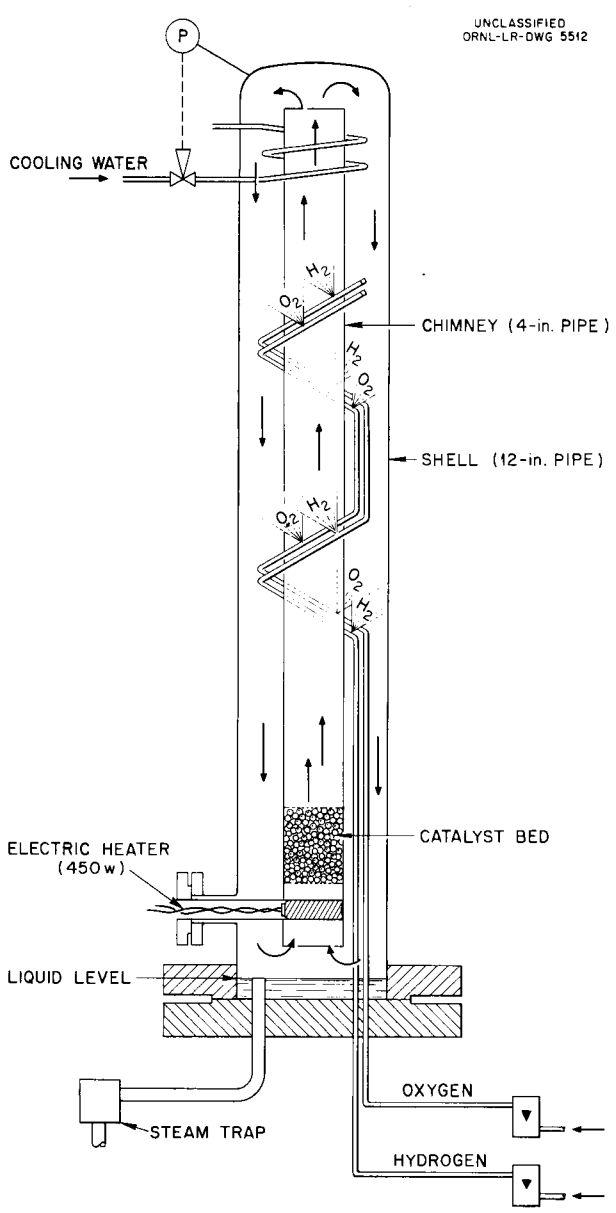

Fig. 6.1. Low-Pressure Thermal Circulating Recombiner.

the reaction is condensed at the top of the annulus. An electric heater is provided for starting the circulation and for preheating the catalyst.

[4]J. G. Smith, I. Spiewak, and D. S. Toomb, Jr., *HRP Quar. Prog. Rep. Oct. 31, 1954*, ORNL-1813, p 109–110.

[5]I. Spiewak *et al.*, *HRP Quar. Prog. Rep. July 31, 1954*, ORNL-1772, p 39–40.

6.2 DUMP-VALVE TEST LOOP

J. G. Smith I. Spiewak
D. S. Toomb

The design of the loop for testing dump-valve performance and life[4] was completed, and construction was started late in December. Operation of the system should begin during the next quarter.

6.3 LOW-PRESSURE ENTRAINMENT SEPARATOR TESTS

P. H. Harley I. Spiewak

A low-pressure glass loop for testing entrainment separators has been described previously[5] in connection with the evaluation of wire-mesh entrainment separators for use in the HRT.

Some additional ideas for improving the efficiency of wire-mesh separators were tested qualitatively. The tests were run by entraining $NiSO_4$ solution in air and then impinging the exhaust of the entrainment separator onto cotton wads saturated with dimethylglyoxime. The intensity of red color on the cotton served as a semiquantitative basis of comparison between runs. The experiments and results were as follows:

1. The mist-laden gas was washed with a pure water stream in a length of pipe containing turbulent fluid, and the washed gas was then passed through 6 in. of coarse wire mesh and 6 in. of fine mesh. This procedure was 10 to 20 times more effective than the one in which mesh alone was used.
2. The depth of the wire mesh was doubled, but it was found that 1 ft of coarse mesh plus 1 ft of fine mesh was only twice as effective as 6 in. of each.
3. The wire-mesh pads were backwashed with fine water spray, but no measurable improvement in entrainment separation was detected.

6.4 5000-gpm GAS SEPARATOR[6]

J. A. Hafford I. Spiewak

New vanes have been installed in the 14-in. experimental pipeline separator. They are geometrically scaled up from those in the HRT gas separator. It is expected that they will provide higher rotational velocities and, therefore, a more stable gas void than the previous set.

[6]C. B. Graham *et al.*, *HRP Quar. Prog. Rep. Jan. 31, 1954*, ORNL-1678, p 34.

6.5 SMALL REACTOR COMPONENTS

6.5.1 500-gpm Pump and 20-cfm Gas Circulators

W. L. Ross W. H. Stahlheber

A proposal from Allis-Chalmers for fabrication and operational testing of a totally enclosed 500-gpm pump and associated test loop is being evaluated. The pump design features top maintenance and hydrostatic bearings.

Proposals from Allis-Chalmers and Westinghouse for the fabrication of totally enclosed 20-cfm gas circulators and their testing at high temperature and pressure are being evaluated. Both circulator designs feature operation at high pressure and temperature, top maintenance, water-cooling, and water-lubricated bearings. The Allis-Chalmers design proposes hydrostatic, fluid-pressurized bearings, while the Westinghouse design uses the hydrodynamic-type (Graphitar) bearings.

6.5.2 ORNL 5-gpm Pump

W. L. Ross

An ORNL 5-gpm pump, which has been operating on an endurance test, suffered an electrical failure. This pump, designed for 1000-psi operation, had run a total of 4850 hr while circulating water at a temperature of 250°C. The significant operating history has been summarized previously.[7]

The pump stator is cooled by the use of copper coils on the iron laminations and has class A insulation on the windings. The stator had operated for a total of 6750 hr at the time that failure occurred. The failure was caused by deterioration of the insulation, with resultant electrical shorts between adjacent conductors. Most of the damaged insulation was on the end turns of the windings. No other defects were observed in the pump and motor.

The stator was rewound with class A insulated wire, and the pump is ready for additional testing. The possibility of using class H insulation is being investigated.

The ORNL pump design has been modified to allow operation at 2000-psi pressure. One model has been received from the ORNL shops. The pump characteristic curves have been determined at atmospheric pressure (Fig. 6.2) and are quite similar to those of the 1000-psi model. Fabrication of a 2000-psi test loop is nearing completion.

6.6 DEVELOPMENT OF LARGE HEAT EXCHANGER

L. F. Goode L. R. Weissert
W. L. Ross

The tubing for the HRT heat exchangers has been subjected to two of the methods of inspection which are being investigated by Foster Wheeler as part of the heat-exchanger development contract.

The first method was an application of the Sperry reflectoscope (ultrasonic method). The inspection was performed at the tubing redraw mill on the 1-in.-OD × 0.120-in.-wall tube rounds. The rounds were checked both circumferentially and longitudinally; the high rejection rate of approximately 45% was caused by failure of the rounds to pass the circumferential check. The number of rounds accepted was sufficient to provide the required redraw stock. Results of the inspection are being interpreted.

The second method was an application of a high-frequency-induced eddy current in the tube. Flaws in the tubing caused eddy-current disturbances, which resulted in a signal from the eddy-current measuring device. The machine, which can inspect 120 ft of tubing per minute, was used to check the finished $\frac{3}{8}$-in.-OD × 0.065-in.-wall tubing. Of the 502 tubes tested, 16 were rejected (about 3%). Examination of one fault indicated by the test revealed a nonmetallic inclusion measuring approximately 22 mils in depth by 1 in. in length and extending radially through a portion of the tube wall.

While tubes for the HRT will have passed both the above tests, in addition to other, more common, tests, it must be recognized that these two methods have not yet been proved to be reliable. The testing indicates that the further development of the methods will very likely result in more reliable tubing in the future.

6.7 4000-gpm LOOP[8]

B. A. Hannaford D. S. Toomb
W. E. Stapf J. S. Culver

After 290 hr of intermittent operation with water at 1000 psi and 250°C, the 4000-gpm loop was

[7] C. C. Hurtt, A. B. Daffron, and W. L. Ross, *HRP Quar. Prog. Rep. Oct. 31, 1954*, ORNL-1813, p 111.

[8] J. R. McWherter *et al.*, *HRP Quar. Prog. Rep. Nov. 15, 1951*, ORNL-1221, p 18.

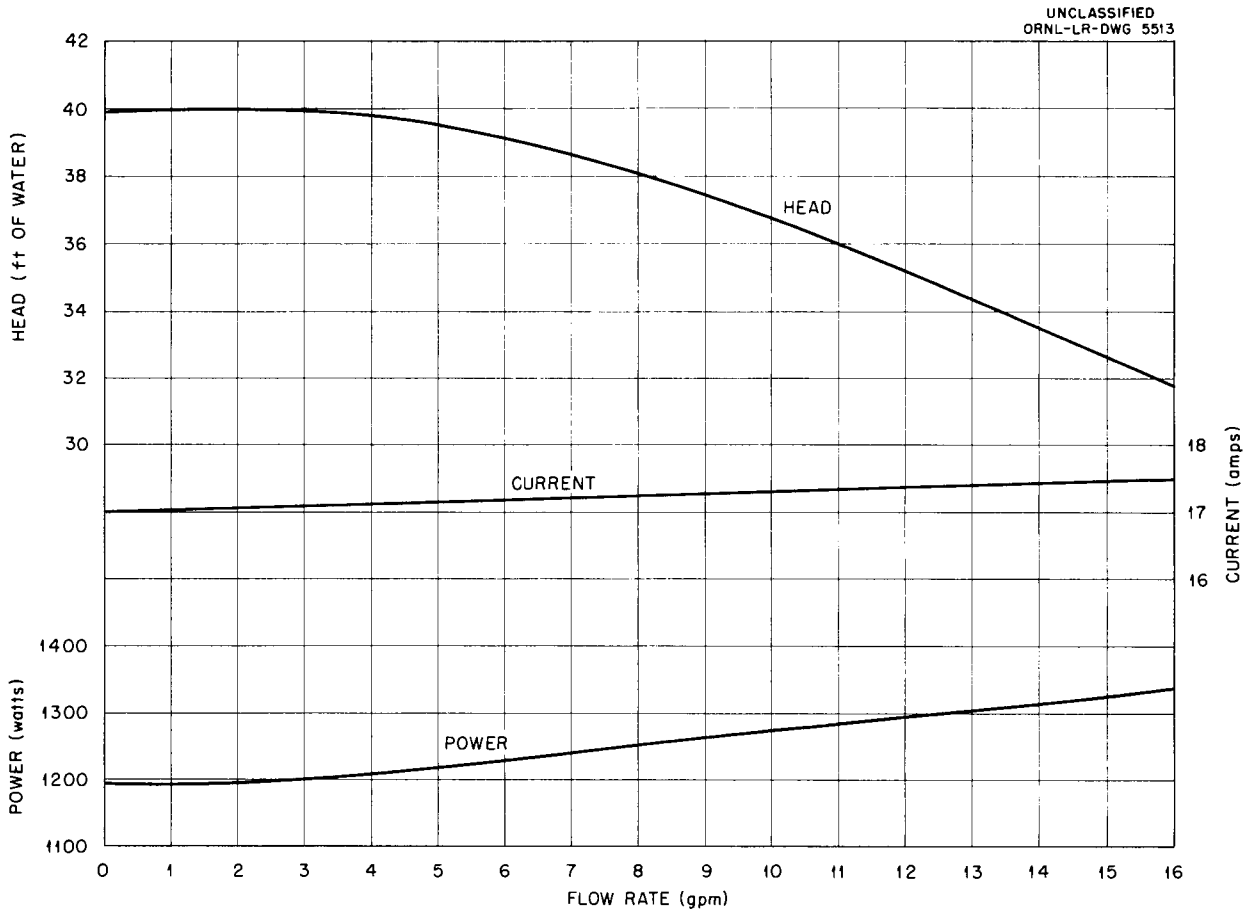

Fig. 6.2. Characteristics of 2000-psi Model ORNL 5-gpm Pump.

shut down in order to observe the effects of temperature-cycling and to prepare it for operation with UO_2SO_4 solution. The loop was drained, and the 6-, 8-, and 10-in. ring joint flanges were tested for tightness with a helium leak detector. No change in leak rate was observed, and all joints were below the HRT tolerance of 0.1 cc of helium per day at atmospheric pressure.

After checking for leaks, the large pipe loop was dismantled, inspected, and reassembled. Three of the stainless steel O-rings were replaced with rings which had been gold plated. No special wrench extensions or impact wrenches were used for reassembly. A leak test showed the loop to be as tight as before.

The Byron Jackson 4000-gpm pump was dismantled, the critical parts were photographed, and the impeller was weighed to provide a base for corrosion studies. Three $\frac{5}{8}$-in. bolts used for holding the stator assembly together were found to have broken during the run. Examination of them revealed a Rockwell hardness of 50 C, whereas a bolt removed intact had a Rockwell hardness of only 40 C. These bolts were made of nitrided 18-8 W stainless steel, which has also given poor experience at Byron Jackson and Westinghouse. All these bolts have been removed and are being replaced with type 316 stainless steel, lubricated with Molykote Z (molybdenum disulphide powder, dry). Various thread forms and antigalling compounds reported by other AEC installations will be tested.

Wear and leakage difficulties have been encountered with the packing and pistons on two Milton Roy pumps which return condensate and solution to the high-pressure system. The following combinations have been tried, but the results were unsatisfactory: Teflon packing,

Garlock Teflon rings, alternate layers of shredded and solid Teflon, and Neoprene chevron rings. Packless pumps have been ordered to replace those mentioned above.

When the 4000-gpm circulating pump has been reassembled, the loop will be operated with dilute UO_2SO_4 solution after a short shakedown with water.

6.8 SLURRY-INJECTION PUMP LOOP

J. S. Culver D. S. Toomb
E. L. Youngblood

The slurry-injection pump loop test has demonstrated the feasibility of pumping ThO_2 slurry with a diaphragm injector pump[9] similar to that used for the fuel system of the HRT. A standard Hammel-Dahl valve with a Stellite 6 plug and a Stellite 12 seat was used to throttle the 1000-psi slurry stream.

All runs were made with a ThO_2 concentration of 500 g/liter at about 30°C and with a single-head pump operating at 72 rpm.

The results of the tests are summarized in Table 6.1, and photographs of the valve trims after service are shown in Figs. 6.3 through 6.6.

[9] J. M. Baker, E. L. Youngblood, and D. S. Toomb, Jr., *HRP Quar. Prog. Rep. Oct. 31, 1954*, ORNL-1813, p 114–115.

TABLE 6.1. RESULTS OF SLURRY-INJECTION PUMP LOOP TEST

Trim	Duration (hr)	Thoria Used	Reason for Termination
A	67	Ames	Valve would no longer hold 1000 psi
B	45	Lindsay No. 8 – oxalate calcined at 900°C	Valve would no longer hold 1000 psi
C	52.1	Lindsay No. 8 – oxalate calcined at 900°C	Valve would no longer hold 1000 psi
D	298.6	ORNL-prepared oxide; calcined at 650°C from mantle-grade oxalate containing 0.7–1.0% sulphate	Valve froze in packing
	772	ORNL-prepared oxide; calcined at 650°C from mantle-grade oxalate containing 0.7–1.0% sulphate	Run was made to finish preceding test (no failure but trim slightly eroded)

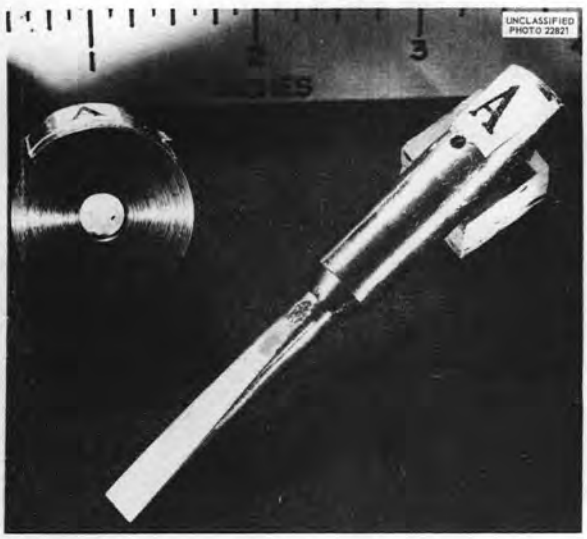

Fig. 6.3. Valve Trims After Use in Slurry Injection Pump Loop.

Fig. 6.4. Valve Trims After Use in Slurry Injection Pump Loop.

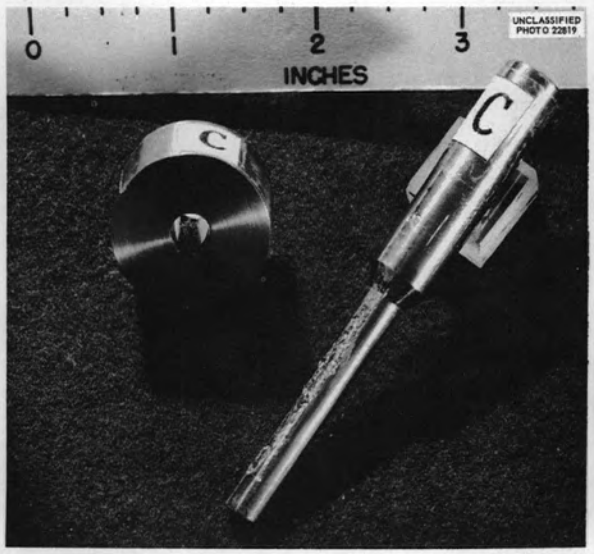

Fig. 6.5. Valve Trims After Use in Slurry Injection Pump Loop.

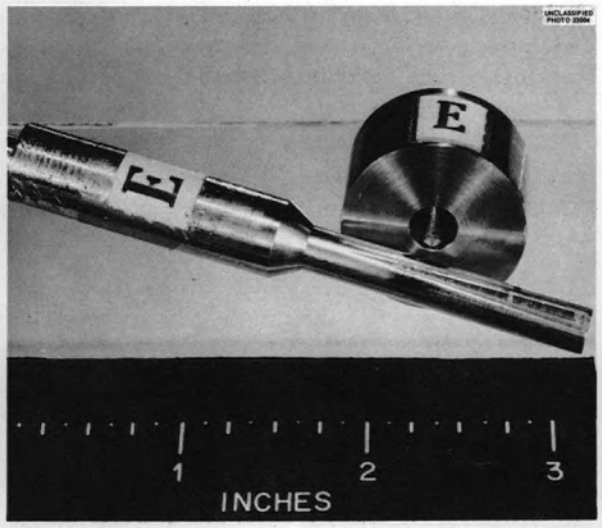

Fig. 6.6. Valve Trims After Use in Slurry Injection Pump Loop.

7. DEVELOPMENT OF BLANKET-SYSTEM COMPONENTS

R. N. Lyon

R. V. Bailey[1]
P. R. Crowley
D. G. Davis
R. B. Gallaher
W. Q. Hullings
A. S. Kitzes
B. A. Kress
C. G. Lawson
L. E. McTaggart
R. H. Nimmo
L. F. Parsly
J. D. Perret
M. Richardson
J. A. Russell
D. S. Toomb
P. C. Zmola

7.1 SLURRY ENGINEERING AND COMPONENT DEVELOPMENT

A. S. Kitzes
P. R. Crowley
R. B. Gallaher
W. Q. Hullings
B. A. Kress
C. G. Lawson
J. D. Perret
J. A. Russell
D. S. Toomb

7.1.1 Slurry-Circulation Studies

During the quarter, additional data have been obtained from the 100-gpm loops[2] and from a 5-gpm loop. In particular, further information was obtained about the influence of sulfate on the erosive-corrosive properties of the slurry and the tendency for the slurry to form cakes. In one test, the oxygen, usually injected into the loop, was replaced by hydrogen.

(a) Summary of Loop Runs. Table 7.1 is a summary of the runs which were made in order to determine the corrosion-erosion resistance of type 347 stainless steel to slurries of various oxide preparations containing oxygen and varying amounts of sulfate. A measured quantity of oxygen was injected into the cold pressurizer at the beginning of the run and whenever the run was interrupted; it was distributed throughout the system by allowing condensed oxygen-containing steam from the pressurizer to flow into the motor end of the pump while the Graphitar pump bearings were being flushed with pure water.

Although there was no pretreatment of the stainless steel prior to loading the loop with slurry, the golden-brown oxide film which had developed on the stainless steel during previous oxygenated slurry runs was not removed between loop tests.

(b) Effect of SO_4^{--} on ThO_2 Concentration and on Caking. It will be seen from Table 7.1 that the sulfate in slurry samples which were withdrawn during operation was largely associated with the ThO_2 solids, at least after the slurry was cooled to room temperature. The influence of sulfate on the slurry is illustrated, in part, by results from run S-54. In this run a slurry of 350 g of ThO_2 per kilogram of water was charged into the loop. After an initial startup period, the concentration in the circulating part of the system, which is about equal in volume to that of the pressurizer, was approximately the same as the charged concentration. Measurement of gamma radiation from the pressurizer also indicated that the solids were about evenly distributed between the loop proper and the pressurizer. The sulfate content during this part of the run was found by analysis to be between 250 and 330 ppm.

The loop was shut down after 69 hr, and sufficient thorium sulfate was added to raise the concentration to about 3500 ppm. When the loop was started up again, it was found that the concentration in the loop proper had almost doubled and that the concentration in the pressurizer was greatly reduced.

Raising the sulfate concentration to about 7000 ppm had little additional effect on the concentration.

In the other runs which are reported this quarter, the only one in which the pressurizer appeared to have a higher concentration than the circulating system was T-47, where the sulfate concentration was slightly below 3000 ppm. In the other runs the thorium concentration in the loop proper ranged from about 20% to about 70% higher than the concentration of the original charge.

In run S-51 (see ref. 3) serious caking had been observed in a slurry containing 12,000 ppm sulfate and 1200 g of thorium per kilogram of slurry. Similar caking was found to occur in a 5-gpm loop[4] test this quarter when a slurry was used that contained 10,000 ppm sulfate and a concentration of

[1]Consultant, Tulane University.

[2]R. N. Lyon *et al.*, *HRP Quar. Prog. Rep. Oct. 31, 1953*, ORNL-1658, p 127.

[3]R. N. Lyon *et al.*, *HRP Quar. Prog. Rep. Oct. 31, 1954*, ORNL-1813, p 116.

[4]R. N. Lyon *et al.*, *HRP Quar. Prog. Rep. April 30, 1954*, ORNL-1753, Fig. 119, p 164.

1000 g of ThO_2 per kilogram of H_2O. The ThO_2 was made from Thorex nitrate converted to oxalate and calcined at 320, 520, and 650°C, successively. Within 28 hr at 250°C essentially all the solids had been removed from suspension; they had been plated out both in the pressurizer and in the pipes. In contrast, the circulating slurry in run S-55 contained only about 5000 to 6000 ppm sulfate with 1200 g of thorium per kilogram of slurry, and no caking tendency was observed.

A portion of the material from the same batch as that charged into the 5-gpm loop at a concentration of 1000 g of ThO_2 per kilogram of H_2O and 10,000 ppm sulfate stalled a Waring blender in 15 min at room temperature.

That sulfate concentrations of 10,000 ppm and above can cause serious caking of slurries appears now to have been established. The theory can also be advanced that appreciable but lower sulfate concentrations cause looser, less adherent flocs which drop out of the pressurizer and do not plate out seriously on the walls. In this way the thorium concentration of the circulating slurry may be raised above that of the original charge. Non-plating flocculation with the resulting increase in the settling rate would be an advantage in the blanket pressurizer of the HRT but might cause excessive concentration gradients within the HRT blanket itself because of the low flow velocities expected there.

(c) Attack on Stainless Steel. A survey of previous tests shows a strong interrelationship between attack on stainless steel, pH, thorium sulfate content, oxygen content, and shear stress at the wall.

Attack in the loops is measured in two ways: by analysis for iron, nickel, and chromium in samples of slurry withdrawn during a run and by examination of loop components after the end of a run. The most complete examination can be given to the pump impeller, the orifice flow restrictor, and, when present, a rod which passes through a venturi so that it is subjected to a variety of shear stresses and velocities along its length. Visual examination of the pump volute is also easily accomplished. Earlier indications that these more accessible components were, by far, the most drastically attacked and that the piping was not seriously affected were strongly supported when a large portion of piping from S loop was removed and opened for inspection. The loop had accumulated a total service time, at 250°C, of about 5000 hr with all types and concentrations of ThO_2 slurry plus about 10,000 hr with $UO_3 \cdot H_2O$ slurries and water. The pipe, elbows, and welds showed essentially no attack; in most places they were covered with a very thin golden film. Hence, no defilming was required to examine the surfaces for attack. Attack was found to have occurred downstream from the orifice, on the wall, and at a weld downstream from the elbow. On the other hand, no appreciable attack appeared to have occurred on the sampler tube which extended into the stream or on the pipe wall downstream from the sampler tube. A more complete examination will be made, and the information obtained will be presented in the next report.

In the previous report,[3] two runs, S-53 and T-46, were described in which the principal difference between the slurries appeared to be in the amount of sulfate present as an impurity. In each run the ThO_2 had been prepared by calcination of the oxalate at 650°C, but the slurry in run S-53 averaged almost 5000 ppm SO_4^{--}, while the slurry in run T-46 averaged only about 225 ppm SO_4^{--}. Both runs were made with oxygen. In run T-46 the attack rate was high, the slurry remained strongly alkaline, and the concentration of solids appeared to remain about equal in the circulating stream and the pressurizer. In contrast, during run S-53 the slurry became acid, the attack rate was low, and solids appeared to settle out of the pressurizer into the circulating stream. The influence of the sulfate on this behavior was not demonstrated conclusively, since the high attack rate was obtained in a system with a stainless steel impeller, while the system which showed a low attack rate contained a titanium impeller. Also, it was recognized that there might have been other important, unknown differences between the slurries themselves. To clarify the results of these two tests and to determine whether $Th(SO_4)_2$ added to a slurry was as effective in reducing attack on stainless steel as $Th(SO_4)_2$ present as an impurity within the slurry solids, run S-54 was begun last quarter. The results of run S-54 are shown in Table 7.1 and are compared with those of runs T-46 and S-53 in Fig. 7.1.

The run was made in the same loop that was used for run S-53, but the slurry was from the same batch as that used in run T-46. During the first 69 hr, when the sulfate content was about 300 ppm,

TABLE 7.1. CIRCULATION OF THORIUM OXIDE SLURRIES AT 250°C

Sample No.	Circulation Time (hr)	Solids (Based on Total Slurry)									Filtrate				Materials in System			Gas Analysis		
		Th (g/kg)	Fe (ppm)	Ni (ppm)	Cr (ppm)	SO_4^{--} (ppm)	Ti (ppm)	pH	Fe (mg)/Th (g)	Cr (mg)/Th (g)	pH	Fe (ppm)	Ni (ppm)	SO_4^{--} (ppm)	Impeller	Orifice Plate	Seal Rings	Volume of Gas (ml)	O_2 (ppm of Slurry)	H_2 (ppm of Slurry)
Run S-54 – Oxide Prepared by Lindsay Chemical Co. from Cold Precipitated Oxalate Calcined at 650°C																				
0	1	401	28	5	12	300	<20	9.5	0.07	0.03	8.9	<1	<1	<10	Ti (weight loss, 2 g; light yellow color)	Ti (weight loss, 68 g)	Ti	36	320	0
1	21	320	320	51	92	246	<20	9.3	1.0	0.29	6.4	<1	<1	<10						
2	45	318	580	89	155	281	65	7.6	1.82	0.49	7.6	<1	<1	<10				45	290	0
3	69	324	750	116	176	252	71	8.8	2.30	0.85	7.8	<1	<1	16						
50 g of $Th(SO_4)_2$ Added After 69 hr of Circulation																				
4	71	530	670	89	220	3180	51	6.5	1.26	0.42	5.9	<1	7	31	Ti (maximum velocity at tip, 120 fps)	Ti (velocity, 83 fps)	Ti			
5	89	586	813	129	257	3170	54	6.5	1.40	0.44	6.2	<1	14	40				77	470	0
6	151	582	892	144	234	3460	129	6.0	1.53	0.40	6.0	<1	21	46						
7	198	602	1080	146	227	3520	136	6.3	1.80	0.38	6.1	<1	27	50				48	270	0
8	202	574	1000	103	294	3600	215	5.9	1.74	0.51	5.8	<1	26	54						
9	222	580	1070	165	330	3690	250	6.0	1.85	0.57	5.9	<1	29	68						
50 g of $Th(SO_4)_2$ Again Added After 222 hr of Circulation																				
10	248	572	1090	146	277	5650	267	4.2	1.90	0.49	4.2	<1	54	126	Ti (maximum velocity at tip, 120 fps)	Ti (velocity, 83 fps)	Ti			
11	313	556	1155	155	328	7880	274	3.7	2.08	0.59	3.7	<1	68	53				49	370	0
Run S-55 – Oxide Prepared by Lindsay Chemical Co. from Hot Precipitated Oxalate Calcined at 650°C																				
0	2	1255	120	34	37	5540	<20	8.0	0.10	0.03	6.8	<1	<1	22	SS, Ti hubs (tip velocity, 100 fps; weight loss, 17 g; loose black film, no pits; no film on much of system)	SS (velocity, 41 fps; weight loss, 370 mg)	Ti			
1	19	1258	496	95	131	6260	<20	6.8	0.40	0.10	6.1	<1	<1					48	300	0
2	91	1190	1325	248	341	6000	100	6.2	1.10	0.29	6.1	<1	22	44						
3	139	1225	1875	317	420	5670	100	5.4	1.53	0.34	5.9	<1	30	65						
5	193	1258	2310	383	608	5850	280	5.8	1.84	0.46	6.0	<1	36	81						
6	259	1190	3100	380	603	4600	276	6.6	2.60	0.48	5.7	160	5	435						
7	283	1155	3600	412	733	6200	314	6.8	3.12	0.51	5.7	<1	16	49				47	11	44
8	307	1155	4420	580	1000	5230	314	6.8	3.84	0.87	5.7	235	2	540				47	0	63
Run T-47 – Oxide Prepared from Oxalate Calcined at 375°C and Then at 650°C (prior to loading in loop for run, axide was circulated for 300 hr at 250°C: run S-53)																				
0	1	316	166	57	41	3000	49	5.7	0.52	0.13	5.4	<1	8	51	SS, Ti hubs	SS	Ti and SS	82	875	0
1	19	260	135	47	30	2100	48	5.2	0.52	0.12	5.4	<1	8	33						
2	67	212	140	44	33	1800	36	5.4	0.66	0.16	5.4	<1	7	33						
3	93	235	135	32	46	2760	41	6.1	0.57	0.20	6.1	<1	7	50						
4	159	197	126	33	32	2450	49	5.5	0.64	0.17	5.3	<1	7	43						
5	183	182	124	30	29	2310	39	5.4	0.68	0.16	5.6	<1	6	33						
6	231	179	116	30	29	2440	45	5.4	0.64	0.17	5.5	<1	5	29						
7	257	176	127	35	24	2220	73	5.3	0.72	0.14	5.3	<1	5	32				13	150	0
Run T-48 – Oxide Prepared by Lindsay Chemical Co. from Formate Calcined at 650°C; 60 g of $Th(SO_4)_2$ Added																				
0	13	460	110	21	18		<20	5.7	0.24	0.04	5.8	<1	2	12	SS, Ti hubs	Ti	Ti and SS	86	940	0
1	37	523	189	40	39	3000	<20	6.1	0.36	0.07	6.3	<1	4	40						
2	61	594	265	40	61	3150	61	6.1	0.44	0.10	6.2	<1	7	25						
3	133	650	470	70	77	3400	110	5.7	0.72	0.12	5.8	<1	14	43						
4	157	641	489	70	82	3600	132	5.5	0.76	0.13	5.7	200	2	480						
5	205	666	594	85	79	3200	111	5.7	0.89	0.12	5.7	<1	18	56						
6	299	666	714	78	90	3200	128	5.4	1.10	0.14	5.7	<1	2	48				87	725	0
Run T-49 – Oxide Prepared from Oxalate Calcined at 375°C and Then at 650°C; 100 psi H_2 Added																				
0	2	330	14	5	8		<20	8.4	0.04	0	8.2	<1	<1	66	SS, Ti hubs (weight lass, 15 g; tip velocity, ~120 fps)	SS (weight loss, 2.3 mg; enlarged from 3/4 to 7/8 in.; velocity, 80 fps)	Ti and SS			
1	65	352	297	14	58		<20	8.4	0.84	0.17	8.2	<1	<1	212				62	0	56
2	113	424	484	21	112	3440	<20	8.3	1.13	0.27	8.2	<1	<1	263						
3	161	454	730	23	133	3670	<20	8.3	1.61	0.29	8.2	<1	<1	307				67	0	134
4	233	550	1240	25	290	4400	<20	8.2	2.32	0.53	8.1	<1	<1	387						
5	281	539	1608	34	405	3700	<20	8.2	2.98	0.75	7.8	<1	<1	452				60	0	72
6	329	531	1835	21	504	3570	<20	8.2	3.46	0.95	7.5	<1	<1	389						
7	400	510	2460	34	585	3470	37	8.0	4.82	1.15	7.0	<1	<1	510				36	0	46

[redacted]

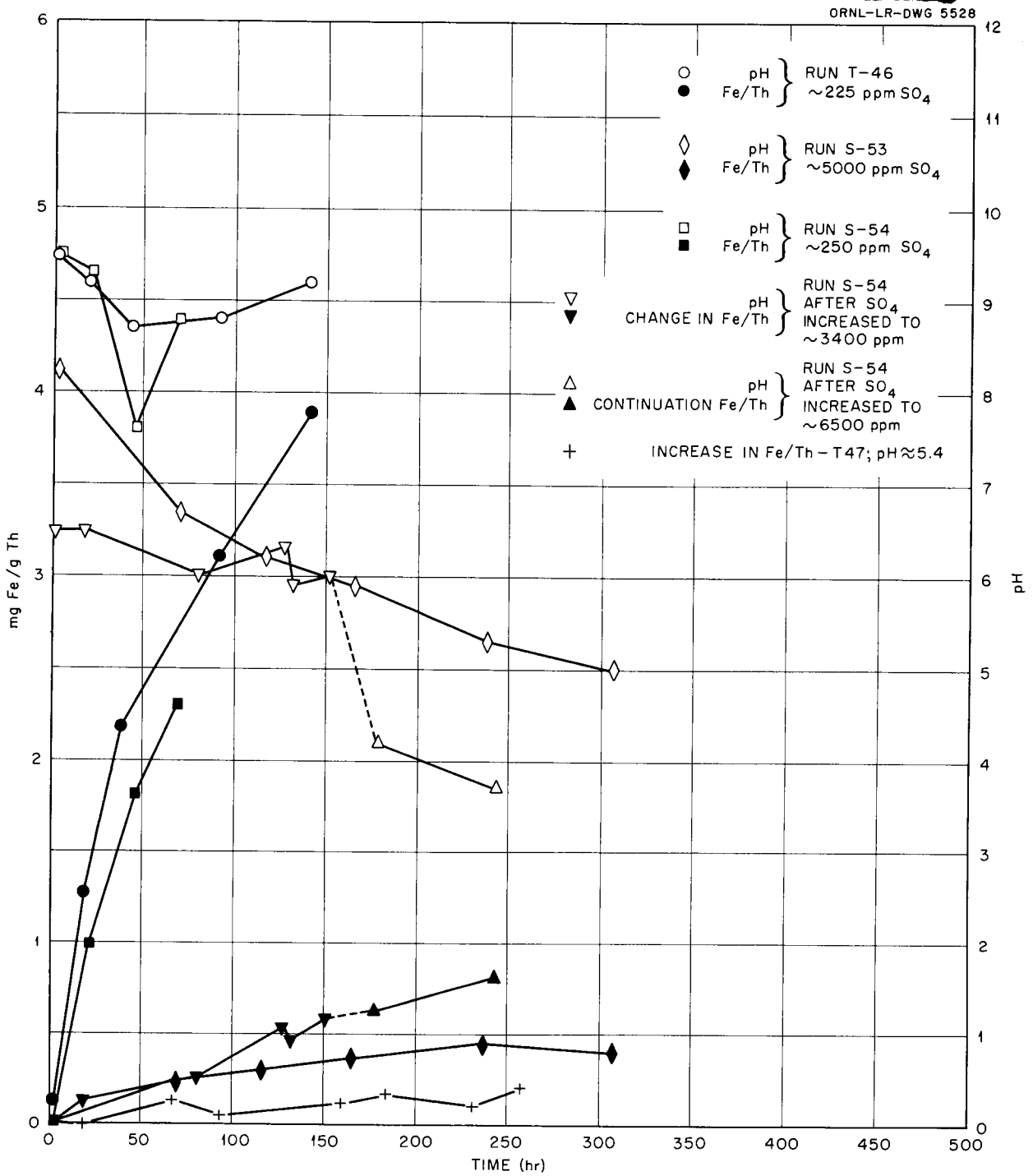

Fig. 7.1. Iron-Thorium Ratio and pH vs Time (Runs S-53, S-54, T-46, T-47).

the attack rate was comparable to that in run T-46, the slurry remained alkaline, and the circulating concentration remained at about that of the original charge. With the addition of $Th(SO_4)_2$, which raised the SO_4^{--} content to about 3400 ppm, both the slurry and the filtrate became acid, and solids began to settle into the circulating stream. The iron-to-thorium ratio indicated by the symbol ▼ in Fig. 7.1 represents the increase in the ratio after addition of sulfate. It is seen at once that the magnitude of this increase is of the same order as the increase found in run S-53. Coincident with the addition of more $Th(SO_4)_2$, which increased the concentration to about 6500 ppm, the pH dropped still further but no startling change in attack rate occurred.

It will be observed that the titanium concentration in the slurry solids rose to an unusually high value in runs S-54 and S-55. This may be compared with run S-53.[3] It does not appear possible at this time to draw valid conclusions regarding the relationship between titanium accumulations and other slurry variables. At the present time it is believed that the titanium attack is less important than the type of attack on stainless steel which was demonstrated, for example, in runs S-55 and T-49.

In an effort to round out the evidence further, slurry which had been pumped for 300 hr in run S-53 was charged into T loop, which contained a stainless steel impeller and an orifice plate. Unfortunately, the ThO_2 concentration was not so high as in the other runs of this series, but at least an indication is given that the attack rate is less with this slurry than with the fresh material (Fig. 7.1).

In run T-48, sulfate was added as thorium sulfate to Lindsay oxide of low sulfate concentration. The results obtained were essentially the same as those obtained[5] in run S-49, which used oxide, prepared at ORNL, containing the same amount of sulfate as a contained impurity instead of as an additive. Both oxides were prepared by calcination of thorium formate at 650°C. It is concluded that sulfate as an impurity in the oxide has the same effect as thorium sulfate added to the slurry.

When hydrogen was present instead of oxygen, as in run T-49, both the attack rate and the pH remained high throughout the run, even though 3500 ppm sulfate was present. In run S-55 in which oxygen was present at the beginning of the run and was then inadvertently permitted to become depleted until hydrogen appeared, the pH at first dropped and then began to rise. It appears correct to conclude that $Th(SO_4)_2$ is not effective unless oxygen is present and, conversely, that oxygen is not effective unless $Th(SO_4)_2$ or some other additive is present. It does not appear that pH is not controlled directly by corrosion-product concentration.

Additional studies will be required to elucidate the relationships between thorium concentration, thorium oxide preparation, sulfate concentration, pH, oxygen concentration, shear stress at the wall, and extent of attack on stainless steel and titanium. The available evidence suggests that oxygen is beneficial, that oxide preparations involving calcination at temperatures of 900°C provoke greater initial attack than do preparations calcined at temperatures of 650°C, that high concentrations of sulfate cause agglomeration and more rapid settling of slurries, and that the tendency for a given slurry to attack stainless steel is diminished by the changes resulting from circulating this slurry at high temperatures.

7.1.2 Thermal Decomposition of Thorium Sulfate

Since it has been observed that a correlation exists between calcining temperature and sulfate content of thorium oxide, a short study was made to determine whether thorium sulfate was stable at high temperature.

The results of tests on the thermal stability of thorium sulfate are shown in Table 7.2. Decomposition of the sulfate to the oxide became pronounced between 800 and 850°C and was essentially complete at 1000°C.

High-temperature calcination also appeared to remove sulfate from thorium oxide. Removal of the sulfate became pronounced at 850°C and was essentially complete at 1100°C. X-ray diffraction studies on the thorium oxide prepared by calcining thorium formate showed that the half-widths of the characteristic bands for ThO_2 narrowed (0.75 to 0.35 deg) as the temperature was increased, indicating an increase in crystallinity.

7.1.3 Pressure Drop in Slurry Systems

For those thorium oxide slurries which are non-Newtonian, the viscosity is not constant at a given

[5] R. N. Lyon *et al.*, *HRP Quar. Prog. Rep. July 31, 1954*, ORNL-1772, p 114.

TABLE 7.2. THERMAL STABILITY OF THORIUM SULFATE AND FORMATE

Initial Material	Calcination Temperature (°C)	Time (hr)	Chemical Composition (mg/g Solids)		ThO_2 X-Ray Pattern (Half-Width, deg)
			Th	SO_4^{--}	
$Th(SO_4)_2$	650	2	568	407	
	750	2	564	412	
	850	2	637	331	
	1000	2	873	3.1	
$Th(OOCH)_4$	600	2	870	8.9	0.75
	750	2	872	8.3	0.52
	850	2	873	6.9	0.45
	950	2	877	3.1	0.42
	1100	2	875	0.4	0.35

temperature and concentration but is variable, depending upon the pipe diameter and fluid velocity. The flow properties of such slurries will have to be determined experimentally before flow systems in which they are to be used can be designed properly.

It has been reported[6] that the apparent viscosity of a pumped thorium oxide slurry was high at relatively low shear rates. An apparent viscosity of 43,000 centipoises was measured with a Brookfield viscometer at the lowest spindle speed (6 rpm) for a pumped slurry containing 730 g of thoria per liter. In order to extend the data to high shear rates, measurements were made of the pressure drop required to produce a given flow rate of slurry through a length of tubing. Figure 7.2 gives the stress-strain curves at 25°C (shear diagrams) for slurries recovered from runs S-52, S-54, and S-55. These data indicate that the three slurries, each containing 1000 g of thorium per liter of slurry, are Bingham plastics or pseudoplastics at 25°C; the apparent viscosity in each case decreased as the shear rate increased. The coefficient of rigidity was approximately 5 centipoises, ranging from 4.6 to 7.4 centipoises for the three slurries.

Shear diagrams at 25°C for various concentrations of the same slurry are shown in Fig. 7.3. The slurry from run S-54 was diluted from 970 to 380 g of thorium per liter of slurry by adding distilled water.

Pressure-drop measurements for flow through tubes of different length were made in order to determine whether or not thorium oxide slurries were thixotropic. Shear diagrams were obtained for the same slurry (run T-48) by measuring the pressure drop required to force the suspension through two tubes of the same size but of different lengths. One tube was 24.3 in. long; the other was 60.1 in. long. The data in Fig. 7.4 indicate that the slurry may be thixotropic, since the apparent viscosity decreased with longer lengths of pipe.

Excellent agreement was obtained between Brookfield viscometer data and pipeline viscometer data, as shown in Fig. 7.5. The following ex-

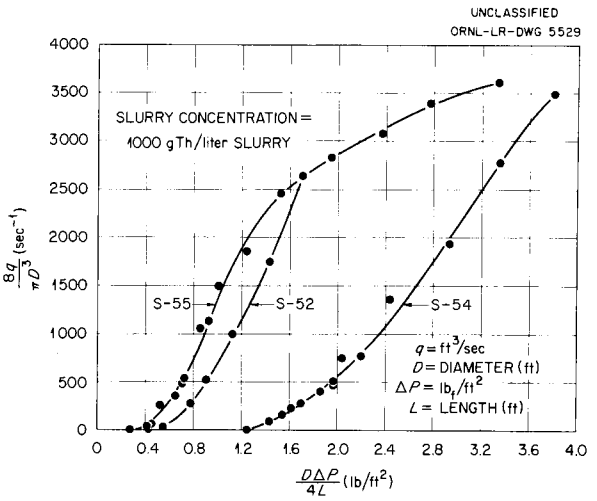

Fig. 7.2. Shear Diagram at 25°C for Thorium Oxide from Loop Runs S-52, S-54, and S-55.

[6]R. N. Lyon *et al.*, *HRP Quar. Prog. Rep. Oct. 31, 1954*, ORNL-1813, p 116.

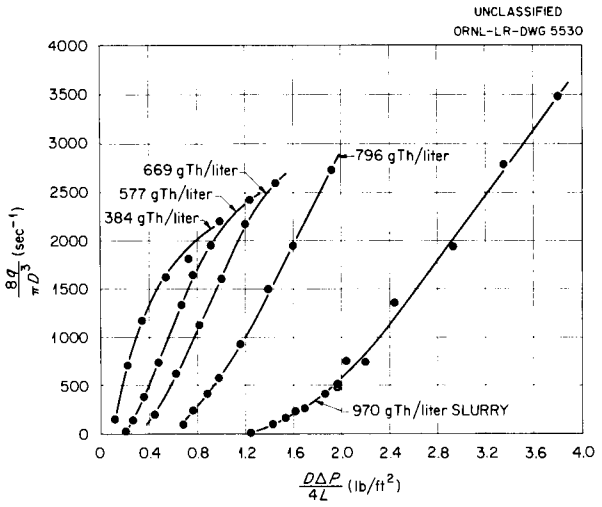

Fig. 7.3. Shear Diagram at 25°C for Thorium Oxide Slurry from Loop Run S-54 at Various Concentrations of Thorium.

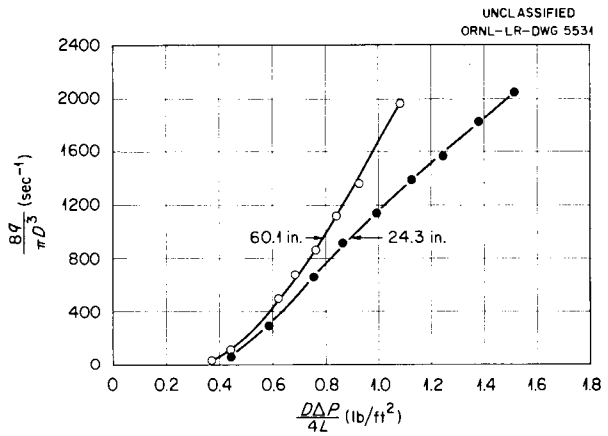

Fig. 7.4. Effect of Pipe Length on Shear Diagram of Pumped ThO_2 Slurry (T-48) Containing 565 g of Thorium per Liter of Slurry.

pressions[7] were used to correlate the two sets of data:

$$-\left(\frac{dV}{dr}\right)_i = 2\tau_i \frac{d\omega}{d\tau_i} ,$$

[7]G. E. Alves, D. S. Boucher, and R. L. Pigford, *Chem. Eng. Progr.* 48, 385 (1952).

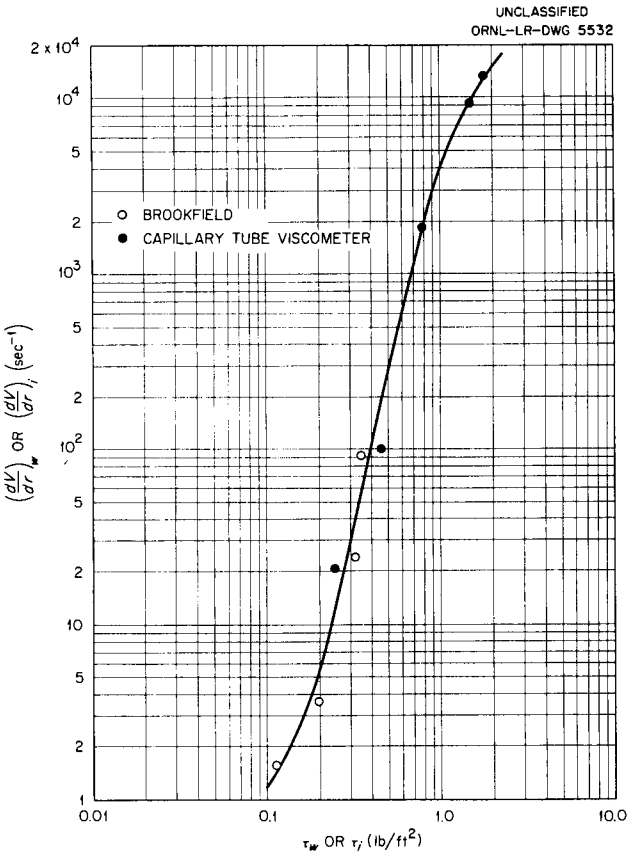

Fig. 7.5. Shear Diagram at 25°C for Thorium Oxide Slurry Containing 1000 g of Thorium per Liter of Slurry (Run S-52).

$$-\left(\frac{dV}{dr}\right)_w = 3\left(\frac{8q}{\pi D^3}\right) + D\,\frac{\Delta P}{4L}\left[\frac{d(8q/\pi D^3)}{d(D\Delta P/4L)}\right] ,$$

where

$-(dV/dr)_i$ = rate of shear at inner cylinder wall, fps/ft,
$-(dV/dr)_w$ = rate of shear at tube wall, fps/ft,
V = velocity, fps,
q = volume rate of flow, cfs,
D = inside tube diameter, ft,
L = length of tube, ft,
ΔP = pressure drop due to friction, lb force/ft^2,

τ_i = shear stress at inner cylinder wall, lb force/ft^2,
ω = angular velocity, radians/sec,
r = radius.

7.1.4 Slurry Component Development

(a) Allis-Chalmers 5-gpm Pump. Tests of the Allis-Chalmers 5-gpm slurry pump were discontinued; it was impossible to balance the pump hydrodynamically after a run with slurry.

The pump, designed to deliver 5 gpm with a head of approximately 35 ft, is of an all-stainless-steel canned-rotor type. All bearings are of the fluid piston type; the radial bearings of stainless steel are an integral part of the rotor and run against a hollow stationary stainless steel shaft as the journal. Process fluid is used to lubricate the bearing surfaces.

Failure of the pump during the slurry run was due to the accumulation of solids in the stationary hollow shaft and rotor chamber. As a result, the impeller rubbed against the front of the pump casing.

(b) Westinghouse 200A Slurry Pump. The Westinghouse 200A pump designed specifically to handle slurries was received. Fabrication of the loop[8] to test the pump is about 50% complete.

(c) Pressurizer Studies. Loop T was modified to study various schemes for pressurizers suitable for use in the HRT. The following major modifications to loop T were made (Fig. 7.6):

1. A bypass stream from the main circulating loop to the pressurizer just below the normal liquid level was installed. This will permit a net downward flow in the pressurizer and will tend to maintain the pressurizer at the same slurry concentration as the rest of the system.

2. A surge tank was installed in the water line from the pressurizer to the back of the pump. This will permit increased flows through the back of the pump and in some cases a net upward flow in the pressurizer. Accumulation of solids in the pressurizer as a function of the net upward or downward flow will be determined.

[8] R. N. Lyon *et al.*, *HRP Quar. Prog. Rep. July 31, 1954*, ORNL-1772, p 114.

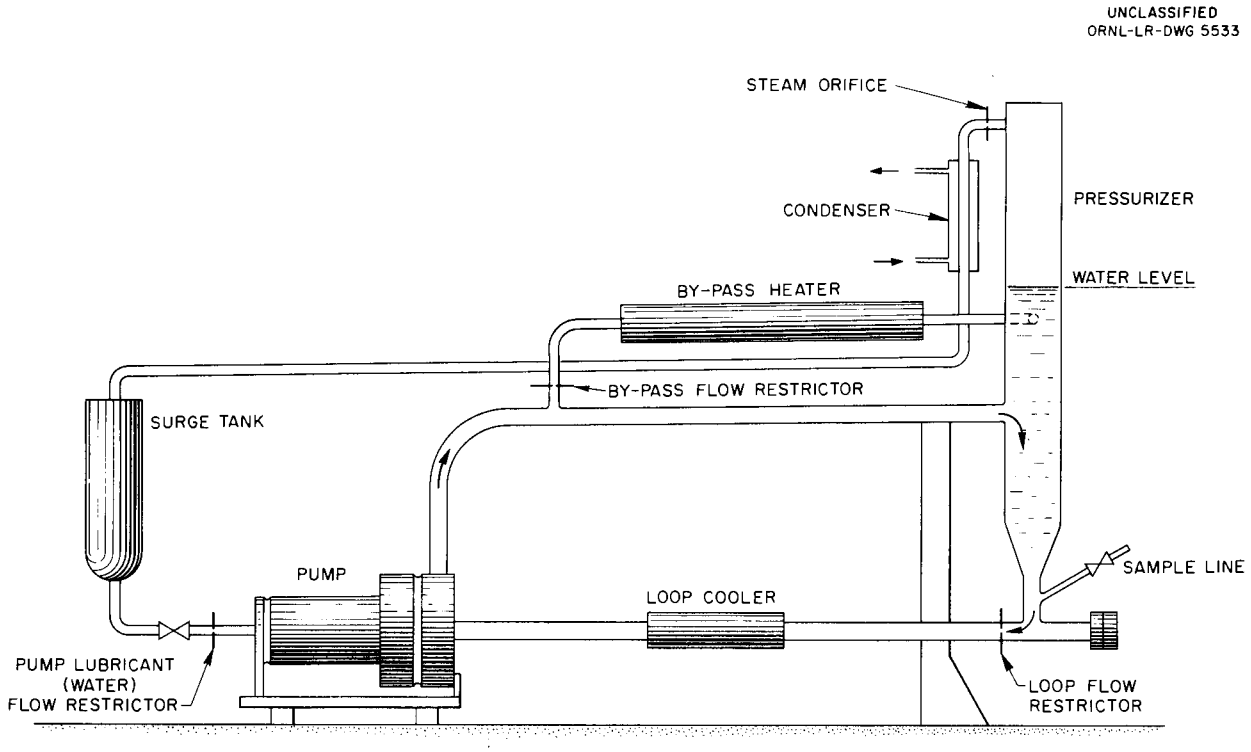

Fig. 7.6. Modification of Loop T for Pressurizer Studies.

In addition to the above studies, the following problems will be investigated:

1. solids entrainment as a function of steam removal,
2. the use of the pressurizer as a gas separator and as a steam generator,
3. a sloping horizontal pressurizer in which only a small fraction of the circulating fluid passes through the pressurizer,
4. a vertical pressurizer fed at the top by a mixture of slurry and steam.

(d) Pressure-Vessel Studies. Water tests in the 18-in. steel mockup of the blanket vessel, described previously,[8] were completed. Pressure drops across the blanket vessel and heat transfer coefficients from the core wall to the blanket fluid were determined for various flow rates. The temperature distribution, a measure of the homogeneity of the blanket fluid, was also determined at a flow rate which gave the velocity, at the equator (0.035 fps), anticipated for the HRT pressure vessel.

The fluid entered the pressure vessel tangentially through the two inlets and swept across the bottom of the vessel to pick up solids which had settled during a long shutdown. A take-off annulus around the core outlet was installed to prevent settling on top of the core vessel. The temperature of the core vessel was maintained between 140 and 170°C with building steam; the temperature of the blanket fluid was varied between 25 and 100°C. A Westinghouse 30A canned-rotor pump was used to circulate the slurry.

Preparatory to the blanket-vessel studies with slurry, water tests were made in order to compare the results with those obtained with slurry. The following characteristics of the system were determined with water:

1. At a flow rate through the blanket vessel of 0.035 fps, the pressure drop across the vessel measured at room temperature was 17 ft of water, due largely to the inlet nozzles.

2. Under steady-state conditions, the temperature distribution data at a flow rate of 0.035 fps indicated the presence of a hot layer, near the core vessel, surrounded by a well-mixed region filling the remainder of the sphere. The temperature of the bulk fluid, except for the layer next to the core wall, was constant and was lower than the temperature of the fluid leaving the vessel. Mixing of the hot and cold layers apparently occurred near the outlet of the vessel.

3. The heat transfer data indicate that the flow through the blanket is turbulent. A straight line whose slope is 0.8 was obtained from a logarithmic plot of the blanket-side heat transfer coefficient, h, against the flow rate (gpm). Apparent heat transfer coefficients in the temperature range between 25 and 100°C for various flow rates are shown in Table 7.3.

TABLE 7.3. APPARENT HEAT TRANSFER COEFFICIENTS FOR VARIOUS FLOW RATES THROUGH BLANKET VESSEL

Flow Rate (gpm)	Average Over-All Heat Transfer Coefficient, U_0 (Btu/hr·ft^2·°F)	Average Blanket-Side Coefficient, h (Btu/hr·ft^2·°F)
21 (0.035 fps)	349 ± 10%	435 ± 10%
15.5 (0.027 fps)	289 ± 10%	346 ± 10%
10.0 (0.018 fps)	212 ± 15%	241 ± 15%

Tests with a slurry containing 500 g thorium per kilogram of water are now in progress. Pressure drops and heat transfer coefficients for comparison with water will be determined.

7.2 HRT BLANKET MOCKUP

L. F. Parsly

D. G. Davis R. H. Nimmo
L. E. McTaggart

A major revision was made in the blanket mockup flow sheet; the revised flow sheet is shown in Fig. 7.7. The principal change from earlier flow sheets was the elimination of heating and partial vaporization of a side stream to provide purge steam for diluting the radiolytic decomposition gases. In the new arrangement, steam for purge purposes will be provided by vaporizing the bulk of the condensate returned from the low-pressure system. The purge steam will be passed through the vapor space in the pressurizer, then through a superheater and into a gas-slurry separator. Sufficient heat will be added in this superheater to heat to saturation the liquid content of the gas-liquid stream separated in the primary gas separator. The separated slurry from the gas-slurry separator will be returned to the circulating loop, while the gas, diluted below explosive limits by the purge steam, will be let down to low pressure.

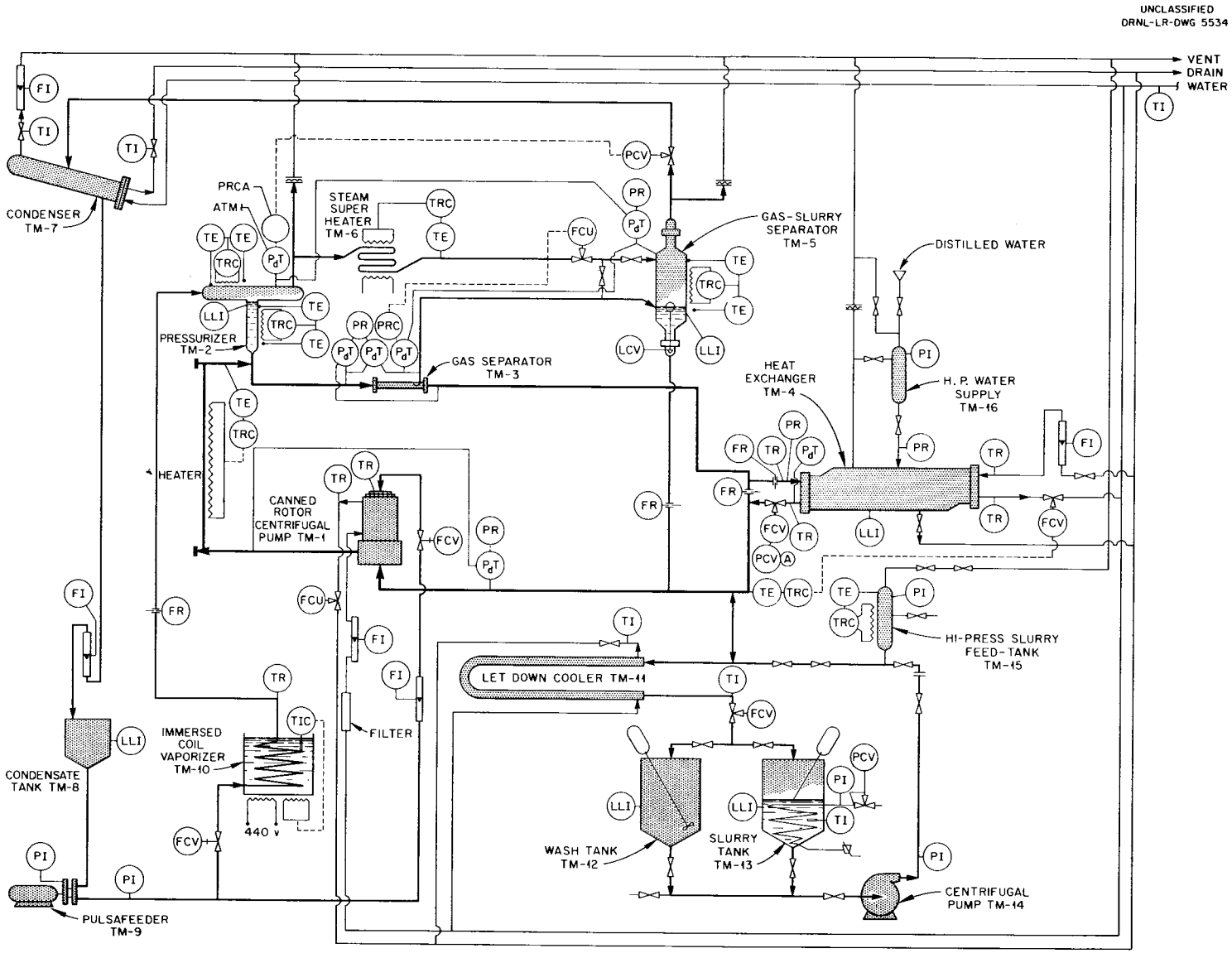

Fig. 7.7. HRT Slurry Blanket Mockup, Model II.

This revision has at least three advantages over the original plan: (1) the high-temperature heat requirement will be reduced; (2) the pressurizer may be located close to the reactor outlet without requiring an auxiliary pump to run slurry through a bypass heater, which would have been necessary with the previous proposal unless the pressurizer were located at the circulating pump suction; (3) plugging, which might occur with partial vaporization of the slurry, will be avoided.

The Newport News Shipbuilding & Dry Dock Co. mockup of the pressure vessel for the HRT will be used for tests at about 200°C.

A study is now under way for determining whether the pressurizer can remove sufficient gas without the supplementary gas system and for evaluating the saving in mockup cost which would accompany the elimination of the in-line gas separator and its auxiliary equipment.

The target completion date of the mockup was deferred approximately three months because of these design changes. Drawings were completed for several equipment items unaffected by the proposed flow-sheet changes.

7.3 BOILING STUDIES

P. C. Zmola R. V. Bailey
M. Richardson

7.3.1 Vapor Transport

In the last quarterly report,[9] a method of presenting experimental data was outlined which indicated that the local vapor velocity is most strongly dependent upon the local vapor fraction. An expression for the local vapor velocity, U, based on the entire cross-sectional area was given by

$$U = (U_s + U_0)\frac{f}{1-f}, \tag{1}$$

where f is the local vapor fraction, U_0 is the liquid velocity based on the total cross-sectional area, and U_s is a factor which accounts for the relative velocity of the vapor to liquid and appears to be only a slowly varying function of geometry and fluid physical properties. For a system in which the power input is uniform, the vapor velocity is given as a function of the height, z, from the point of initiation of boiling by

$$U = \frac{P}{A}\frac{v_g}{h_{fg}}\frac{z}{Z}, \tag{2}$$

where P is the total power from which vaporization results, A is the cross-sectional area of the flow channel, v_g is the specific volume of the vapor, h_{fg} is the latent heat, and Z is the total boiling height. Equations 1 and 2 can be combined to give

$$\frac{z}{Z_0} = \left[\frac{Z}{Z_0}\frac{h_{fg}}{v_g}\frac{A}{P}(U_s + U_0)\right]\frac{f}{1-f}, \tag{3}$$

which defines the void fraction and, hence, density distributions; Z_0 is the total test-section height.

Values of U_s can be determined from experimental data obtained under conditions of uniform power input by employing Eq. 3. Data obtained from the 1.25 × 4 in. circulating apparatus yield values of U_s in the range of 1 to 3 fps. Data obtained at 600 psi at ANL[10] yield values of about 2 fps. There is agreement between the experimental data and the predicted density distribution given by Eq. 3, except for a systematic deviation of the data in the direction of lower void fraction at the test-section exit for operation at high power. Further work is planned to determine the influence of operating conditions on U_s.

Instrumentation required to determine the density distribution in a boiling ThO_2 slurry is being built. Some preliminary experiments indicated that measurement of the attenuation of the 1.3-Mev gamma ray from Co^{60} will provide a satisfactory indication of the vapor fraction of the boiling slurry.

7.3.2 Transient Behavior

A few experiments were performed with the 1.25 × 4 in. volume-heated natural-circulation apparatus in which power, system pressure, and circulation flow rate were obtained as functions of time after cooling-water cutoff for a number of initial steady-state power levels.[11]

[9] P. C. Zmola, R. V. Bailey, H. A. MacColl, and M. Richardson, *HRP Quar. Prog. Rep. Oct. 31, 1954*, ORNL-1813, p 126–128.

[10] *Quarterly Progress Report on Reactor Development. 4000 Program*, ANL-5358 (Oct. 31, 1954), p 25–28.

[11] M. Richardson and L. G. Alexander, *Boiling Experiment: Transient Effects*, ORNL CF-55-1-104 (Jan. 11, 1955).

8. METALLURGY

E. C. Miller

R. G. Berggren
G. E. Elder
J. I. Federer
W. J. Fretague
W. O. Harms
W. J. Leonard
G. B. Wadsworth
J. C. Wilson
C. H. Wodtke

8.1 WELDING DEVELOPMENT

8.1.1 Welding of 1-in. Carbon-Steel Plates Clad with Type 347 Stainless Steel

W. J. Leonard

The previously described[1] experimental weldments, butt-joining 1-in. composite plates of carbon steel (ASTM A201 grade A) clad with a 20% thickness of type 347 stainless steel, were completed. The four basic designs used were proposed by Newport News Shipbuilding & Dry Dock Co., the subcontractor fabricating the HRT pressure vessel.

In the first method, type 347 stainless steel weld metal was used to join the two edges of the stainless steel cladding. This weld metal was used for the root pass and successive weld passes until the groove was filled to the carbon steel–stainless steel interface. The face of the stainless steel weld deposit was then machined flat and flush with the interface, and an ingot-iron strip, approximately $\frac{1}{16}$ in. thick, was placed over the surface of the stainless steel weld metal. The ingot-iron strip was welded to the adjacent carbon-steel base metal (but not bonded to the underlying stainless steel weld deposit), and the weld was then completed with an electrode made of low-hydrogen-type carbon steel.

In the second method the procedure was the same as in the first, up to the point of the carbon steel–stainless steel interface. At this point a layer of type 310 stainless steel weld deposit was placed over the type 347 stainless steel welded surface, followed by one layer of ingot-iron weld metal over the type 310. The weld was then completed, as in the first method, with the electrode made of low-hydrogen carbon steel.

In the third method, type 347 weld metal filled the groove to a point about $\frac{1}{16}$ in. below the carbon steel–stainless steel interface, and two layers of type 308L stainless steel weld metal over the type 347 weld metal brought the weld deposit to a point approximately $\frac{1}{8}$ in. above this interface. Next, one layer of ingot-iron weld metal was placed over the type 308L weld metal, and the groove was then finished with carbon-steel electrodes.

The fourth method was the same as the third, except that no ingot-iron metal was used. Instead, the carbon-steel weld metal was placed directly on the type 308L weld deposit. The weld was then completed, as in the previous methods, with the carbon-steel electrodes.

Figures 8.1, 8.2, 8.3, and 8.4 are macrophotographs of sections from these welded plates. All except the weldments made by the first method appear to be sound as welded. Macroscopic examination of the sound-appearing weldments revealed no cracks or fissuring in the joint.

Side-bend tests made on specimens cut from each of the four plates are shown in Figs. 8.5, 8.6, 8.7, and 8.8. In the specimen welded according to the second method, considerable dilution of the carbon-steel passes by the previous ingot-iron deposits occurred, and the diluted weld metal tended to pull away from the base metal on bending. This same effect of ingot iron on the carbon-steel weld deposits was noted to a lesser extent in the specimen represented in the third method. The iron-to-stainless-steel interfaces did not show this effect in the bend test.

Tensile bar specimens for obtaining the mechanical properties of the composite carbon steel–stainless steel welded joints have been made but have not yet been tested.

At present the joint achieved by the third method appears to be the most acceptable of those attempted. The joints made by the fourth method also appear to be satisfactory, but more detailed metallurgical examination should be made of those factors which may influence the performance of the joint in the contemplated service.

[1] W. J. Leonard, *HRP Quar. Prog. Rep. Oct. 31, 1954*, ORNL-1813, p 133.

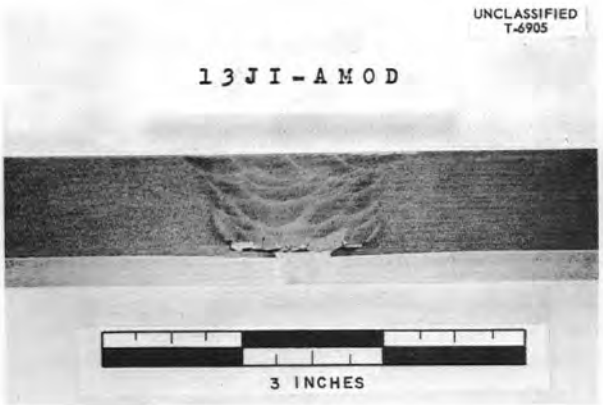

Fig. 8.1. Method 1 Weld. Type 347 SS; ingot iron strip; low-hydrogen-type carbon steel.

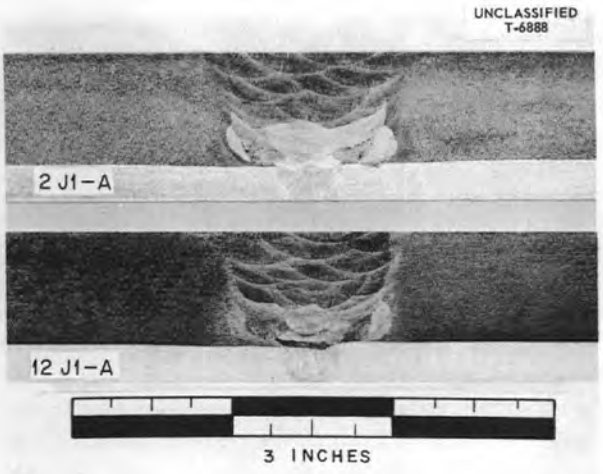

Fig. 8.2. Method 2 Weld. Type 347 SS; type 310 SS; ingot iron weld metal; low-hydrogen-type carbon steel.

8.1.2 Welding of Type 347 Stainless Steel with Fully Austenitic Filler Metal

One-quarter-inch plates of type 347 stainless steel were beveled for welding in accordance with welding specification HRP-2. A fully austenitic, modified, type 347 welding wire was used instead of the specification type 347 weld wire, which usually results in 6 to 10% ferrite in the weld deposit. By using the Heliarc process and the welding procedure of HRP-2, successful welds were made with the same techniques as are used

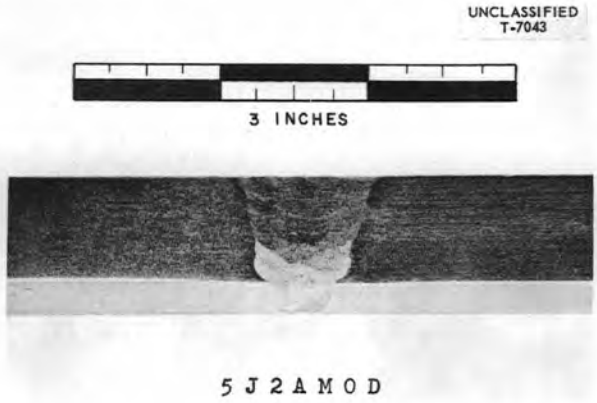

Fig. 8.3. Method 3 Weld. Type 347 SS; type 308L SS; ingot iron weld metal; low-hydrogen-type carbon steel.

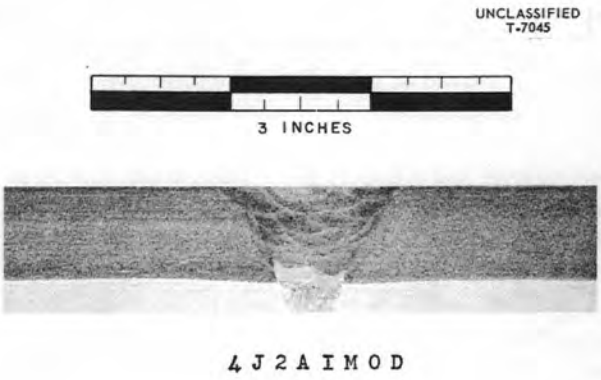

Fig. 8.4. Method 4 Weld. Type 347 SS; type 308L SS; low-hydrogen-type carbon steel.

on the standard ferrite-producing wire. X-ray radiography, microscopic examination, and bend tests were used to evaluate the welds. Figure 8.9 is a typical microstructure of the fully austenitic weld metal. There is no cracking or microfissuring in the root area. Figure 8.10 is a root-bend test made on this weld. Bending the specimens through the maximum arc possible on the jig (160 to 180 deg) produced no cracking on or adjacent to the root face.

Welding has also been done on type 347 seamless tubing, $\frac{1}{2}$ and $1\frac{1}{2}$ in. in diameter, with the use of the weld wire described above and in accordance with the HRP-2 procedure. Liquid-penetrant in-

Fig. 8.5. Side-Bend Test of Method 1 Weld.

Fig. 8.7. Side-Bend Test of Method 3 Weld.

Fig. 8.6. Side-Bend Test of Method 2 Weld.

Fig. 8.8. Side-Bend Test of Method 4 Weld.

spection during welding and radiographic inspection after completion indicate sound welds.

8.2 PHYSICAL METALLURGY OF CORROSION

W. O. Harms J. I. Federer
G. B. Wadsworth

8.2.1 Stress-Corrosion Cracking of Austenitic Stainless Steels

A program has been initiated for establishing an acceptable testing procedure for evaluating the stress-corrosion susceptibility of austenitic stainless steels in homogeneous reactor environments and for studying systematically the various factors which may influence this susceptibility. Initial studies have been directed toward the development of a satisfactory test specimen, and preliminary testing has been carried out in boiling 42 wt % magnesium chloride, an accelerated laboratory test environment. After testing techniques and methods for studying the associated variables have been investigated in magnesium chloride, similar studies will be carried out in uranyl sulfate solutions under conditions similar to those in

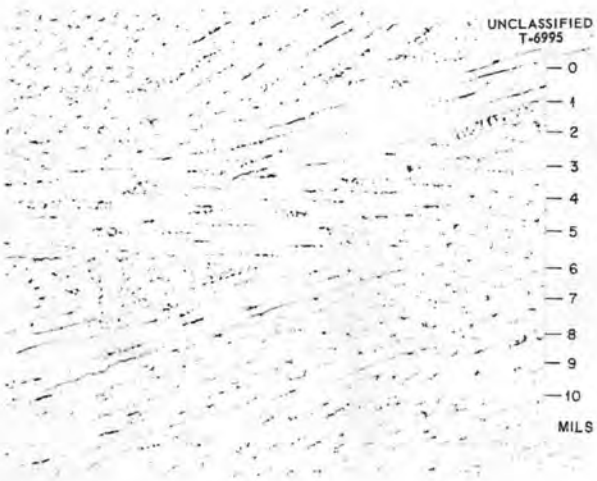

Fig. 8.9. Typical Microstructure of Fully Austenitic Weld Metal.

Fig. 8.10. Root-Bend Test of Fully Austenitic Weld.

various parts of the reactor systems. It is anticipated that this experimental program will provide information regarding the mechanism of stress-cracking in homogeneous reactor systems which can be used in evaluating HRP materials specifications as they pertain to minimizing stress-corrosion failures.

Among several designs used by previous investigators in this field, the one introduced by Waber and co-workers[2] appeared to be attractive, since theoretically it presented a large area of constant outer-fiber tensile stress and minimized uncertainties associated with designation of the stress at which cracking occurred. Specimens based on a modification of this design[3] were machined from single lots of types 347, 304, 309SCb, and 316 stainless steel and from two lots of type 304L stainless steel, covering a wide range of martensite-forming susceptibilities. It was observed, by electric-strain-gage measurements, that the stress on the straight portion of the specimens was not constant but was characteristic of a given specimen and varied by as much as 30%. In addition, the stress distribution was neither uniform nor reproducible. The specimens were subjected to tests in boiling magnesium chloride at stresses equivalent to 50 and 90% of the yield strength to obtain preliminary data on the effect of composition on stress cracking. After an exposure as long as 30 hr, it was observed that only the tie rods and nuts had cracked. These parts were then covered with three coats of primer and three coats of Teflon, each application requiring baking periods of from 15 to 30 min. When no cracks appeared on the specimens after a 30-hr exposure, it was decided that this type of specimen was not acceptable, and therefore the study of a direct-loading-type specimen was undertaken.

The equipment was modified so that wire specimens of about 0.050 in. in diameter could be tested by use of direct loading. A sketch of the apparatus appears in Fig. 8.11. A glass tube was joined to the opening in the bottom of a cylindrical flask, and a hole was punched in the heating jacket to accommodate this tube. In the present setup the specimen extends through the system from a lever arm at the top and is fixed at a point beneath the apparatus. Air is forced through a glass tube, which encloses the specimen to a point just below the liquid level, to prevent contact between the specimen and solution vapors. The wire is stressed by hanging weights on the lever arm; when failure occurs, the falling weights will actuate a microswitch, which will stop an electric clock and thus indicate the moment of failure. The magnesium chloride contained in the protruding tube beneath the heating jacket remains solid during the test and prevents escape of the solution. Initial tests with this apparatus indicate that heavily stressed wires of type 347 stainless steel break after about

[2] J. T. Waber, H. J. McDonald, and B. Longtin, *Corrosion and Material Protect.* 3, 13 (1946).

[3] W. O. Harms and E. C. Miller, *Met. Semiann. Prog. Rep. April 10, 1954*, ORNL-1727, p 20.

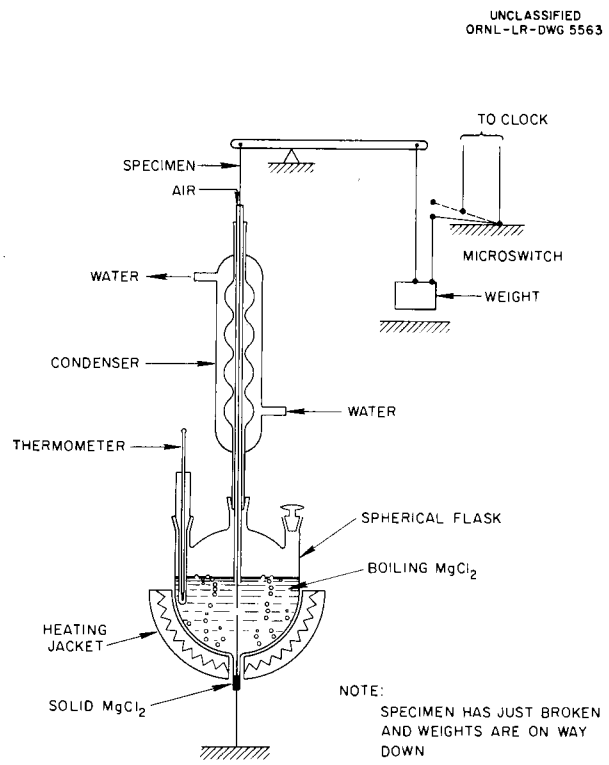

Fig. 8.11. Direct-Loading Stress-Corrosion-Cracking Apparatus.

1 hr, but additional work will be necessary to prove the acceptability of this method.

8.2.2 Dynamic Corrosion of Austenitic-Stainless-Steel Weld Specimens

The results of dynamic corrosion tests of 200-, 400-, and 800-hr duration on special flat-plate-type coupons[4] machined from 1-in. weldments are represented in Fig. 8.12. The test environment was 0.17 *m* uranyl sulfate at 250°C and 20 fps. All-wrought metal specimens were included for comparison. Two anomalies appear in the data: (1) the resistance of type 309SCb was extremely poor in the 800-hr run; (2) except in two cases, the specimens in holder B lost considerably more weight after 400 hr than they did after 800 hr. It should be emphasized that the same specimens were used in all three tests and that they were electrolytically polished prior to each run.

[4]W. J. Leonard and W. O. Harms, *HRP Quar. Prog. Rep. April 30, 1954*, ORNL-1753, p 115.

The poor showing of wrought type 309SCb may be due to the presence of about 2% ferrite in the form of stringers. This specimen was practically film-free after the 800-hr run, which indicates that its critical velocity had been reached; enough time had elapsed so that this was manifested as a substantial weight loss. The inconsistency in holder B may be due to partial plugging of the by-pass line in the 400-hr run, resulting in a mean solution velocity somewhat higher than 20 fps. If these data are excluded, it appears that a reasonable correlation exists between similar specimens in the two holders. In both holders the weldments involving type 308L welds showed the lowest corrosion resistance, and those involving composition H (an experimental fully austenitic 18% Cr–13% Ni–5% Mn, Cb-stabilized alloy) weld metal compared favorably with wrought type 347 specimens.

8.2.3 Dynamic Corrosion Study of Factors Associated with Grain Size in Wrought Austenitic Stainless Steels

Dynamic corrosion pin-size specimens of types 304L and 347 stainless steel have been swaged and machined and are being heat-treated to give ASTM grain sizes of 2, 4, 6, and 8 (20 specimens each). These specimens will be submitted to the HRP Dynamic Corrosion Group for a systematic study of the effect of grain size on corrosion resistance.

Sigma-phase alloys of compositions 45% Cr–55% Fe and 5% Ni–45% Cr–50% Fe are being prepared for corrosion testing. Iron, chromium, and nickel metals of 99.98, 99.95, and 99.92% purities were arc-melted in a purified argon atmosphere. The alloys were remelted several times to ensure homogeneity and were hot rolled at 1200°C to a minimum thickness of 0.210 in. Dynamic corrosion pin specimens are being machined from these coupons and will be heat-treated at 800°C to promote transformation of alpha to sigma phase. Sigma phase, in contrast to ferrite, is hard, brittle, and nonmagnetic, and so the transformation can be followed by hardness and Magne-Gage measurements as well as by metallography and x-ray diffraction analysis. A knowledge of the corrosion behavior of sigma phase is desirable, since certain type 300 stainless steels develop this brittle phase during welding or as the result of heat treatment during fabrication.

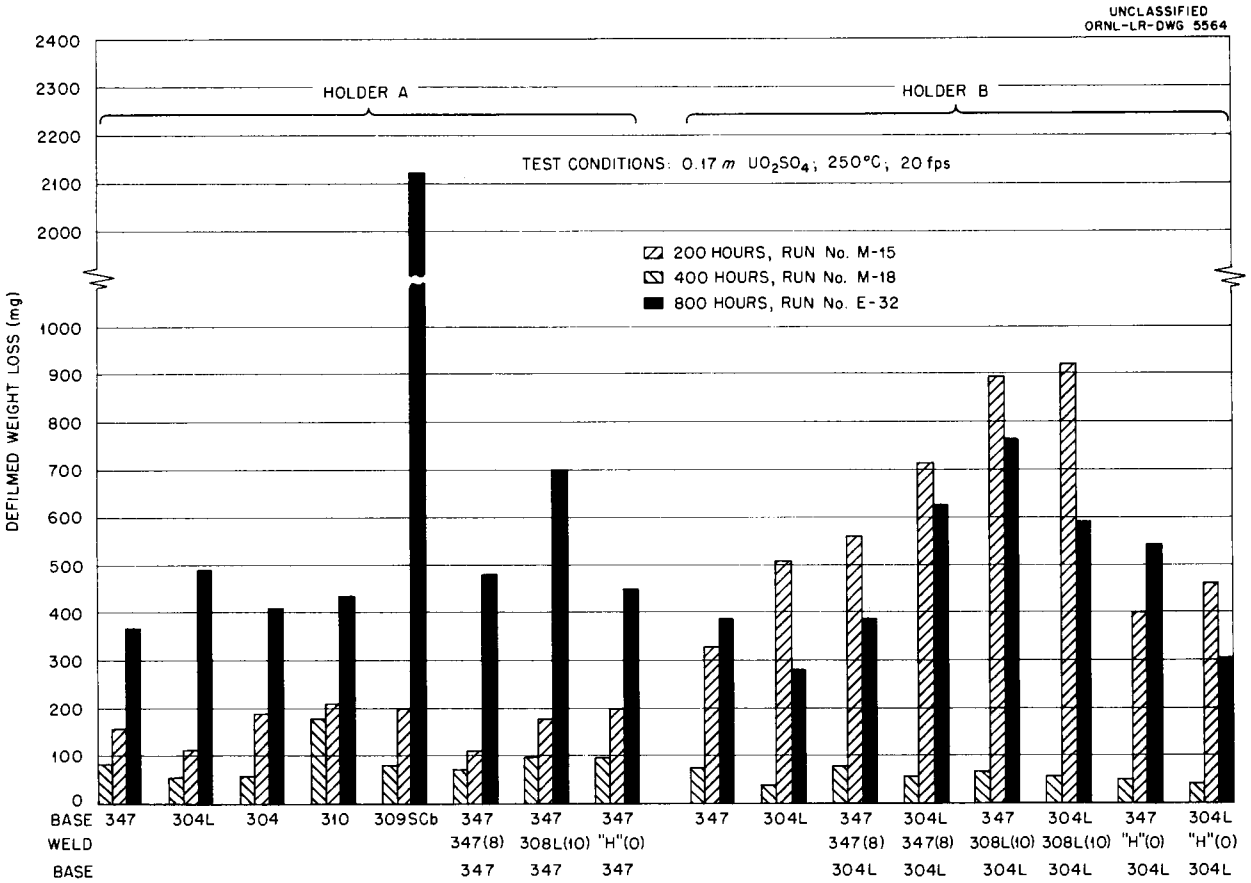

Fig. 8.12. Corrosion of Austenitic Stainless Steel Welds.

8.2.4 Effect of Hydrogen on Properties of Zirconium and Its Alloys

An apparatus has been designed and constructed for admitting known quantities of gas to metal specimens at a given temperature. It will be used to study the effects of alloying elements and surface conditions on the rate of absorption of hydrogen by zirconium and its alloys.

The apparatus is capable of holding steady vacuums of the order of 10^{-7} mm Hg at room temperature, which pressure is necessary for accurate pressure-volume calculations and for ensuring against contamination of the purified hydrogen. Oil-pumped tank hydrogen gas is purified by being dried and passed through titanium turnings and zirconium powder at 700°C and is absorbed by titanium turnings at 400°C. When hydrogen is needed for an experiment, it is generated by heating the titanium hydride to 700°C. High-purity hydrogen is required because other gaseous impurities alter both the quantity of hydrogen absorbed and the properties of the metal itself. Slow-bend or impact-type specimens are suspended from a quartz hook in a quartz reaction tube, and hydrogen is admitted to this system through a liquid-nitrogen-cooled trap from a gas buret.

8.2.5 Role of Oxide Films on Rate of Hydrogen Adsorption by Zirconium and Its Alloys

Experiments designed to evaluate the possibility of hydrogen embrittlement of zirconium and zirconium alloy reactor components, as the result of exposure to radiolytic gas, were initiated during the quarter. The first phase of the work is concerned with the cathodic treatment of zirconium specimens in sulfuric acid at temperatures up to 300°C, since in this way the role of oxide films as diffusion barriers to hydrogen atoms in aqueous environments can be studied. The reactor vessel

is a zirconium-lined, type 347 stainless steel autoclave, containing a tubular gold anode surrounding a zirconium cathode, which is machined in the form of a multiple-break-type subsize impact specimen. A coil of platinum wire, heated to approximately 50°C higher than any other part of the system, is to be used to catalyze the recombination of hydrogen and oxygen in the gas phase. The effects of cathodic treatments under several sets of conditions will be evaluated by impact testing, hydrogen analyses, and metallography. The bomb and associate parts have been designed, and construction and assembly are in progress.

8.3 MECHANICAL TESTING OF TITANIUM AND ZIRCONIUM

W. J. Fretague

8.3.1 Commercial Titanium

Investigations are continuing for determining the cause of the embrittlement of a commercial titanium specimen holder described in a previous report.[5] Debye patterns of filings prepared from the exposed corrosion specimen holder gave extraneous lines which could not be attributed to any known compounds of titanium. Metallographic examination of samples from the material reveals an unidentified second microconstituent. Attempts are being made to identify this constituent by electron-diffraction methods.

8.3.2 Zirconium Alloys (Zircaloy-2)

Zircaloy-2 impact test specimens exposed to radiation in the first in-pile loop (run DD) were tested over the temperature range −196 to 280°C, and the results are plotted in Fig. 8.13. Similarly, impact test results from specimens exposed to loop conditions out-of-pile, run CC, are plotted in Fig. 8.14. Impact test results from unirradiated

[5] W. J. Fretague, *HRP Quar. Prog. Rep. Oct. 31, 1954*, ORNL-1813, p 135–137.

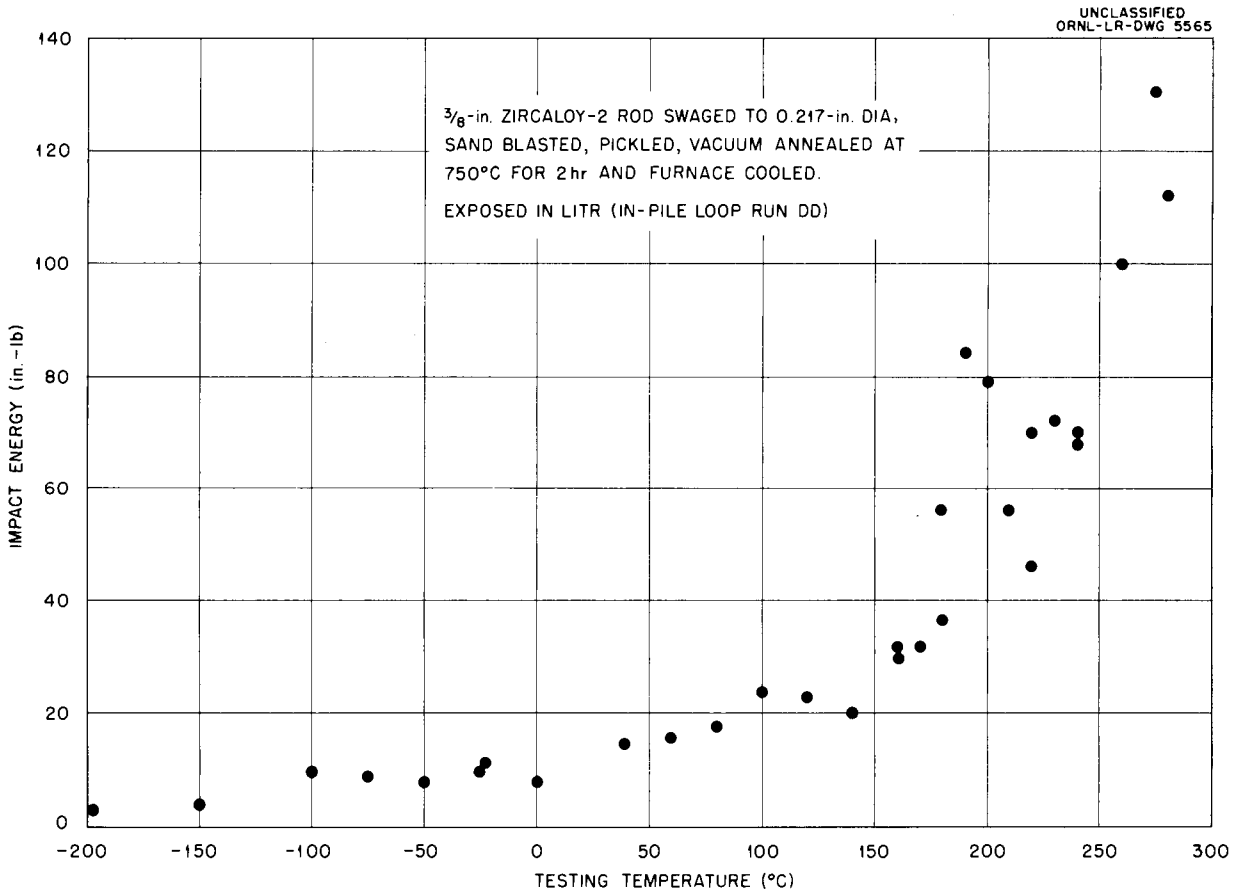

Fig. 8.13. Impact Energy vs Testing Temperature for Zircaloy-2 Exposed in LITR.

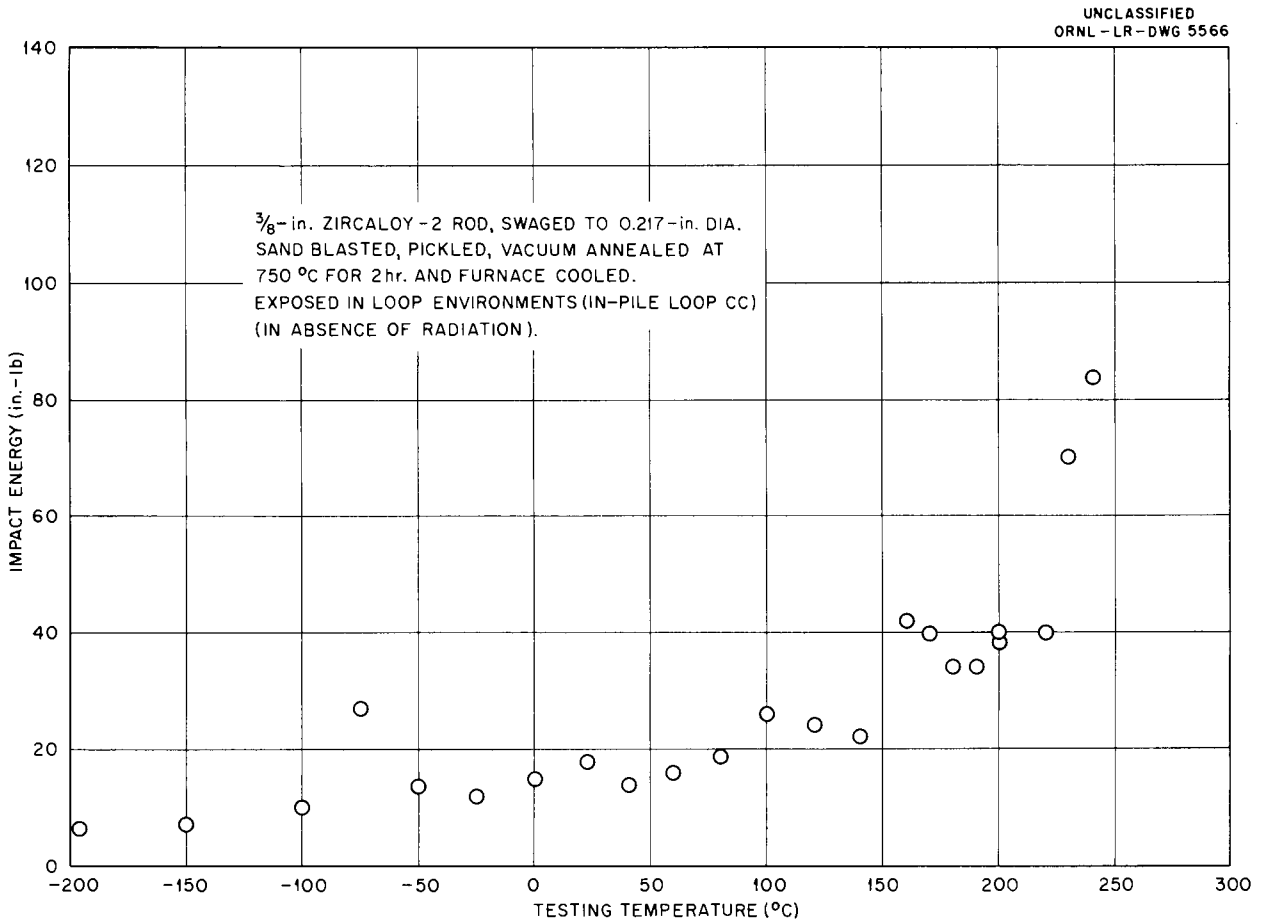

Fig. 8.14. Impact Energy vs Testing Temperature for Zircaloy-2 in Loop Environments Without Irradiation.

Zircaloy-2 control specimens are plotted in Fig. 8.15. Comparisons of Figs. 8.13 and 8.14 with Fig. 8.15 suggest that no significant changes in transition temperature resulted from either the in-pile exposure in UO_2SO_4 solution (Fig. 8.13, run DD) or from out-of-pile exposure in UO_2SO_4 solution (Fig. 8.14, run CC).

Elevated-temperature tensile tests were performed on a variety of Zircaloy-2 plate specimens obtained from plate scraps left over from fabrication of the Zircaloy-2 core tank for the HRT. The data are presented in Table 8.1.

8.4 METALLURGICAL ENGINEERING SERVICE

G. E. Elder

8.4.1 Fabrication of HRT Zircaloy-2 Core Vessel

Developmental research required in forming and fabricating the Zircaloy-2 core vessel is proceeding under a subcontract with the Newport News Shipbuilding & Dry Dock Co. The geometry of the component parts of the vessel is such that relatively complex jigs and fixtures are required.

(a) Forming. The component parts of the sphere were hot-formed from $^5/_{16}$-in. plate with the dies and press shown in Fig. 8.16. The formed quadrants were clamped to the male die as shown in Fig. 8.17 and were machined to obtain the fit-up required for the Electric Boat, preplaced, consumable type of insert used for the root weld. The halves of the 30- and the 90-deg cones were hot-formed from $^3/_8$-in. plate. Some reworking of the dies was necessary to allow for spring-back of the Zircaloy-2. After they were assembled and welded, the cones and the sphere halves were re-formed, as illustrated in Fig. 8.18.

(b) Welding. Producing a sound weldment with Zircaloy-2 requires complete blanketing of the

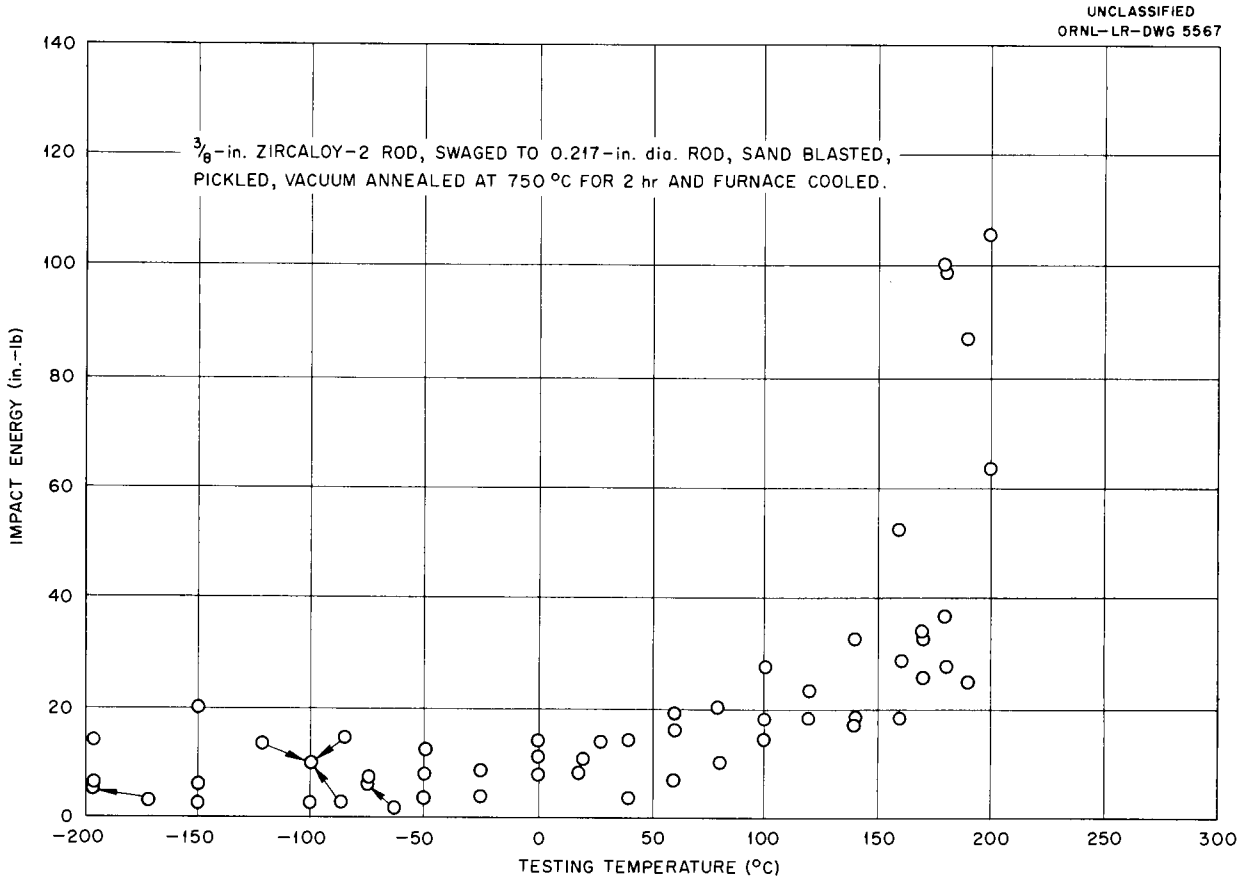

Fig. 8.15. Impact Energy vs Testing Temperature for Zircaloy-2 Unirradiated Control Specimens.

weld area with helium or argon. An individual shield was designed for, and constructed to conform with, each weld geometry, as shown in Fig. 8.19. Inert gas was supplied to the shield, both at the Heliarc torch and behind the torch, through holes in the center copper tubing of the shield. Small notches at the contact edge of the shield permitted the gas to flow out of the shielded area and prevented ingress of the outside atmosphere. Figure 8.20 is a close-up of the welding head and demonstrates conformation of the shield to the work surface. A hollow copper bar, Fig. 8.21, conforming to the inner surface, served as a backing shield for the welds on the sphere. A positive pressure of inert gas was maintained inside the bar, with the gas flowing over the weld area from regularly spaced holes. The back of the weld on the two cones and on the pipes was shielded by plugging both ends of the piece and maintaining an inert atmosphere therein.

The consumable insert was used as the root pass on all welds. After assembly and fit-up of the parts, a Heliarc hand torch was used to tack-weld the insert in place. In all cases the welding head was held stationary, and the work was moved by an automatic positioner. Figure 8.22 shows the 30-deg cone in welding position. Tabs of Zircaloy-2 were tack-welded at both ends of the weld pass to assure a sound weld at the start and finish of the pass. Figure 8.23 shows the sphere in welding position. The jig used was that designed and used for constructing the aluminum prototype vessel. Figure 8.24 is a photograph of the completed weld on the 90-deg cone. Figure 8.25 shows the setup used for welding the 30-deg cone to a pipe section. The two knobs on the left of the shield were used to adjust the arc length and to center the head on the weld bead. One operator manipulated the arc length knob to maintain a constant arc length as indicated by the voltmeter

TABLE 8.1. MECHANICAL PROPERTIES OF ZIRCALOY-2 TENSILE SPECIMENS TESTED IN AIR AT 600°F

Specimen No.	Stress (psi)		Tensile Strength (psi)	Elongation (%)	Reduction in Area (%)
	At 0.1% Offset	At 0.2% Offset			
1[a]	13,500	14,700	27,500	46.0	66.8
2[b]	16,700	17,500	25,000	46.0	74.3
3[b]	17,100	17,700	24,600	47.5	71.7
ZR 3/8[c]	15,600	16,200	24,900	48.0	72.3
ZR 1/4	13,500	14,400	21,400	40.0	71.5
ZR G1	14,900	16,000	22,600	11.5[d]	73.6
ZR FB	14,600	15,600	21,900	27.5	71.1
ZR 2	15,100	16,100	22,900	25.0	65.0

[a]Specimen axis parallel to rolling direction of plate.
[b]Specimen axis perpendicular to rolling direction of plate.
[c]Specimen taken from plate used in conical section of core tank.
[d]Broke outside gage marks, 17.2% elongation between shoulders.

mounted above the head. The other operator positioned the arc laterally and fed the weld rod used for the cover passes through the hole in the lower right corner of the glass front on the shield. The weld speed was controlled by the welding positioner which supported the jig. Figure 8.26 shows two of the diffuser plates welded in the 30-deg cone. The welding was done with a Heliarc hand torch. Shielding was accomplished by capping the small end of the cone and covering all the diffuser plate, except for a small area around the particular ligament being welded, and by maintaining a helium atmosphere in the cone by injecting the gas through a fitting in the end plug.

8.5 EFFECTS OF RADIATION ON STRUCTURAL METALS AND ALLOYS

R. G. Berggren J. C. Wilson

Irradiation of impact specimens of hot-rolled ASTM-A-212B boiler plate, SAE 1040 steel in two heat treatments, and annealed type 301 stainless steel was completed in the HB-3 facility of the LITR, and testing is in progress. Impact specimens of types 301 and 446 stainless steel were irradiated in the HB-3 facility of the MTR, and tests will be made when the specimens are received at ORNL.

An irradiation was completed in an LB piece of the MTR, and the specimens are being returned to ORNL for testing. Included in this group are impact and tensile specimens of types 301, 302, 302B, 304L, 305, 321, and 347 stainless steel. All specimens were annealed before irradiation.

An experiment was installed in the HB-3 facility of the MTR, and the irradiation is now in progress. The experiment utilizes light water in the plug and the concrete of the cubicle doors to introduce the necessary radiation shielding; thus a lighter and more economical experiment results. The experiment contains tensile and impact specimens of ASTM-A-212B boiler plate in three heat treatments – normalized, quenched and tempered, and spheroidized – type 446 stainless steel, high-purity iron in two heat treatments – a subcritical and supercritical anneal – 8½% nickel steel, Croloy 5, vacuum-annealed Ti-75A titanium, and vacuum-annealed Zircaloy-2.

Construction has been started of an experiment plug which will incorporate improvements made as a result of experience gained in building and

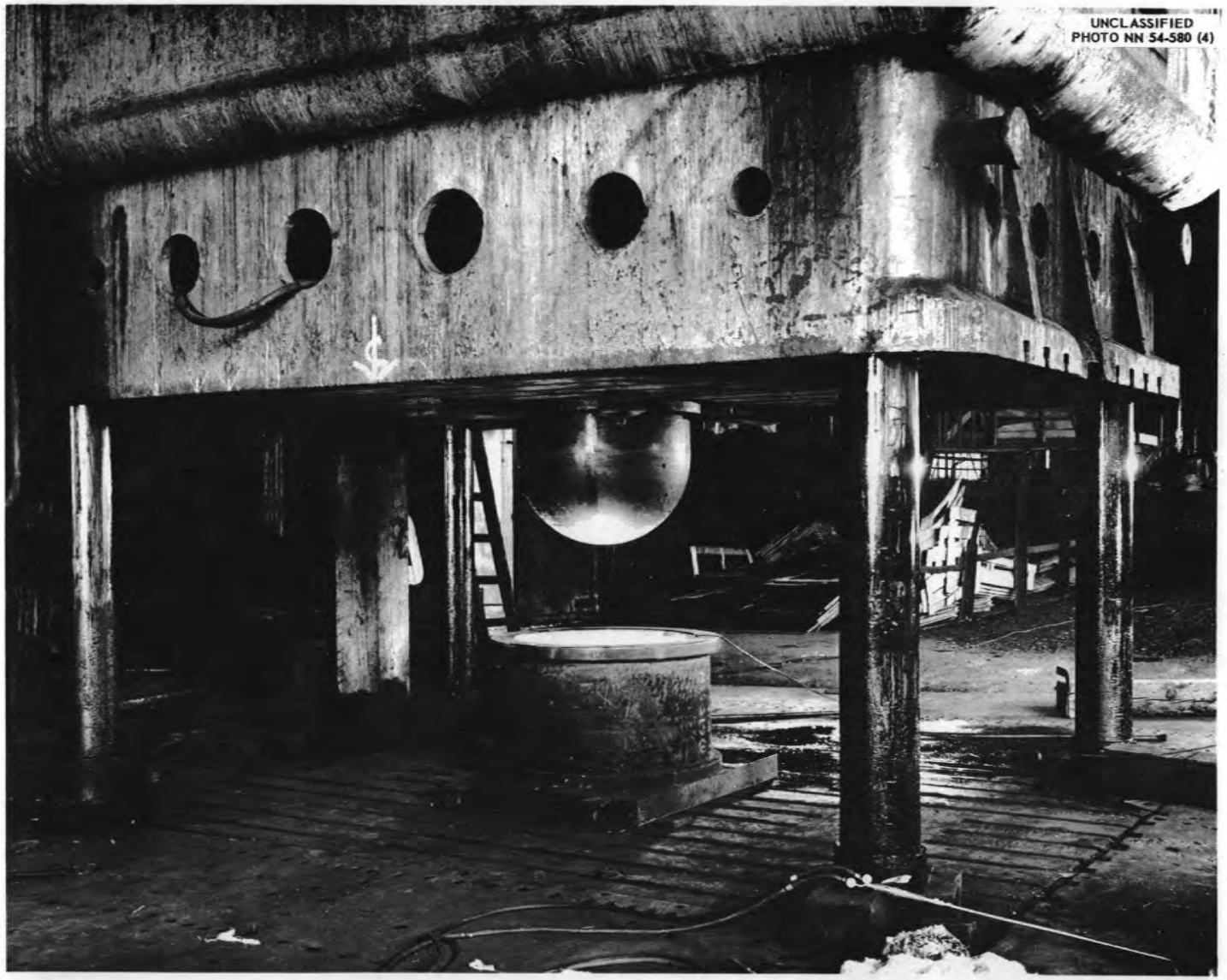

Fig. 8.16. View of the Hydraulic Press Showing the Male and Female Dies in Place Ready for Forming Sphere Sections of the Core Tank.

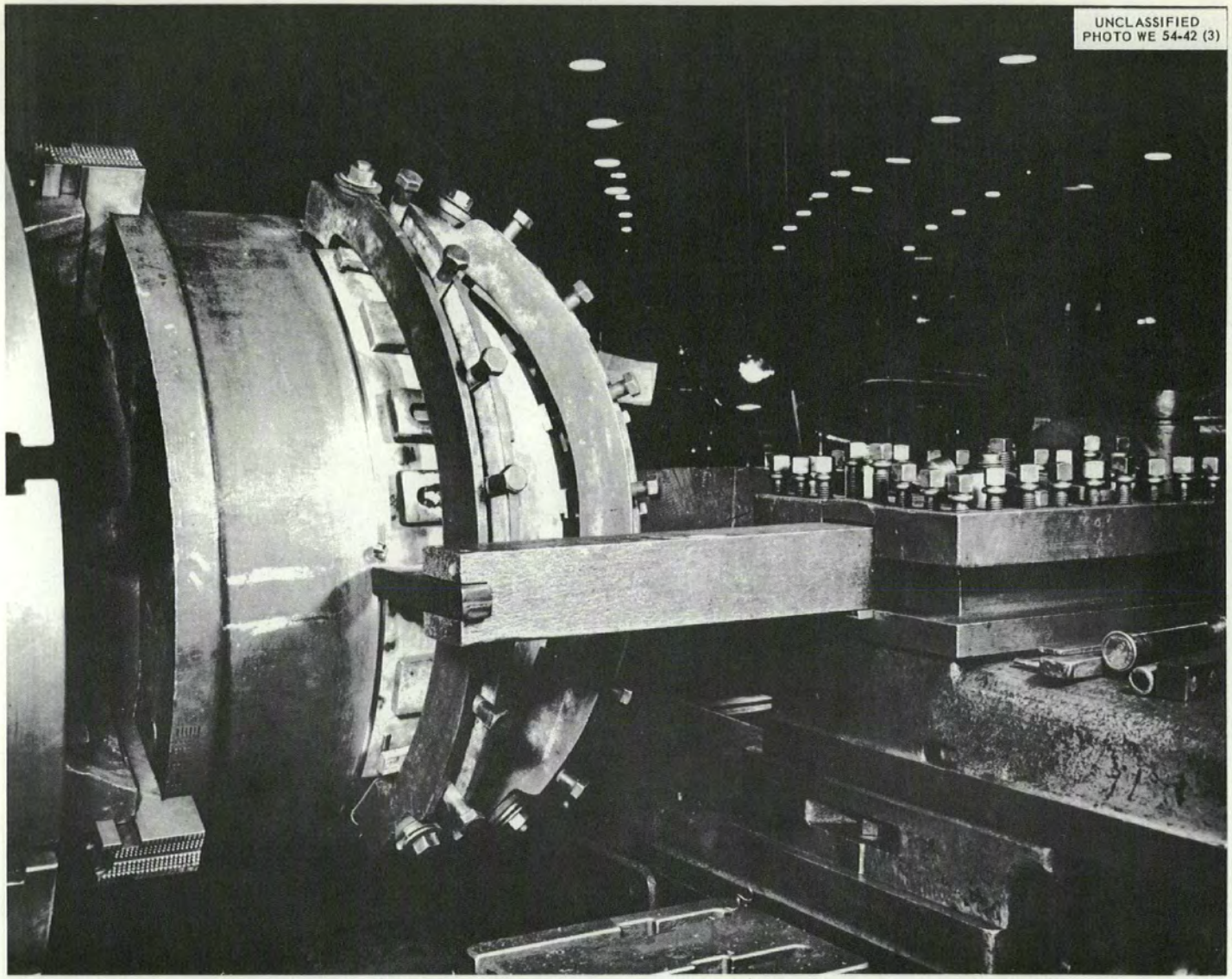

Fig. 8.17. Close-up Side View Showing the Method of Holding and Machining Spherical Sections of the Core Tank on a Large Lathe.

Fig. 8.18. Close-up View of the Male and Female Dies Used for the Final Forming Operation of the 30-deg Cone Section of the Core Tank.

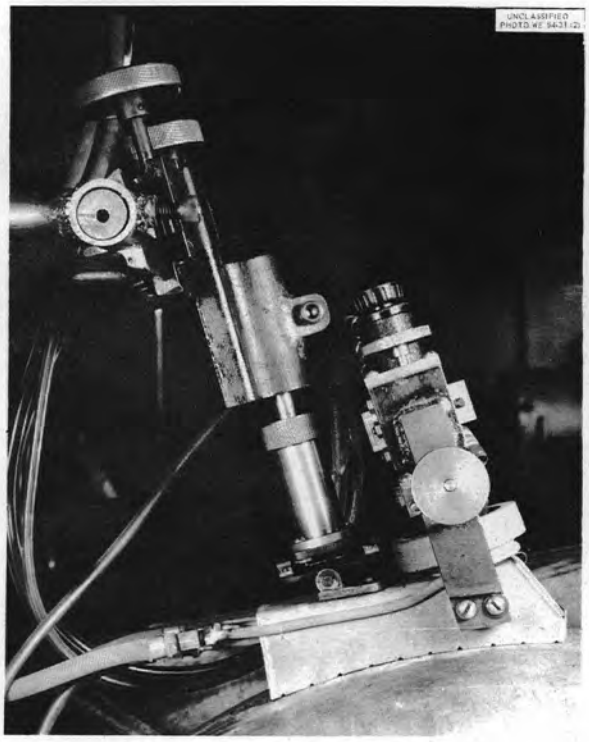

Fig. 8.20. Side View (Close-up) Showing Details of the Welding Torch and Shield Positioning and Manipulating Fixtures.

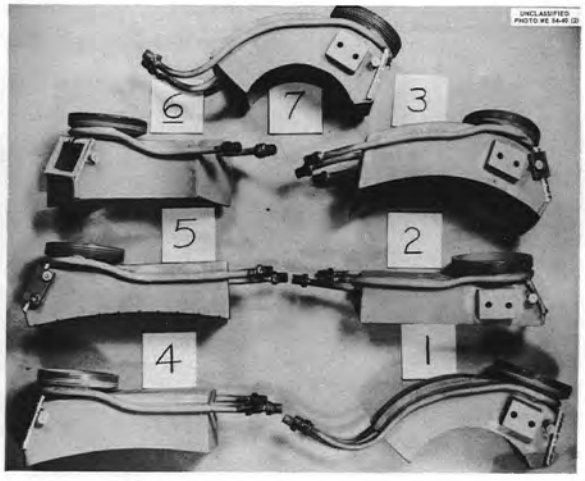

Fig. 8.19. Side Views of the Seven Welding Shields Used to Perform Welding Operations on Core-Tank Joints.

Fig. 8.21. View of Copper Bar Used for Gas Shielding on Back Side of Mid-Body Joints of Core Tank.

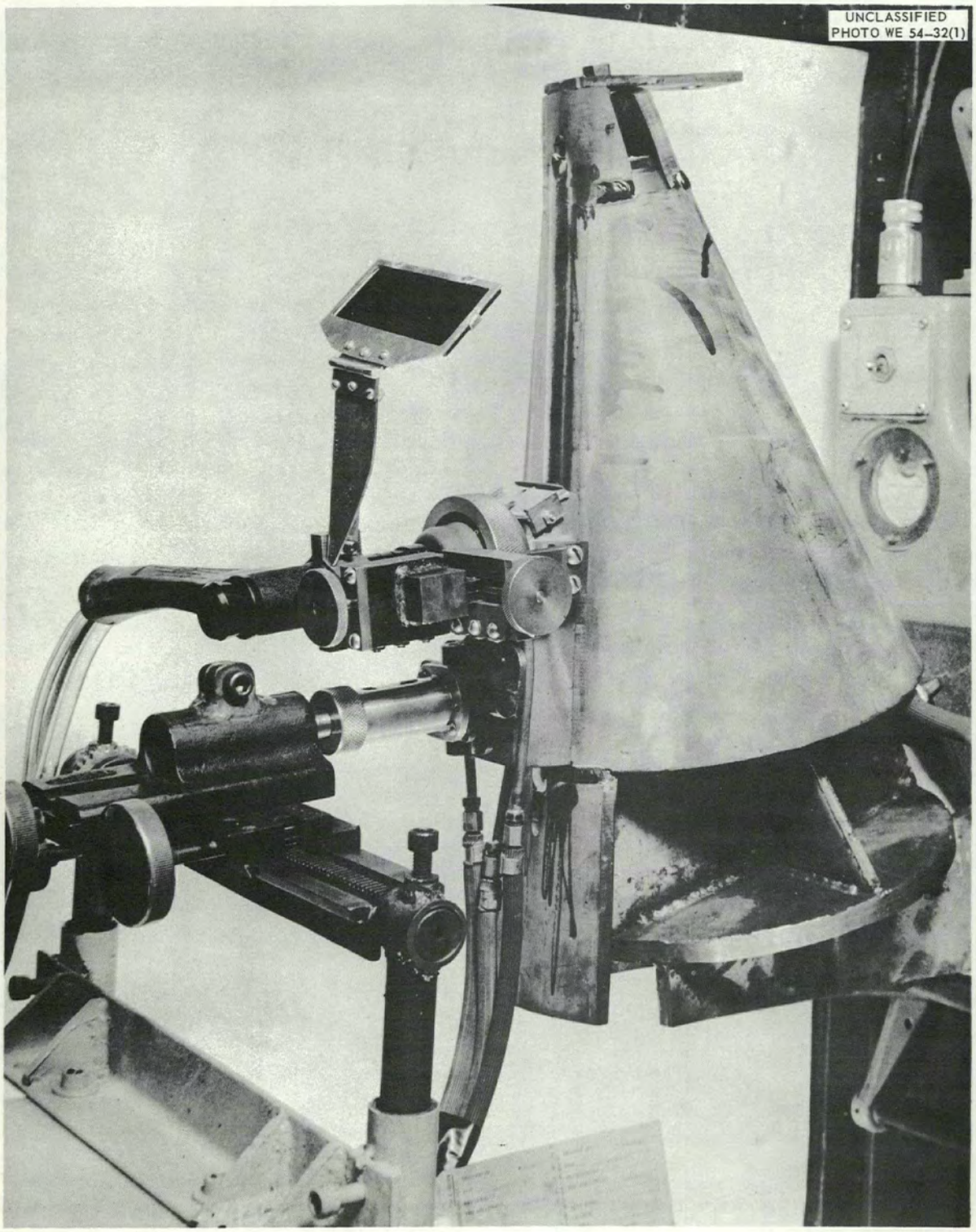

Fig. 8.22. Side-Top View Showing Arrangement for Making Seam Welds of 30-deg Cone Section of Core Tank.

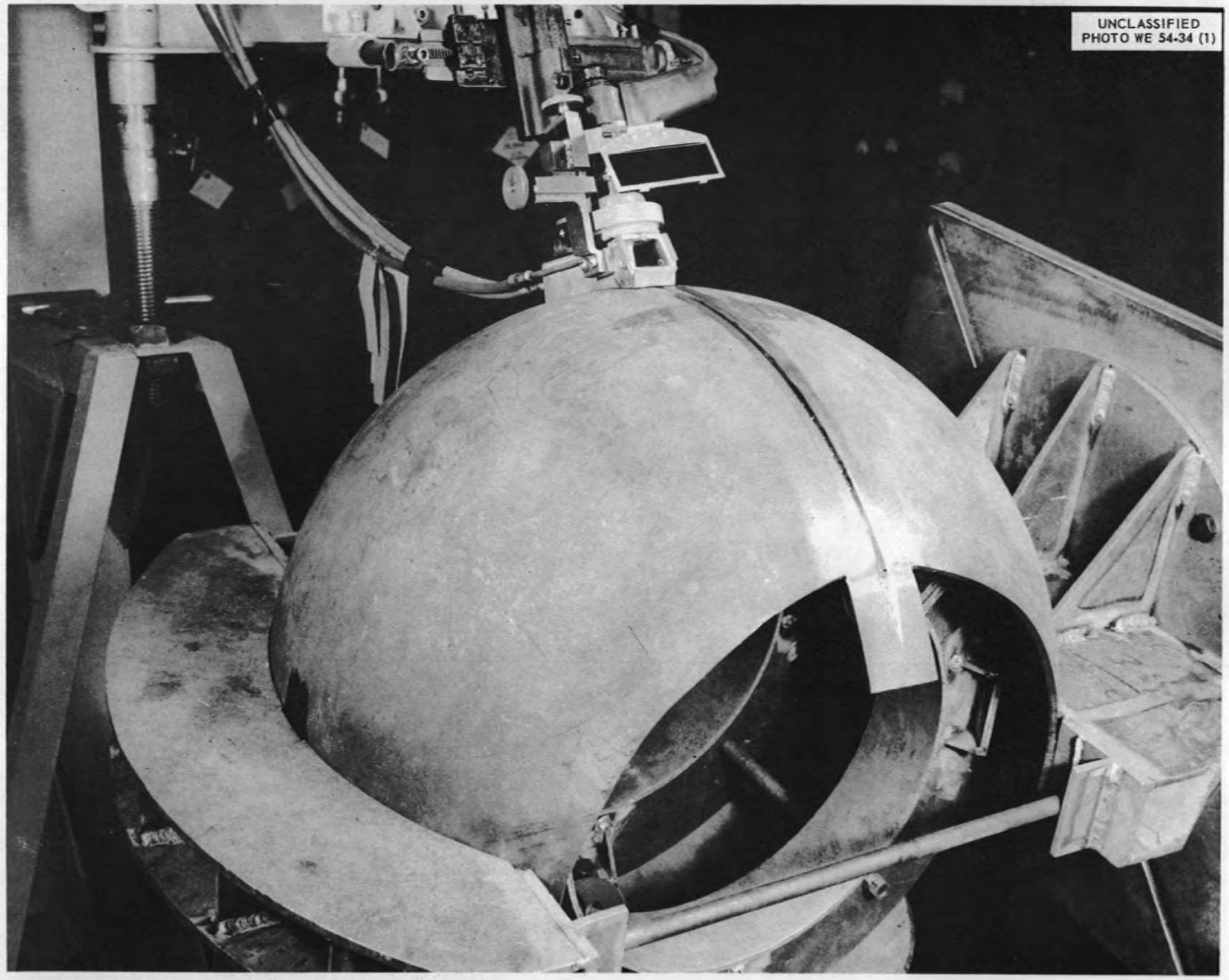

Fig. 8.23. View Showing Arrangement for Making a Weld Joining Spherical Pieces of the Mid-Body Section of Core Tank.

operating the above experiment. Data from the above experiment have also permitted resumption of design on an experiment plug for irradiation of specimens at elevated temperatures.

Impact specimens of Carilloy T-1, Croloy 5, 8½% nickel steel, experimental low-manganese modifications of ASTM-A-212B and ASTM-A-242 steels, and ASTM-A-106 steels made by both commercial coarse-grain practice and by fine-grain practice are being irradiated in the HB-3 facility of the LITR.

Zircaloy-2 scrap from the plates used in fabricating the HRT core tank was received, and impact and tensile specimens are being fabricated for irradiation tests.

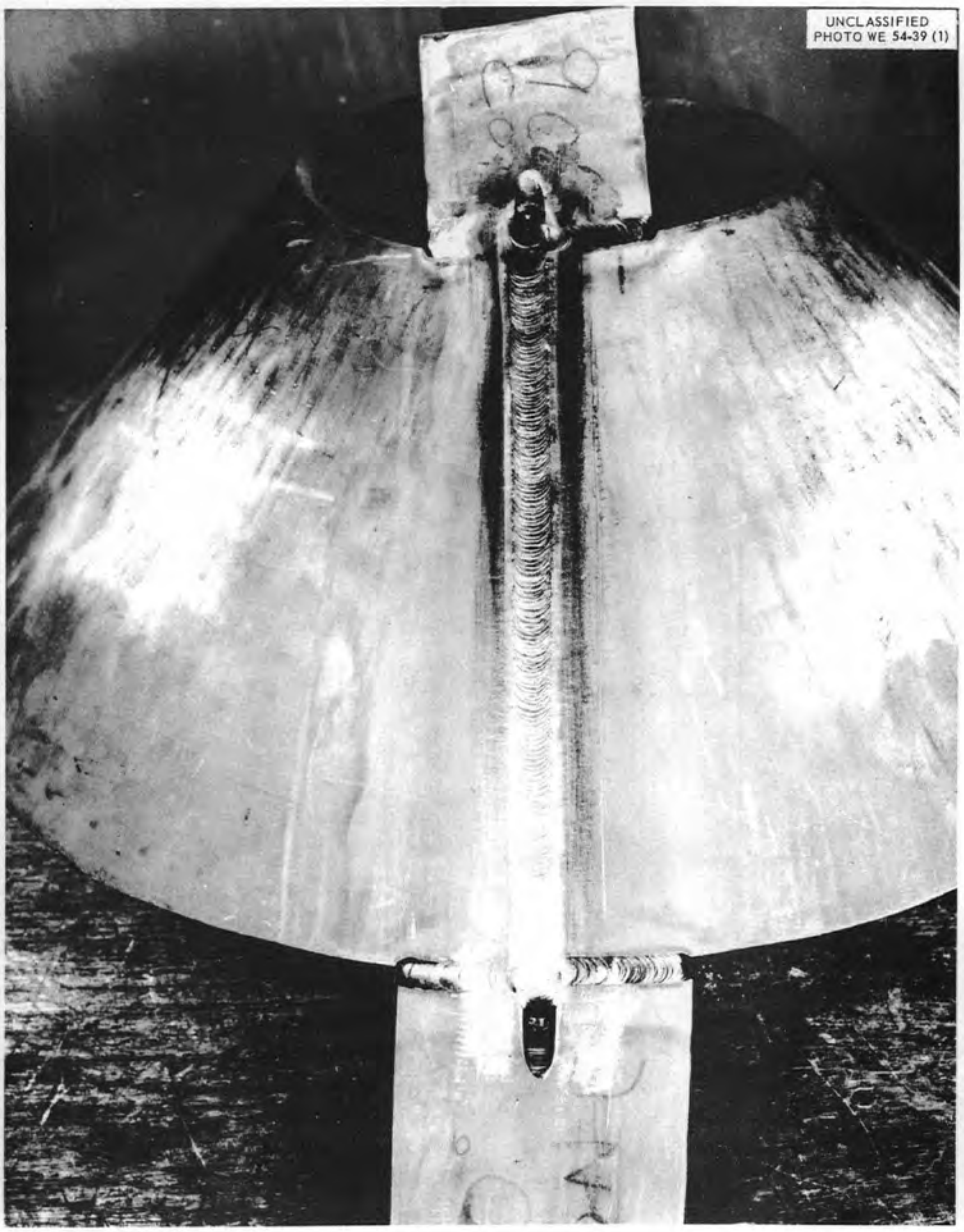

Fig. 8.24. View Showing Outside of Completed Seam Weld in 90-deg Cone Section of Core Tank.

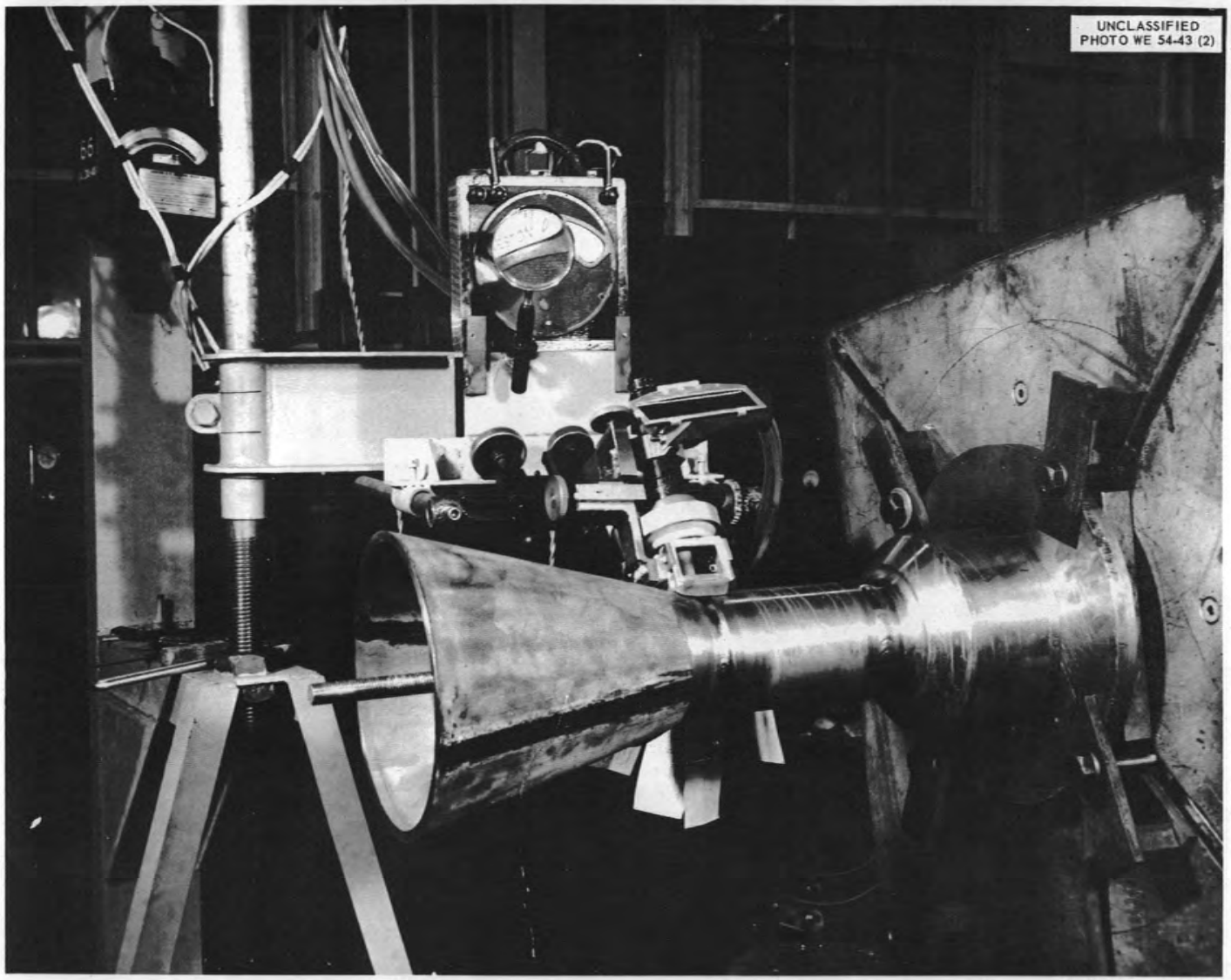

Fig. 8.25. Side-Front View of Arrangement for Making Weld Joining Inlet Cylinder and Flange to 30-deg Cone Section of Core Tank.

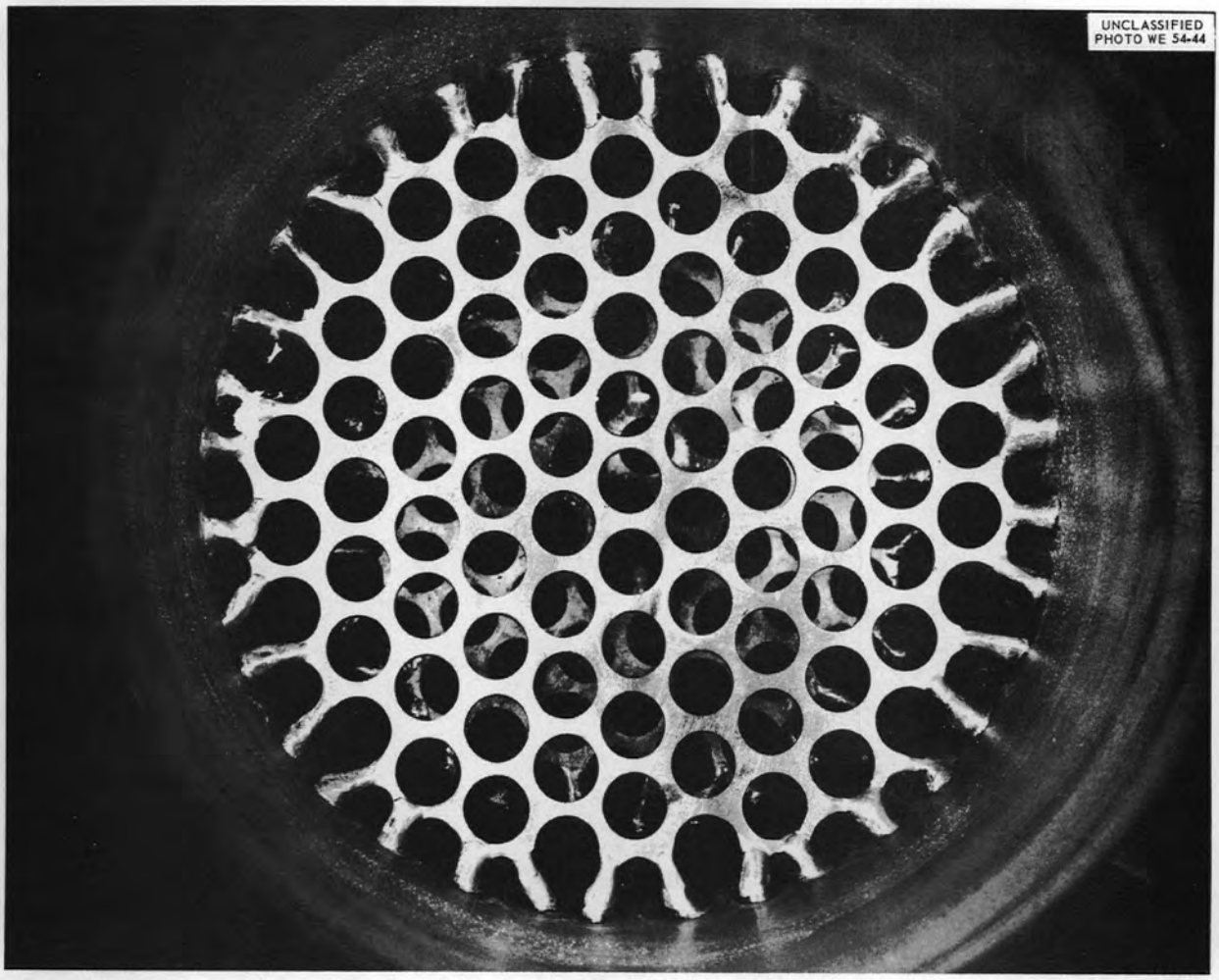

Fig. 8.26. Interior View of Core Tank 30-deg Cone Section Showing Welds Attaching Diffuser Plate No. 2 to Side Walls of Cone.

Part V

CHEMICAL ENGINEERING DEVELOPMENT

F. R. Bruce

9. SLURRY FUEL AND BLANKET STUDIES

D. E. Ferguson
J. P. McBride

V. D. Allred
L. E. Morse
C. E. Schilling
J. T. Roberts
D. G. Thomas
E. V. Jones
S. R. Buxton
A. R. Jones
N. A. Krohn
W. M. Woods

Work on the development of an aqueous thorium oxide slurry for use in the blanket of a thermal power breeder has been intensified, with an increase in effort from the 4 man-year level, at which it has operated for the last 1½ years, to a 12 man-year level. The immediate objective of this program is the development of a slurry for use in the blanket of the HRT. The program includes the demonstration of slurry radiation stability and the acquisition of sufficient understanding of slurries to support the over-all effort and to assure the success of the thorium blanket experiment.

The work of the past quarter has been concentrated on the development of apparatus and techniques for laboratory-scale study and characterization of slurries at room and elevated temperatures for both in-pile and out-of-pile use. The irradiation effort has been augmented by the use of hole C-44 in the LITR. A shielded hood, for use in the remote opening and handling of the irradiated bombs, has been designed and partially constructed. Further slurry irradiations have been made in the ORNL Graphite Reactor. Additional gas recombination studies have been made, with particular attention being given to the catalytic effect of copper. Studies on the preparation of fine-particle oxide and the evaluation of the Thorex product as a source material for the preparation of pure oxide have been initiated. A nitrogen adsorption apparatus for the measurement of surface areas by the Brunauer-Emmett-Teller method is ready for operation. A thermo-gravimetric and adsorption balance is nearly complete. It will be used in the measurement of surface areas by water adsorption, the characterization of slurry solids by measuring their surface activity, and the study of the thermal properties of slurry solids.

9.1 THORIUM DIOXIDE SLURRY IRRADIATION STUDIES

A. R. Jones
N. A. Krohn
J. T. Roberts
W. M. Woods

9.1.1 Slurry Irradiations in the LITR

The bomb developed for slurry irradiations in the LITR (see Sec. 9.1.3) was tested with water. In an 88-hr irradiation at 300°C, no difficulty was encountered. Counting data obtained from a gold wire inserted to calibrate the hole flux indicated that the thermal-neutron flux was approximately 2.7×10^{13} neutrons/cm^2/sec. An aqueous slurry of thorium dioxide prepared from thorium oxalate by calcination at 900°C (Lindsay No. 8) and containing 530 g of thorium per kilogram of H_2O was irradiated for 115 hr at 300°C. The stirrer ceased to operate after the first 24 hr of irradiation. Temperature gradients obtained after stirring had ceased indicated that the thorium dioxide had settled to the bottom of the bomb. The bomb has not yet been opened, and it is not known whether the difficulty with stirring was due to a mechanical failure or to a radiation effect on the slurry. A systematic program of extensive pretesting of bomb assemblies before insertion in the reactor has been initiated to minimize the possibility of mechanical troubles during the irradiation.

9.1.2 Slurry Irradiations in the ORNL Graphite Reactor

In further irradiation studies in the ORNL Graphite Reactor, a slurry containing 530 g of thorium, 40 g of U^{235}, and 6.3 g of copper per kilogram of H_2O as the mixed oxide was irradiated at 275 to 280°C in hole 11 at a flux of 7×10^{11} neutrons/cm^2/sec for ten days. Stirring became labored, and ceased

after 24 hr of irradiation. No gas pressure in excess of steam was observed either before or after the stirring stopped. This indicated that complete recombination of the radiolytic gases was occurring, as was predicted by out-of-pile test results.[1] No difficulty with stirring was encountered in an out-of-pile control run in which hydrogen and oxygen were added from time to time to simulate as closely as possible the in-pile conditions.

The pure thorium oxide slurry irradiated for 30 days at 250 to 300°C in the ORNL Graphite Reactor[2] was removed from the bomb. No change in color was found, and slurry properties seem to have been unaffected by the irradiation. The slurry from the ORNL Graphite Reactor irradiation containing 530 g of thorium and 40 g of U^{235} as the mixed oxide, which was irradiated at 290 to 300°C for six days,[3] was also recovered. This slurry was very viscous, and dilution with water was required before it could be poured from the bomb. The slurry solids were dark tan rather than orange in color and were readily dispersable in the diluted suspension. No evidence of caking on the bottom of the bomb could be discerned. During the original irradiation the stirrer failed to operate at the end of four days, possibly as a result of increased slurry viscosity.

9.1.3 Development of Facilities for Slurry Irradiation Studies

A standard hood being modified for use in the opening and handling of reactor-irradiated bombs has been reinforced mechanically to support heavier shielding, and an air-operated impact wrench and an air-operated shaker have been installed and tested. Design of the permanent shielding has been completed, and construction should be completed by early February.

A stainless steel bomb of 14-ml capacity for use in irradiation studies in hole C-44 of the LITR has been developed and has been tested in-pile (see Sec. 9.1.1). The gas pressure in the bomb is transmitted through a capillary tube to a strain-gage type of pressure cell; a continuous record of the pressure is obtained. The bomb contains an electromagnetically operated dash-pot type of stirrer similar in principle to the one already in use in the ORNL Graphite Reactor.[2] It differs, however, in that the thermocouple well enters at the bottom of the bomb (does not penetrate the gas phase) and the stirrer goes through its cycle completely submerged in the slurry. An induction coil wound around the activating solenoid and feeding into an oscilloscope permits observation of the stirrer operation during the irradiation. The shape of the tracing also gives qualitative information on the condition of the slurry.

Gamma absorption heating in hole C-44 of the LITR is sufficient to raise the temperature of the bomb to any desired value. The temperature is then controlled by air-cooling. The direction of air flow is such as to keep the bomb under continuous reflux, thus minimizing the possibility of the formation of dried solids in the gas phase.

An intensified program for the development of specialized apparatus for the study of slurry properties at high temperatures and pressure and under irradiation has been initiated. A plunger type of bomb viscometer is under consideration. Design of the viscometer is essentially complete, and a Plexiglas model for testing is under construction. Instrumentation to operate the plunger electromagnetically is being developed and assembled in the Instrumentation and Controls Division. The plunger is powered on both the up and down strokes by means of double solenoids. The device is self-timed, since the circuit utilizes the change in impedance in the actuating solenoids to detect the end of one stroke of the plunger and to initiate the next. The plunger was designed to make the resistance to its movement predominantly the result of slurry viscosity. At a constant actuating voltage in the solenoids it is expected that the frequency of the plunger cycle will give a semiquantitative measurement of any change in slurry viscosity.

A bomb for use with slurry experiments in the Co^{60} source is under construction.

9.2 GAS RECOMBINATION STUDIES

L. E. Morse

A reactor blanket containing a thorium oxide slurry in which 10 kw of fission heat per liter of slurry is generated may be expected to produce as much as 4.5 moles of radiolytic gas (D_2 and O_2) per hour per liter of slurry. An internal catalyst to promote the recombination of the evolved gases

[1] D. E. Ferguson *et al.*, *HRP Quar. Prog. Rep. Oct. 31, 1954*, ORNL-1813, p 143.

[2] D. E. Ferguson *et al.*, *HRP Quar. Prog. Rep. July 31, 1954*, ORNL-1772, p 139.

[3] D. E. Ferguson *et al.*, *HRP Quar. Prog. Rep. Oct. 31, 1954*, ORNL-1813, p 144.

would greatly simplify blanket design. It is the ultimate objective of the gas recombination studies to develop such a catalyst for use in thorium oxide slurries which, at the same time, would not adversely affect desirable slurry properties.

Gas recombination studies were carried out with various thorium oxide preparations and thorium oxide slurries containing 0.001 to 0.09 *m* $CuSO_4$ plus 0.0025 *m* H_2SO_4. None of the pure thorium oxide slurries exhibited sufficient catalytic activity for use without an additional catalyst. The catalytic activity of the slurries containing copper sulfate increased as the copper sulfate concentration and temperature increased and decreased with increasing slurry concentration. The recombination rates obtained with slurries containing 0.09 *m* $CuSO_4$ plus 0.0025 *m* H_2SO_4 were more than sufficient to maintain a blanket slurry in a thermal breeder reactor at less than 2000 psi total pressure (D_2O, D_2, O_2) over the temperature range of 253 to 307°C at a concentration of 660 g of thorium per kilogram of H_2O and a thorium concentration range of 660 to 1320 g of thorium per kilogram of water. In all cases most of the copper sulfate was adsorbed on the slurry solids by an apparently reversible process. The catalytic activity appeared to be associated mainly with the copper sulfate in solution. The activation energy calculated from the data on temperature dependence was approximately 20,000 cal per mole of copper, which is in good agreement with the data obtained in uranyl sulfate solutions.

The experimental details and methods of data analyses have been described previously.[1,4] The reaction rate constant, k_π, is given by the expression

$$k_\pi = \frac{\Delta P}{\Delta t} \times \frac{1}{\bar{P}} ,$$

where ΔP is the observed decrease in total pressure in time Δt, and $\bar{P}$ is the average pressure in the time interval. The number of moles of hydrogen, n, removed from the gas phase per liter of slurry per unit time Δt, at a hydrogen partial pressure of p, was calculated from the expression

$$\frac{\Delta n}{\Delta t} = k_\pi \times \frac{pV_g}{RT} \times \frac{1000}{V_s} ,$$

where V_g and V_s are the gas and slurry volumes in cubic centimeters, T is the absolute temperature, and R is the gas constant in appropriate units. The hydrogen removed from the slurry phase during the experiment has been ignored, since only a small fraction of the total hydrogen is dissolved. The calculated recombination rates therefore may be low by as much as 10 to 20%.

The catalytic activity of the various thorium oxide slurries investigated varied slightly, depending on the method of preparation, with the low-burned thorium oxalate giving the highest recombination rate, 0.04 mole of H_2 per hour per liter at 500 psi of H_2 and 300°C (see Table 9.1). The increase, by a factor of 3, in the activity of the oxide prepared from the formate after being circulated in the pumping loops is of interest, since the pumped slurry contained corrosion products and the slurry particles had been degraded.[5]

The addition of 0.09 *m* $CuSO_4$–0.005 *m* H_2SO_4 to a slurry of Ames oxide increased the hydrogen recombination rate from 0.007 to 31 moles/hr/liter at 307°C and a hydrogen partial pressure of 500 psi (see Table 9.2). The copper sulfate was largely adsorbed on the slurry solids but could be at least partially removed by recovering the solid, reslurrying in fresh H_2O, and reheating in the reaction vessel. The distribution of copper between the liquid and solid phases and the marked increase in catalytic activity as soon as reasonable amounts of copper sulfate appeared in the liquid phase indicate that the catalytic activity was more dependent upon the amount of copper sulfate in solution than upon the total amount of copper sulfate added to the slurry.

The slurries containing copper sulfate and sulfuric acid were found to have increased in pH upon recovery from the reaction vessel, indicating that a reaction between the acid and the thorium oxide had occurred. No apparent deterioration of slurry properties was observed, although no effort was made to study settling rates or to measure particle growth. The slurry containing the 0.09 *m* $CuSO_4$ and 0.0025 *m* H_2SO_4 was carried through six recombination experiments, with no decrease in catalytic activity or apparent physical change.

The recombination rate increased with increasing temperature (see Table 9.3). Raising the temperature from 253 to 307°C increased the recombination

[4] H. F. McDuffie *et al.*, *Reactor Sci. Technol.* 4, No. 2, 23–42 (1954) (TID-2013).

[5] D. E. Ferguson *et al.*, *HRP Quar. Prog. Rep. Oct. 31, 1954*, ORNL-1813, p 145.

TABLE 9.1. EFFECT OF METHOD OF THORIUM OXIDE PREPARATION ON CATALYTIC RECOMBINATION OF HYDROGEN AND OXYGEN BY THORIUM DIOXIDE SLURRIES

Reaction temperature: 300°C
Initial pressure: 960 psi H_2, 500 psi O_2 (at 25°C)
Concentration: 660 g of thorium per kilogram of H_2O

Thorium Oxide Preparation	k_π (hr^{-1})	H_2 Recombination Rate at Hydrogen Partial Pressure of 500 psi (moles/hr/liter)
Thorium oxalate calcined above 650°C (Ames)	0.023	0.007
Thorium oxalate calcined at 600°C	0.13	0.04
Thorium hydroxide calcined at 500°C	0.015	0.005
Thorium formate calcined at 650°C	0.018	0.006
Thorium formate calcined at 650°C and circulated in loop at 250°C for 1500 hr	0.049	0.018

TABLE 9.2. EFFECT OF COPPER SULFATE CONCENTRATION ON CATALYTIC RECOMBINATION OF HYDROGEN AND OXYGEN BY THORIUM DIOXIDE SLURRIES

Reaction temperature: 307°C
Initial pressure: 960 psi H_2, 500 psi O_2 (at 25°C)
Concentration: 660 g of thorium per kilogram of H_2O (Ames ThO_2), 0.0025 *m* H_2SO_4

Copper Sulfate Concentration (*m*)	pH at 25°C		Copper Adsorbed on Thorium Dioxide at 250°C (% of Total Cu)	k_π (hr^{-1})	H_2 Recombination Rate at Hydrogen Partial Pressure of 500 psi (moles/hr/liter)
	Initial	Final			
				0.023	0.007
0.001	2.3	5.2	99	0.105	0.03
0.01	2.4	4.6	88	1.76	0.51
0.09	2.5	3.4	73	109	31
0.066*			66	62	18

*Solid recovered from 0.09 *m* $CuSO_4$ run; resuspended in H_2O with no additional acid.

rate of a slurry containing 660 g of thorium per kilogram of H_2O and 0.09 *m* $CuSO_4$–0.0025 *m* H_2SO_4 from 7 to 31 moles/hr/liter at a hydrogen partial pressure of 500 psi. Increasing the thorium concentration from 660 to 1320 g per kilogram of water reduced the hydrogen recombination rate from 22 to 9 moles/hr/liter at 293°C and 500 psi H_2 partial pressure (see Table 9.4).

Further work will include an investigation of copper sulfate catalysis without added sulfuric acid, a study of other possible catalysts such as silver and the platinum metals, and an estimation of the Henry's law constant for hydrogen in a slurry of the standard thorium oxide preparation by determining the recombination rates obtained with different gas-to-slurry ratios and extrapolating to zero gas volume.

TABLE 9.3. EFFECT OF TEMPERATURE ON CATALYTIC RECOMBINATION OF HYDROGEN AND OXYGEN BY THORIUM DIOXIDE SLURRIES CONTAINING 0.09 *m* $CuSO_4$

Initial pressure: 960 psi H_2, 500 psi O_2 (25°C)
Concentration: 660 g of thorium per kilogram of H_2O (Ames ThO_2), 0.09 *m* $CuSO_4$, 0.0025 *m* H_2SO_4

Temperature (°C)	k_π (hr^{-1})	H_2 Recombination Rate at Hydrogen Partial Pressure of 500 psi (moles/hr/liter)
253	18	7
269	43	11
293	76	22
307	109	31

TABLE 9.4. EFFECT OF SLURRY CONCENTRATION ON CATALYTIC RECOMBINATION OF HYDROGEN AND OXYGEN BY THORIUM DIOXIDE SLURRIES CONTAINING 0.09 *m* $CuSO_4$–0.0025 *m* H_2SO_4

Reaction temperature: 293°C
Initial pressure: 960 psi H_2, 500 psi O_2 (25°C)
ThO_2 used: Ames

Thorium Dioxide Concentration (g of Th per 1000 g of H_2O)	k_π (hr^{-1})	H_2 Recombination Rate at Hydrogen Partial Pressure of 500 psi (moles/hr/liter)
660	76	22
990	44	12
1320	36	9

9.3 LABORATORY EVALUATION OF THORIUM DIOXIDE SLURRIES

V. D. Allred E. V. Jones
S. R. Buxton C. E. Schilling
D. G. Thomas

A systematic investigation of the variables associated with the preparation and the properties of thorium oxide has been undertaken. The following studies have been initiated this quarter: a laboratory evaluation of the Thorex product as a suitable source material for the preparation of pure thorium dioxide, the measurement of the surface areas of oxide products, the preparation of fine-particle oxide, and the characterization of thorium dioxide slurries at elevated temperatures (250 to 300°C).

Apparatus for measuring surface area by low-temperature nitrogen adsorption was obtained from the Reactor Experimental Engineering Division and is at present being calibrated. This equipment is also being modified to incorporate a method[6] for measuring the surface area of porous solids by the transient-state flow rate. This latter method is reported to be extremely rapid (4 to 5 min of actual measuring time per sample compared with 6 to 8 hr for the nitrogen adsorption method) and also to have accuracy comparable to the nitrogen adsorption technique.

Equipment for determining surface area by water adsorption has been incorporated into a thermogravimetric balance. Apparatus of this type can

[6]G. Kraus and J. W. Ross, *J. Phys. Chem.* 57, 334–36 (1953).

also be used to characterize the chemical nature of the oxide surfaces by determining the type of compounds which are chemisorbed upon them.[7]

A survey has been made of the analytical data obtained on thorium oxide products used in the HRP slurry program. The information is being prepared for issue as a memorandum.

9.3.1 Preparation of Fine-Particle Oxide

The possibility that slurries composed of small, uniform particles (<0.1 μ) calcined at 650°C or higher (900°C) would have markedly improved handling characteristics and a minimum abrasiveness as compared with slurries of a grosser or less uniform particulate nature has prompted an investigation into the preparation of fine-particle oxide. One possible approach, and the one currently being studied, is to prepare fine-particle thorium oxalate and to study the effect of the calcination procedure on the particle size and slurry characteristics of the oxide product.

A method of preparing fine, uniform particles by a controlled precipitation technique[8] has been in use for some time at K-25. This method has been applied at K-25 to the preparation of a sample of a double salt of ammonium and thorium oxalate which is described as being of a uniform and small particle size. A slurry of the product was passed through a Whatman No. 42 filter paper and air-dried. Agglomeration occurred during the drying process, and the dried product was ground in a mortar and pestle before delivery to X-10 for evaluation.

Two calcinations were carried out on the material: a multistage process with the final calcination at 650°C and a simple calcination at 650°C followed by a calcination at 950°C. The final product in both cases had a tan discoloration. Aqueous slurries of the original material and the 950°C oxide product settled rapidly, with the bulk of the settled materials being sandlike plus a small fraction of the material as fines. Adding 0.004 *m* $Na_4P_2O_7$ to the slurries and shaking them overnight failed to produce a good dispersion. Samples of the original material and of both oxide products have been submitted for sedimentation particle-size analysis and electron microscopic examination.

When dried to constant weight at 100°C, the original preparation contained 2.8% NH_4^+, 46.3% Th, 43.7% $C_2O_4^{--}$, and 8.1% H_2O. During the stepwise calcination the double complex was apparently destroyed between 170 and 290°C. Essentially complete decomposition of the oxide was obtained at approximately 320°C.

[7] G. A. Mills, E. R. Boedeker, and A. G. Oblad, *J. Am. Chem. Soc.* 72, 1554–60 (1950).

[8] A. T. Grefig and R. W. Anderson, *Thorium Ammonium Oxalate Sample Thox C-27–24*, KLI-3347 (Dec. 21, 1954).

10. THERMAL BREEDER FUEL PROCESSING

D. E. Ferguson
W. E. Unger

W. L. Carter
R. A. McNees
E. O. Nurmi
J. C. Bresee
J. R. Engel
C. E. Guthrie
P. A. Haas
R. W. Horton
R. B. Lindauer
F. C. McCullough
A. M. Rom
H. O. Weeren
M. E. Whatley
H. E. Williamson

10.1 RARE-EARTH CHEMISTRY

R. A. McNees R. W. Horton

Studies on neodymium sulfate solubility[1] and precipitation behavior were carried out under dynamic conditions in test loop A. This loop has a capacity of 1.6 liters and a circulation rate of about 3 gpm. The main circulating stream operates at 250°C, and the pressurizer, through which there is a flow of about 200 ml/min, operates at 285°C.

Similar studies were made in a 1-liter rocking autoclave and a 10-ml shaker bomb in the laboratory.

10.1.1 Neodymium Solubility

The solubility of neodymium sulfate in simulated reactor fuel solution was found to be 0.06 g per kilogram of H_2O at 260°C. At 285°C, the solubility was 0.02 to 0.03 g per kilogram of H_2O, corresponding to a 0.2% neutron poison level in a two-region thermal breeder reactor.

The tests at 260°C were made in the rocking autoclave. The vessel contained 0.02 *m* UO_2SO_4–0.005 *m* H_2SO_4 solution free of fission products. To this was repeatedly added small amounts of uranyl sulfate solution containing known amounts of mixed rare-earth sulfates traced with Nd^{147}. Samples were taken in such a fashion as to maintain the desired volume of liquid in the pressure vessel. The Nd^{147} in solution increased to a value of 0.06 g of neodymium sulfate per kilogram of H_2O at 260°C. Continued addition of rare-earth-bearing solution did not increase the amount of neodymium sulfate in solution.

The tests at 285°C were made in loop A. In these runs the loop was brought to operating conditions with only 0.03 *m* UO_2SO_4–0.005 *m* H_2SO_4 solution in the system. After stable loop operation was assured, additional uranyl sulfate solution containing known amounts of neodymium sulfate traced with Nd^{147} was pumped into the system, and samples were withdrawn at intervals in such a way that the liquid content of the loop was essentially constant. While the main circulating stream operates at 250°C, the pressurizer, which is at 285°C and acts as a retaining vessel for the rare-earth sulfate solids (see Sec. 10.1.2), controls the amount of neodymium in solution in the loop.

The data are plotted in Fig. 10.1. Data obtained by visual observation[1] of solutions in quartz tubes are included for comparison.

The typical behavior of neodymium sulfate in the loop A solubility tests is shown in Fig. 10.2. These data were obtained during run LR-23 (see Sec. 10.1.2). The amount of neodymium sulfate in the circulating stream increased to 0.032 g per kilogram of H_2O during the first 8 hr in which neodymium sulfate was added to the loop solution. Over the next 8 hr, with continued addition of neodymium sulfate solution, the neodymium sulfate dropped to 0.02 g per kilogram of H_2O and remained at this level until the run was interrupted because of a plug in the pressurizer preheater. At this time the loop temperature was dropped to 140°C and the pressurizer to 160°C. A sample taken under these conditions indicated that 0.210 g of neodymium sulfate per kilogram of H_2O was in solution; 0.240 g per kilogram of H_2O had been injected into the loop.

10.1.2 Rare-Earth Sulfate Precipitation Behavior in Loop A

During the solubility tests[2] in loop A there was a tendency for neodymium sulfate to accumulate

[1] W. K. Eister *et al.*, *HRP Quar. Prog. Rep. April 30, 1954*, ORNL-1753, Fig. 128, p 178.

[2] D. E. Ferguson *et al.*, *HRP Quar. Prog. Rep. Oct. 31, 1954*, ORNL-1813, Fig. 12.3, p 154.

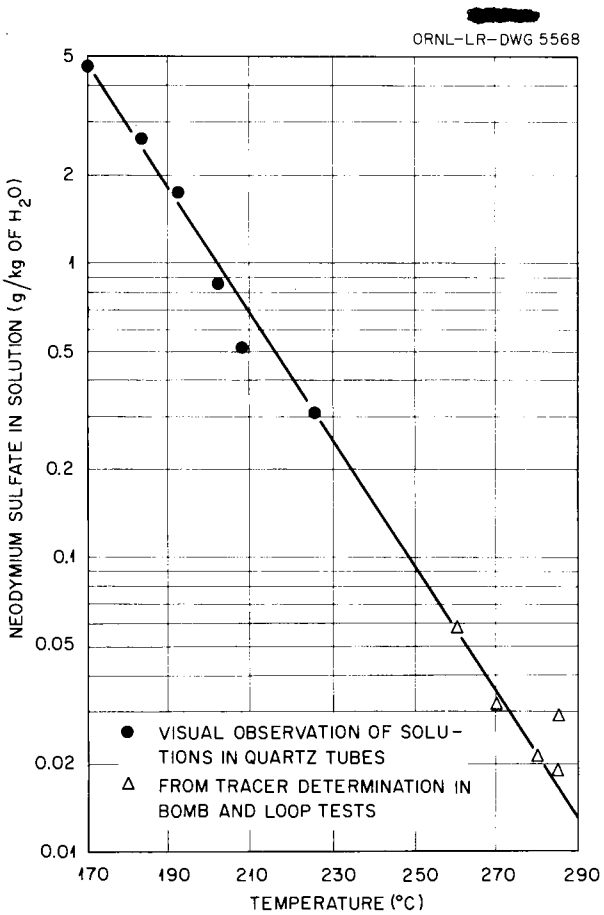

Fig. 10.1. Solubility of Neodymium Sulfate in 0.03 *m* UO_2SO_4–0.005 *m* H_2SO_4 Solution.

in stagnant or low-velocity sections and to scale out on hot metal surfaces. No significant amount of insoluble neodymium sulfate was found suspended in the main loop circulating stream. From activity measurements and inspection of the loop after drainage, it was concluded that the insoluble neodymium sulfate had settled out in the pressurizer and preheater exit tube. Since the pressurizer preheater (and electrically heated 80-mil-ID stainless steel tube) had repeatedly plugged, this tube was removed and inspected after the last run. The exit section of the tube was completely plugged with a scalelike deposit that contained a considerable amount of neodymium and corrosion products.

The results and conditions of the loop A runs are summarized in Table 10.1. Test run LR-16 showed a neodymium material balance of only 20%. The loop was not washed out after this run, and neodymium was present in the loop solution in runs LR-17 and 18 even though none was added. Examination of the pressurizer after run LR-17 showed the presence of loose solids with the composition 4% neodymium, 27% iron, 10% chromium, 1.7% nickel, and 1% uranium. Pitting of the loop was observed at the line of the liquid-vapor interface.

In test run LR-20 the added neodymium sulfate solution was traced with Nd^{147}. After enough neodymium solution had been added to saturate the loop contents, the neodymium sulfate concentration in solution in the loop remained essentially constant at 0.03 g per kilogram of H_2O for several hours. Further addition of neodymium solution resulted in precipitation. The preheater eventually plugged, thus stopping flow through the pressurizer and making the loop inoperable. Lowering the temperature of the loop eventually unplugged the preheater, but subsequent operation was so erratic that equilibrium conditions were not again obtained. When the loop was drained and washed, a material balance of 77% was obtained. Attempts to obtain samples of solids from the loop while it was in operation failed, owing to plugging of sample lines and leaks in the sampler system.

Test run LR-23 was essentially a repetition of run LR-20, except that the rare-earth-bearing solution was pumped into the main circulating loop instead of into the pressurizer. The loop A preheater plugged several times during run LR-23, and, since the highest metal temperatures in the loop were in the preheater, it was considered likely that the plugging was due to neodymium sulfate precipitation. The preheater (see Fig. 10.3) was therefore removed and sectioned at the end of the run, and one section of the tube (80 mils ID) was found to be completely plugged. The section adjacent was coated with a deposit to the extent that the diameter was about half that of the original. These solids accumulations showed a high activity level, which indicated that a considerable amount of neodymium was present.

The delivery tube between the preheater and pressurizer also showed a considerable accumulation of loose solids (Fig. 10.3). A portion of this solid matter was dissolved in water and was analyzed by counting the neodymium tracer activity. The analysis indicated that 7% of the solids was neodymium sulfate. It is presumed that this material was precipitated in the preheater and carried

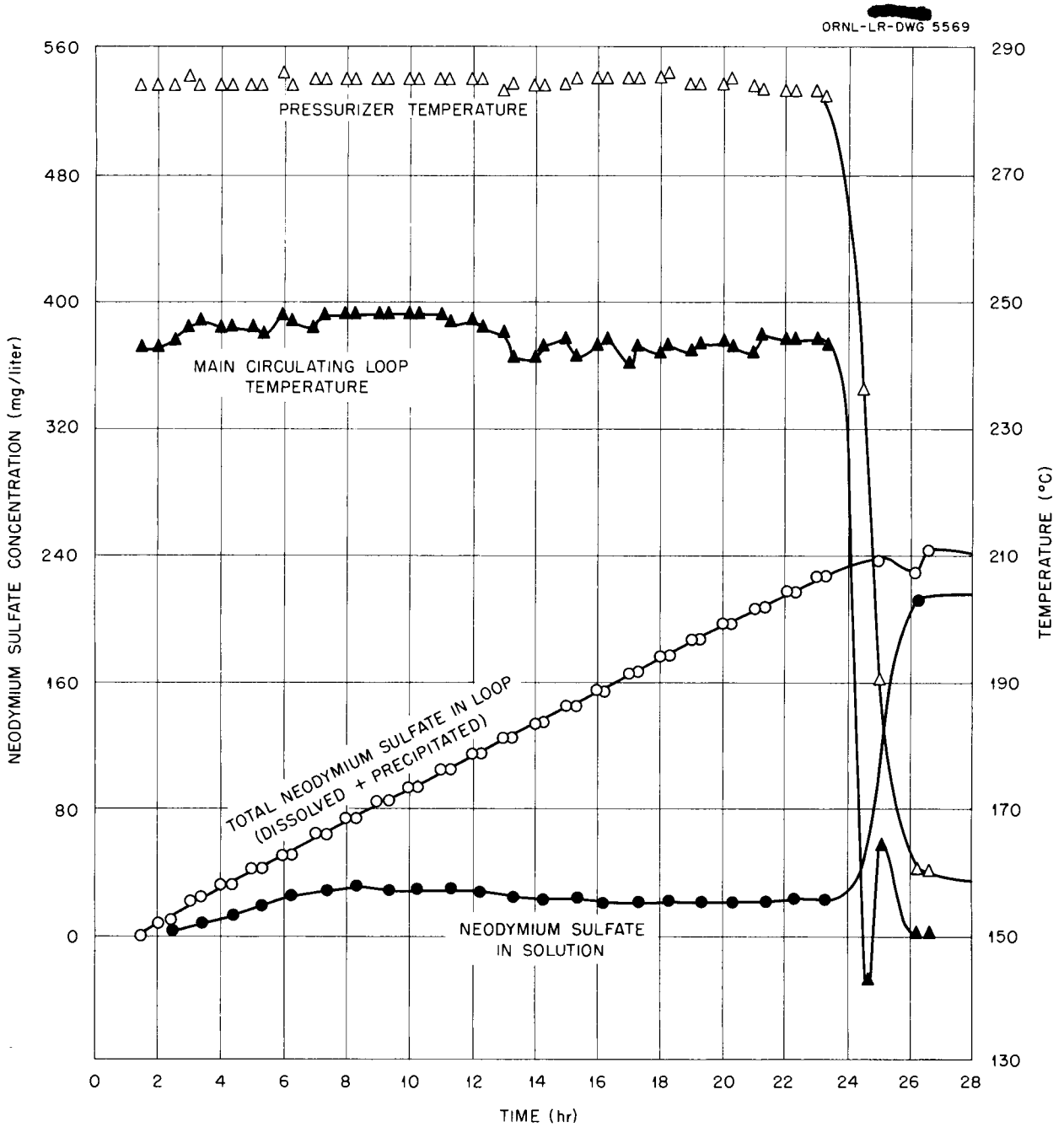

Fig. 10.2. Behavior of Neodymium Sulfate in Solubility Tests in Loop A.

out to the lower-stream-velocity section, where it was found.

A survey of the loop with a radiation detection instrument after run LR-23 indicated that an appreciable amount of the neodymium had also collected in the pressurizer vessel. This vessel has a very slow flow, and the neodymium probably settled out on the bottom of the pressurizer pot.

TABLE 10.1. SUMMARY OF NEODYMIUM SOLUBILITY TESTS MADE IN LOOP A

Loop pressure: 1000 to 1100 psig

Loop temperature: 250°C

Pressurizer temperature: 280 to 285°C

Loop operated with 0.02 *m* UO_2SO_4–0.005 *m* H_2SO_4 (1000 ppm oxygen) until operation was stable; uranyl sulfate solution of approximately the same concentration and containing known amounts of neodymium, traced with Nd^{147} in some runs, was pumped into the system; then samples were withdrawn at intervals in such a way that liquid content of loop remained constant

LR Run No.	Feed Concentrations			Average Loop Concentrations			Material Balance (%)		Operating Time (hr)
	Uranium (g/kg of H_2O)	$Nd_2(SO_4)_3$ (g/kg of H_2O)	Nd^{147} (counts/min/ml)	Uranium (g/kg of H_2O)	$Nd_2(SO_4)_3$ (g/kg of H_2O)	Nd^{147} (counts/min/ml)	Uranium	Neodymium	
16	6.7	3		7.30	0.11–0.16[a]		109	20	65.5
17	10			6.42	0.04–0.06[a,b]		64		46.0
18	10			10.4	0.05[a,b]		104		16.0
20	8.4	0.32	1.7×10^4	8.62	0.03[c]	1.7×10^3	103	77[a]	26.0[d]
23	8.6	0.35	1.4×10^5	9.0	0.02[c]	1.0×10^4	104		104

[a]Based on gravimetric analysis, which is only an order-of-magnitude estimate at this low concentration.

[b]Loop was not washed after run LR-16, and neodymium remaining in system appeared in these subsequent runs.

[c]Based on Nd^{147} radiochemical analysis.

[d]Operated for 40 hr before neodymium addition started.

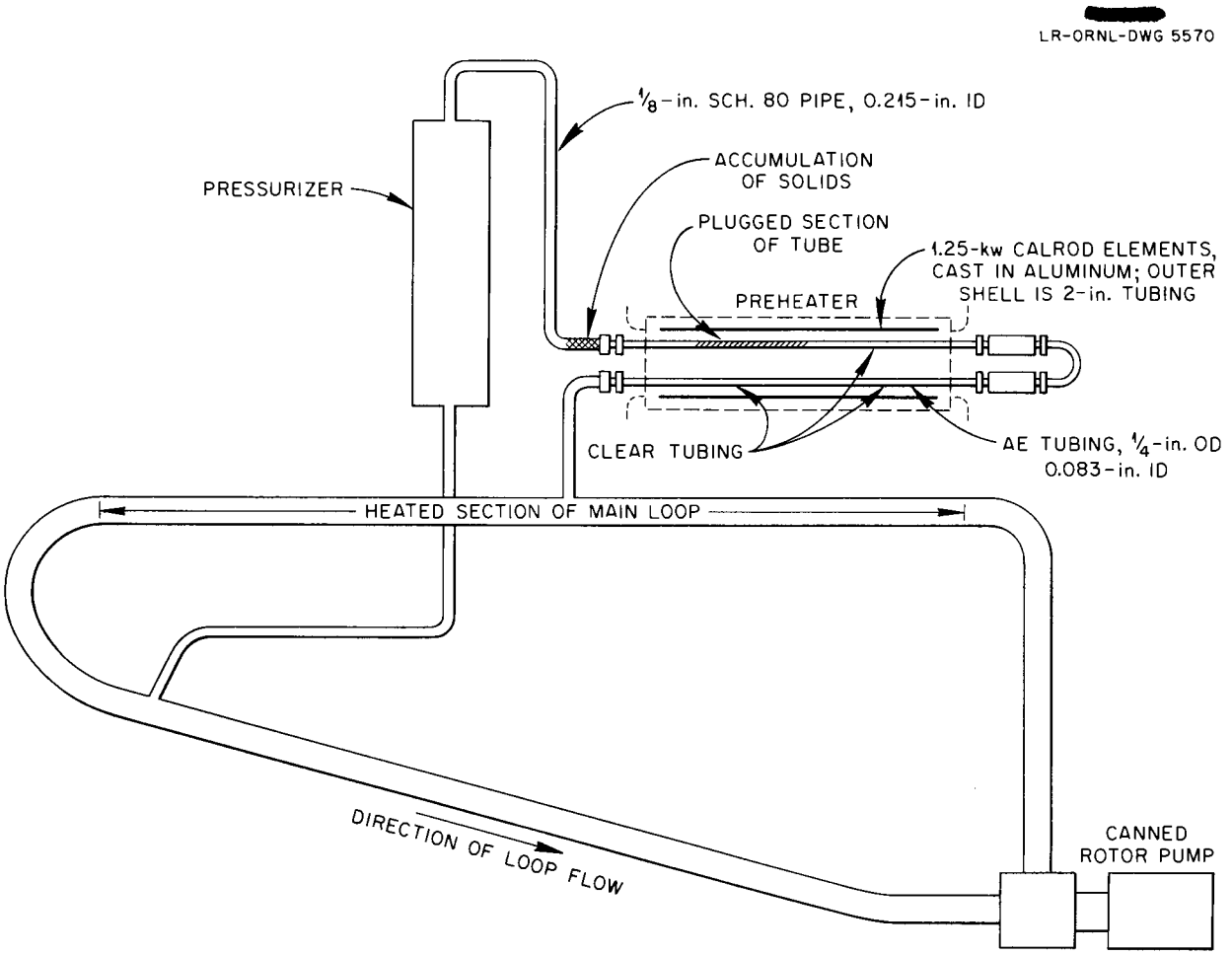

Fig. 10.3. Schematic Diagram of Loop A and Preheater.

10.1.3 Rare-Earth Precipitation Behavior in Laboratory Tests

When rare-earth sulfates were precipitated from a simulated fuel solution in contact with hot metal surfaces, a large fraction (30 to 80%) of the precipitated salt was found attached to the metal surface (see Table 10.2). In the case of Zircaloy-2 pins suspended in the solution, and therefore at solution temperature, the adsorption of rare earths was negligible. Titanium pins, under these conditions, did adsorb a significant amount of rare earth at 275 and 300°C, but not at 250°C. In some cases large rare-earth sulfate crystals formed on the titanium pins.

These data were obtained by heating a simulated fuel solution containing mixed rare-earth sulfates and Nd^{147} tracer in stainless steel and titanium pressure vessels. Each vessel contained 5 ml of fuel solution and two metal test pins. The bombs were heated to the desired temperature with both pins immersed in the liquid. After 30 min at temperature the bomb was inverted and then slowly cooled. One test pin fell with the liquid and was wet while being cooled; the other was held in the gas phase of the vessel. After the bomb was opened, the pins and solutions were examined for activity.

The largest amount of neodymium adsorbed on a titanium test pin was 0.2 mg/cm^2, and the crystals of rare-earth sulfates were visible to the naked eye. Examination under a low-power microscope of some of the other high-activity pins showed definite crystal growth at spots which differed in appearance from the remainder of the pin. Crystal growth

TABLE 10.2. ADSORPTION OF RARE-EARTH SULFATES ON METAL SURFACES

Simulated reactor fuel heated in titanium or 347 stainless steel shaker bombs, with two metal pins suspended in solution; at end of experiment, the bomb was inverted and one pin (wet pin) remained with the solution while the other pin (dry pin) was suspended in the vapor by a platinum wire

Temperature (°C)	Pressure-Vessel Metal	Nd on Vessel Wall (% of Total)	Test-Pin Metal	Neodymium on Pin (mg/cm^2)*		
				Wet Pin	Dry Pin	Difference
250	Titanium	40	Zircaloy-2	0.004	0.02	0.016
	347 SS	70	Zircaloy-2	0.002	0.003	0.001
275	Titanium	50	Zircaloy-2	0.002	0.005	0.003
	347 SS	35	Zircaloy-2	0.003	0.003	0.00
300	Titanium	30	Zircaloy-2	0.01	0.01	0.00
	347 SS	45	Zircaloy-2	0.01	0.02	0.01
250	Titanium	55	Titanium	0.006	0.02	0.014
	347 SS	50	Titanium	0.01	0.03	0.02
275	Titanium	60	Titanium	0.01	0.06	0.05
	347 SS	80	Titanium	0.01	0.07	0.06
300	Titanium	60	Titanium	0.01	0.13	0.12
	347 SS	70	Titanium	0.01	0.20	0.19

*10 mg of neodymium per square centimeter on the core tank of the TBR is equivalent to 1% neutron poison.

seemed to be localized at spots of surface imperfection.

When test pins were subjected repeatedly to precipitating rare earths, the amount of neodymium adsorbed increased with the increasing number of exposures, but the appearance of the corrosion film on the test pin also definitely changed from that observed with a single precipitation. Where the amount of neodymium per square centimeter of test pin was built up, by repeated precipitations, to the level at which crystals were seen in single precipitation tests (0.2 mg/cm^2 on titanium), no crystals could be seen. This indicates that inclusion of rare earths in the corrosion film on hot metal surfaces will occur but that heavy concentration of rare earths as distinct sulfate crystals probably will not occur on well-passivated metal surfaces.

10.2 HYDROCLONE DEVELOPMENT

M. E. Whatley J. R. Engel

The most attractive device for removing precipitated solids from aqueous homogeneous reactor fuel and blanket solutions is a hydroclone (a solid-liquid cyclone separator).[3] During the past quarter, study and evaluation of both the 0.5- and the 0.25-in.-ID hydroclone have continued. The efficiency of each of the two units was determined as a function of throughput, dimensions of the inlet and outlets from the unit, length of the unit, and interior surface conditions. In addition, a method of evaluating efficiency as a function of particle size was devised and was applied to current data.

[3] *Ibid.*, Fig. 12.2, p 152.

The work was carried out at room temperature with demountable hydroclones, assembled from brass and Lucite parts, and with a unit hydroclone from a Dorr TM-3 assembly. The parts of the demountable units could be interchanged with one another so that various inlet nozzles and vortex finders could be used with a given hydroclone body. The slurry used was thorium dioxide processed to narrow the size distribution of the particles (see Table 10.3). The technique consisted in momentarily injecting a small charge of slurry into the water feed to the hydroclone under test and collecting the exit streams until all the injected material was out of the system.

The 0.25-in.-dia hydroclones gave higher separation efficiencies for submicron particles than did the 0.5-in.-dia hydroclones. (The efficiency of a hydroclone is the fraction of the solids in the feed stream that reports to the underflow of the hydroclone. The fraction of the feed stream represented by the underflow, the "underflow ratio," is the lower limit of efficiency.)

TABLE 10.3. FEED PARTICLE-SIZE ANALYSES

Feed Designation	Feed Particle Size (μ)	Amount of Feed Less Than Particle Size (wt %)	Settling Rate (in./hr)
A	8.70	100.0	56
	5.50	90.9	21.8
	2.76	70.7	5.45
	1.53	48.9	1.70
	1.01	25.7	0.74
	0.75	10.9	0.40
	0.62	4.7	0.275
B	16.1	100.0	175
	9.6	90.6	66.0
	7.1	85.5	36.0
	5.1	70.8	18.8
	4.1	50.1	12.1
	3.5	28.5	8.8
	3.0	16.2	6.50
	2.0	4.3	2.86
	1.0	1.7	0.72
C	25.6	96.7	470
	7.1	52.5	36.0
	5.1	41.5	18.8
	4.2	35.4	12.7
	2.33	34.9	3.90
	1.50	20.6	1.62
	1.00	19.2	0.72
	0.82	19.0	0.48
	0.60	18.3	0.26

10.2.1 The 0.5-in.-dia Hydroclone

Efficiencies greater than 95% were obtained with 0.5-in.-dia hydroclones for separation of 2-μ thorium dioxide particles from water at room temperature. The efficiency of the hydroclones depended primarily on the feed pressure to the hydroclones. The feed pressure varied with the flow rate and with the size of the inlet and overflow port openings.

The efficiency of the hydroclones increased from 80% at 0.5 gpm to 95.6% at 1 gpm and reached a maximum of 99.8% at 1.5 gpm under the conditions tested (see Table 10.4). The feed pressure varied with the square of the flow rate through the hydroclone.

TABLE 10.4. EFFECT OF FEED RATE (PRESSURE) ON EFFICIENCY OF 0.5-in.-dia HYDROCLONE

Hydroclone length:	3.5 in.
Feed inlet port area:	10^{-2} in.^{2}
Overflow port area:	13.3×10^{-3} in.^{2}
Vortex finder length:	0.34 in.
Underflow port area:	12×10^{-3} in.^{2}
Underflow ratio:	6%
Feed material:	B (see Table 10.3)

Feed Rate (gpm)	Feed Pressure (psi)	Efficiency (%)
0.5	7.1	81
0.8	20.3	94
1.0	28.9	96
1.5	80.0	99.85
2.0	160.0	99.85

With comparable feed pressures, efficiency was highest when the inlet and overflow areas were both in the range 7×10^{-3} to 12×10^{-3} in.^{2} (see Table 10.5 for typical data). Efficiencies were lower in this range when the two areas differed by as much as a factor of 3.

TABLE 10.5. EFFECT OF FEED INLET AND OVERFLOW PORT AREAS ON EFFICIENCY OF 0.5-in.-dia HYDROCLONE

Hydroclone length: 3.5 in.
Vortex finder length: 0.45 in.
Underflow port area: 12×10^{-3} in.^{2}
Underflow ratio: 10%
Feed material: A (see Table 10.3)

Feed Rate (gpm)	Feed Pressure (psi)	Feed Inlet Port Area (in.^{2})	Overflow Port Area (in.^{2})	Efficiency (%)
0.5	49.5	3.1×10^{-3}	3.1×10^{-3}	84
1.0	61.0	6.9×10^{-3}	6.8×10^{-3}	97
1.0	34.1	12.3×10^{-3}	6.8×10^{-3}	89
0.5	56.0	6.9×10^{-3}	2.1×10^{-3}	78
0.8	51.0	12.3×10^{-3}	3.1×10^{-3}	82

10.2.2 The 0.25-in.-dia Hydroclones

The 0.25-in.-dia hydroclones had a higher efficiency for submicron particles than the 0.5-in.-dia hydroclones and for this reason were studied more exhaustively. Efficiencies of greater than 90% for 1-μ particles were obtained with this hydroclone at flow rates as low as 0.3 gpm. The optimum length for the 0.25-in.-dia hydroclone was 1.5 in.

As was observed with the 0.5-in.-dia hydroclone, the efficiency of the 0.25-in.-dia hydroclone depended primarily on the feed pressure. At constant feed pressure, varying the inlet and overflow port areas over the range 1.3×10^{-3} to 6.0×10^{-3} in.^{2} did not appreciably change the efficiency of the hydroclone (see Table 10.6).

As the feed rate (and pressure) increased from 0.08 to 2.8 gpm, the efficiency of the 0.25-in.-dia hydroclone increased from 54 to 98% with feed material B; with feed material C, which contained a higher proportion of fine particles (20% less than 1.5 μ), the efficiency increased from 45% at a feed rate of 0.15 gpm to 94% at 0.5 gpm (see Table 10.7). The efficiency dropped off drastically below a feed rate of about 0.2 gpm (30 psi feed pressure).

The effect of varying the underflow ratio (see Table 10.8) was much less pronounced than that of varying the feed rate. The efficiency dropped from 88 to 63% when the underflow ratio was decreased from 30 to 1% (see Table 10.8). The concentration factor, defined as the ratio of the underflow concentration to the feed concentration, increased as the underflow ratio decreased to the smallest underflow ratio tried (1%). It should be noted that when any operation variable is changed the effect on efficiency is dependent upon the nature of the feed material used. A material with a wide spread in particle size is much less influenced by operating variables than one essentially uniform and at the critical particle size for the hydroclone.

The optimum cone length for the 0.25-in.-dia hydroclone was ascertained to be about 1.5 in. As seen in Table 10.9, the optimum is not well defined, and a reasonable latitude is allowable without serious decreases in efficiency occurring.

A progressive relation is noted between capacity and cone length. Since the pressure requirement is indicative of the centrifugal field in a hydroclone, a high capacity is indicative of a low centrifugal field. Apparently, increasing the length of the cone increases the drag on the liquid, decreasing the centrifugal field; the optimum reflects a compromise between residence time and centrifugal field. Cones for these studies were made of both brass and Lucite. It may be seen that, in all cases in which the physical dimensions were identical, the brass cone had a higher capacity and a lower efficiency. This, again, is a phenomenon of drag and indicates that Lucite is more amenable to providing a smooth surface. It is thought that, if all the hydroclones had been

TABLE 10.6. EFFECT OF INLET AND OVERFLOW PORT AREAS ON EFFICIENCY OF 0.25-in.-dia HYDROCLONE

Hydroclone length: 1.5 in.
Vortex finder length: 0.24 in.
Underflow port area: 4.4×10^{-3} in.^{2}
Underflow ratio: 6%
Feed pressure: 35 psi
Feed material: C (see Table 10.3)

Feed Inlet Port Area (in.^{2})	Overflow Port Area (in.^{2})	Feed Rate (gpm)	Efficiency (%)	
			1.4-in.-long Cone	1.0-in.-long Cone*
1.4×10^{-3}	1.7×10^{-3}	0.20	65.4	71.0
2.1×10^{-3}	2.2×10^{-3}	0.22	73.2	72.0
3.8×10^{-3}	3.9×10^{-3}	0.34	65.9	69.3
5.9×10^{-3}	3.9×10^{-3}	0.39	63.7	65.1
5.9×10^{-3}	5.8×10^{-3}	0.39	65.5	69.0

*Cone made of Lucite.

TABLE 10.7. EFFECT OF FEED RATE (PRESSURE) ON EFFICIENCY OF 0.25-in.-dia HYDROCLONE

Hydroclone length: 1.5 in.
Feed inlet port area: 1.4×10^{-3} in.^{2}
Overflow port area: 1.6×10^{-3} in.^{2}
Vortex finder length: 0.15 in.
Underflow port area: 4.4×10^{-3} in.^{2}

Feed Rate (gpm)	Feed Pressure (psi)	Efficiency (%)
Feed Material B, Underflow Ratio 10%		
0.08	7.8	54
0.09	8.8	72
0.10	10.6	77
0.28	91.5	98
Feed Material C, Underflow Ratio 6%		
0.15	18.9	45
0.20	31.8	66
0.30	66.9	87
0.40	140.0	86
0.50	244.0	94

TABLE 10.8. EFFECT OF UNDERFLOW RATIO ON EFFICIENCY OF 0.25-in.-dia HYDROCLONE

Hydroclone length: 1.5 in.
Feed inlet port area: 1.4×10^{-3} in.^{2}
Overflow port area: 1.6×10^{-3} in.^{2}
Vortex finder length: 0.15 in.
Underflow port area: 4.4×10^{-3} in.^{2}
Feed rate: 0.20 gpm
Feed material: C (see Table 10.3)

Underflow Ratio (%)	Efficiency (%)	Feed Pressure (psi)	Concentration Factor
1	63	34.1	6300
2	65	33.9	3250
4	68	32.1	1700
6	69	29.2	1150
10	73	29.0	730
20	83	27.9	415
30	88	26.8	290

TABLE 10.9. EFFECT OF CONE LENGTH ON EFFICIENCY OF 0.25-in.-dia HYDROCLONE

Vortex finder length:	0.24 in.
Underflow port area:	4.4×10^{-3} in.^{2}
Underflow ratio:	6%
Feed pressure:	35 psi
Feed material:	C (see Table 10.3)

Cone Length (in.)	Feed Rate (gpm)	Efficiency (%)
Feed Inlet Port Area, 1.4×10^{-3} in.^{2}; Overflow Port Area, 1.7×10^{-3} in.^{2}		
0.5*	0.16	57
0.75*	0.16	70
1.00*	0.18	70
1.41	0.21	64
2.00*	0.19	66
2.50*	0.20	50
3.50	0.24	35
Feed Inlet Port Area, 3.8×10^{-3} in.^{2}; Overflow Port Area, 3.9×10^{-3} in.^{2}		
0.5*	0.27	63
0.5	0.28	60
0.75*	0.28	79
0.71	0.30	75
1.00*	0.31	81
1.41	0.34	87
2.00*	0.36	85
2.00	0.38	80
2.50	0.37	72
3.30	0.39	54**

*Lucite cone; others were brass.

**Pressure dropped to 30 psi.

polished to a smoother surface, the optimum length might have been longer.

10.2.3 Effect of Particle Size on Efficiency

Results of a preliminary analysis confirmed the fact that there is a particle size below which hydroclone efficiency falls off rapidly with decreasing particle size. For the 0.5-in.-dia hydroclones this critical size appeared to be about 1 μ in the case of thorium dioxide in water. The 0.25-in.-dia hydroclones maintained high efficiencies to even smaller particle sizes. The critical size for the smaller hydroclones appeared to lie between 0.7 and 0.2 μ. The uncertainty of these data results from the following:

1. an insufficient fraction of the feed material in the critical particle-size region,
2. inability to obtain representative samples of slurry,
3. inherent errors in particle-size analysis,
4. degradation of particles by the hydroclones.

The first and fourth sources of uncertainty are being minimized by better processing of the feed material. The second and third sources should be minimized by further experience with the system.

10.3 HRT CHEMICAL PLANT

W. L. Carter, R. B. Lindauer, A. M. Rom, F. C. McCullough, C. E. Guthrie, H. O. Weeren, H. E. Williamson

The HRT fuel processing plant will be operated in conjunction with the reactor to demonstrate the feasibility of continuously processing the reactor fuel to remove the fission and corrosion products that would otherwise accumulate in the reactor loop and impair its operation. Two of the outstanding advantages of the homogeneous type of reactor are the ease and economy with which this processing may be accomplished. The fission and corrosion products that are objectionable because of large cross sections are essentially insoluble at the reactor operating temperatures and may be removed by centrifugation. The only means of removing soluble contaminants will be by continuous removal of a small portion of the fuel and replacement with fresh fuel.

The insoluble fission and corrosion products will be centrifuged from a slip stream bypassed around the reactor-loop heat exchanger. Hydroclones, a hydraulic application of the cyclone separators widely used for removing suspended solids from gas streams, will be used to centrifuge the solids from the liquid reactor fuel. The current flow sheet (see Fig. 10.4) differs from the one previously published[4] primarily in that (1) a single stage of hydroclones is now recommended instead of a cascade of two stages and (2) drying and re-solution of the solids removed by the hydroclones will be accomplished in the shielded carrier rather than in equipment designed specifically for this purpose.

[4]D. E. Ferguson *et al.*, *HRP Quar. Prog. Rep. July 31, 1954*, ORNL-1772, Fig. 75, p 155.

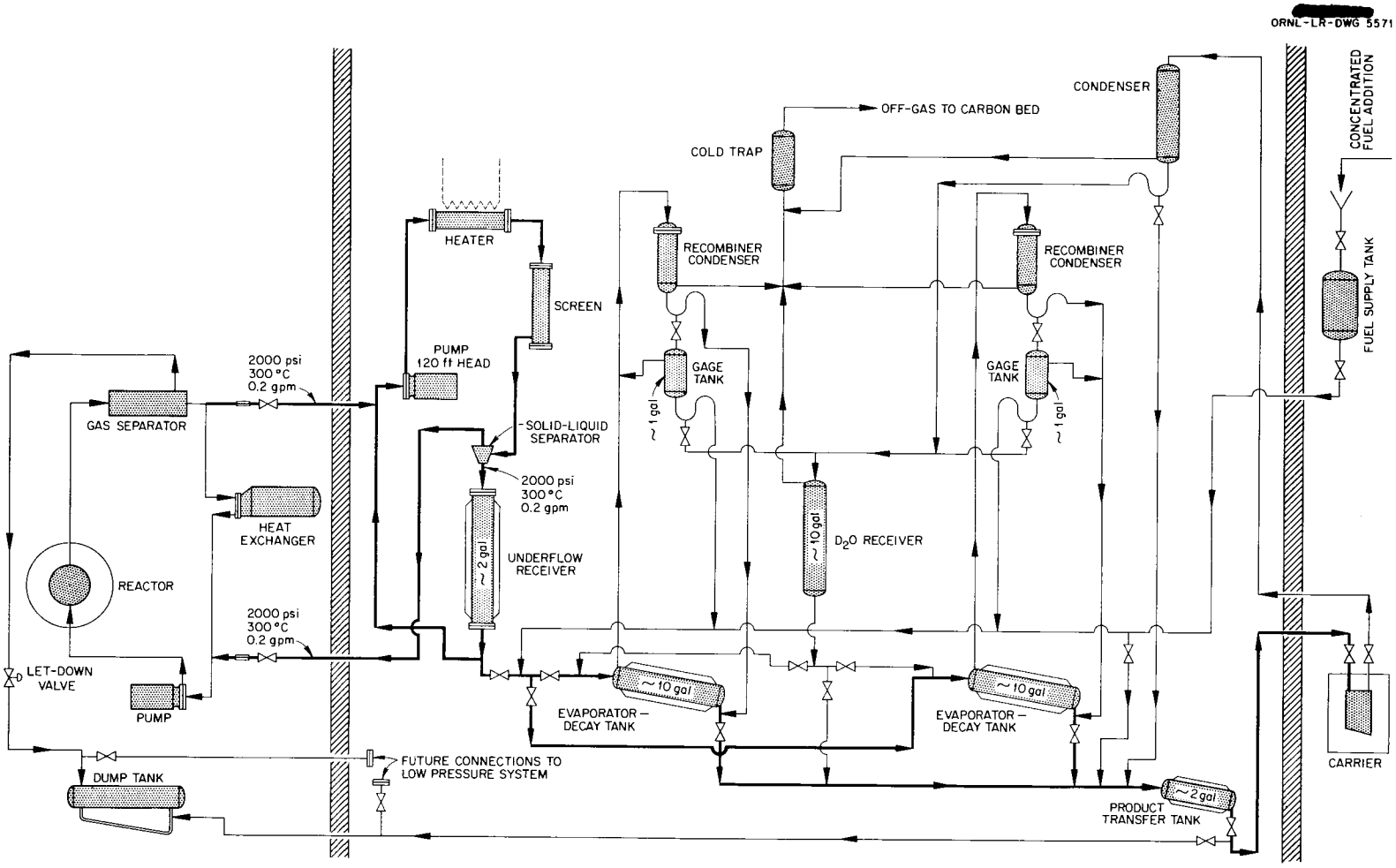

Fig. 10.4. Flow Sheet for HRT Fuel Processing, January 1955.

The slip stream from the reactor loop will be fed to the hydroclone unit by a canned-rotor pump, and the clarified overflow from the hydroclones will be returned to the reactor loop into the suction side of the reactor fuel circulating pump. The underflow of the hydroclones, which will contain the concentrated insoluble material, will be circulated through a retention tank and recycled, for further concentration, through the hydroclone unit so that, in effect, the solids separated by the hydroclones will be trapped in the underflow loop. Periodically, the retention tank will be shut off from the high-pressure system, cooled, and discharged. The frequency with which the pressure in the underflow retention tank is let down and the contents discharged will determine the rate of purging of the reactor fuel.

The concentration factor, the ratio of the solids concentration in the underflow retention tank to that in the reactor fuel at approximately steady state, is influenced by the efficiency of the hydroclones for solids separation and by the ratio of the underflow rate to the feed rate. The concentration of solids in the reactor fuel is influenced by the underflow retention tank volume, the concentration factor, the frequency of the retention tank discharge, and the length of time between operations. The speed of approach to steady state is influenced by the underflow retention tank volume and the underflow rate.

The hydroclone system for the HRT chemical processing plant is designed to keep the fission-product solids concentration below 70 mg/liter under the following conditions:

Unit hydroclone efficiency, %	70
Feed rate, gpm	0.25
Underflow retention tank volume, gal	2
Underflow tank discharged	Once a week
Ratio of underflow rate to feed rate	0.02:1–0.12:1

The hydroclones have repeatedly demonstrated efficiencies above 70% with particles of 1-μ dia and larger. If the fission-product particles are much smaller than this (e.g., 0.1-μ dia), two or more hydroclones, as suggested in the previous[4] flow sheet, may be required to achieve the necessary separation efficiency.

The time that the underflow tank must be operated to permit the solids in the underflow circuit to approach closely steady-state concentration depends on the underflow rate but is not critical. Under the above conditions the minimum time between tank discharges is two days, but up to seven days may be allowed with very little effect on the insoluble fission-product concentration in the reactor fuel. The batch-wise pressure letdown of the underflow retention tank obviates the need for a control valve of small capacity and large pressure drop. The underflow retention tank affords an easy means of restoring to the reactor system the quantity of fuel removed as a purge. Before the processing plant is started up, the tank will be filled with uranium solution of such concentration as to make up the reactor burnup as well as to replenish the fuel purged.

The slurry of centrifuged solids removed from the underflow reservoir will be evaporated for recovery of the heavy water, stored for decay, and transferred to a shielded shipping container for final drying. The shipping container with the dried uranium and fission and corrosion products will be conveyed to a uranium recovery plant, where it will be charged with natural water solution of nitric acid for dissolution of the contents. Shipment of the solids in the dry state will lessen the risk of shipping spills, reduce the loss of the comparatively valuable heavy water, and minimize the possibility of contaminating the heavy-water system with light water.

The evaporation of heavy water from the slurry is expected to be straightforward. It is planned to use the evaporator as a means of dissipating the radioactive heat until decay of the fission products permits storage without elaborate precautions or the risk of excessive temperatures.

The evaporator bottoms, containing the fission and corrosion products and the associated fissionable uranium, will be periodically discharged to a shielded carrier via a transfer tank. The transfer will be accomplished by the vapor pressure of the concentrate. The remaining heavy water will then be removed by evaporation in the carrier, the heavy-water vapor being condensed and returned to the heavy-water storage tanks.

10.3.1 Off-Gas Disposal

In general, the same procedures as those planned for the reactor system and similar equipment will be used in disposing of off-gas and waste.

10.3.2 Hazards

The chemical processing area will consist of four cells: B and C for the blanket and core processing equipment and A and D for the shielding

water pump, remote pump pulsators, instrumentation, samplers, and other equipment which requires access for maintenance but which must be segregated from personnel areas. Cells B and C are separated from the reactor cells by 5 ft of barytes concrete shielding. Through this wall are carried the high-pressure feed and return lines connecting with the hydroclone system. If the reactor fuel feed lines should rupture, the reactor core and blanket (connected for pressure equalization) could be expected to escape into the chemical processing cells. By adiabatic expansion this would raise the pressure to 90 psia, but, if the loss of heat to the cell walls is taken into consideration and if the rate of fluid escaping from a ruptured feed line is limited to 100 lb/min by the pressure drop in the feed line, the maximum pressure that would be attained is computed to be less than 25 psi, and this would occur after 30 min. Operation of the high-pressure shutoff valves or an emergency dump of the reactor in this period of time is feasible and can be relied upon to interrupt the loss of reactor fuel through the parted line.

The chemical processing cells will be designed to contain an internal pressure of 30 psi, and the cells will be sealed by a continuous steel membrane between layers of shield plugs in the same manner as planned for the reactor cells.

10.3.3 Schedule

The reactor is scheduled to start up January 1, 1956, after which time craftsmen cannot work safely in the processing cells. This necessitates completion of the chemical processing plant by January 1, 1956. The reactor will have completed its experimental functions by April 1, 1956. Continued operation of the reactor subsequent to this date will be primarily for separations experiments, and April 1, 1956, thus becomes the startup date of the chemical processing plant.

10.4 EQUIPMENT DEVELOPMENT

P. A. Haas J. C. Bresee

Installation of loop B (see ref. 5), designed for use in the dynamic study of the chemistry of fission-product precipitation and the effects of temperature cycling and attrition on the separability of precipitates, is 95% complete. The slurry in the loop can be drawn off continuously to feed a hydroclone liquid-solid separator. The clarified overflow will be returned to the loop; the underflow can be either returned to the loop or diverted to a receiver for evaluating the hydroclone performance. The loop was leak-tested with water at 2500 psig and with helium. No serious leaks were detected. The system is being flushed with acid and will be passivated with uranyl sulfate solution and oxygen preparatory to starting the experimental program.

An evaporator was designed for use in the study of problems involved in recovery of heavy water from the hydroclone underflow product by evaporation of the product to 50% uranyl sulfate. The evaporator will be a length of 6-in.-dia glass pipe heated by electrical resistance of the solution to simulate the heating produced by the fission-product decay. Problems to be studied include entrainment of uranium and fission products in the water vapor, control of liquid level, spattering of uranium on evaporator walls, and viscosity of final product.

[5] D. E. Ferguson *et al.*, *HRP Quar. Prog. Rep. Oct. 31, 1954*, ORNL-1813, Fig. 12.4, p 155.

11. PLUTONIUM-PRODUCER BLANKET PROCESSING

D. E. Ferguson
R. E. Leuze
R. H. Rainey
W. E. Tomlin

The objective of processing the uranyl sulfate solution blanket of the plutonium producer is to remove plutonium and neptunium as rapidly as possible in order to minimize Pu^{240} buildup. During the quarter the study of the chemistry of plutonium and neptunium under simulated reactor conditions has included the measurement of the adsorption of plutonium on stainless steel, titanium, and zirconium, the rate of plutonium dioxide precipitation, and the neptunium adsorption on manganese dioxide.

11.1 ADSORPTION OF PLUTONIUM ON STAINLESS STEEL, TITANIUM, AND ZIRCONIUM

R. H. Rainey

The apparent saturation value for plutonium adsorption on zirconium is about 0.05 mg/cm^2 from 1.7 *m* UO_2SO_4 (erroneously reported before as 1.25 *m*) solution containing 105 mg of plutonium per kilogram of H_2O at 250°C, rather than the 0.03 mg/cm^2 previously reported.[1] Type 347 stainless steel has adsorbed 0.80 mg/cm^2 and titanium has adsorbed about 1.00 mg/cm^2, with no indication of an approach to equilibrium (see Fig. 11.1).

The experiment previously reported[1] was continued through 53 cycles of adding 1.7 *m* UO_2SO_4 containing 105 mg of plutonium per kilogram of H_2O [91% Pu(IV)], heating to 250°C under 150 psi oxygen and 150 psi hydrogen for 12 hr, removing the solution and precipitate, and rinsing with water. The amount of plutonium adsorbed on the walls of various metal containers was determined by material-balance calculations, with the plutonium found neither in solution nor in the precipitate assumed to have been adsorbed.

About 10% of the plutonium added to the zirconium vessel during the first 13 cycles was adsorbed, resulting in a plutonium buildup of 0.05 mg/cm^2. During the next 27 cycles, there appeared to be a slight increase in the plutonium adsorption, to 0.06 mg/cm^2, followed by a drop to a little less than 0.05 mg/cm^2. This may be real or it may be a result of small errors in the material balance. In either event, the saturation value for plutonium adsorption appears to be about 0.05 mg/cm^2 under these conditions.

Plutonium was being adsorbed by titanium and type 347 stainless steel, even after 53 cycles, with no indication of an approach to steady-state conditions. The break in the curves (Fig. 11.1) in the thirty-seventh cycle was a result of excessive evaporation in which the concentrated uranyl sulfate stripped some plutonium from the walls. About 50% of the plutonium added to the titanium was adsorbed on the surface, resulting in a plutonium buildup on the two vessels of 1.04 and 0.93 mg/cm^2, respectively. About 60% of the plutonium added to the stainless steel vessel was adsorbed, resulting in a plutonium buildup of 0.70 mg/cm^2. Since there was excessive corrosion in a duplicate stainless steel vessel, it was eliminated from the adsorption test.

It should be emphasized that the validity of these results is not known, since the experiments were carried out under static conditions, in the absence of a neutron flux, and with much higher plutonium concentrations than are expected in the plutonium-producer blanket. This series is being terminated, and other experimental methods will be used to check the results and to obtain the desired data more rapidly.

11.2 PRECIPITATION RATE OF PLUTONIUM DIOXIDE

R. H. Rainey

The time required for plutonium to precipitate after being formed and the equilibrium solubility (~3 mg per kilogram of H_2O) determine the amount of dissolved plutonium in the plutonium-producer blanket. Experimental data under simulated reactor conditions, but with no neutron flux, indicate that the dissolved plutonium will exceed the solubility by less than 0.3 mg per kilogram of D_2O. This will have only a slight effect on the amount of Pu^{240} in the product.

A study of the precipitation rate was made by injecting 15 ml of 1.25 *m* UO_2SO_4 containing Pu(IV) into an autoclave loaded with 35 ml of 1.25 *m* UO_2SO_4 under an atmosphere of 80 psi

[1] D. E. Ferguson *et al.*, *HRP Quar. Prog. Rep. Oct. 31, 1954*, ORNL-1813, p 147.

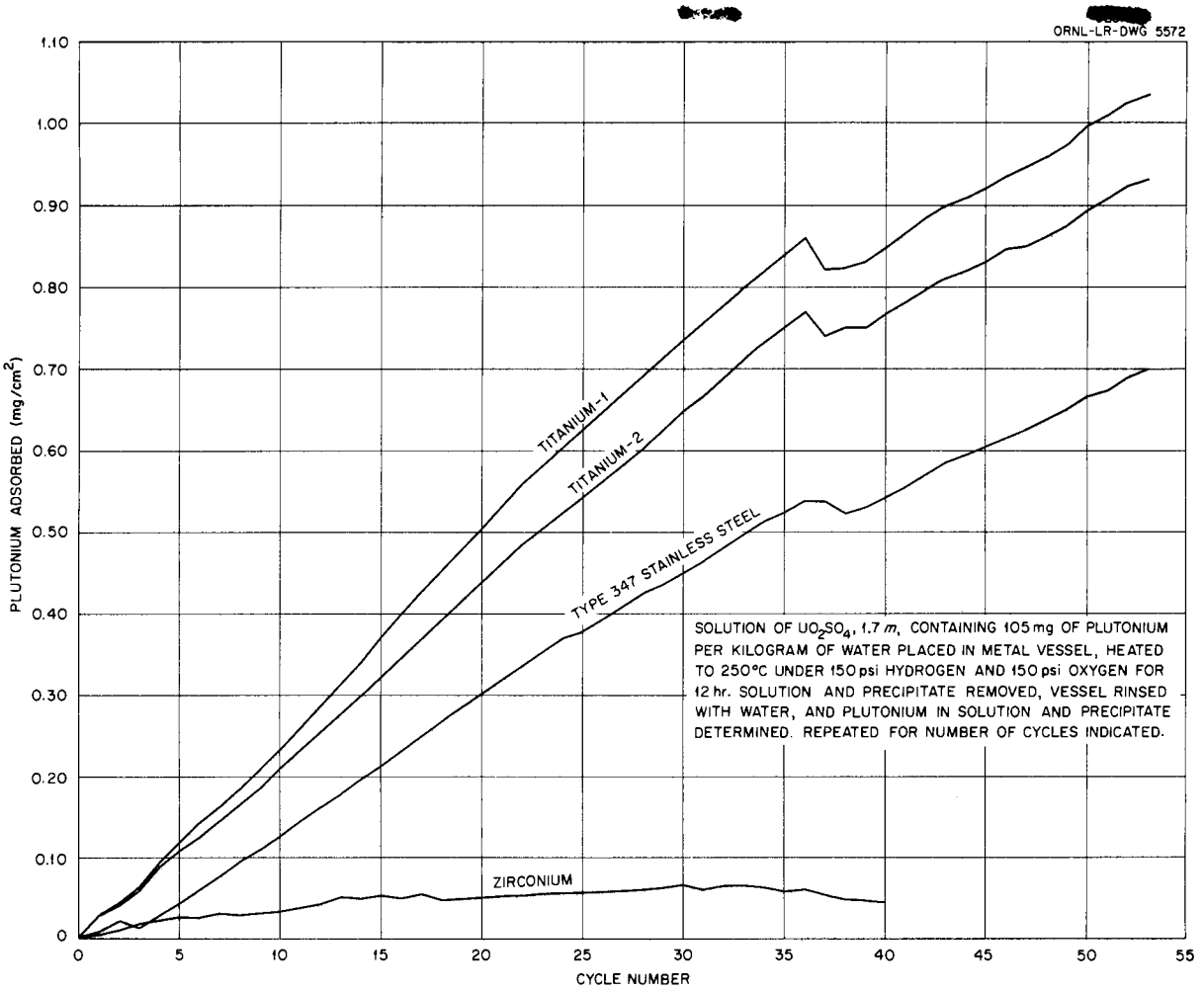

Fig. 11.1. Adsorption of Plutonium on Type 347 Stainless Steel, Titanium, and Zirconium.

oxygen and 160 psi hydrogen at 250°C. The solutions were mixed and then sampled at short intervals to determine the amount of plutonium remaining in solution. Results (see Fig. 11.2) show different behavior for different initial plutonium concentrations. The logarithm of the plutonium concentration vs time is essentially linear between 2.5 and 4 mg of plutonium per kilogram of H_2O, which is the range expected in the reactor. The reaction half lives calculated from the experimental data in this concentration range for initial plutonium concentrations of 50, 20, and 10 mg of plutonium per kilogram of H_2O were 5, 15, and 19 min, respectively. Even at the slowest rate, the plutonium solubility in the blanket will be greater than the saturation value by less than 0.3 mg per kilogram of D_2O.

The reason for the difference in precipitation behavior for solutions with different initial plutonium concentrations is not known. A test was made in order to determine whether the precipitation rate was a function of the amount of plutonium dioxide present; however, there was no difference in precipitation rate when a solution containing 20 mg of plutonium per kilogram of H_2O was spiked into a uranyl sulfate solution containing no plutonium or when the uranyl sulfate solution initially contained 15, 25, or 35 mg of plutonium dioxide per kilogram of H_2O.

When Pu(VI) was used in similar experiments, more than 90% of the plutonium was reduced to Pu(IV) in 5 min, and the precipitation rates were essentially the same as in the experiments in which Pu(IV) was used.

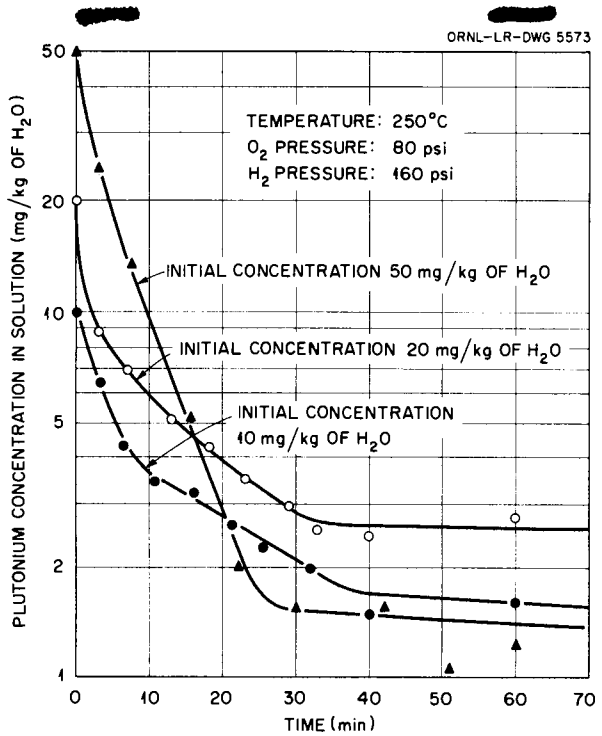

Fig. 11.2. Precipitation of Plutonium Dioxide from 1.25 *m* UO_2SO_4 with Initial Plutonium Concentrations as Shown.

11.3 ESTIMATE OF Pu^{240} CONTENT OF PRODUCT

With the information now available, an estimate can be made of the amount of Pu^{240} to be expected in the plutonium product of the plutonium producer. Neutron capture of Np^{239} to give Np^{240}, which decays by beta emission to Pu^{240}, and the neutron capture of Pu^{239} are the main sources of Pu^{240}. The estimate (see Table 11.1) that has been made is preliminary and includes a number of approximations, but it indicates what might be expected of the proposed chemical flow sheet. It also points out the importance of developing a continuous neptunium removal process, since neutron capture by Np^{239} is the largest source of Pu^{240}. One of the assumptions made was that more than 95% of the insoluble plutonium dioxide will be removed by the hydroclones. This may not be the case, since the particle size of plutonium dioxide in the reactor is unknown. The efficiency of a 0.25-in.-dia hydroclone for removing plutonium dioxide precipitated under simulated reactor conditions will be determined. Although the adsorption of plutonium on metal walls has not yet been completely studied, the data indicate that this is perhaps a minor source of Pu^{240}; however, adsorption of about 1 mg/cm^2

TABLE 11.1. ESTIMATED BUILDUP OF Pu^{240} IN K-49 BLANKET PRODUCT

Source	State	Amount	Resulting Pu^{240} in Product (%)
Neptunium	Soluble	50 mg/kg D_2O	0.42 ± 0.10[a]
Plutonium	Soluble	3 mg/kg D_2O	0.12
	Supersaturated	0.3 mg/kg D_2O	0.012
	PuO_2	4.6 mg/kg D_2O[b]	0.19
	Adsorbed on zirconium core tank	5.3 g[c]	0.05[d]
	Adsorbed on blanket wall	420 g[e]	0.036[f]

[a]Neptunium completely soluble and $\sigma_c(Np^{239}) = 80 \pm 20$ barns.
[b]Amount processed per day = 100,000 liters, assuming 95% efficiency of solids separation.
[c]Plutonium on 6-ft zirconium core tank = 0.05 mg/cm^2.
[d]Neutron flux assumed to be five times average blanket flux.
[e]Equilibrium value not known; 1 mg of plutonium per square centimeter assumed for estimation.
[f]Neutron flux assumed to be $\frac{1}{25}$ of average blanket flux.

on titanium will hold up one day's production on the blanket wall and several times this amount in the heat exchanger loop.

11.4 NEPTUNIUM CHEMISTRY

W. E. Tomlin

It was previously reported[2] that neptunium could be adsorbed on manganese dioxide from a uranyl sulfate solution but that the capacity was not known. A single experiment with Np^{239} used as a tracer in 0.06 *m* UO_2SO_4 indicated the capacity to be less than 1 part of neptunium per 10^9 parts of manganese dioxide.

[2]D. E. Ferguson *et al.*, *HRP Quar. Prog. Rep. Oct. 31, 1954*, ORNL-1813, p 149.

12. THERMAL-BREEDER BLANKET PROCESSING

D. E. Ferguson
R. E. Leuze W. E. Tomlin

At the present time, the most obvious method for processing the thorium dioxide blanket is to recover the heavy water by evaporation and to dissolve the thorium dioxide as feed for the Thorex process. A study of thorium dioxide dissolution was started, and leaching methods for removal of protactinium and uranium from thorium dioxide were investigated.

12.1 DISSOLUTION OF THORIUM DIOXIDE

W. E. Tomlin

A small amount of hydrofluoric acid must be added to refluxing nitric acid in order to dissolve thorium dioxide within a reasonable length of time. The results of dissolution experiments (see Table 12.1) show that 2 g of thorium dioxide was not dissolved by refluxing in 160% excess 16 *N* HNO_3 for 4 hr when no hydrofluoric acid was present but that, when 0.04 *N* HF was added, complete dissolution was accomplished in 11 min. Since the Thorex process feed is acid deficient, it is desirable to dissolve the thorium dioxide in a minimum amount of acid. It should be noted that when 30% excess 8.0 *N* HNO_3 containing 0.04 *N* HF was used, 2 g of thorium dioxide was completely dissolved in 1 hr, resulting in a 1.4 *M* $Th(NO_3)_4$ solution containing 2.5 *N* HNO_3. When 15% excess 7.0 *N* HNO_3 containing 0.04 *N* HF was used in an attempt to obtain a final concentration of 1.4 *M* $Th(NO_3)_4$ and 1.5 *N* HNO_3, dissolution was not complete in 3 hr.

TABLE 12.1. DISSOLUTION OF THORIUM DIOXIDE

2.0 g of thorium dioxide (calcined at 650°C) refluxed in 5 ml of HNO_3

Nitric Acid (*N*)	Nitric Acid (% excess)	Hydrofluoric Acid (*N*)	Dissolution Time (min)
16	160	0.08	8
		0.06	7
		0.04	11
		0.032	30
		0.02	120
		0	240*
13	110	0.04	28
9.6	60	0.04	55
8.0	30	0.04	60
7.0	15	0.04	180*

*Not completely dissolved.

As the calcination temperature of thorium dioxide increased, the dissolution time also increased (see Table 12.2). This effect was more pronounced as the nitric acid concentration was lowered. In 30% excess 8 *N* HNO_3 containing 0.04 *N* HF, it required over twice as long to dissolve thorium dioxide calcined at 800°C as that calcined at 650°C. When 110% excess 13 *N* HNO_3 was used, the thorium dioxide calcined at 800°C required only a slightly longer time to dissolve than that calcined at 650°C.

TABLE 12.2. EFFECT OF CALCINATION TEMPERATURE ON THORIUM DIOXIDE DISSOLUTION

2.0 g of thorium dioxide refluxed in 5 ml of HNO_3 containing 0.04 *N* HF

Nitric Acid (*N*)	Thorium Dioxide Calcination Temperature (°C)	Dissolution Time (min)
8 (30% excess)	650	60
	800	150
	1000	225
13 (110% excess)	650	28
	800	29
	1000	38

12.2 LEACHING OF THORIUM DIOXIDE

W. E. Tomlin

In a series of scouting tests, 12 *N* H_2SO_4 was the most effective reagent for leaching protactinium from irradiated thorium dioxide. When 14 mg of thorium dioxide that had been irradiated 62 hr in the ORNL Graphite Reactor was refluxed with 3 ml of 12 *N* H_2SO_4 for 4 hr, 70% of the Pa^{233} was

leached and only 0.2% of the thorium was dissolved. Analyses showed that 1.46×10^7 protactinium beta counts per minute was dissolved and that 5.85×10^6 protactinium beta counts per minute remained in the solids.

A 14-mg sample of blue thorium dioxide (from irradiated thorium metal) was refluxed with 5 ml of 12 *N* H_2SO_4 for 4 hr. Approximately 45% of the beta activity and 30% of the alpha activity (U^{233}) were leached from the thorium dioxide. This was repeated with another sample of blue thorium dioxide, and 43% of the U^{233} was removed.

13. SUMMARY OF WORK OF VITRO LABORATORY[1]

A high-temperature circulating loop was incorporated in the existing calcium fluoride adsorption pilot plant, and the apparatus is being used to study the chemistry of rare-earth and corrosion-product precipitation in a flowing stream. A preliminary test run was completed in which a mixture of rare-earth, ferric, and chromic sulfates in 0.02 *m* UO_2SO_4 solution was continuously added to the loop operating at 280° C. A sample of solids filtered from the loop solution at 280° C was dried at temperature and removed for examination. This run will be followed by a test run in which a rare-earth tracer will be used so that material balances may be obtained and the extent of deposition of rare-earth sulfates on the hot surfaces of the loop may be studied.

Further batch tests carried out in quartz-lined stainless steel bombs showed that the amount of iodine in 0.02 *m* UO_2SO_4 can be reduced from 0.001 g of iodate per kilogram of water to 0.02 ppm, or 98 to 99% removal, by the reaction of iodine vapor with metallic silver in the gas phase above such a solution at 310° C. A continuation of this study is planned in order to provide kinetic data applicable to the design of a unit for removing fission-product iodine from the core of the HRT, thus diminishing the poisoning effect of Xe^{135} and the hazard of cesium buildup.

An experiment designed for the study of the removal of cesium from a simulated fuel solution by an inorganic ion-exchange material was carried out. A column containing zirconium phosphate cation exchanger was operated at room temperature with 513 bed volumes of 0.02 *m* UO_2SO_4, containing 0.2 g of cesium per liter as cesium sulfate, before breakthrough occurred. A loading of 67 mg of cesium per gram of adsorber was obtained. The test will be repeated at 100° C.

Attempts to measure adsorption of tagged elements on metal surfaces by Geiger-Mueller counting showed that the uranium salts used in making up simulated fuel solution would have to be freshly extracted before each test to eliminate interfering beta counts from UX_1 and UX_2. The beta activities having maximum energies in the range 0.5 to 3.0 Mev could not be measured quantitatively in the presence of these interferences by conventional absorption methods.

[1] W. A. Bain, *HR Fuel Reprocessing. Quar. Prog. Rep. Oct. 1–Dec. 31, 1954*, KLX-1741.

Part VI

SUPPORTING CHEMICAL RESEARCH

E. H. Taylor

14. RADIATION DECOMPOSITION OF THORIUM NITRATE SOLUTIONS

J. W. Boyle H. A. Mahlman

14.1 GAMMA-RAY DECOMPOSITION

Previous results[1] showed that thorium nitrate solutions decompose under reactor irradiation and fission-particle irradiation to give hydrogen and oxygen from decomposition of the water and to give nitrogen, oxygen, and oxides of nitrogen from decomposition of the nitrate. The hydrogen yield decreases with increasing thorium concentration for mixed fast-neutron, beta, and gamma radiations (ORNL Graphite Reactor) and for fission-fragment irradiation. The nitrogen yield for fission-particle irradiation at a dose of 1.4×10^{21} ev/ml increases with increasing thorium nitrate concentration. The amount of N_2O produced is about one-tenth the nitrogen yield, and NO_2 and nitrite (in solution) are observed in trace quantities.

Yields of hydrogen and nitrogen from the gamma-ray decomposition of thorium nitrate solutions have now been determined with the use of a 1000-curie cobalt source.

The total energy absorbed in the solutions was based on the ferrous sulfate dosimeter,[2] and the mass absorption coefficients (at 1.25 Mev) for the various solution components were taken from the work of Richardson[3] and of Snyder and Powell.[4] The 100-ev yields of hydrogen and nitrogen for various concentrations of thorium nitrate and for the different radiations are summarized in Table 14.1.

The results show that the more densely ionizing radiations cause the greater decomposition and that the effect of solute concentration is essentially the same for all types of radiation. The yields were determined for a particular dose and may not represent initial yields.

14.2 YIELD-vs-DOSE STUDIES IN REACTOR-IRRADIATED SOLUTIONS

Gas yields have been determined for 2.76 *m* $Th(NO_3)_4$ solutions as a function of irradiation time in the ORNL Graphite Reactor at a temperature of 30 to 40°C and are presented in Fig. 14.1. The values for the ordinates are to be multiplied by the factors given on the curves. The thermal-neutron flux was determined for each experimental point and varied between 4.7×10^{11} and 7.2×10^{11} neutrons/cm^2/sec. It was assumed that the energy input varied directly as the slow-neutron flux. Half-filled spherical silica ampoules of 1 to 2 ml total volume were used in this study. It is seen that there was some decrease in rate of gas evolution during the time of the experiment, which was about one week.

---

[1] J. W. Boyle and H. A. Mahlman, *Chem. Semiann. Prog. Rep. Dec. 20, 1954*, ORNL-1832, p 69.

[2] C. J. Hochanadel and J. A. Ghormley, *J. Chem. Phys.* 21, 880 (1953).

[3] D. M. Richardson, *Calorimetric Measurement of Radiation Energy Dissipated by Various Materials Placed in the Oak Ridge Pile*, ORNL-129 (Oct. 1, 1948).

[4] W. S. Snyder and J. L. Powell, *Absorption of γ-Rays*, ORNL-421, Supp. I (Nov. 7, 1949).

TABLE 14.1. RADIATION DECOMPOSITION OF THORIUM NITRATE SOLUTIONS

Total energy input: 10^{20} to 10^{21} ev/ml

$Th(NO_3)_4$ (*m*)	G_{H_2}			G_{N_2}		
	Gamma Radiations	Graphite Reactor Radiations	Fission-Fragment Radiations	Gamma Radiations	Graphite Reactor Radiations	Fission-Fragment Radiations
0.26	0.070	0.26	1.11	0.00004	0.003	0.002
0.55	0.053	0.17	0.93	0.0005	0.003	0.016
1.5	0.026	0.10	0.51	0.0015	0.005	0.047
2.7	0.014	0.05	0.33	0.0011	0.006	0.063

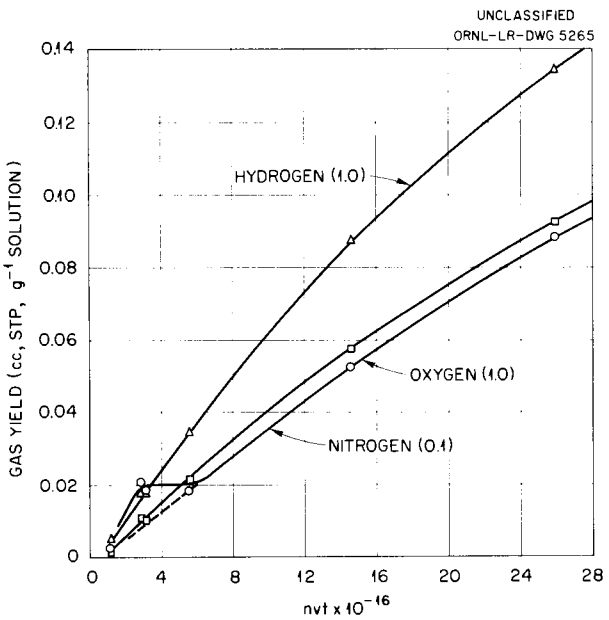

Fig. 14.1. Gas Yields from 2.76 *m* $Th(NO_3)_4$ Solutions vs Radiation Time.

Further experimentation will be carried out to verify the shape of the nitrogen curve. The apparent leveling-off of the nitrogen curve between 3×10^{16} and 6×10^{16} neutrons/cm^2/sec is supported by other data not included on the graph and is believed to be real. The shape of the nitrogen-yield-vs-time curve is similar to the shape of the hydrogen-yield-vs-time curve[5] for pure water irradiated in the ORNL Graphite Reactor. In the test with pure water the rise in pressure after the apparent steady state was attributed to impurities entering the water from the silica container walls. Perhaps in the present study there is a similar explanation – the buildup of some substance which was not initially present – for the shape of the curve.

14.3 EFFECT OF ULLAGE

Three ampoules containing different fillings of degassed 2.76 *m* $Th(NO_3)_4$ solution were irradiated together in the Graphite Reactor. The resulting total decomposition gas pressure and relative yields of gas after one week of irradiation are presented in Table 14.2.

Although the ampoules contained aliquots of the same stock solution and were irradiated together for the same length of time, the energy input per gram differed for each sample. If all the Th^{233} beta-decay energy were absorbed in the sample, it would amount to about 20% of the total energy. However, a considerable fraction of the energy of the 1.2-Mev beta ray is lost because of the geometry of small samples. No correction was made for this loss. In spite of the fact that there is less energy absorbed in the smaller samples (thus a lower gas yield would be expected), the relative yields for both hydrogen and nitrogen increased with an increase in ullage (vapor fraction). The nitrogen-yield results are in agreement with those of the studies discussed in the next paragraph.

TABLE 14.2. EFFECT OF ULLAGE ON RADIATION DECOMPOSITION OF THORIUM NITRATE SOLUTIONS

	Ampoule (% filled)		
	91	52	7
Total final pressure, atm	3.6	0.48	0.039
Relative H_2 yield per gram	1	1.32	1.61
Relative N_2 yield per gram	1	1.02	1.09

14.4 EFFECT OF ADDED GASES

Known amounts of hydrogen, oxygen, air, and nitrogen were added singly to ampoules containing 2.76 *m* $Th(NO_3)_4$ solutions before irradiation in the reactor in order to determine the effect of the various gases on the nitrogen yield. One irradiation time was used for the ampoules containing hydrogen, oxygen, and air, and two different exposure times were used for the ampoules containing nitrogen. The gas yields were compared with the yields for degassed samples irradiated for the same length of time.

The comparison of yields indicated that hydrogen added at the start increased the nitrogen yield somewhat, that oxygen had no effect, and that air and nitrogen decreased the nitrogen yield. The amount of nitrogen added at the start was about ten times that produced in a similar sample degassed and irradiated for the same length of time. The 100-ev nitrogen yield was smaller for the shorter period of radiation. It is not known whether the decrease in nitrogen yield was due to an interference with the formation of nitrogen or to fixation of the nitrogen present.

[5] A. O. Allen *et al.*, *Decomposition of Water and Aqueous Solutions under Pile Radiation*, ORNL-130, Fig. 1 (Oct. 11, 1949).

15. INORGANIC CHEMISTRY

15.1 ADSORPTION OF RARE EARTHS ON INORGANIC MATERIALS

T. A. Carlson K. A. Kraus
J. S. Johnson, Jr. H. O. Phillips

Exploratory investigations of the adsorptive properties of various inorganic materials in aqueous media have been started. Primary emphasis was given to a number of compounds containing zirconium. It was shown in earlier preliminary work that a commercial preparation of zirconium oxide could adsorb europium tracer even from relatively acidic solutions (~0.01 *M* HCl and H_2SO_4). These experiments were repeated with small (~1-ml, 2.5-cm-high) columns. As shown in Fig. 15.1, this particular commercial zirconium oxide showed excellent adsorption of europium tracer at low acidities. It further showed reversibility of adsorption, which permitted elution at higher acidities.

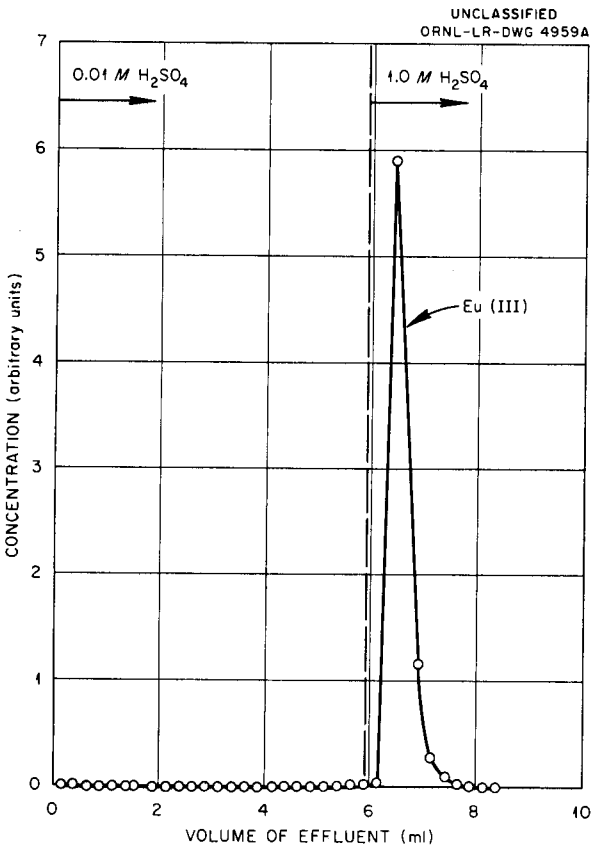

Fig. 15.1. Adsorption and Elution of Eu(III).

In an attempt to establish whether this adsorption was due to the zirconium oxide or to impurities, a number of preparations were made from doubly recrystallized zirconium oxychloride ($ZrOCl_2 \cdot 8H_2O$) (Table 15.1). None of these preparations showed any significant adsorption in 10^{-2} or 10^{-3} *M* HCl, suggesting that adsorption in the commercial zirconium oxide is due to impurities. This explanation was further substantiated by rough measurements of the capacity of the commercial zirconium oxide for rare earths, which was found to be less than 10^{-5} mole of rare earths per liter of bed.

A series of precipitations of zirconium hydroxide in the presence of various metals [Ca(II), Fe(III), Bi(III), and Sn(IV)] was carried out, and the resulting products were washed, dried, ignited, and tested for Eu(III) adsorption. No significant adsorption was found for these materials from 10^{-2} or 10^{-3} *M* HCl (Table 15.1).

Since a spectrographic analysis of the commercial zirconium oxide indicated the presence of phosphorus, some of the adsorption characteristics of pure zirconium phosphate were investigated. The material prepared by precipitating Zr(IV) with H_3PO_4 from a solution of recrystallized $ZrOCl_2$ and drying at 110°C showed very strong adsorption for Eu(III) from 0.01 *M* HCl (or H_2SO_4) and slow elution with 0.1 *M* HCl (or H_2SO_4) in a manner similar to the commercial zirconium oxide. However, its adsorption for cobalt tracer was considerably better than that of the commercial zirconium oxide, leaving considerable doubt that zirconium phosphate was responsible for the adsorptive properties of the commercial preparation.

It was found that Eu(III) tracer adsorbed on a material prepared from purified hydrous zirconium oxide (zirconium hydroxide dried at 110°C) after it had been pretreated with a dilute phosphoric acid solution. One milliliter of the hydrous oxide adsorbed phosphoric acid from approximately 13 ml of a 10^{-3} *M* H_3PO_4 solution, which should make the adsorptive capacity of the final material of the order of 10^{-2} mole per liter of bed. In rough capacity measurements with Ce(III), this adsorptive capacity was essentially confirmed. In contrast to this capacity of the phosphate-treated hydrous oxide, precipitated zirconium phosphate (dried at 110°C) showed an adsorptive capacity for rare earths of approximately 0.2 mole of Ce(III) per liter of bed.

TABLE 15.1. ADSORPTION OF Zr(IV)-CONTAINING PREPARATIONS

Material	Method of Preparation	Adsorption
ZrO_2	Commercial	Good (10^{-2} *M* HCl)
ZrO_2	Precipitation, $ZrOCl_2 + NH_4OH$, dried at 130°C	Negligible (3×10^{-3} *M* HCl)
ZrO_2	Precipitation, $ZrOCl_2$ (boiled) + NH_4OH, dried at 130°C	Negligible (3×10^{-3} *M* HCl)
ZrO_2 + 16 mole % Fe_2O_3	Precipitation, $ZrOCl_2 + FeCl_3 + NH_4OH$, dried at 150°C, fired over night at 600°C	Negligible (4×10^{-3} *M* HCl)
ZrO_2 + 1 mole % SnO_2	Precipitation, $ZrOCl_2 + SnCl_4 + NH_4OH$, dried at 25°C	Negligible (2×10^{-3} *M* HCl)
ZrO_2 + 2 mole % Bi_2O_3	Precipitation, $ZrOCl_2 + Bi(ClO_4)_3 + NH_4OH$, dried at 150°C	Negligible (1.5×10^{-3} *M* HCl)
ZrO_2 + 5 mole % CaO	Precipitation, $ZrOCl_2 + CaCl_2 + NH_4OH$, dried at 150°C	Negligible (1×10^{-3} *M* HCl)
ZrO_2 + 5 mole % CaO	Precipitation, $ZrOCl_2 + CaCl_2 + NH_4OH$, dried at 150°C, fired at 600°C	Negligible (1×10^{-3} *M* HCl)

15.2 PEPTIZATION OF OXIDE POWDERS

K. A. Kraus H. O. Phillips

During attempts to prepare adsorption columns from finely divided oxide powders, the following incidental observations were made regarding peptization of these oxides.

The commercial ZrO_2 was of small particle size (0.1 to 1 μ), and it tended to peptize on repeated washing. Because of the small particle size, it appeared very difficult at first to make adsorption columns. However, it was noticed that at low electrolyte concentrations the oxide tenaciously clung to glass, making it possible to prepare reasonably-well-flowing columns by filling them with a mixture of fine-mesh glass beads (~200 mesh) and oxide powder.

When these columns were washed with water or with dilute HCl solutions, the effluent was cloudy, probably as a result of continued peptization of the oxide in the column. The effluent, however, clarified suddenly when the columns were treated with 0.1 *M* HCl or more concentrated solutions. The effect was reversible; that is, returning to more dilute HCl solutions produced cloudy effluents (peptization), whereas returning then to more concentrated HCl solutions clarified the effluents. The effect of sulfuric acid on the peptization properties of the oxide columns was very interesting: Substitution of 10^{-3} *M* H_2SO_4 for a dilute HCl solution (in which peptization occurred) caused immediate clarification. After this treatment with dilute sulfuric acid, return to dilute HCl solutions did not cause peptization as before, indicating that the effect of sulfate was essentially irreversible. Since it was suspected that the effect of sulfate was related to a residual anion-exchange property of the oxide, the column was treated with 1 *M* HCl in an attempt to displace adsorbed sulfate. After this treatment, dispersion at low HCl concentration could again be achieved, as was anticipated.

Similar observations were made with columns containing Fe_2O_3 of small particle size. Since these observations are reproducible, it is suggested that a column technique of this type might be useful in general in a study of the effect of additives on the dispersion properties of finely divided materials.

16. PHASE STUDIES OF AQUEOUS SYSTEMS AT ELEVATED TEMPERATURES

C. H. Secoy
F. J. Loprest W. L. Marshall

16.1 THE SYSTEM URANYL CHROMATE–WATER

Phase equilibria in the system uranyl chromate–water have been investigated from 0°C to the ice eutectic at –0.145 ± 0.015°C and to temperatures at which hydrolytic precipitation of a solid phase occurs. From a probable $UO_2CrO_4 \cdot 5\frac{1}{2}H_2O$ a transition has been found to occur at 66.30 ± 0.30°C. The maximum solubility of UO_2CrO_4 attainable for this system was that for the monohydrate from 66.30 to 145°C, the saturated solution being approximately 70 wt % UO_2CrO_4 over this entire concentration range.

Hydrolytic precipitation of a basic uranyl chromate occurred in the temperature region 110 to 140°C over the entire soluble concentration range of UO_2CrO_4.

The system is unique for a uranyl salt in that the solubility of the $5\frac{1}{2}$ hydrate increases markedly from 0.08314 *m* at 0.0°C to 6.19 *m* at 66.3°C. This solubility behavior may be of practical importance in purification or production operations involving aqueous uranyl systems.

It has not been possible to prepare uranyl dichromate in this laboratory as a stable solid at room temperature; however, solutions of mole ratio Cr/U = 2.0 have been investigated at elevated temperatures and are phase stable at *higher* temperatures than are uranyl chromate solutions.

The investigation of the UO_2CrO_4-H_2O system is essentially complete and is being reported elsewhere.[1]

16.2 PRELIMINARY OBSERVATIONS OF THE SYSTEM ThO_2-CrO_3-H_2O

The system ThO_2-CrO_3-H_2O at 25°C has been studied by Britton.[2] His data indicate that at this temperature it is possible to dissolve as much as 190 g of thorium per 1000 g of solution (near point A in Fig. 16.1), which is perhaps as much as 360 g of thorium per liter.

To obtain preliminary information about the high-temperature phase behavior of this system, samples of solutions of various compositions, unsaturated at room temperature, were heated in sealed capillary tubes, and the temperatures at which solid phases appeared were determined by visual observation.

16.2.1 Experimental

Initially, a mixture of ThO_2, CrO_3, and H_2O was prepared using pure ThO_2 that had been prepared from the oxalate by ignition. A solid phase, which appeared to be ThO_2, remained after this mixture was stirred for one week, even though its total composition lay in the unsaturated region of the 25°C ternary isotherm. It therefore seemed that the rate of solution of ThO_2 would be too low for the planned experiments to be done in a reasonable length of time. For this reason, a solid phase of composition fairly close to that of the formula $Th(CrO_4)_2 \cdot 3H_2O$ was prepared by adding dilute K_2CrO_4 solution (0.25 *M*) in a dropwise manner to boiling dilute $Th(NO_3)_4$ solution (0.5 *M*); both solutions were prepared from Baker and Adamson cp reagents. The method of preparation is practically the same as that described by Britton.

The thorium chromate precipitated as an orange crystalline solid, which was filtered, washed with

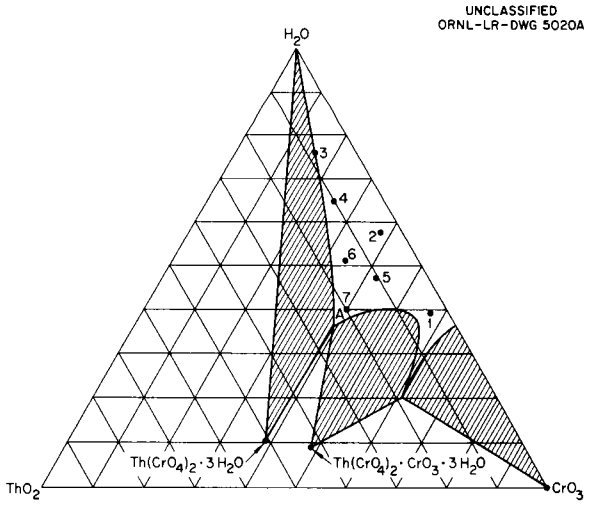

Fig. 16.1. The System ThO_2-CrO_3-H_2O at 25°C.

[1] F. J. Loprest, W. L. Marshall, and C. H. Secoy, *The System UO_2CrO_4-H_2O*, ORNL-1848 (in press).

[2] H. T. S. Britton, *J. Chem. Soc.* 123, 1429 (1923).

distilled water, and analyzed, with the following results: ThO_2, 51.52 wt %; CrO_3, 34.55 wt %. Thorium was determined gravimetrically by precipitation and ignition of the oxalate. Chromate was determined in two ways. Volumetrically, it was determined by initial oxidation with perchloric acid, reduction with excess standard ferrous solution, followed by a titration of the excess ferrous with standard potassium permanganate solution; calorimetrically, it was determined by complexing with diphenylcarbazide after initial sodium bismuthate oxidation. Single determinations of potassium and nitrate by flame photometry and the Kjeldahl method, respectively, yielded values of 1.2% potassium and 0.17% nitrate. It was assumed that the impurities would have little effect on these preliminary experiments.

The mixtures were prepared by weighing the solid thorium chromate, chromic oxide standard solution (58% CrO_3), and water. The mixture was magnetically stirred in a closed vessel, and the solid dissolved readily. The unsaturated solution was sealed in small capillary tubes and heated.[3]

TABLE 16.1. TEMPERATURE OF PRECIPITATION IN THE SYSTEM ThO_2-CrO_3-H_2O

Solution No.	ThO_2 (wt %)	CrO_3 (wt %)	Mole Ratio CrO_3/ThO_2	Observed Precipitation Temperature (°C)
1	3.94	57.01	38.21	320
2	4.7	38	21.4	170
3*	8.33	16.00	5.07	
4	10.14	25.19	6.56	156
5	10.54	42.24	10.58	250
6	14.83	34.28	6.11	166
7**	20.16	40.09	5.25	160

*Prepared from ThO_2. The solution did not become unsaturated after one week of stirring at room temperature.
**Density = 1.91 at room temperature.

16.2.2 Results

Figure 16.1 is a schematic reproduction of the 25°C isotherm of the system ThO_2-CrO_3-H_2O according to Britton.[2] The points in the unsaturated region represent the compositions of the mixtures prepared in this study and recorded in Table 16.1. Also in Table 16.1 are given the temperatures at which solid phases are observed to form when the unsaturated solutions are heated at a rate of about 2°C per minute. The true saturation temperatures are less (by undetermined amounts) than the temperatures recorded, which presumably are dependent on the rate of heating and the tendency of the various solid phases to supersaturate. The solids precipitated from solutions 2 and 4 to 7 were orange and crystalline, and all redissolved completely within 4 hr at 100°C. The solid precipitated from solution 1 was very dark in color and was not reversibly soluble. This solid probably contained Cr(III) oxides.

It appears from these preliminary observations that probably only those solutions with relatively high CrO_3/ThO_2 mole ratios will contain a sufficient concentration of thorium for breeder-blanket purposes at least in the temperature range 100 to 250°C. The thermal cross section of natural chromium, 2.9 barns, is probably too high for these solutions to be of practical value as a breeder blanket unless an isotopic separation is effected, in which case the 83.8% isotope of 0.72 barn and the 2.4% isotope of 0.006 barn might be utilized. However, even in this case, the question of thermal and radiation stability of aqueous hexavalent chromium ions must be answered.

[3] W. L. Marshall, H. W. Wright, and C. H. Secoy, *J. Chem. Educ.* 31, 34 (1954).

17. HOMOGENEOUS REACTOR ANALYTICAL DEVELOPMENT

M. T. Kelley C. D. Susano

17.1 HIGH-RADIATION-LEVEL ANALYTICAL FACILITY

L. T. Corbin D. J. Fisher
U. Koskela

The construction of the High-Radiation-Level Analytical Facility is progressing according to schedule, and the completion date for the contractor's portion of the work is April 1, 1955. A realistic date for completion of ORNL participation and equipping the laboratory is probably about July 1, 1955, although some limited operation will probably be undertaken prior to that time.

It is planned to have the cells equipped so that the following analytical operations can be performed without the samples having to be removed from the cells: weighing, dissolution of solids, centrifugation, measurement of liquid sample volumes and dilution to measured volume, spectrophotometric analyses, polarographic analyses, potentiometric titrations, coulometric titrations, pH measurement, specific-gravity measurement, ion-exchange resin separations, solvent-extraction separations, electrolytic separations, qualitative and semiquantitative spectrochemical analysis.

According to present plans, the training of personnel will begin even before the facility is ready for occupancy so that by the time of the startup of the HRT the personnel will have considerable experience in the operation of the cell equipment.

17.2 ION-EXCHANGE SEPARATION OF ALUMINUM FROM HRT FUEL

A. D. Horton

Since aluminum may occur as a contaminant in fuel solutions from chemical processing or from corrosion of alloys which may be used, a method of analysis for aluminum in such solutions was sought.

When the fuel solution is adjusted to 9 *M* in hydrochloric acid and passed through a Dowex-1 chloride-form ion-exchange column, aluminum and nickel pass through quantitatively.

Uranium, zirconium, tin(II), titanium(II), cobalt, copper, and most of the manganese(II) are strongly adsorbed on the column. Two column volumes of 9 *M* hydrochloric acid rinse are sufficient to recover the aluminum quantitatively. The effluent containing the aluminum is evaporated to dryness, and aluminum is determined colorimetrically by the method of Luke and Braun.[1]

17.3 SPECTROPHOTOMETRIC DETERMINATION OF NICKEL IN THE PRESENCE OF SULFATE

M. L. Druschel O. Menis
M. L. Hubbard C. K. Talbott

An extensive study was made to determine the optimum conditions for the determination of nickel in uranyl sulfate by the dimethylglyoxime method. It was found that the best results were obtained by use of an ammonium carbonate medium to complex the uranium. The use of ammonium citrate and sodium carbonate plus ammonium hydroxide was possible, but conditions were more critical and the color was less stable than with ammonium carbonate. In an ammonium carbonate medium the color seemed to be stable for at least 1.5 hr. A precision of 1% can be attained either with uranium present or absent. It was found that an ammonium citrate medium was suitable for the determination of nickel in 2 *M* aluminum nitrate solution after the nitrate had been eliminated by a preliminary evaporation with concentrated hydrochloric acid. The concentration of ammonium citrate used is rather critical, since a large excess will retard the development of the nickel color.

17.4 AMPEROMETRIC TITRATION OF HALIDES

C. M. Boyd

It was found that amperometric titration can be used for each of the halide ions separately down to the 10-μg level in uranyl sulfate, with about 5% precision. The conditions necessary for the titration are different in each case; so it would seem possible to titrate the halides in the presence of each other. However, it is found that the titration of mixtures leads to errors of about the same order as those encountered when potentiometric titration of mixed halides is attempted. In the amperometric case the individual halides must be determined by difference, since titration under chloride conditions

[1] C. L. Luke and K. C. Braun, *Anal. Chem.* **24**, 1120 (1952).

gives total halides, titration under bromide conditions gives iodide plus bromide, etc. Uranyl sulfate has no deleterious effect on the determination of any of the halides.

17.5 DETERMINATION OF DISSOLVED OXYGEN IN URANYL SULFATE SOLUTION

C. M. Boyd

It has been found that the modified Winkler method may be used for the determination of dissolved oxygen in uranyl sulfate solution after it has been passed through a bed of mixed ion-exchange resin (Dowex-1 in chloride form and Dowex-50 in the hydrogen form). However, there seems to be a loss of about 20 μg of oxygen in the resin bed, the exact cause of which has not yet been determined.

Attempts to determine dissolved oxygen by use of a polarographic technique without removing the ionic components have met with little success. The diffusion current of the oxygen plus the other components of the system does not seem to be strictly additive under these conditions.

17.6 ANALYSIS FOR IMPURITIES IN THORIUM OXIDE

O. Menis

Considerable effort was expended in developing methods for the analysis of impurities in thorium oxide to be used in the blanket-slurry program. It was found that a rapid estimation of the soluble impurities present could be obtained by an electrolytic conductivity measurement on the slurry. The impurities indicated by this test were mostly salts of the alkali and alkaline-earth metals.

17.7 ALUMINUM IN THORIUM OXIDE

H. R. Hunt

Aluminum can be determined in the presence of thorium by the 8-hydroxyquinoline method in which the aluminum complex is extracted with chloroform. The method is applicable in the range from 20 to 200 μg of aluminum, and a precision of 5% can be expected.

17.8 ZIRCONIUM IN THORIUM

F. L. Layton

Zirconium was separated from thorium by Dowex A-1 resin by using 9 *M* hydrochloric acid to elute the thorium. After elution from the column, zirconium is determined by the chloranilic acid method. Thorium is determined in the hydrochloric acid effluent by using the Versene titration technique.

17.9 TITANIUM IN THORIUM

H. R. Hunt I. B. Rubin

Preliminary investigation showed ascorbic acid to be unsatisfactory as a chromogenic agent for the determination of titanium when thorium was present. It was found, however, that the 8-hydroxyquinoline complex of titanium could be extracted from an acetate medium (pH 3 to 6) with chloroform. Iron, nickel, chromium, and manganese interfere in this method, and, while the interference of small amounts of iron can be eliminated by addition of hydroxylamine hydrochloride, the interference of the other elements can be eliminated only by removal with a mercury cathode from a perchloric acid medium. A precision of 3 to 5% can be attained by this method.

17.10 PALLADIUM IN THORIUM OXIDE

T. C. Rains

The α-furildioxime qualitative test for palladium has been adapted to test for the presence of this element in thorium oxide slurries.

17.11 SULFATE IN THORIUM OXIDE

T. C. Rains

The turbidimetric determination of sulfate has been adapted for use with thorium oxide samples. By careful control of conditions a precision of 5% may be expected in the range of 100 to 600 μg of sulfate.

18. CONCENTRATION OF NITROGEN-15[1]

J. S. Drury

L. L. Brown A. A. Palko
B. B. Klima W. T. Ward
R. R. Wiethaup

Experiments on the concentration of N^{15} for possible use in a breeder reactor containing thorium nitrate solution in the breeder blanket have been reported previously.[2,3] Further laboratory experiments on the ammonia vs ammonium carbonate system (the Carbonate system) have been performed, and some pilot-plant data have been accumulated. An initial survey has been made of a proposed new system in which the exchanger between gaseous NO and aqueous nitric acid is utilized to produce isotopic concentration. The cost of producing 95% N^{15} by these two processes has been estimated.

18.1 LABORATORY STUDIES OF THE CARBONATE SYSTEM

The favorable possibilities of the Carbonate system for separation of the isotopes of nitrogen made a study of the temperature variation of the isotopic separation factor desirable. Knowledge of the temperature dependence of the separation factor is necessary for a proper choice of operating conditions for a plant or laboratory exchange column. In a simple system, elevation of the temperature usually results in a lower separation factor. The Carbonate system, however, is not a simple system because of the chemical equilibrium involved and because of the solubility changes that occur with temperature variations. The nitrogen-containing solution species consist largely of dissolved ammonia, ammonium ion, and carbamate ion. The total and relative amounts of these species vary with temperature and change the effective separation factor.

To determine the separation factor as a function of temperature, single-stage batch equilibrations were performed at different temperatures. The separation factor does not depend on the amount of material present in either phase, since it is the ratio of the isotopic ratios in the two phases. It is necessary only to bring the gas and solution to equilibrium at the desired temperature, separate the phases, and prepare samples from the two phases for isotopic analysis. The liquid phase was simultaneously saturated with gaseous ammonia and commercial ammonium carbonate and then held at constant temperature for at least five days to ensure equilibrium. Isotopic exchange was carried out between 60 ml of the solution and 1 liter of gaseous ammonia in a stirred flask immersed in a constant-temperature bath. Stirring was continued for 2½ hr to ensure equilibrium. After this time the gas and liquid were separated and samples were taken for chemical and isotopic analysis. Isotopic samples were converted to nitrogen by oxidation with alkaline hypobromide solution. Four runs were made at temperatures of 15.6, 25.8, 35.9, and 44.3°C. Table 18.1 shows the results of chemical analysis of the liquid phases used in these runs. The total ammonia is divided into the species NH_3, NH_4^+, and $COONH_2^-$. The carbon dioxide is present as $COONH_2^-$, CO_3^{--}, and HCO_3^-.

TABLE 18.1. CHEMICAL COMPOSITION OF LIQUID PHASES – CARBONATE SYSTEM

Temperature (°C)	Total NH_3 (M)	Total CO_2 (M)	$COONH_2^-$ (M)	pH
15.6	19.35	3.94	3.71	10.8
25.8	20.05	6.20	5.82	10.9
35.9	20.10	7.50	6.68	10.5
44.3	18.10	8.03	6.81	

In no case was the chemical composition equal to that expected from published phase studies.[4] The compositions obtained were consistently lower in NH_3 and CO_2 content than were the published values. Table 18.2 shows the separation factors calculated from the mass analyses. Each sample

[1] A program of the Materials Chemistry Division.

[2] J. S. Drury, *Chemical Separation of Isotopes Section Semiann. Prog. Rep. Dec. 31, 1953*, ORNL-1706, p 13.

[3] J. S. Drury, *Chemical Separation of Isotopes Section Semiann. Prog. Rep. June 30, 1954*, ORNL-1815, p 19.

[4] E. Jaenecke, *Z. Elektrochem.* 35, 716 (1929).

TABLE 18.2. SEPARATION FACTORS* FOR NITROGEN ISOTOPES IN THE CARBONATE SYSTEM

Temperature (°C)	Replicate Separation Factors*	Average Separation Factors* (95% C.I.)
15.6	1.0124	1.015 ± 0.003
	1.0160	
	1.0158	
	1.0159	
25.8	1.0180	1.019 ± 0.002
	1.0184	
	1.0185	
	1.0185	
	1.0212	
35.9	1.0213	1.021 ± 0.003
	1.0222	
	1.0227	
	1.0191	
44.3	1.0179	1.022 ± 0.004
	1.0238	
	1.0232	
	1.0223	

*$(N^{15}/N^{14})_{soln}/(N^{15}/N^{14})_{gas}$.

was submitted several times to increase the precision of the numbers obtained. From the data it can be seen that the separation factor increases with temperature as a result of the increased solubility of NH_3 and increased amount of NH_4^+ in solution at higher temperatures. However, because of the negative temperature dependence of the separation factors, the effect is decreased at the higher temperatures, and the separation factor is approaching, or has passed through, a maximum. The data are not complete enough to prove exactly where this maximum value for α occurs. Ammonium carbonate solutions decompose at higher temperatures, which makes higher temperature runs difficult.

Two final column runs (runs 9 and 10) were made with the apparatus and methods described previously,[3] in order to check the effect of temperature on the total separation attained. The operating temperature was increased to 40°C, while flow rates and concentrations of the opposing streams remained essentially the same as those shown previously. During run 9 a crack developed in the reflux column, and the column had to be replaced. Run 10 proceeded satisfactorily, and the reflux losses of NH_3 from the stripping column were found to be 0.0066% of the interstage flow. The isotopic data from run 10 are plotted in Fig. 18.1 along with the data from run 8 made previously at 30°C. Approximate extrapolation of the two curves to equilibrium yields total separation values of 1.41 and 1.46, respectively, for the 30 and the 40°C runs. This is the order of magnitude of difference that would be expected when the single-stage α determinations reported above are taken into consideration and indicates that the advantage of using a temperature higher than 30°C would be small.

18.2 THE NITROX SYSTEM

An interesting system for enriching N^{15} was described recently in a preliminary report[5] by W. Spindel and T. I. Taylor of Columbia University. In this system, $NO_{(g)}$ passes countercurrent to $HNO_{3(aq)}$, and N^{15} concentrates in the aqueous

[5] W. Spindel and T. I. Taylor, *Concentration of Nitrogen-15 by Chemical Exchange*, NYO-6241 (Nov. 29, 1954).

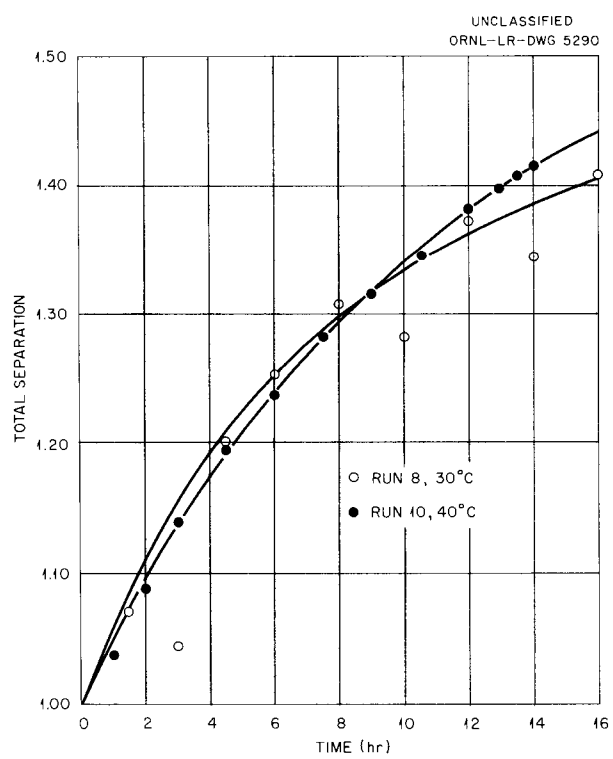

Fig. 18.1. Total Separation vs Time for Runs 8 and 10: Ammonia–Ammonium Carbonate System.

phase as indicated by the following reaction:

$$N^{15}O_{(g)} + HN^{14}O_{3(aq)} \longrightarrow N^{14}O_{(g)} + HN^{15}O_{3(aq)}$$

The single-stage isotopic fractionation factor for the reaction as written is about 1.05. Conversion of the $HNO_{3(aq)}$ to $NO_{(g)}$ at the product end of the system is accomplished by addition of gaseous SO_2 and appears to proceed according to the over-all equation:

$$2H_2O + 2HNO_{3(aq)} + 3SO_{2(g)} \longrightarrow 2NO_{(g)} + 3H_2SO_{4(aq)}$$

Reflux at the waste end of the system is effected by oxidizing the NO to NO_2 with air or oxygen and then absorbing the NO_2 in water, forming HNO_3.

In view of the large separation factor, the apparent low cost of chemicals needed to reflux the waste end of the system, and the production of a useful chemical, H_2SO_4, in one reflux reaction, a preliminary economic evaluation of the HNO_3-NO system was made.

18.3 ECONOMIC COMPARISONS OF THE CARBONATE AND THE NITROX SYSTEMS

An estimate of the cost of producing 95% N^{15} by the Carbonate system was already in preparation, and for comparison purposes a preliminary cost estimate, based, as far as possible, on the same criteria, was made of the Nitrox system. These estimates have been reported in detail elsewhere[6,7] and will be only summarized here. It should be emphasized that the cost criteria used are believed to be optimistic. For example, in the cascade design in both estimates, it is assumed that there is no loss of enriched material in the refluxers. Loss of enriched material in the refluxers would require a larger cascade and would result in a higher product cost. For the Nitrox system the concentration of sulfuric acid produced in the reflux reaction was taken as 60°Bé, and the isotope facility was assumed to be located adjacent to a sulfur dioxide manufacturer so that a very low contract price, free of transportation charges, could be used for the sulfur dioxide. The separation factor assumed for the Nitrox system (1.049) was the result of preliminary measurements; the exact value has not been determined.

Table 18.3 gives a summary of the basic criteria used in the two cost estimates. Table 18.4 shows the final results of the estimates. The cost of N^{15} produced by the Nitrox system is about 48% of that produced by the Carbonate system. It is estimated[6] that, in the case of the Carbonate system, scaleup to a plant producing 50 lb of N^{15} per day at the 95% level would reduce the cost of N^{15} to $2.38 per gram. Scaleup of the Nitrox process would be expected to reduce the cost also, although not proportionately.

TABLE 18.3. N^{15} COST-ESTIMATE CRITERIA

	Carbonate System	Nitrox System
Single-stage separation factor (N^{15} concentrated in aqueous phase)	1.020	1.049
Production rate	1 lb of N^{15} per day	1 lb of N^{15} per day
Mole fraction of N^{15}		
At product level	0.9500	0.9500
At feed level	0.0037	0.0037
At waste level	0.0017	0.0017
Number of enriching stages	591	244
Number of stripping stages	73	29

TABLE 18.4. COMPARATIVE COST OF PRODUCING N^{15}

	Carbonate System	Nitrox System
Total plant investment	$3,251,240	$863,748
Production cost		
Per pound	4,014	2,752
Per gram	8.85	6.07
Net cost (after credit is taken for by-products)		
Per pound	3,989	1,908
Per gram	8.79	4.21

[6] B. B. Klima and W. T. Ward, *Estimate of the Cost of Producing Nitrogen 15 by Chemical Exchange: Ammonia-Ammonium Carbonate System Using Calcium Hydroxide Reflux*, ORNL CF-55-1-20 (Jan. 12, 1955).

[7] B. B. Klima, W. T. Ward, R. R. Wiethaup, and J. S. Drury, *Estimate of the Cost of Producing Nitrogen-15 by Chemical Exchange: Nitric Acid–Nitric Oxide System Using Sulfur Dioxide Reflux*, ORNL CF-55-1-22 (Jan. 14, 1955).